THE DESIGN OF ANTENNA SYSTEMS ON COMPLEX STRUCTURES USING CHARACTERISTIC MODES

Thesis submitted in accordance with the
requirements of the University of Liverpool
for the degree of Doctor in Philosophy by

Kevin Paul Murray

March 1993

To
My Mum and Dad,
and
My wife Lesley

ABSTRACT

Antenna design for complex structures has always presented engineers with problems. The properties of a particular antenna my be dramatically altered by spurious current flow on the structure on which it is mounted. This study investigates an alternative approach to complex structure antenna design using the method of Characteristic Modes (CM). This allows a structure and the antenna to be considered as one, defining a unique set of orthogonal functions or modes. Useful insight may then be gained into the radiation characteristics of the complete composite structure by the examination of the individual modes. Further the orthogonal properties of the modes make them ideal for optimization purposes, which allows the previously spurious currents to be utilised to beneficial effect. In the work described a Characteristic Modal calculation routine is developed using the MININEC3 Method of Moments computer code. Further modal optimization software to achieve far-field pattern synthesis is also developed. The successful application of the technique to a HF vehicular antenna design problem demonstrates its general purpose suitability as a tool for complex structure antenna design. Appropriate wire grid models are generated to represent the various complex vehicular structures that are analyzed. This requires the development of a set of antenna modelling guidelines specific for the MININEC3 code which add to those in the literature.

Acknowledgements

I would like to express my gratitude to my supervisor throughout this research programme, Dr.B.A.Austin. His comments, suggestions and advice have always proved invaluable. The financial support of the Science and Research Engineering Council is also gratefully acknowledged.

My special thanks go also to my colleague Dr.Riyadh Najm. Our frequent informal discussions on many wide ranging engineering aspects could not be forgotten.

Finally the friendship and help of numerous people in the Department of Electrical Engineering could not be forgotten. In particular special thanks go to Andy Greenwood and Roman Surowiec. The support of the technical staff, particularly Mr.Fred Ormesher LFC OBE, is also much appreciated.

Table of Contents

List of Figures

List of Tables

Glossary of Terms

a	wire radius (m)
f	frequency (Hz)
λ	wavelength (m)
λ_n	modal eigenvalue
ψ	characteristic angle (°)
k_0, β	wave number ($2\pi/\lambda$)
ϵ	electric permittivity (Fm^{-1})
ϵ_0	electric permittivity of free space (8.85×10^{-12} Fm^{-1})
μ	magnetic permeability (Hm^{-1})
μ_0	permeability of free space ($4\pi \times 10^{-7}$ Hm^{-1})
Z_0	characteristic impedance of free space (377Ω)
A	magnetic vector potential (Wbm^{-1})
Φ	electric scalar potential (Vm^{-1})
E	electric field intensity (Vm^{-1})
H	magnetic field intensity (Am^{-1})
CM	Characteristic Modes
EFIE	electric field integral equation
HF	high frequency
MM	Method of Moments
MFIE	magnetic field integral equation
NVIS	Near Vertical Incidence Skywave
$[Z]$	generalized impedance matrix

The coordinate system

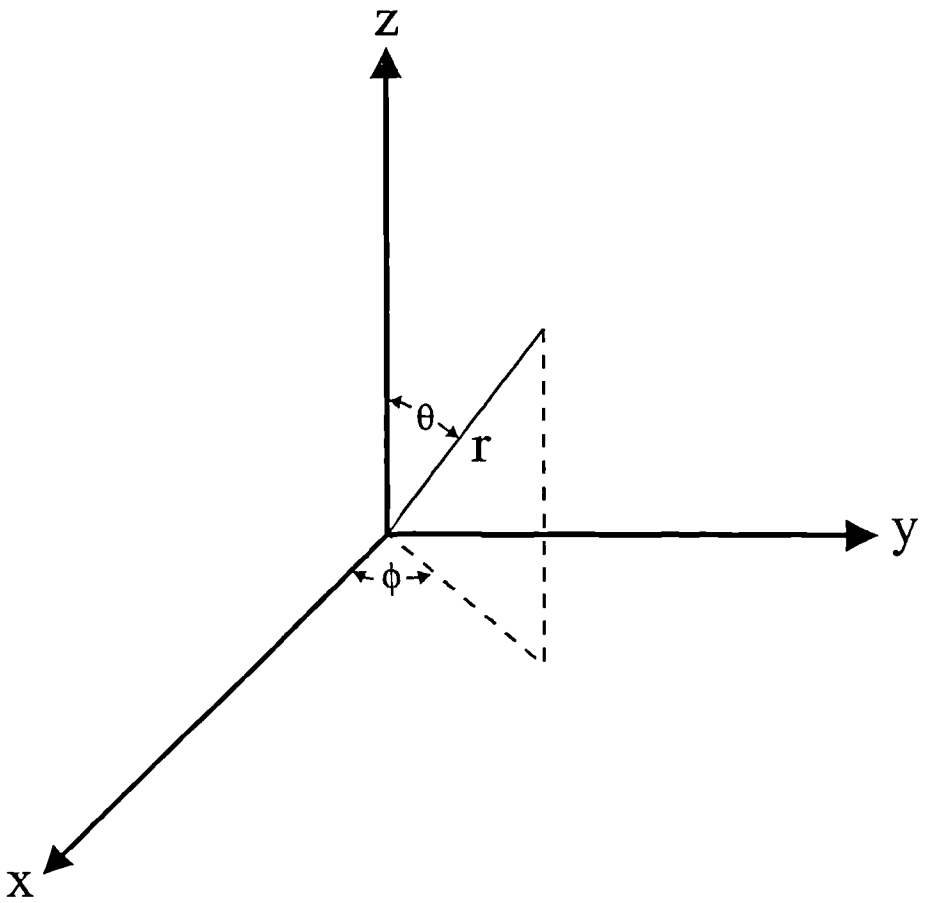

CHAPTER 1

INTRODUCTION

Designing antenna systems for mounting on complex structures has always presented engineers with problems. Where the structure and the antenna are of comparable electrical size, spurious current flow on the structure may dramatically alter the antenna's characteristics. The research described in this thesis addresses this problem by presenting an alternative approach to the design of antennas on complex structures. This is achieved using the method of Characteristic Modes which was initially developed by Garbacz (1968). The method permits the structure and antenna to be considered as one by defining a unique set of orthogonal modes. The individual properties of these modes allow greater insight to be obtained into the radiation characteristics of the complete composite structure. They may further be optimized to enable the utilization of the previously spurious structure currents and thus used to develop an antenna system with desirable characteristics.

Various techniques have been employed to assess the performance of antenna systems on complex structures. Experimentally, both full-scale measurements (eg. Cox and Vongas 1991) and scale modelling (eg. Nishikawa 1984) have been widely used. Computer simulation is also an appropriate method (eg. Najm 1992, Baldwin *et al* 1991). In such assessments of antenna performance various authors have suggested the existence of particular radiation modes

associated with the structures. It has been implied that the type and mounting position of an antenna may serve to strongly excite such modes thus making the overall radiation characteristics of the system due predominantly to current flow on the structure. For example both Pavey (1980) and Burberry (1982) recognised so called loop and dipole modes when examining HF aircraft and land vehicle antenna systems. Baker (1991) identified similar modes when assessing the performance of a helicopter HF antenna system. Further Lindenmeier (1989) described how the excitation of the resonant modes of a car body allowed an effective diversity system to be employed.

The aim of the research programme described in this thesis was threefold. Firstly to develop general purpose software to identify the Characteristic Modes of any arbitrary conducting structure. Secondly to investigate their form and structure, particularly of those associated with complex geometrical configurations. Finally, since the technique allows the definition of a unique set of orthogonal functions, to investigate the viability of using these modes in optimization routines. A particularly useful application is the ability to control the modes of a structure for far-field pattern synthesis.

The technique used here to calculate the Characteristic Modes of a structure follows that of Harrington and Mautz (1971b) and uses the Method of Moments (MM) (Harrington 1968). Conventionally the Method of Moments is used as a tool for the analysis of radiating and scattering structures (eg. Miller and Burke 1992). The technique solves the continuous function representing the current flow on a structure due to a defined excitation. Once the current

distribution is known other characteristics such as far-field may be evaluated. The novel combination of the Moment Method and Characteristic Modes used here however is more useful in that the defined modal set are ideal for both analysis and optimization purposes. In all the previous published work the method of Characteristic Modes has only been employed with simple structures (eg.Yee and Garbacz 1973 and Garbacz and Newman 1980). One reason for this is computer CPU time required when using the Method of Moments with complex structures. This increases with the electrical size and complexity of the test structure. The dramatic increase in the speed of computers over the last two decades however now allows the successful application of the Method of Moments and thus Characteristic Modes to analyze highly complex structures.

This thesis begins, in chapter 2, with a review of the Method of Moments and its application for antenna analysis. In particular issues that affect the accuracy of the final solution are addressed. This includes the application of different expansion and testing functions which are used to represent the current distribution. In using the Method of Moments as the basis of a Characteristic Modal calculation routine it is vital that a so called Galerkin formulation is employed. This necessitates that identical expansion and testing functions are used in the definition of the generalised impedance matrix. This effectively ruled out the use of the Numerical Electromagnetics Code (NEC) which is one of the most popular, widely used codes. Hence a modified version of the MININEC computer code was used for the work of this thesis. This is Galerkin and uses pulse expansion and testing functions. In chapter 2 this code is described and its

various features are examined. Also described in chapter 2 are the various, mainly empirical antenna modelling guidelines that have been suggested by various authors. A section is also included that examines the representation of continuous surfaces by wire grid models. This is vital to ensure the accurate electromagnetic representation of the modelled structures.

In chapter 3 the theory of Characteristic Modes is developed from first principles. Modal calculation using the Method of Moments is described and the relationship between the modes and the conventional matrix inversion currents and fields is examined. Also illustrated is the useful orthogonality conditions that exist between each member of the set of modes associated with a structure. These are of vital importance for later chapters where modal optimization is considered. Other useful modal formulations such as representing a structure as a N-port network and alternative modal orthogonality conditions are examined.

Chapter 4 demonstrates techniques by which the Characteristic Modes associated with a structure may be exploited to beneficial effect. This includes simple techniques whereby individual modes may be controlled by the position of a feed-point or passive loads. These methods are suitable for relatively uncomplicated structures where only a few modes control the overall radiation. Other techniques where the modes are collectively optimized to produce a desirable far-field are also described. These are suitable for complex structures with numerous significant modes.

Chapter 3 also describes the theoretical background of the MININEC computer code which was modified and used as the basis of work described in

this thesis. This code had not previously been used to model complex structures because the original code was written in the BASIC language and compiler constraints previously limited the size of structure to no more few wavelengths of wire. Conversion of the MININEC to FORTRAN effectively removed this constraint but the code's ability to model complex structures accurately was not known. In chapter 5 the validation of the modified MININEC code is addressed. Three method are used to assess its ability to model complex antenna structures accurately. Firstly analytical data is used, although this is limited to simple dipoles and loops. Secondly the results predicted by MININEC3 for a number of complex structures, represented as wire grid models, are compared to those from the NEC code. Lastly experimental data is used to assess the accuracy. The results of these simulations led to a set of modelling guidelines for MININEC which complement those made by other authors.

Chapters 6 and 7 concentrate on the practical application of the method of Characteristic Modes for antenna analysis and far-field pattern synthesis. Firstly in chapter 6 the software implementation of the techniques outlined in chapters 2, 3 and 4 is described. Then antenna analysis and pattern synthesis is demonstrated using a number of different antenna configurations. The usefulness of a Characteristic Modal approach is clearly apparent. In chapter 7 the Characteristic Modes of a number of complex structures are examined. In particular the modes of a land-based motor vehicle are investigated. Pattern synthesis is carried out to produce desirable a far-field pattern for a specific HF communication antenna system. This shows how the current flow on the complete

surface of complex structure may be utilised to beneficial effect. Suggestions are also made concerning the practical implementation of systems of voltage sources and loads to physically realise the results.

In chapter 8 the viability of using Characteristic Modes for complex structure antenna design is discussed. This is followed by the conclusions and recommendations for future work.

There are two appendices in this thesis. The first shows additional MININEC validation data, relevant to chapter 5. The second details the 6 publications that have resulted from the research programme.

For the numerical analysis described in this thesis an IBM 3081 mainframe computer and a 80386 PC were employed.

CHAPTER 2

ANTENNA MODELLING USING THE METHOD OF MOMENTS

2.1 Introduction

With the rapid increase in computer speed and sophistication over the past two decades, the Method of Moments (MM) has become one of the most widely used methods of antenna analysis. As, using this method, the electrical size of an antenna structure governs the required computer resources, only simple geometries were considered when the theory was initially formulated. Today however the analysis of relatively complex, electrically large structures using the Method of Moments is feasible.

The ultimate aim of the work described in this thesis was to use the theory of Characteristic Modes as a tool for the analysis and then far-field pattern synthesis of complex radiating platforms such as motor vehicles. As this involves the use and manipulation of a Method of Moments computer code it is useful here to review the underlying theory.

This chapter therefore, examines the basic principle of the Method of Moments. Section 2.2 traces the development of the basic theory by Harrington (1968) who formalised the underlying concept. Also included is a discussion of the application of the Moment Method theory for the solution of electromagnetic problems. This is achieved by obtaining the approximate solution of the various

integral equation representations which are typical of electromagnetic field relationships. A review of the numerous implemented computer codes is also undertaken to demonstrate different practical considerations.

Section 2.3 goes on to describe in detail the Method of Moments computer code that was used for a large proportion of the work in this thesis. This includes a full review of all the calculation features incorporated into the code and the reasoning behind why the code was chosen for the project.

Section 2.4 addresses some of the issues that affect the accuracy of the results obtained using Moment Method codes. It includes a discussion about segmentation schemes and also on wire grid modelling whereby a continuous surface is approximated by a conducting mesh.

2.2 The Method of Moments

2.2.1 The General Theory

The Method of Moments (Harrington 1968) is a powerful general purpose technique for solving a continuous functional equation. The theoretical basis of the method is the reduction of a continuous integral equation to a finite set of linear equations. Matrix techniques may then be applied to solve them. Since a continuous equation is reduced to a finite set of equations the calculated result is only an approximation to the exact result, with many factors affecting the accuracy. Following Harrington (1968) the Method of Moments in its most general form is summarized here. The applicability of the method for electromagnetic problems and the various factors that affect the accuracy of the

results obtained are discussed in later sections.

Initially a general inhomogeneous equation is defined as:

$$Lf=g \tag{2.1}$$

where L is a known operator, g is a known function and f is an unknown function to be determined. The first step is to express the unknown function f as an expansion of a series of N linear terms such that:

$$f \approx a_1 f_1 + a_2 f_2 + \cdots + a_N f_N = \sum_{n=1}^{N} a_n f_n \tag{2.2}$$

where a_n are constants and f_n are so called expansion or basis functions. Because of the finite nature of equation 2.2 it is noticed that the summation is an approximation to the continuous function f. For an exact result N must equal infinity. Now substituting equation 2.2 into equation 2.1 yields:

$$\sum_{n=1}^{N} a_n L f_n = g \tag{2.3}$$

which reduces the continuous operator equation 2.1 to a single equation with N unknowns, which is still unsolvable. In order to generate a solvable representation it is then necessary to define a suitable inner product of the functions f and g:

$$\langle f,g \rangle \tag{2.4}$$

which satisfies the general laws of linear spaces and operators reviewed by Harrington (1968 p213).

Next a set of M ($M \geq N$) so-called weighting or testing functions w_m are then defined. The inner product of the individual elements of equation 2.3 is then

taken with each w_m yielding:

$$\sum_{n=1}^{N} a_n \langle w_m, L\, f_n \rangle \approx \langle w_m, g \rangle \qquad m=1,2,3,....M \tag{2.5}$$

Equation of 2.1 has now been reduced to a set of M linear equations each with N unknowns which may be represented in matrix format as:

$$[L][A] = [G] \tag{2.6}$$

where $[L]$ is an M by N matrix with elements:

$$l_{mn} = \begin{bmatrix} \langle w_1, L\, f_1 \rangle & \langle w_1, L\, f_2 \rangle & \cdots & \langle w_1, L\, f_N \rangle \\ \langle w_2, L\, f_1 \rangle & \langle w_2, L\, f_2 \rangle & \cdots & \langle w_2, l\, f_N \rangle \\ \vdots & \vdots & \cdots & \vdots \\ \langle w_M, L\, f_1 \rangle & \langle w_M, L\, f_2 \rangle & \cdots & \langle w_M, L\, f_N \rangle \end{bmatrix} \tag{2.7}$$

and $[A]$ is a column matrix of the unknown constants a_n with elements of the form:

$$a_n = \begin{bmatrix} a_1 \\ a_2 \\ \vdots \\ a_N \end{bmatrix} \tag{2.8}$$

and $[G]$ is a further column matrix with elements g_m of the form:

$$g_m = \begin{bmatrix} \langle w_1, g \rangle \\ \langle w_2, g \rangle \\ \vdots \\ \langle w_M, g \rangle \end{bmatrix} \tag{2.9}$$

Equation 2.1 has now been reduced to a set of solvable simultaneous

equations. Hence for the case N=M the matrix $[L]$ is square and may be inverted using standard matrix techniques to yield the unknown $[A]$ where:

$$[A] = [L]^{-1} [G] \tag{2.10}$$

Clearly the theory outlined by equations 2.1 to 2.10 above demonstrates a general purpose method to solve any continuous equation. Clearly many factors govern how accurately the discretized form of the equation represents the continuous one. The choice of expansion functions f_n and testing functions w_m and also the number of samples taken N are vitally important. These, along with other important aspects of applying the method to electromagnetic problems, are discussed in following section.

2.2.2 Electromagnetic Problems

The starting point with any electromagnetic problem is Maxwell's Equations. Various methods of manipulation are used depending on the problem in hand to produce different desirable formulations. For the class of problem considered in this thesis, that is those of wires excited by fixed voltage generators, the most appropriate format is initially that of the Helmholtz equations, which may be solved and manipulated to yield expressions for magnetic vector potential **A** and electric scalar potential Φ. Considering any body S composed of an homogeneous material the expressions relating these two quantities to current and charge density may be defined as (Moore and Pizer 1986):

$$\mathrm{A}(r) = \mu \iint_S J(r') K(r,r') \, dS \tag{2.11}$$

$$\Phi(r) = \frac{1}{\epsilon}\iint_S \rho(r') \, K(r,r') \, dS \qquad (2.12)$$

where r and r' are two points on the surface of the body S, termed the observation point and the source point respectively, μ is the permeability, ϵ the permittivity, ρ the charge density and K the kernel or Green's function which will be defined later. Equations 2.11 and 2.12 are surface integrals because the assumption is made in this case that the material under consideration is a good conductor and hence any current flow will be on the surface. J is therefore the current density in Am^{-2}.

The class of structure that will be analyzed in this thesis is that of cylindrical wires of finite radius. A typical example of such a wire orientated along the z-axis is shown in Figure 2.1, where L is the wire length and a is the wire radius.

To analyze such a geometry requires manipulation of equations 2.11 and 2.12. If the wire is considered to be thin such that

$$a << \lambda \qquad (2.13)$$

where λ is the wavelength, then a number of assumptions may be made to reduce the complexity of the required manipulation.

Firstly, transverse current may be assumed to be negligible compared to the current flowing axially along the wire. Also any circumferential variation of the current may be ignored and the current may therefore be assumed to flow along a filament on the axis of the wire.

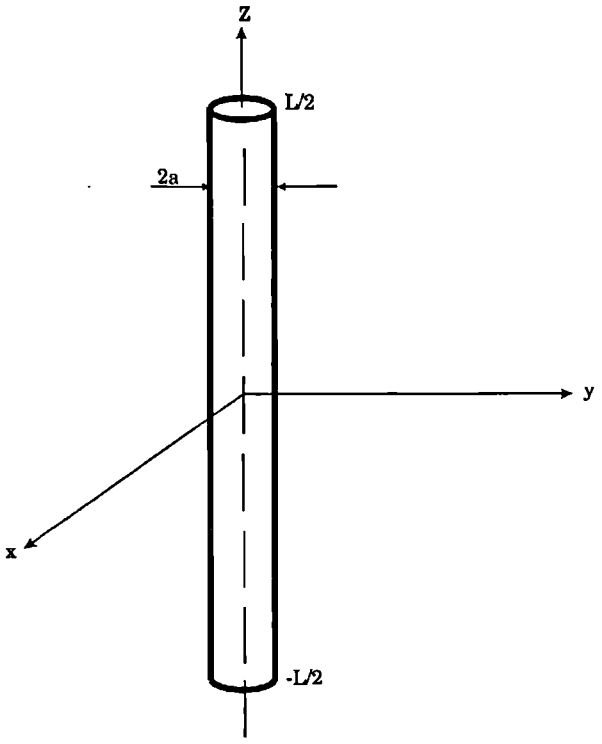

Figure 2.1 Typical vertically directed wire

Hence for the geometry shown in Figure 2.1 the current at a point z' may be defined as:

$$I(z') = J(z')\ 2\pi a \tag{2.14}$$

and so equations 2.11 and 2.12 may now be reduced to:

$$A(z) = \mu \int_{-L/2}^{L/2} I(z')\ K(z,z')\ dz' \tag{2.15}$$

$$\Phi(z) = \frac{1}{\epsilon} \int_{-L/2}^{L/2} \rho(z')\ K(z,z')\ dz' \tag{2.16}$$

where ρ is simply the charge per unit length defined as:

$$\rho(z') = -\frac{1}{j\omega} \frac{dI}{dz'} \tag{2.17}$$

and the kernel K is the free space Green's function for a point charge (Stutzman

and Thiele 1981 p12):

$$K(z,z') = \frac{e^{-j\beta R}}{4\pi R} \tag{2.18}$$

Here β is the wave number and R is the absolute distance between the source and observation points z' and z. Hence enforcing the thin wire criteria described above, the geometry shown in Figure 2.1 is reduced to the equivalent model shown in Figure 2.2 with an arbitrary source and observation point.

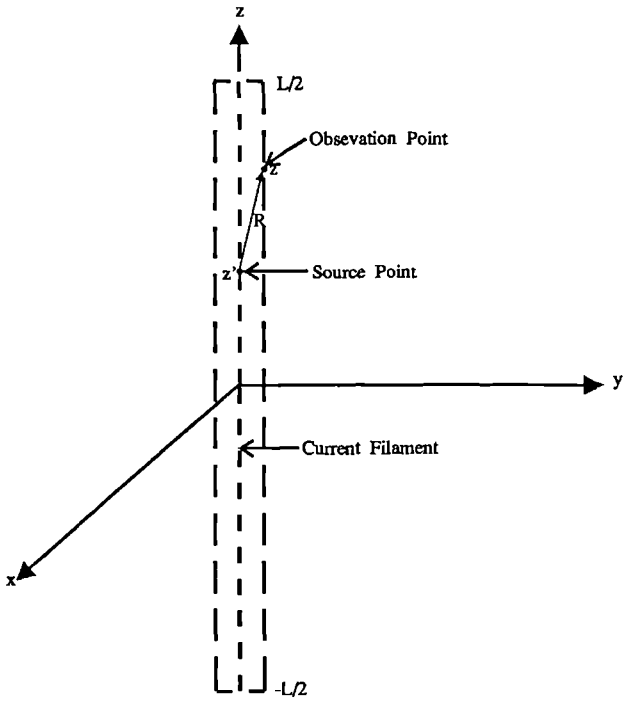

Figure 2.2 Thin wire representation of a z-directed wire

The now entirely z-directed electric field E_z, due to A and Φ, may be defined from Maxwell's equations as (Kraus 1988 p389):

$$E_z = -j\omega\mu_0 A_z - \frac{\partial\Phi}{\partial z} \tag{2.19}$$

and using the Lorentz condition (Stutzman and Thiele 1981 p10) and equation 2.16

it may be further shown that:

$$E_z = \frac{1}{j\omega\epsilon_0}\left(\frac{\partial^2 A_z}{\partial z^2} + \beta^2 A_z\right) \tag{2.20}$$

Then for an elemental section of the wire *dl* the magnetic vector potential is defined, using equation 2.11, as:

$$dA_z = \frac{I(r')K(r,r')}{4\pi}dl \tag{2.21}$$

Combining equations 2.20 and 2.21 yields the electric field due to a elemental wire section:

$$dE_z = \frac{I(z')}{j\omega 4\pi\epsilon_0}\left(\frac{\partial^2}{\partial z^2}K(z,z') + \beta^2 K(z,z')\right)dz' \tag{2.22}$$

which may be integrated over the complete wire length to give:

$$E_z = \frac{1}{j\omega 4\pi\epsilon_0}\int_{-L/2}^{L/2}\left(\frac{\partial^2}{\partial z^2}K(z,z') + \beta^2 K(z,z')\right) I(z')\, dz' \tag{2.23}$$

This equation is known as Pocklington's Electric Field Integral Equation (EFIE). Clearly this is of a form that is solvable using the Method of Moments. It is the basis of numerous Moment Method computer codes for the calculation of antenna characteristics such as the Numerical Electromagnetics Code (Burke and Poggio 1981) and its derivative MININEC (Julian *et al* 1982). Although it is only shown for a z-directed wire here, the theory is easily extended to arbitrary configurations, either in free space or above a ground plane of defined characteristics.

The Pocklington's EFIE is not a unique method of describing the relationship between current flow on a wire and electric field. Other integral formulations are available and include Hallen's integral equation (eg. Balanis 1982 p304) and those based on Rumsey's Reaction Quantity (Richmond 1974a). In addition Pocklington's Magnetic Field Integral Equation (MFIE) (Burke and Poggio 1981) may be implemented. More will be said about the choice of the specific integral equation later in this chapter. All the formulations to be considered are for bodies having good conductivity and can be expressed by an integral equation of the general type:

$$\iint_{surface} I(r') \; H(r,r') \; dS = E(r) \tag{2.24}$$

with a known excitation E on the right hand side of the integral and an unknown current I and response function H within the left hand side integral.

In order to use the Method of Moments to solve an equation of the form of 2.24 requires the geometrical configuration under consideration to be divided or segmented into a number of discrete regions or elements. The currents flowing in each section are then the expansion functions described by equation 2.2. The known excitation is of the form either of fixed voltage sources or an incident plane wave. The resultant matrix equation required to solve for the unknown currents may be considered to be similar to that describing the response of an N-port electrical network:

$$[Z] \; [I] = [V] \tag{2.25}$$

Here $[Z]$ is a square matrix of order N known as the Generalized Impedance Matrix, $[I]$ and $[V]$ are matrices of the currents and voltages associated with each

port respectively. The diagonal elements of the [Z] matrix are termed the Self Impedances of the individual ports and the off diagonal elements are termed the Mutual Impedances between the ports. Hence considering an electrical network with N ports numbered n=1,2,3,...,N, the self impedance of port 1 may be defined:

$$Z_{11} = \frac{V_1}{I_1} \qquad (I_{n\neq 1} = 0) \tag{2.26}$$

which is simply the voltage at port 1 due to a 1A current flowing into that port with all other ports open circuited. Similarly the mutual impedance between ports 1 and 2 may be defined as:

$$Z_{12} = \frac{V_1}{I_2} \qquad (I_{n\neq 2} = 0) \tag{2.27}$$

which is the voltage at port 1 due to a 1A current flowing into port 2 with all other ports open circuited.

The above definitions may be extended to cover a complete network and hence define the Generalized Impedance Matrix associated with it. Applying this representation to an antenna problem is straightforward as the Method of Moments reduces the continuous problem to that of a number of fixed sampling points. The electromagnetic interaction of each defined point with every other point is approximated by the matrix [L] of equation 2.6. It has units of impedance or impedance per unit length or area and is easily comparable to that of the network problem.

Using this notation the Generalised Admittance Matrix associated with a

geometry defined:

$$[Y] = [Z]^{-1} \tag{2.28}$$

may be determined to solve for the unknown currents due to a defined excitation.

2.2.3 Computation Considerations

As stated at the end of section 2.2.1 many factors affect the results obtained when using a Method of Moments technique to solve an integral equation. Miller (1989) describes three desirable attributes of any such Moment Method computer model as accuracy, efficiency and utility. Accuracy is the degree to which the model conforms to the real physical situation. This is affected initially by the choice of integral equation and then also by the choice of expansion functions and weighting functions used in the discretization process. Efficiency describes the relative cost of obtaining the computed results, in terms of human and computer resources used. This may again be affected by the choice of the specific integral equation. A certain representation may produce highly accurate results but require a restrictive amount of computer CPU time, for example. Expansion and testing functions, if complex, may also inhibit the solution speed. Utility simply describes the applicability of the model to a range of problems. It may also include the type of hardware that a computer code requires for successful operation.

Considering accuracy firstly, numerous Method of Moment computer codes use different integral representations and choices of expansion and testing

functions. Some of the most widely used codes are detailed and referenced in Table 2.1.

Table 2.1 Comparison of Various Moment Method Codes

CODE	INTEGRAL	ANALYSIS STRUCTURE	BASIS FUNCTION	TEST FUNCTION
NEC (Burke and Poggio 1981)	Pocklington (EFIE) Pocklington (MFIE)	Thin Wires Surface Patches	Constant+ Sine+ Cosine	delta
MININEC3 (Logan and Rockway 1988)	Pocklington (EFIE)	Thin Wires	Pulse	Pulse
Richmond (Richmond 1974a,b)	Rumsey's Reaction (EFIE)	Thin Wires	Sine	Sine
WIRES (Kuo *et al* 1972)	Pocklington (EFIE)	Thin Wires	Triangle	Triangle
AWAS (Djordjevic *et al* 1990)	Pocklington (EFIE)	Thin Wires	Polynomial	Pulse

It is noticeable that a wide range of dissimilar expansion functions have been employed in the codes listed. Miller (1989) and Balanis (1982 p308) recommend that an important aspect in the choice of expansion functions is their ability to accurately resemble and approximate the anticipated form of the unknown current distribution. It is noticeable that both the NEC and AWAS codes use relatively complex functions. NEC uses a three term representation of the

current and AWAS code uses a so called "nearly entire domain" (Djordjevic *et al* 1990) polynomial expansion, the order of which may be defined by the user. The use of such relatively complex expansion functions does not however invalidate the use of the simpler examples shown in Table 2.1. Miller (1983) shows that accuracy of the results obtained using a three term expansion and those obtained using a triangular pulse representation are comparable, but that the convergence of the former with the number of samples or segments used is faster. The simpler functions shown may hence accurately approximate the current, but more samples need to be taken. The implication of this result therefore is that the method and procedure used to divide an antenna geometry into a number of sections is more critical when using a Moment Method code that uses relatively simple expansion functions.

Considering the choice of testing function, two basic approaches may be defined. The first method is termed Point Matching and involves the use of a delta function at the centre of the point where the expansion function is applied. Hence the integral equation is solved exactly at the defined points and it is assumed that the boundary conditions are not substantially violated between points. The second method is to use another function that is defined across the complete sampling interval, as is the case with the expansion function. In this case the integral equation is not satisfied exactly at any point but a Weighted Residual of the boundary condition is defined and minimized in a least mean squared sense across the interval as is demonstrated by Stutzman and Thiele (1981). This is the main advantage of this method over that of Point Matching,

because with Point Matching the boundary conditions may be violated to an unsatisfactory level between individual sampling points. For the case where the same expansion and testing functions are employed, it is known as a Galerkin implementation of the Method of Moments (Harrington 1968 p7). A considerable benefit of using a Galerkin approach is detailed by Moore and Pizer (1986), who show that using the same expansion and testing functions ensures that the reciprocity condition between segments is enforced. Hence the individual elements of the generalized impedance matrix [Z] conform to the relationship:

$$Z_{nm} = Z_{mn} \tag{2.29}$$

where the mutual impedance between two elements is the same, enforcing the physical analogy to electrical networks described by equations 2.25 to 2.28. The generalized impedance matrix is therefore symmetric which is a further advantage, as only half of it needs to be calculated. This property reduces both the storage requirements of the computer system and also decreases execution time. The theory of Characteristic Modes, which will be discussed in Chapter 3, relies, for their calculation, on the generalised impedance matrix being symmetrical. It was therefore vitally important to use a Galerkin procedure to generate the impedance matrix for the work described in this thesis. Hence a modified version of the MININEC3 code was chosen as the basis for the majority of the computational work in this thesis. A full description of the code and the reasons for choosing it are presented in section 2.3 below.

2.3 The MININEC Antenna Analysis Computer Code

2.3.1 Code Evolution

The Mini-Electromagnetics Code (MININEC) was initially developed by Julian *et al* (1982) as a Method of Moments code for the analysis of simple, relatively small (in terms of wavelengths), antenna structures. The original purpose of the code was to provide a tool for the rapid analysis of such simple antennas on small micro or desktop computers. It allowed the computation of a number of the basic characteristics such as current distribution and far field pattern that were also calculated by the larger mainframe based Numerical Electromagnetics Code (NEC) developed by Burke and Poggio (1981).

There were many limitations to the initial version of MININEC. The antenna being analyzed could only be situated in free space or over a perfect ground plane. Point reactive loading was available, although this was not allowed for wire segments intersecting the perfectly conducting ground plane. Also any wire that did intersect the ground plane had to do so at an angle of 90°. Also the computer technology of the time introduced further constraints. Computer memory and the available BASIC compilers limited the size of analyzable geometries to around 30 segments. This meant that the maximum size of antenna that could be handled confidently was of the order of 1 wavelength.

A second version of the code was developed by Li *et al* (1983) which addressed some of the ground plane constraints listed above. The next major step in the progression of the code however was the development of MININEC3 by Logan and Rockway (1986), together with the rapid development of computer

technology. Although the code was still written in the BASIC language, compilers were available that could address up to 64k of memory, enabling antenna structures of up to 125 segments or of the order of 8 wavelengths to be analyzed. The relative increase in desktop computer speed also made the analysis of such structures feasible within a reasonable period of time.

This third version of MININEC also included many more of the features that are available with the mainframe NEC code. As with the previous codes, current distribution and hence input impedance, along with far field patterns could be calculated. The feature of point loading the antenna was improved to include the ability to add either fixed or frequency dependant s-domain loading. The antenna could now be situated in either free space or over a perfect or finite conducting ground plane. This feature used the Fresnel reflection coefficient to allow five changes in ground impedance using either circular or linear boundaries. Near fields were also calculated by the code, if required.

Other variants of the MININEC code have been developed that have improved the interface with the user and also presented improved routines for the display of calculated data. Such codes are detailed by Lewallen (1991) and include The MININEC System Logan (1988), MN4 Beezley (1992) and ELNEC Lewallen (1991). These codes although not improving the capabilities of the basic algorithm or speed present an attractive "user friendly" interface and rapid methods of displaying calculated data graphically.

The algorithms used in the MININEC3 code and its variants provide a reliable, stable method for the calculation of generalized antenna

characteristics. There is no theoretical limit to the size of geometry that can be analyzed using these algorithms, although it is limited by two external factors. Firstly, as discussed above, the size of core memory that a BASIC compiler can address limits the physical size of the problem. Secondly, the speed of operation of the computer on which the software is mounted places a further practical constraint on the time available.

The first of these constraints was addressed with the implementation of a version of MININEC3 in FORTRAN as described by Miller (1989). The FORTRAN programming language overcomes all the inherent constraints of BASIC compilers. There is no theoretical limit to the size of memory that can be addressed and the greater efficiency of the language for numerical calculations improves execution time. Also the code may be used with a wider range of computers including mainframes.

2.3.2 MININEC - Version 3

This section discusses in more detail the features of the MININEC3 code. The code uses a Galerkin formulation of the Method of Moments (Harrington 1968), using pulses for expansion and testing functions as shown in Table 2.1. The MININEC3 algorithm obtains a numerical solution to a generalized form of the Pocklington Electric Field Integral Equation (EFIE) shown for a z-directed wire in equation 2.23. The thin wire conditions described in section 2.2.2 are assumed and geometries are specified in terms of straight wires, defining the coordinates of the two endpoints and also a fixed radius. Each wire is divided into a number

of user defined segments. Figure 2.3a shows two arbitrary orientated segmented wires which illustrate these points. The pulse expansion functions are defined for the geometry between the midpoints of each adjacent segment as shown in figure 2.3b. Notice that at the free ends of the wire a half pulse of zero amplitude is defined to enforce the boundary condition of zero current at the wire end. Notice also that an overlapping pulse scheme is employed at wire junctions. For wire junctions of more than two wires, multiple overlapping pulses will reside at the junction endpoints. In this case Kirchoff's current law is enforced in order to calculate the resultant current for the end of each wire. Figure 2.3c shows how a possible resultant current distribution on the two wires due to an arbitrary voltage source may be resolved.

Lumped impedance loading at the centre of any current pulse may be specified with MININEC3. The loads are specified as either a fixed resistance and reactance or as an s-domain frequency dependant polynomial. As added lumped loads do not affect the mutual impedance between elements, only the diagonal self impedance term of the relevant pulse is modified. Hence, for a geometry loaded with a lumped load Z_l at pulse n the diagonal generalized impedance matrix element Z_{nn} will be modified to Z'_{nn} such that:

$$Z'_{nn} = Z_{nn} + Z_l \tag{2.30}$$

If we consider a structure situated over an infinite, perfectly conducting ground plane, image theory allows the geometry to be replaced by the original structure plus its image below the ground plane. Hence the generalized impedance matrix of this modified structure is twice its original size. Because

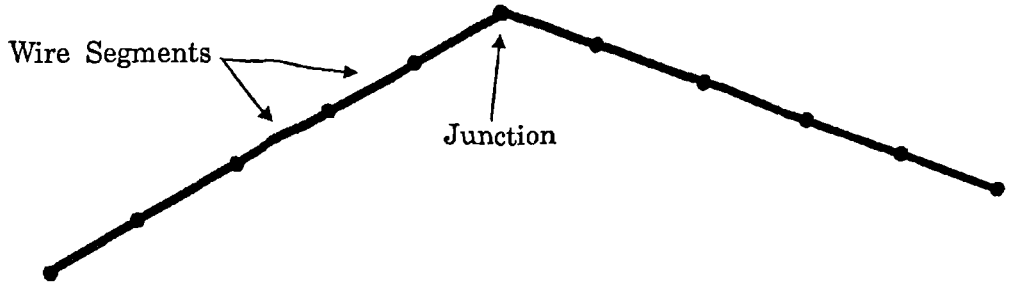

(a) Segmented wires

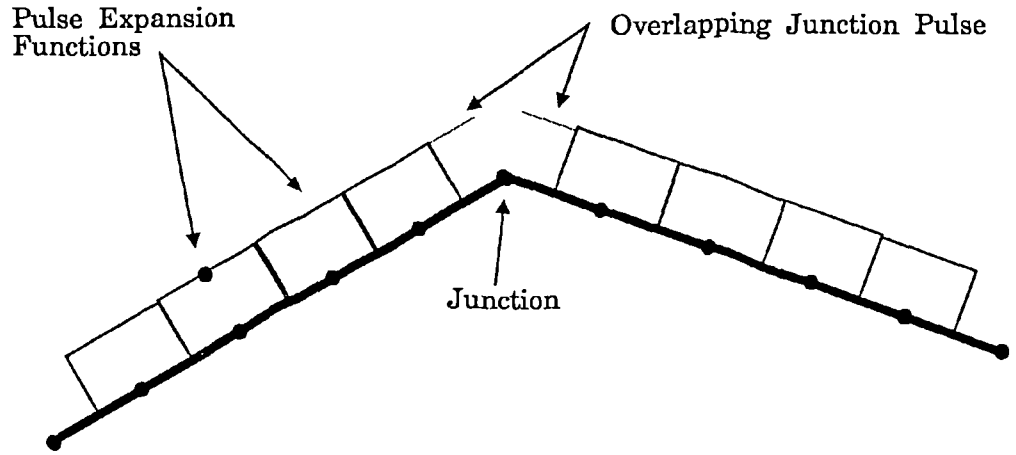

(b) Pulse Expansion Functions Applied

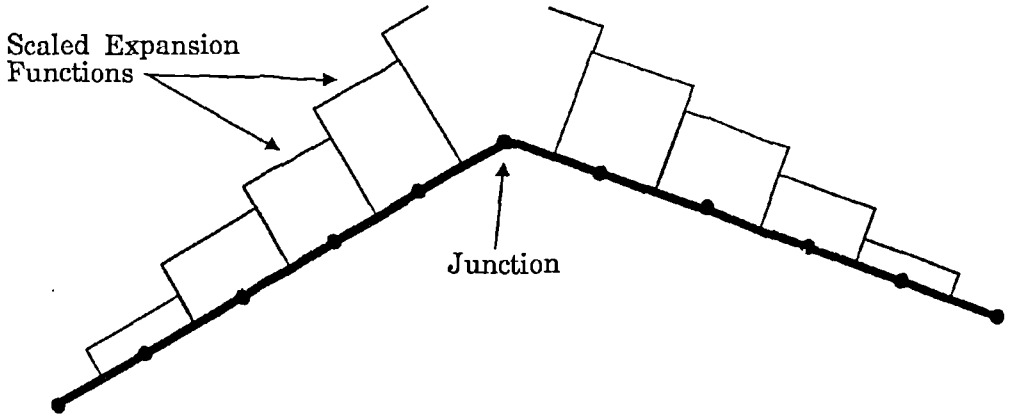

(c) Possible Resultant Current Distribution

Figure 2.3 MININEC3 geometry segmentation scheme

of symmetry this matrix will contain redundant, repeated information. Therefore MININEC3 uses a method of compression, described by Stutzman and Thiele (1981, p343), which allows the matrix to remain the same size as that of the original geometry in free space. Hence, for a structure and image of N current pulses, the elements of the modified impedance matrix Z'_{mn} are:

$$Z'_{mn} = Z_{mn}+Z_{mn+N/2} \qquad \begin{matrix} n=1,2,...,N/2 \\ m=1,2,...,N/2 \end{matrix} \qquad (2.31)$$

The time taken to invert the generalized impedance matrix of a geometry situated over a perfect ground plane will therefore be the same as that for the geometry in free space.

Upon solving the initial matrix equation to obtain the current distribution associated with a particular source configuration, both near-fields and far-fields may be calculated by the MININEC3 code. This is achieved by considering the effect due to each individual current pulse, and then summing the results to find the total. For far fields the theta and phi components are calculated in either absolute values in Vm^{-1} for a defined fixed distance or relative power gain in dBi. The resultant far fields may also be modified to take into account real lossy ground conditions. This is achieved using the Fresnel Reflection Coefficient, which takes into account the existence of both a direct and reflected component of the resultant far field. It should be noted that as with the NEC code, on which this feature is based, the real ground condition in no way affects the initial calculation of current distribution. When a real ground is specified the initial calculation assumes that the antenna is situated over perfect ground in

calculating the unknown currents. Only the resultant far-fields from this calculation are then modified. Care therefore needs to be taken when assessing the results obtained using this feature.

Overall the MININEC3 algorithm was chosen as the basis of the Characteristic Mode calculation routine for a number of beneficial reasons. Firstly as stated previously, the algorithm uses a Galerkin procedure which yields a symmetrical generalized impedance matrix. Reciprocity of the mutual impedance elements is therefore maintained which is required for Characteristic Mode calculation. Secondly the code is relatively compact compared to other codes, which implies that modification may be carried out in a straightforward, rapid manner. Lastly there is great similarity in the methodology used to specify antenna geometries with MININEC3 and that used with the NEC code. This allows the wide range of pre- and post-processors available for use with the NEC code to be utilised for MININEC3 analysis with minimal modification. These include NECPLOT (Burke and Poggio 1981), a routine for the display of antenna geometries and resultant current distributions. Also various routines available with the NEEDS system (1988) may be employed including IGUANA (1987), a graphical geometry generation program and GRAPS (Laird 1985), a general purpose plotting routine for the display of output data.

2.4 Antenna Modelling Guidelines

2.4.1 Antenna Geometry Definition

Before the modification of MININEC code from BASIC to FORTRAN, its use has been limited to relatively small geometries. In addition little validation material is available in the literature, compared to other codes such as NEC.

Amongst the data that are available is that in the initial publication document (Logan and Rockway 1986). Here the convergence of the input impedance with segmentation and the overall accuracy of results is tested for simple antenna configurations. The input impedance of three centre fed dipoles: a short dipole where the length is much less than half of a wavelength, a halfwave dipole close to resonance and a one wavelength anti-resonant dipole, is calculated as the segmentation density is increased. The accuracy is examined by comparison with the widely accepted theoretical analytical results due to King and Harrison (1969 p727).

Both the short and the halfwave dipoles show excellent convergence, whereas the anti resonant case does not. The half wave dipole shows the best convergent behaviour. Both the conductance and susceptance component percentage error compared to King and Harrison varies at a rate less than 0.2% per further added segment, for segmentation schemes where over 20 segments per wavelength of wire are employed. A similar rate of convergence is obtained for the short dipole for segmentation schemes when over 36 segments per wavelength are used. Considering the accuracy of these converged results of both

cases, both input conductance and susceptance are within 6% of the results due to King and Harrison.

Regarding the one wavelength anti-resonant dipole, Logan gives no explanation for the lack of convergence of the result, but suggests that this case is problematic when considered using other Method of Moment codes such as NEC. Examining the results that he presents however it is noticeable that despite the apparent lack of convergence the input conductance and susceptance components are never more than 5% in error compared to King and Harrison. This is for segmentation schemes ranging from 6 segments per wavelength up to over 40 segments per wavelength. The most accurate result for both components is obtained when using approximately 20 segments per wavelength.

It can be concluded from these results that as a "rule of thumb", around 20 segments per wavelength of wire are needed to obtain an acceptable degree of accuracy for straight dipoles. It should be noted that these figures are appropriate for vertical monopoles over perfect ground, due to the use of the method of images. Clearly in using this segmentation figure as a general "rule of thumb" for arbitrary geometries, convergence of the results should always be tested.

Logan and Rockway (1986) also investigated the MININEC3 results obtained for circular loops and closely spaced parallel wires. The circular loops were approximated by polygons and the convergence characteristic, as the order of the polygon was increased, was determined. In considering two parallel wires, accurate results for the mutual impedance between the wires were obtained

down to the closest spacing considered by King (1971) of a tenth of a wavelength. For MININEC3 results below this spacing no comparison to other data was made, but the output data continues to vary smoothly in a manner expected by the geometrical configuration.

2.4.2 Wire Grid Modelling

When using a Method of Moments computer code to model a continuous surface one of two basic approaches is usually adopted. The first is to use a code that employs a Magnetic Field Integral Equation (MFIE), which is the most suitable formulation for modelling such surfaces. NEC employs such a facility as shown in Table 2.1, but the modelling restrictions enforced inhibit the usefulness of the approach. When using the MFIE formulation all surfaces must be closed. This clearly limits the class of structure that may be analyzed. Apertures will exist on most practical continuous structures such as ships, aircraft and land vehicles. The most versatile and therefore most widely adopted method of analyzing continuous structures is that of wire grid modelling (Richmond 1966). Here the EFIE formulation is employed and a continuous surface is approximated by a wire mesh of appropriate dimensions. As all the Method of Moment codes shown in table 2.1 utilize an EFIE they may all be used to model continuous surfaces using this method. When using a wire grid model, the accuracy with which the resultant current distribution obtained approximates the actual current flow on the continuous surface is clearly controlled by the configuration and composition of the defining grid. The methodology used to construct the grid is

therefore of vital importance. Factors that need to be considered include the shape of the individual cells of the mesh, the size or resolution of the cells and the size of the radii of the wires of the cells.

Considering firstly the type of wire grid, the most commonly used configuration is of grids consisting of rectangular or quadrilateral calls. This type of configuration, which is relatively simple to implement, has been used with great success by many authors. A criticism of this approach however is its relative inability to accurately simulate the true current path because of the perpendicular nature of the grid elements. Hence other formulations have been introduced to overcome this problem. Moore and Pizer (1986 p107) prefer the use of triangular mesh cells. This introduces a diagonal current component to the perpendicular components of a rectangular mesh. Ferguson and Balestri (1988) also recognise the problem and investigate the use of polygonal cells, although no concluding recommendations were made regarding which configuration is best. Overall though it is apparent from the literature that rectangular or quadrilateral grid cells are adequate, provided that the other wire grid modelling design criteria, grid size and wire radius, are chosen with care.

As the size of the grid used affects the number of unknowns to be determined and therefore the computer time necessary for solution, various authors have investigated the maximum allowable size of the grid apertures. Two basic methods exist which consider either the total area of an individual cell or the spacing between adjacent elements of a grid. Moore and Pizer (1986 p107) recommend an empirically determined result of a maximum cell area of $0.02\lambda^2$

to $0.03\lambda^2$. For a square cell this would correspond to a maximum grid spacing of approximately $\lambda/7$ to $\lambda/6$. Ludwig (1987) considers a standard canonical problem and concludes that a grid spacing of $\lambda/5$ generally produces acceptable accuracy. Lin and Richmond (1975) used wire grid modelling to determine the radar cross section (RCS) of various military aircraft. For this application it was concluded that a grid spacing of $\lambda/4$ provides accurate results. Poggio and Miller (1973) state another grid spacing "rule of thumb" maximum as $\lambda/10$ to $\lambda/20$. As the other references specify a larger grid spacing, this rule has been widely adopted as a general starting point for initial models. It has been the experience of other modellers however that denser meshes need sometimes to be used in critical regions of structures where relatively large current will flow such as the feed-point. Cox (1991) found it necessary to use a grid spacing of $\lambda/500$ at the feed-point to obtain accurate results for input impedance of HF antennas mounted on aircraft. Similarly Kubina (1991) decreased the grid spacing from an initial value of $\lambda/10$ to yield accurate results for input impedance for his aircraft models. Clearly then when selecting grid spacing the general $\lambda/10$ "rule of thumb" is a sensible starting point. The experience of others though (eg. Austin and Najm 1991) stresses the importance of trying to refine and change the resultant model after initial calculation by comparison with experimental results.

Upon deciding the size and shape of the wire grid representation it is then necessary to choose a radius for the individual wires of the mesh. Two methods have been adopted by various authors. The first is to choose a radius that is simply a defined fraction of a wavelength or a fraction of the grid size.

Nishikawa (1984) used wire grids to model motor vehicles and set the radius of the model's wires empirically at $\lambda/200$. No reason was given for the choice. Similarly Richmond (1975) chose a wire radius of $w/25$, where w was the spacing between adjacent elements.

The second preferable method, which has been more widely adopted, is to relate the radius of the grid wires to the surface area of the structure being modelled. This is achieved by comparing the surface area of the wires to that of the continuous surface. Consider a continuous surface where A_S is the surface area. If the structure is approximated by a wire grid model then A_W is the total surface area of the grid wires. Both Oyekanmi and Watkins (1989) and Najm (1991) have reviewed the various recommended wire radius criteria of different authors. Table 2.2 lists these and those due to other authors for a rectangular mesh by stating the recommended relationship between A_S and A_W, from which a value for wire radius may be calculated.

Clearly the predominant recommendation is the so called "twice surface area" rule. This is referred to by some authors as the "equal surface area" rule. This description is used when considering wire grids excited by plane waves. Then the area is that which is parallel and therefore visible to one polarization. For the work considered in this thesis it was thought more meaningful to consider the actual surface area of the structure and use the first description to describe the relationship with wire radius. It is also useful to look at the type of structure analyzed by the authors shown in table 2.2 in arriving at their recommendations.

Table 2.2 Wire Radius Modelling Criteria

Author	Surface Area Criteria
Moore and Pizer (1986)	$A_w = A_S$ to $5A_S$
Lee *et al* (1976)	$A_w \approx 2A_S$
Ludwig (1987)	$A_w = 2A_S$
Elliot and McBride (1990)	$A_w = 2A_S$ (open surface) $A_w = 4A_S$ (closed surface)
Burke and Poggio. (1981)	$A_w = 2A_S$
Paknys (1991)	$A_w = 2A_S$

The results of both Ludwig (1987) and Paknys (1991) are for a canonical problem of an infinitely long cylinder. Their analytical methods shows that for this geometry the "twice surface area" rule is optimum. The error is increased if the so called area factor is either increased or decreased. Lee *et al* (1976) consider a perfectly conducting sphere. An approximate expression for the excess, erroneous inductance of the wire grid representation is defined. This expression is minimized when the "twice surface area" rule is invoked. The wire radius recommendations of Elliot and McBride (1990) for both closed and open surfaces were an interpretation of the Lee *et al* (1976) results. Here rectangular surface patches were analyzed using wire grid modelling.

It is clear that the majority of the results shown in table 2.2 are for uncomplicated, regular geometries. The exception to this is those of Moore and Pizer (1986). Their recommendations stem from the analysis using wire grid modelling of a wide range of complex structures such as aircraft and land based motor vehicles. Although their guidelines are empirically determined the antenna

structures considered are the most practically-based. In choosing wire radius for wire grid models therefore, it is clear that the conclusions from both the analytically and empirically determined guidelines must be considered. Overall though an initial surface area criterion of twice the actual surface area is the most widely recommended option.

2.5 Summary

As the Method of Moments is the basis of the work considered in this thesis, this chapter has reviewed the underlying theory, especially as applied to complex radiating antenna systems.

The basis and initial formulation of the theory were reviewed in section 2.2, particularly as applied to electromagnetic problems. The importance of the integral representation and the expansion and testing functions used have also been investigated. Section 2.2 also studied a number of the most widely available Moment Method computer codes, in order to determine the most suitable for the Characteristic Mode research. The final choice of code was made after full consideration of the features and characteristics of various widely available software implementations. One of the most important considerations was the fact that much of the future analysis required that a Galerkin implementation of the Method of Moments be used. This excluded one of the most commonly used computer codes (NEC). The less commonly used code (MININEC) exhibited the most desirable features of the available Galerkin based codes and is similar to NEC in many of its data input and output routines and was therefore chosen

for this task. Clearly though not as much validation data is available in the open literature for MININEC as there is for NEC, although section 2.3 reviewed what is available. Also the results of further validation exercises are shown in chapter 5.

Section 2.4 has described some of the most important modelling guidelines that are necessary to achieve the most accurate results. These include both analytically obtained guidelines and practically inferred so called "rules of thumb" that stem from others' modelling experiences. The important method of wire grid modelling which allows the simulation of continuous surfaces was also described.

CHAPTER 3

THE CONCEPT AND THEORY OF CHARACTERISTIC MODES

3.1 Introduction

In simple terms the method of Characteristic Modal analysis is a mathematical technique which suggests that any radiating structure has associated with it a particular infinite set of currents and corresponding fields. This set of basis functions or modes are independent of the excitation and exhibit various orthogonality conditions. Such properties are shown to be beneficial for the analysis of such radiating structures because the properties of the individual modes may be examined separately. Also the prospect of optimizing individual modes to obtain certain desirable characteristics is considerable. This chapter therefore discusses and reviews the underlying theoretical background of Characteristic Modes and also examines their application to practical antenna and scatterer problems.

Firstly section 3.2 examines the initial development of the theory from first principles. The contributions of both Garbacz and Turpin (1968, 1971) and Harrington and Mautz (1971a, 1975) are examined. The approach taken by Garbacz is of limited practical application because no general purpose method of modal calculation was shown. It does however clearly demonstrate the theoretical fundamentals and their relationship to classic electromagnetic

theory.

In the literature the contribution of Harrington and Mautz represents the most important contribution to the theory of Characteristic Modes in terms of its application to practical problems. This is because the theoretical representation is expressed in a form which is solvable using the Method of Moments discussed in chapter 2. This leads to generalized Characteristic Mode calculation algorithms for arbitrary structures.

With the initial underlying Characteristic Mode theory defined in section 3.2, section 3.3 goes on to examine the properties of the Characteristic Modes of radiating structures. Various useful orthogonality conditions that exist between the members of each Characteristic Mode set are examined. Methods of exploiting these conditions for analysis are explored. The examination shows how Characteristic Modes allow greater insight into the radiation properties of antenna geometries than other purely numerical methods provide.

In certain practical situations the Characteristic Modes of a complete radiating structure may be of little interest. For example a complex radiating structure may have a number of fixed point, at which either loads or sources may be placed. In these constrained circumstances information about the full modal composition of the structure is of limited use. Section 3.3 therefore addresses this situation by discussing how the Characteristic Modes of an N-port system may be calculated. The properties of such modes, which are similar to those of complete radiating systems, are examined.

Finally alternative Characteristic Mode formulations to those discussed

in the earlier sections are examined in section 3.4. These overcome some of the constraints imposed by the other earlier formulations. The various methods are compared and recommendations are made regarding appropriate formulations for different types of problems.

3.2 Theoretical Concepts

3.2.1 Generalized Scatterers

The theoretical basis of Characteristic Modes was presented by Garbacz and Turpin (1968, 1971). He used the fact that any conducting or dielectric object may be considered as a device which transforms a convergent wave incident on it into a scattered divergent wave, using the so called Scattering Operator S (eg. Newton 1966) to describe the interaction. Consider a wave function E_i incident upon a scatterer, the Scattering Operator S is that which operates upon E_i producing E_o :

$$E_o = SE_i \tag{3.1}$$

It follows that in the absence of an obstacle the incident field is undisturbed and represented by :

$$E_o = IE_i \tag{3.2}$$

where I is defined as the Identity Operator or the Scattering Operator of unbounded free space.

It then follows from equations 3.1 and 3.2 that the difference between an outgoing wave function with an obstacle at the origin and that without an

obstacle at the origin may be defined :

$$\Delta E_o = (S-I)E_i \tag{3.3}$$

This could be defined as the perturbation although Garbacz and Turpin introduced a factor of one half for ease of later manipulation by defining a perturbation operator as:

$$P=\frac{1}{2}(S-I) \tag{3.4}$$

Hence this operator gives a measure of how much an ingoing function will be displaced by the presence of an obstacle. Therefore a so called scattered wave function E_s may be defined (Garbacz 1968) such that:

$$E_s = \Delta E_o/2 \tag{3.5}$$

and hence:

$$E_s = PE_i \tag{3.6}$$

Hence the concept of operators provides a useful mathematical description of the actual physical situation. Garbacz and Turpin (1968, 1971) demonstrated that both S and P are completely continuous, symmetric operators. These properties were then used to produce the basis of the theory of Characteristic Modes. The principle of the theory is the expression of the incident and outgoing field functions in terms of a infinite orthogonal set of spherical vector wave functions or multipoles $\{E_n\}$, considered as a convenient basis set. Hence using a fixed coordinate system the incoming fields are the complex conjugate of the outgoing and therefore E_i, E_o and E_s may be defined

as (Harrington and Mautz 1971a, 1975):

$$E_i = \sum_{n=1}^{\infty} a_n E_n^* \tag{3.7}$$

$$E_o = \sum_{n=1}^{\infty} b_n E_n \tag{3.8}$$

$$E_s = \sum_{n=1}^{\infty} c_n E_n \tag{3.9}$$

where a_n, b_n and c_n are complex numbers and * denotes complex conjugate. Hence using this formulation the continuous $\boldsymbol{S}$ and $\boldsymbol{P}$ operators are reduced to the so called scattering and perturbation matrices $[S]$ and $[P]$ respectively. These matrices represent the transformation of all incoming multipoles into their respective outgoing multipoles, describing the transformations shown by equations 3.1 and 3.6. Clearly these matrices will be infinite in extent which follows from the infinite nature of the original operators. Also the orthogonal mode representation infers that the matrices will be diagonal.

Garbacz and Turpin (1968, 1971) showed that although these matrices are infinite in extent they may be reduced and approximated by finite dimensional matrices. This is possible because in practice only a finite number of the diagonal elements of the scattering matrix differ from unity by a significant amount. Hence using equation 3.4 the perturbation matrix will have diagonal elements, only a finite number of which will differ from zero. Hence this implies that only a finite number of the set of fields E_n are significant and the effect of the rest

is negligible. Hence the following relationships may be stated:

$$[B] = [S][A] \tag{3.10}$$

$$[C] = [P][A] \tag{3.11}$$

where $[A]$, $[B]$ and $[C]$ are N-dimensional column matrices containing the significant scaling factors of equations 3.7 to 3.9, where N is the number of significant fields.

Garbacz and Turpin (1968, 1971) therefore defined a set of so called Characteristic Modes for any radiating structure. It is clear that these modes will be unique to a particular geometry configuration at a fixed frequency of operation. Clearly these modal fields, when used individually to excite a structure, are transformed into their complex conjugates and further shifted in phase by a fixed amount. Hence an equiphase current and associated equiphase impressed electric field or voltage must be associated with each modal field. The extent of the phase shift is an indication of the relative significance of each mode.

Garbacz and Turpin (1968, 1971) showed, using the passive nature of the scattering system and the scaling introduced in equation 3.4, that the diagonal elements of the perturbation matrix p_{nn} would lie on the circumference of a unit half circle of centre (-1/2,j0) in the real-imaginary plane. Further the diagonal elements of the scattering matrix s_{nn} would lie on the circumference of a unit circle centred at the origin (0,j0) of the real-imaginary plane. A bilinear transform may also be employed to relate both p_{nn} and s_{nn} to a additional real

quantity λ_n ($-\infty<\lambda_n<+\infty$) associated with each mode. Hence:

$$p_{nn} = \frac{-1}{1+j\lambda_n} \tag{3.12}$$

$$s_{nn} = \frac{1+j\lambda_n}{1-j\lambda_n} \tag{3.13}$$

This was carried out predominantly for ease of plotting on the Smith Chart. It does however easily allow the phase angle by which each mode is shifted when incident on the geometrical configuration to be defined. Hence a so called characteristic angle ψ_n (Garbacz and Turpin 1968, 1971) associated with each mode, is defined where:

$$\psi_n^\circ = 180^\circ - \tan^{-1}(\lambda_n) \tag{3.14}$$

which lies in the range $90^\circ<\psi_n<270^\circ$. The factor of 180° accounts for the fact that the complex conjugate is used in the original definition of the basis functions in equation 3.7. Hence a characteristic angle of 180° represents the case when a structure most effectively radiates or scatters a mode which suggests a resonant current with zero stored energy. Characteristic angles of 90° and 270° therefore correspond to when a mode is least effective at radiating or scattering. The phase angle between the imposed current and associated voltage is 90° so all energy is stored. Clearly $\psi_n=90^\circ$ implies inductively stored energy whereas $\psi_n=270^\circ$ defines the capacitive case.

The preceding section has shown how it is possible to define a particular set of orthogonal Characteristic Modes associated with any structure. Each mode is of the form of a Characteristic Field E_n and corresponding equiphase current

I_n which exists upon the structures surface. A number of defined variables p_{nn}, s_{nn}, λ_n and ψ_n allow the significance of each mode to be assessed and compared to others. A limitation of the theory defined up to this point is the difficulty associated with the actual calculation of the modes. Garbacz and Turpin (1968, 1971) were only able to calculate the Characteristic Modes of a number of simple structures such as a sphere and a square loop, where the modal structure was merely an extension of the resonant fields and currents associated with it. Similar analysis was carried out by Turpin (1969). The next section shows how Harrington and Mautz (1971a, 1975) developed an alternative formulation of Characteristic Modes by using a procedure which may be solved by the Method of Moments. The significance of the defined real constant λ_n will also become apparent.

3.2.2 Generalized Radiating Structures

In the previous section it was shown that a set of Characteristic Modes could be defined for any radiating structure. These modes are specific to a defined geometrical configuration at a fixed frequency and are independent of any particular excitation. An alternative formulation of Characteristic Modes was developed by Harrington and Mautz (1971a, 1975). They defined a similar modal set to those specified by Garbacz and Turpin (1968, 1971) shown in the previous section, but developed the theory from a different starting point. This section will describe the development of this theory and also discuss why it is preferable to that shown in the previous section.

Equation 2.1 shows a general homogeneous equation. Now considering any conducting surface S, an operator equation of this general type relating the impressed electric field E to a current I flowing on it may be defined as:

$$ZI = E \tag{3.15}$$

Z is a linear operator and is the so called impedance operator of the structure. This is the basic equation which may be solved using the Method of Moments as outlined in Chapter 2 with Z defined from Maxwell's equations as a combination of magnetic vector and electric scalar fields A and Φ as shown by equations 2.11 and 2.12.

For general antenna or scattering problems the Method of Moments allows the discretization of the Z operator to form a matrix equation as shown by equation 2.25. Solution of the problem is achieved by factorization or inversion of the matrix to form the generalized admittance matrix and hence the resultant current due to an applied source. The method of Characteristic Modes developed by Harrington and Mautz (1971a, 1975) takes a different approach involving the determination of the eigenvalues and associated eigenvectors of an appropriate operator equation. Various orthogonality relationships that exist between the elements of the defined modal set, comparable to those outlined for the modes defined by Garbacz and Turpin (1968, 1971) in the previous section, demonstrate that this method has many benefits compared to the standard Moment Method technique.

Initially it is necessary to define a number of properties of the Impedance operator which make the analysis possible. The reciprocity theorem suggests that

Z is a complex, symmetric, non-Hermitian operator. This is discussed for the Galerkin-derived, discretized matrix form of the Impedance operator $[Z]$ (the Generalized Impedance matrix) in Chapter 2, equation 2.29. Also two real, symmetrical operators R and X are derivable from the Z operator (Harrington and Mautz 1971a, 1975) such that:

$$Z = R+jX \tag{3.16}$$

These correspond to the real and imaginary components of generalized impedance matrix $[Z]$ such that:

$$[Z] = [R]+j[X] \tag{3.17}$$

By definition the R operator is positive definite which implies that any current which flows on the surface S will radiate some power.

Using the above stated properties of the impedance operator Harrington and Mautz (1971a, 1975) showed how it is possible to define a set of Characteristic Modes. Initially the following weighted eigenvalue equation may be set up:

$$ZI_n = v_n RI_n \tag{3.18}$$

where v_n are the complex eigenvalues of the system and I_n are the eigenvectors or so called Characteristic Mode currents, comparable to those defined by Garbacz and Turpin (1968, 1971) in the previous section. R in this equation is employed as a weight function. The purpose of this is that it ensures that various orthogonality relationships which will be discussed later, exist between mode currents.

Next defining:

$$v_n = 1 + j\lambda_n \tag{3.19}$$

and substituting into equation 3.18 yields:

$$XI_n = \lambda_n RI_n \tag{3.20}$$

which is the basic defining Characteristic Mode equation for any conducting structure. Solution of this modified equation produces a set of eigenvalues λ_n each with the same associated eigenvector or Characteristic Mode current I_n as that defined by equation 3.18. The symmetrical nature of the R and X operators ensures that both these quantities are real. Hence a unique set of Characteristic Modes are definable, each being expressed as a real equiphase current and an associated real constant. The considerable benefit of using this formalisation is that various orthogonality conditions may be defined when the structure is perfectly conducting. This is a result of using R as a weight in equation 3.18 and by the fundamental mathematical definition of the solutions of equation 3.20 (eg. Gourley and Watson 1973). Hence defining an inner product of two arbitrary functions B and C which may exist on the surface of the structure S as:

$$\langle B,C\rangle_S = \iint_S B.C \; dS \tag{3.21}$$

the following current orthogonality conditions may be stated:

$$\langle I_m,RI_n\rangle_S = D\delta_{mn} \tag{3.22}$$

$$\langle I_m,XI_n\rangle_S = D\lambda_n\delta_{mn} \tag{3.23}$$

$$\langle I_m, ZI_n \rangle_S = D(1+j\lambda_n)\delta_{mn} \tag{3.24}$$

where δ_{mn} is the Kronecker delta.

Clearly D is a real constant and is the power radiated by each mode. For further convenience it is desirable to normalise all modes to radiate unit power such that:

$$\langle I_m, RI_n \rangle_S = 1 \tag{3.25}$$

Hence equations 3.18 to 3.20 have demonstrated how a set of Characteristic Modes can be defined for any arbitrary antenna geometry. The modes radiate unit power and are orthogonal over the source region as shown by the three conditions in equation 3.22 to 3.24. In physical terms these equations show that the modes will radiate power independently from each other and there is hence zero modal coupling. The importance of the eigenvalue λ_n associated with a mode is also clearly demonstrated. Notice that this is the same variable defined in equation 3.12 using the formulation of Garbacz and Turpin (1968, 1971). Examination of equation 3.24 shows that it is the ratio of stored to radiated power of that particular mode. The eigenvalue is therefore an indication of how prevalent a mode will be compared to others. Modes that have eigenvalues closest to zero will hence be the most effective at radiating. It is also clear that modes with a negative eigenvalue may be considered capacitive whereas modes with a positive eigenvalue are inductive.

Next, considering the far electric and magnetic fields E_n and H_n associated with each modal current I_n, it may be shown that they too are

orthogonal over the sphere at infinity. For each pair of real modal currents I_n and I_m the power coupling and hence power radiated $P_{mn(rad)}$ may be defined as:

$$P_{mn(rad)} = Re(\ <I_m, ZI_n>_S\ ) = <I_m, RI_n>_S \tag{3.26}$$

Also, considering the far-fields associated with each pair of modal currents, the Poynting vector (eg. Plonus 1986 p492) may be applied to calculate the radiated power over the sphere at infinity. Assuming lossless free space conditions:

$$P_{mn(rad)} = \iint_{S\infty} E_m \times H_n^* \, dS \tag{3.27}$$

where * denotes complex conjugate. Then writing the Characteristic Impedance of free space Z_0 as the ratio of E_n and H_n (eg.Collin 1985 p23):

$$Z_0 = \frac{E_n}{H_n} = \sqrt{\frac{\mu_0}{\epsilon_0}} \tag{3.28}$$

where μ_0 and ϵ_0 are the permeability and permittivity of free space respectively, equation 3.27 may be rewritten for the individual E and H components:

$$P_{mn(rad)} = \frac{1}{Z_0} \iint_{S\infty} E_m \cdot E_n^* \, dS \tag{3.29}$$

$$P_{mn(rad)} = Z_0 \iint_{S\infty} H_m \cdot H_n^* \, dS \tag{3.30}$$

Equating equations 3.29 and 3.30 with equation 3.26 and using the current orthogonality condition shown by equation 3.22, the power coupling between

modal fields is defined as:

$$\frac{1}{Z_0}\int\int_{S\infty} E_m \cdot E_n^* \, dS = \delta_{mn} \tag{3.31}$$

$$Z_0\int\int_{S\infty} H_m \cdot H_n^* \, dS = \delta_{mn} \tag{3.32}$$

Hence the modal fields too are orthogonal over the sphere at infinity and radiate power independently from each other.

3.3 Characteristic Mode Calculation

3.3.1 Mode Calculation and the Method of Moments

Section 3.2.2 showed how Harrington and Mautz (1971a, 1975) defined a set of Characteristic Modes for any radiating or scattering structure.This was achieved by setting up a weighted eigenvalue equation involving the impedance operator Z associated with the particular structure. The Method of Moments, which was described in chapter 2, is a suitable technique for finding a discretized form of the operator, which is defined as the Generalized Impedance matrix $[Z]$. Also the defining Characteristic Mode equations of section 3.2.2 for the continuous operator are relevant to the discretized matrix form of Z. Hence a straightforward, practical method of Characteristic Mode calculation is defined. The matrix form of equation 3.20 is (Harrington and Mautz 1971b, 1975):

$$[X]I_n = \lambda_n[R]I_n \tag{3.33}$$

where $[R]$ and $[X]$ are the so called resistive and reactive components of $[Z]$ defined by equation 3.17. The mode currents I_n are now of course matrix

representations of the continuous current distribution sampled at discrete points. The issues affecting the accuracy of this form of representation were discussed in chapter 2. The set of modes defined by equation 3.33 will be finite in extent, where the number of modes is the same as the order of the generalized impedance matrix. It is also therefore possible to define a similar set of current orthogonality conditions to those of the continuous operator. Firstly though, it is necessary to define an inner product for two arbitrary matrix functions $[B]$ and $[C]$ which exist on the surface S of the structure, analogous to the case of the two continuous functions shown by equation 3.21:

$$\langle B,C\rangle_S = [B]^T[C] \tag{3.34}$$

where ^{T} denotes matrix transpose. As before, this represents the symmetric vector product of the two functions which exist on the surface defined by S.

The current orthogonality conditions comparable to those shown by equations 3.22 to 3.24 are therefore:

$$\langle I_m,RI_n\rangle_S = I_m^T[R]I_n = \delta_{mn} \tag{3.35}$$

$$\langle I_m,XI_n\rangle_S = I_m^T[X]I_n = \lambda_n\delta_{mn} \tag{3.36}$$

$$\langle I_m,ZI_n\rangle_S = I_m^T[Z]I_n = (1+j\lambda_n)\delta_{mn} \tag{3.37}$$

As with the continuous operator case the procedure described by equations 3.26 to 3.32 may be repeated to show that the far-fields associated with each modal current in this discretized form are also orthogonal over the sphere at infinity.

The Method of Moments therefore allows a relatively simple, straightforward procedure for Characteristic Mode calculation to be implemented. The implication of using this technique is that provided a Galerkin based code, as discussed in chapter 2, is employed then the modal structure of any arbitrary geometry configuration can be calculated easily. The method may therefore be looked upon as an extension of the more usual function of the various Moment Method codes described in chapter 2.

3.3.2 Modal Summation

It is now necessary to show how the Characteristic Mode currents I_n relate to the total current flow I due to an applied source. Because of the mode current orthogonality, the total Method of Moment current shown by equation 2.25 is a linear superposition of the modal currents such that:

$$I = \sum_{n=1}^{N} \beta_n I_n \tag{3.38}$$

where β_n are complex scaling factors and N is the total number of Characteristic Modes. The modal fields too may be summed in a similar manner to find the total field due to an applied source:

$$E = \sum_{n=1}^{N} \beta_n E_n \tag{3.39}$$

In order to find the scaling factors β_n associated with each mode we combine equation 3.38 with equation 2.25 yielding:

$$\sum_{n=1}^{N} \beta_n [Z] I_n = V \tag{3.40}$$

with the E of equation 2.25 changed to voltage V for the antenna rather than the scatterer situation. Next taking the inner product of each side of this equation with each I_n such that:

$$\sum_{n=1}^{N} \beta_n \langle I_n, Z I_n \rangle_S = \langle I_n, V \rangle_S \tag{3.41}$$

yields:

$$\sum_{n=1}^{N} \beta_n I_n^T [Z] I_n = I_n^T V \tag{3.42}$$

Now combining this equation with equation 3.37, the current orthogonality condition, yields:

$$\sum_{n=1}^{N} \beta_n (1 + j\lambda_n) = I_n^T V \tag{3.43}$$

and hence the complex scaling factor for each mode due to an applied excitation is:

$$\beta_n = \frac{I_n^T V}{(1 + j\lambda_n)} \tag{3.44}$$

Expressions for the total current flow I and the total field E due to an applied source V are therefore:

$$I = \sum_{n=1}^{N} \frac{I_n^T V}{(1+j\lambda_n)} I_n \tag{3.45}$$

$$E = \sum_{n=1}^{N} \frac{I_n^T V}{(1+j\lambda_n)} E_n \tag{3.46}$$

It is clear therefore from equations 3.45 and 3.46 that two factors affect the extent to which each mode will contribute to the total current or field. Firstly the inverse $(1+j\lambda_n)$ scaling shows that the modal significance is inherently controlled by the structure's dimensions and fixed operating frequency. Secondly the direct scaling of the complex constant $I_n^T V$ shows that the contribution of each mode is also directly affected by the position and magnitude and phase of the applied voltage sources. This linear modal summation is an attractive property of the method of Characteristic Modes, as it implies that insight may be gained into a structure's radiation properties by consideration of the attributes of the individual modes. Certain radiation features of a structure may be due to specific Characteristic Modes, hence implying that action may be taken to enhance or suppress the feature as desired. Chapter 4 will discuss in detail, methods of modal control leading to various techniques for far-field pattern synthesis which may be achieved by feed-point positioning or the addition of loading.

3.3.3 N-Port Networks

The Characteristic Mode theory considered up to this point has demonstrated how the modal structure of any continuous radiating system may be defined. As stated previously, the modes are defined independently of excitation for a fixed frequency and depend on the self resonances of the structure. The aim of this thesis is to investigate the use of these Characteristic Modes to achieve desirable radiation properties, by methods of modal control which will be outlined in chapter 4. Clearly this will involve the correct positioning of appropriate sources or loads to suppress or enhance the effects of defined modes as desired. For many relatively simple structures, where only a few modes are significant, this form of action is clearly feasible. Here only a few easily positioned sources or loads will be necessary to regulate the contribution of these few modes. However in many practical situations consisting of complex, relatively large structures, the number of significant modes may be substantial. This suggests that an unreasonably large number of control mechanisms are required to attain correct modal control. Also the positioning of sources or loads may be restricted to certain areas of the structure. In this case therefore the Characteristic Modes of the full, continuous structure are of limited practical value.

This problem may be overcome by a procedure suggested by Mautz and Harrington (1973). They demonstrated that if the useable feed-points of a radiating structure were known, then it could be considered as an N-port network, where N is the number of feed-points. Hence an alternative

Characteristic Mode set could be defined which is related to this restricted set of feed-points. The procedure is outlined below.

Previous sections of this thesis have discussed the solution of a weighted eigenvalue equation which was set up using the real and imaginary components of the generalized impedance matrix [Z]. This matrix contains information relating to the interaction of every point on the structure to every other point, within the limits of the discretization used. If however it is only possible to use a limited number of fixed points to excite the structure then it may be represented as an N-port network. Figure 3.1 demonstrates the transformation for a typical simple structure with two fixed sources.

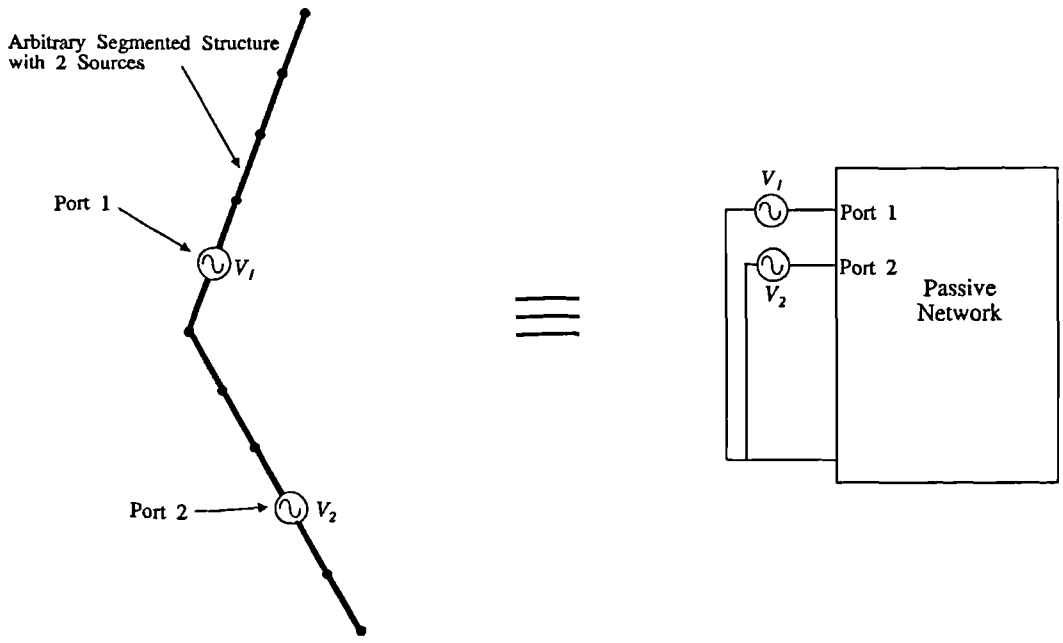

Figure 3.1 N-Port network representation of an arbitrary structure

The above feed-point limitation indicates that the characteristics of the structure may be categorised by a considerably reduced amount of information from the generalized impedance matrix [Z]. Hence a port impedance matrix [Z_p]

may be defined. The elements are analogous to the circuit theory case, described in chapter 2 for the generalized impedance matrix. Z_{pij} is defined as the voltage at port *i* due to a *1A* current flowing into port *j*. In order to determine the port impedance matrix it is therefore necessary to firstly obtain the generalized admittance matrix [*Y*] by inversion of [*Z*]. Next with the fixed ports defined a port admittance matrix $[Y_p]$ may be defined. The elements of this matrix are easily obtained by deleting all rows and columns of [*Y*] except those associated with the defined feed ports. Figure 3.2 demonstrates the procedure for a five element structure with two ports defined at segment numbers 2 and 5.

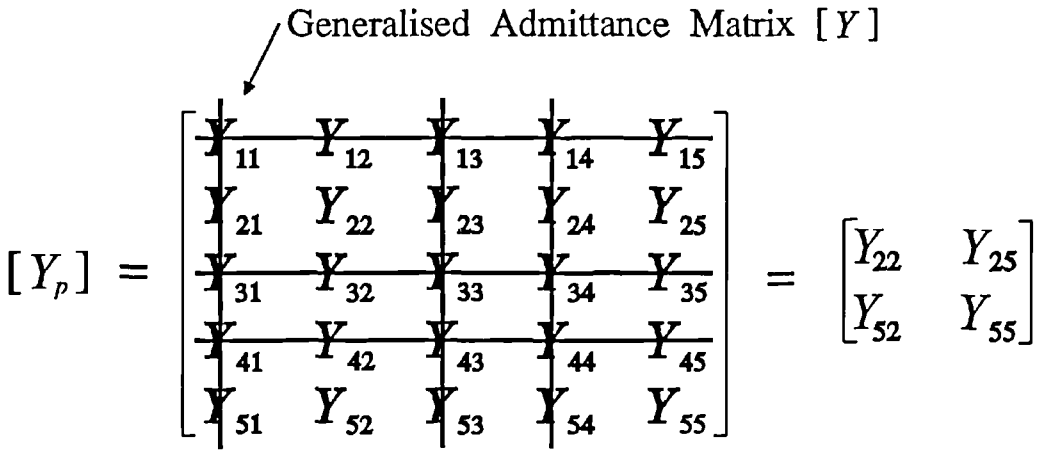

Figure 3.2 Conversion of [*Y*] to $[Y_p]$ for an arbitrary structure

Clearly the Port Impedance matrix $[Z_p]$ is then determined by the inversion of $[Y_p]$:

$$[Z_p] = [Y_p]^{-1} \tag{3.47}$$

Hence any size structure, with a fixed number of feed-points, may be completely categorised by considering it as an *N*-port network. All the required information may be represented by the port matrix formulation described above.

The port matrices are square matrices whose ranks are the same as the number of feed-points defined.

Mautz and Harrington (1973) further showed that Characteristic Modes could be defined for an *N*-port system, similar to those of the continuous structure. Hence a similar weighted eigenvalue equation to that of equation 3.33 is defined by:

$$[X_p]I_{pn} = \lambda_n[R_p]I_{pn} \tag{3.48}$$

where $[R_p]$ and $[X_p]$ are the real and imaginary parts of the port impedance matrix $[Z_p]$, λ_n are the eigenvalues each with an associated eigenvector or port mode current I_{pn}. It may be shown that the orthogonality conditions discussed for the continuous structure are relevant for this formulation. Thus:

$$I_{pm}^T[R_p]I_{pn} = \delta_{mn} \tag{3.49}$$

$$I_{pm}^T[X_p]I_{pn} = \lambda_n\delta_{mn} \tag{3.50}$$

$$I_{pm}^T[Z_p]I_{pn} = (1+j\lambda_n)\delta_{mn} \tag{3.51}$$

The port modal fields E_{pn} associated with each mode may also be shown to be orthogonal over the sphere at infinity, as is the case for the modal fields of the continuous structure such that:

$$\frac{1}{Z_0}\int\int_{S\infty} E_{pm}\cdot E_{pn}^* \, dS = \delta_{mn} \tag{3.52}$$

The port formulation of Characteristic Modes is a procedure which therefore overcomes the limitation described earlier of complex structures with

feed-point constraints. Another practical consideration is that it reduces the number of modes associated with a particular structure. This is advantageous with complex, relatively large structures as a manageable number of modes are defined compared to perhaps, an unreasonable number associated with the continuous structure. The obvious disadvantage of this is that this reduced number of modes may not be as easily exploited to produce some desirable radiation property. Clearly when considering the continuous, complete set of Characteristic Modes of a complex radiating platform such as a motor vehicle, a wider range of performance characteristics will be more easily available by correct modal scaling than those from a constrained port formulation. The use of port Characteristic Modes is therefore a trade-off between the practical constraints of exciting a structure and the possible full radiation potential of it. Few data are available in the literature for port Characteristic Modes. Chapter 6 therefore shows the advantages of using the approach for the far-field pattern synthesis of a particular antenna configuration and compares the results with those obtained using the full, continuous modes.

3.4 Alternative Formulations

3.4.1 Variable Orthogonality

It has been shown in previous sections that a set of Characteristic Modes are definable for any arbitrary structure. It has been further shown that these modes are orthogonal over the structure's surface and over the sphere at infinity. The usefulness of this form of representation has also been discussed. The

orthogonality of the far-fields over the sphere at infinity, as shown by equations 3.31 and 3.32 is enforced because the real part of the Impedance operator R is used as a weight function in equation 3.18. In certain practical situations however it would be possibly more useful to define a set of modes that were orthogonal over any defined sector of space, not the complete sphere at infinity. This would be useful in the situation where the radiation characteristics of a structure are only of interest in the defined sector, the remaining part of the sphere being unimportant. Inagaki and Garbacz (1978, 1982) addressed this problem and showed how it was possible to formulate such a modal set. Hence a set of so called Inagaki Modes were defined, comparable to the original Characteristic Modes of Garbacz and Turpin (1968, 1971) and Harrington and Mautz (1971a, 1975), but with different orthogonality relationships between the elements of the modal set.

Pozar (1984) refined the theory by demonstrating how a Moment Method calculation routine could be specified, which leads to a straightforward method of computation for any arbitrary structure. From the generalized impedance matrix $[Z]$ of a structure the following weighted eigenvalue equation is set up (Pozar 1984):

$$[Z]^*[Z]I_n = \tau_n[H]I_n \tag{3.53}$$

where τ_n are the eigenvalues of the system and I_n are the associated eigenvectors or Inagaki Mode currents. The main difference between this formulation and that given by equation 3.33 is the introduction of the so called weight matrix $[H]$. Whereas the $[R]$ matrix, employed initially, represents the

real radiation power coupling between every discrete point on the structure, the elements of the $[H]$ matrix H_{ij} are defined, using the inner product relationship of equation 3.21, as:

$$H_{ij} = \langle WF_i, WF_j \rangle_{S\infty} \tag{3.54}$$

where W is a weight function defined over the complete sphere at infinity. F_i and F_j are the far-fields associated with a unit current flowing on segments i and j respectively. By setting the weight function W to unity in a sector of the sphere of interest S' and zero elsewhere, different $[H]$ matrices may be formed representing the power coupling between the fields in the defined sectors. Hence with correct normalisation the following orthogonality expressions maybe obtained:

$$I_m^T [Z][Z]^* I_n = \tau_n \delta_{mn} \tag{3.55}$$

$$I_m^T [H] I_n = \delta_{mn} \tag{3.56}$$

$$\frac{1}{Z_0} \int\int_{S'} E_m \cdot E_n^* \, dS = \delta_{mn} \tag{3.57}$$

This set of modes are orthogonal over the source region as before but now the far-fields are orthogonal only over the defined sector S', where the weight function W is unity.

Similar sets of modes with user defined far-field orthogonality were investigated by both Mayhan (1990) and Liu *et al* (1990). Here a different weighted eigenvalue equation was employed but Liu *et al* compared their modal

set with a one calculated using the method outlined by Pozar (1984) and found negligible differences.

3.4.2 Operator Considerations

A further addition to the theory of Characteristic Modes was made by Nalbantoglu (1982). The Characteristic Mode Theory considered up to this point has relied on the generalized impedance matrix obtained from the Method of Moments described in chapter 2. As shown the method usually involves the approximate solution of a so called Electric Field Integral Equation (EFIE). Nalbantoglu (1982) demonstrated that for relatively thick structures it is better to use a Magnetic Field Integral Equation (MFIE). This is because the EFIE may produce an ill-conditioned matrix. He therefore defined a different formulation of Characteristic Modes involving another operator equation. The various orthogonality conditions for the modes by Harrington and Mautz (1971a, 1975) are all relevant in this case too. Therefore this method presents an alternative calculation technique for possible problematic geometrical configurations.

A further operator consideration is that the Characteristic Modes discussed up to this point are all for perfectly conducting structures situated in either free space or over a perfectly conducting ground plane. Harrington and Mautz (1972) showed how operator equations could be defined for dielectric and magnetic bodies which were either lossy or lossless. The limitations of the approach were also outlined, with the main one being the loss of the attractive modal field orthogonality conditions. Thus when considering a non-ideal situation

with Characteristic Modes it is better to examine an idealised model and assess the validity of the assumptions made later.

3.5 Summary

This chapter has discussed the method of Characteristic Modes. Firstly, section 3.2.1 examined the contribution of Garbacz and Turpin (1968, 1971). It was shown how a set of orthogonal fields and associated currents could be defined for any radiating structure. This was achieved by manipulation of the scattering and perturbation operators of the structures to yield diagonal scattering and perturbation matrices which show the interaction of all spherical multipoles incident upon the structure. The limitation of the initial theory was the difficultly in obtaining these matrices, except for the most simple geometrical configurations.

The fundamental work of Harrington and Mautz (1971a, 1975) addressed the inherent mode calculation problems of Garbacz and Turpin (1968, 1971) and was reviewed in section 3.2.2. Here an alterative formulation of Characteristic Modes was presented involving the Impedance Operator. Section 3.3 demonstrated how this led to the development of a straightforward method for Characteristic Mode calculation using the Method of Moments. It showed how total field or current flow can be considered simply as a linear superposition of the elements of the modal set. It is also clear from the orthogonal properties of the modes that insight can be gained into the radiation and scattering characteristics of a structure by consideration of the current distributions , far-

field patterns and eigenvalue λ_n of the individual modes. The possibility too of implementing synthesis procedures for the generation or suppression of certain modes is also considerable and is discussed in more detail in chapter 4.

Further operator considerations were also discussed. Section 3.3.3 addressed the problems associated with large, complex structures or those where the choice of feed or control points is constrained. Here the theory of *N*-port networks was used to overcome the problem and to define constrained impedance matrices to represent the restricted situation.

Section 3.4.1 examined formulations of Characteristic Modes that have user-defined orthogonality of the modal fields. Hence orthogonality may be enforced only in a user defined sector of the sphere. This is useful when considering geometrical configurations where the characteristics are only of interest in a small constrained area and the rest are unimportant. Although this formulation may give more freedom for modal exploitation, there is difficulty in relating the results to the generalized impedance matrix for physical implementation.

Section 3.4.2 discussed how the Characteristic Modes of magnetic and dielectric bodies may be defined. Although this formulation allowed more practical structures to be considered, the main disadvantage is that the fields are not orthogonal. Many of the attractive features of the Characteristic Modes of lossless systems are therefore lost.

CHAPTER 4

CHARACTERISTIC MODE CONTROL TECHNIQUES

4.1 Introduction

The previous two chapters have described how, by using the Method of Moments, a set of Characteristic Modes may be defined for any arbitrary structure. It has been shown that the mode currents are orthogonal over the source region. Also the associated fields too are orthogonal over the sphere at infinity. They are therefore useful for allowing greater insight into the fundamental resonances associated with any conducting geometrical configuration. This permits greater understanding of the radiation or scattering characteristics associated with such structures.

This chapter examines methods by which Characteristic Modes may be further utilised in optimization routines to produce desirable far-field radiation patterns. Firstly, however section 4.2 examines some of the numerous existing antenna far-field control techniques that are available in the literature. The advantages and disadvantages of each method are outlined. Their results are later compared to those obtained using methods involving Characteristic Modes.

Section 4.3 then goes on to discuss the feasibility of using Characteristic Modes as a set of basis functions for optimization and pattern synthesis purposes. Section 4.3.1 firstly examines the fundamental limitations of using each

individual mode in such routines. The reduction in the potential total contribution of each mode, due to the inverse proportionality of the contribution to the associated eigenvalue, is investigated. Recommendations are then made regarding the maximum value that the modulus of the eigenvalue, associated with each mode, should exhibit. This addresses the problem of discarding modes that may have desirable attributes but would be practically difficult to excite because of their insignificance compared to others.

Because of modal orthogonality, simplistic methods of modal control are possible merely by the visual inspection of the individual properties of each mode. Direct excitation or suppression is then possible by the correct positioning of sources or loads. Section 4.3.2 therefore illustrates methods of individual modal control by the correct positioning of sources. A method is also outlined by which a particular mode may be brought to resonance, with an eigenvalue of zero, by the addition of lumped, passive loads.

Section 4.3.3 investigates and then further develops two far-field pattern synthesis techniques using Characteristic Modes. The first method enables an equiphase current whose associated far-field pattern is a least mean squared error approximation to a defined desired pattern to be calculated. Although an advantage of the method is that the resultant algorithm is simple in terms of the computer time required for a typical example, the equiphase condition may sometimes overly constrain the approximating current. The second method overcomes this constraint with the optimization of the modes to produce a current that is not phase-restricted. Clearly this greater level of freedom implies

that more accurate approximations will be obtainable using this second method. The one disadvantage of this latter approach is the dramatic increase in the required computer resources.

Section 4.3.4 addresses the implementation of feed systems to physically realise any synthesized current. A method is developed which relates to the modal summation techniques discussed in the previous chapter. Issues that affect the feasibility of such feed systems are also discussed.

Finally section 4.3.5 examines methods by which a reduction in the final mean squared error of a synthesized pattern can be obtained. Here if the phase of the final result is unimportant then a substantial reduction in the error may be obtained by using a convergent, iterative technique, which will be outlined. A similar approach is followed to develop a method of error reduction which may be used if the polarization of the final result is unimportant. Again this method is iterative and the result converges monotonically.

4.2 Review of Pattern Synthesis Techniques

4.2.1 Antenna Pattern Control

This section looks briefly at some of the many existing antenna pattern control techniques that have been described in the literature. Its purpose is examine the fundamental principles involved for later comparison with the Characteristic Mode techniques.

Many of available pattern synthesis techniques are only easily applicable to regular, simple structures such as linear arrays or straight-wire line sources.

The basic principle of many is the optimization of the coefficients of a mathematical series that exhibits certain desirable characteristics. Thus a set of expansion functions must be assumed to exist for the structure. Clearly the choice of series directly affects the ease with which a certain radiation characteristic may be optimized.

The method of Characteristic Modes presents an orthogonal set of currents and fields associated with any structure. These may be looked upon as an alternative set of expansion functions to those of some arbitrary mathematical series. Their orthogonal properties makes such a modal set ideal for optimization purposes. One significant advantage of using Characteristic Modes as the set of expansion functions for pattern synthesis is that they are directly related to the generalized impedance matrix associated with the structure. An assessment may therefore be made about how easily the resultant current would be to realise physically. Also possible, as section 4.3.4 will demonstrate, is a straightforward method by which a feed system, consisting of voltage sources, may be found that causes any synthesized current to flow on a structure.

4.2.2 Existing Techniques

4.2.2.1 Pattern Multiplication

One of the most fundamental techniques of antenna pattern control is the so called method of pattern multiplication (eg. Stutzman and Thiele 1981 p134). Here, arrays of sources or elements with identical patterns are arranged to produce a desired far-field. This is achieved by simply multiplying the pattern

functions of an individual element by the so-called array factor which takes into account their spacing and orientation. By changing the magnitude and phase of the pattern associated with each element widely varying results may be obtained. Kraus (1988 p130) uses the method initially with isotropic sources and later with arrays of linear elements with great success. The great advantage of the technique is its simplicity in that if the pattern of an individual element is known then the pattern of an array of elements can be easily be found with little computational effort. The obvious disadvantage of the technique is that each element must be considered independently from each other. In practice however mutual coupling which exists between elements is ignored in the calculation. The difficulty in applying this method to the problem of interest in this thesis, that of antennas on complex radiating structures, is also clearly apparent.

4.2.2.2 Mathematical Series

Another widely used practical method for controlling the far-field pattern of a linear array or straight wire line source is to relate the current flow to a mathematical series. For the array case the magnitudes and phases of the currents on each element are related to the individual coefficients of the members of the series. The complexity of the resultant series hence governs the required number of elements and therefore the level of control of the resultant pattern. Similarly for the line sources the number of components involved in the basis function expansion relates to the complexity of the resultant current and

hence the level of possible control.

The various different series that can be employed using this technique ensure that a wide range of different pattern attributes are controllable. Stutzman and Thiele (1981 p521) lists some antenna characteristics that a user may wish to optimize. These include beamwidth, side lobe level (SLL) and the overall accuracy of the shape of the pattern compared to some defined, desired far-field. The choice of expansion function is important therefore and must be related to the desired antenna characteristic, as different series are more suitable for certain types of desired result. Kummer (1992) reviewed many of the possible expansion series that have been employed successfully for far-field pattern synthesis of linear arrays.

One of the simplest forms of series is the binomial series and its use is described by Kraus (1988 p159) for a linear array. If the current flow on each element is in phase and proportional to the coefficients of the binomial series and the element spacing is $\lambda/2$, then the resultant pattern has maximum broadside directivity with zero side lobe level. The simplicity of this approach is demonstrated in figure 4.1 which shows a six element array. Notice that the element excitation coefficients are easily found from the corresponding row of the Pascal Triangle.

The binomial series is therefore a simple method to implement for maximum broadside directivity when no side lobes are required. Clearly though as the size of the array increases the change in current between each element becomes dramatic. Also enforcing the side lobe level to be zero means that the

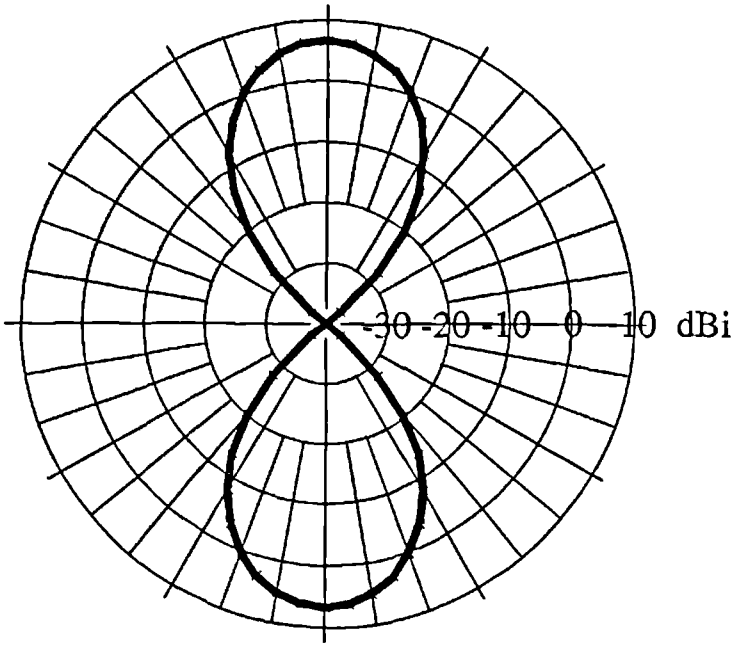

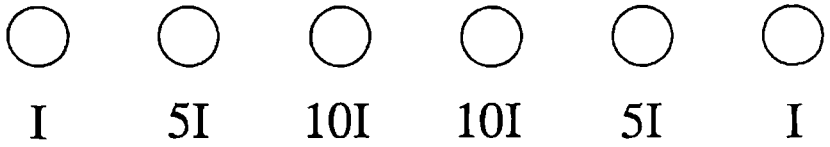

6 Equi-spaced Linear Elements
Length = $\lambda/2$
Spacing = $\lambda/2$
Wire Radius = 0.001λ

Pascal Trinangle

n	
1	1
2	1 1
3	1 2 1
4	1 3 3 1
5	1 4 6 4 1
6	1 5 10 10 5 1

Figure 4.1 Binomial series synthesis of a six element array

width of the main beam may be larger than required.

Other examples of more versatile series that have been utilised include the Fourier transform method (eg.Stutzman and Thiele 1981 p523), the Chebychev polynomial method (eg. Collin and Zucker 1969 p260) and the

Woodward-Lawson sampling method. These methods are more versatile because the user has a greater degree of choice of the accuracy of the synthesizing field. For example Kraus (1988 p162) uses the Chebychev polynomial method to generate a pattern for a linear array. The characteristics of the Chebychev series allowed the selection of an acceptable degree of side lobe level. This action then permits the width of the main beam to be controlled with greater accuracy.

It is clear then that many of the existing pattern synthesis techniques are unique to particular applications. They rely on the user selecting the correct, appropriate method for the problem at hand. A number of the most popular methods have been outlined here so that the versatility and general applicability of the methods using Characteristic Modes, which are discussed in the following section, can be demonstrated. Chapter 6 describes the software implementation of these methods and compares various results with those obtained by using some of the methods outlined in this section.

4.3 Pattern Synthesis Using Characteristic Modes

4.3.1 Basic Principles

It was shown in chapter 3 how a set of Characteristic Modes could be defined for any arbitrary structure by the solution of the weighted matrix eigenvalue equation 3.33. The equation was generated from the Method of Moment generalized impedance matrix associated with the structure and hence available software could be modified to produce a simple, straightforward

calculation method. The defined modal set is specified in terms of real currents and associated eigenvalues λ_n, each with a related far-field pattern. By assuming that the structure under analysis is perfectly conducting and is situated in a lossless environment, the mode currents are orthogonal over the surface of the structure and also the far-fields are orthogonal over the sphere at infinity. It is the purpose of this section to examine and assess the viability of various available methods of Characteristic Mode control. The objective of the analysis is the excitation or suppression of the attributes of certain modes in order to realise desirable radiation characteristics. Far-field pattern synthesis will be concentrated upon, especially as related to complex radiating platforms such as motor vehicles. Hence the analysis will involve the modification of existing methods for this particular purpose and also the development of new, novel techniques.

4.3.2 Mode Significance

Chapter 3 also described how, when considering the properties of each individual Characteristic Mode, two factors affect the ease with which each mode may be excited. Equation 3.45 repeated here for convenience

$$I = \sum_{n=1}^{N} \frac{I_n^T V}{1+j\lambda_n} I_n \tag{4.1}$$

shows an inverse scaling of each mode current by $(1+j\lambda_n)$. This factor is inherently controlled by the structure's geometrical dimensions and orientation. Hence when considering the excitation of a mode this scaling factor is constant,

except, for example, if the geometrical configuration is changed in some way by loading. Various authors have therefore specified numerical limits on this value in order to assess the radiation potential of each mode. Thus modes with a scaling factor below the defined level may be assumed to have a negligible contribution.

It is desirable therefore to investigate the extent which the eigenvalue affects the contribution of each mode. Since the mode currents I_n are real and equiphase, the real and imaginary parts of $1/(1+j\lambda_n)$ directly scale the contribution of each mode current. This corresponds to the real part clearly adding a proportionate value to the total conductance G of the system whereas the imaginary part adds to the total susceptance B. Figure 4.2 demonstrates how the so called modal scaling is affected as the modulus of the associated modal eigenvalue λ_n changes. The real and imaginary parts of $1/(1+j\lambda_n)$ are plotted along with the resultant magnitude of the scaling.

The plot clearly shows that as λ_n becomes significant compared to 1, the real part of $(1+j\lambda_n)$, then the contribution to G decreases at a rate of approximately $1/\lambda_n^2$ whereas that to B approximately as $1/\lambda_n$. It can be seen therefore, for eigenvalues with a modulus greater than approximately 3, the contribution of a mode adds almost entirely to the imaginary part of the resultant total current and hence B. It is also clear that modes where the modulus of the associated eigenvalue is below this level will be significant because of the non-linearity of the scaling in this region. When examining the modal spread of a structure therefore, this non-linearity of the eigenvalue

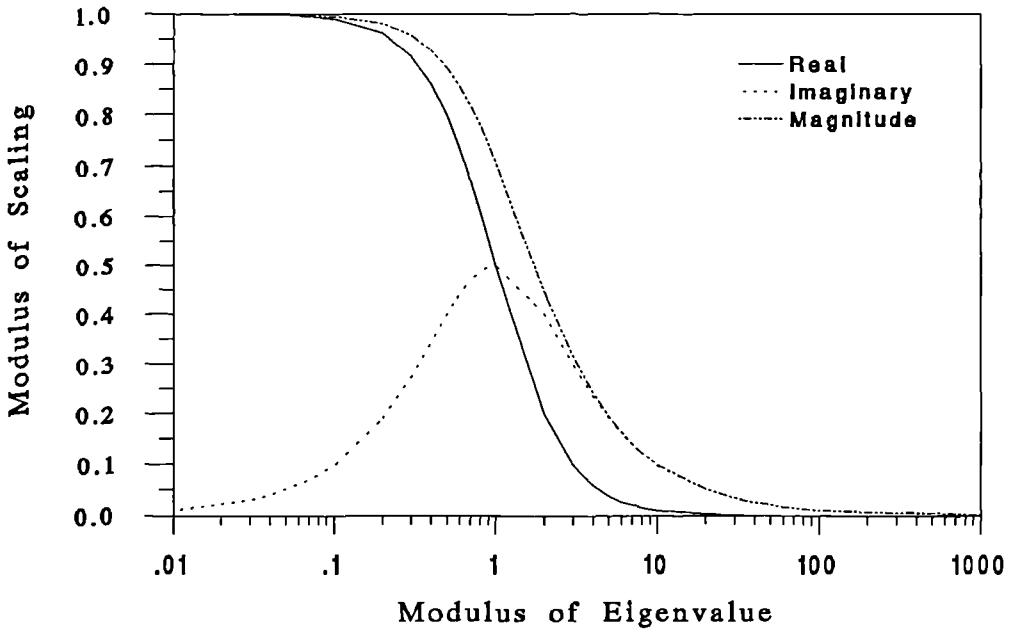

Figure 4.2 Variation of modal scaling with eigenvalue

scaling needs to be considered. A single mode with an eigenvalue around this level will be dominant, compared to others, and therefore difficult to suppress. It is a desirable feature of any synthesis routine to use the most significant modes as this will result in a current that is easier to implement physically.

Both Harrington and Mautz (1971b) and Pozar (1984) arbitrarily limited the modal spread of a structure by similar empirical methods. These involved calculating the power radiated by each mode current with unit excitation such that $I_n{}^T V$=1. A power level may then be defined such that any mode radiating power below it is discarded. Harrington and Mautz used a method which involved finding the eigenvalues of the generalized resistance matrix [R] alone before the Characteristic Mode weighted eigenvalue equation is solved. Since the matrix [R] is by definition positive definite, all the eigenvalues will be positive corresponding to a finite amount of radiated power and may be arranged in

ascending order. By forcing certain of these, with moduli below a certain value to zero, the generalized impedance matrix [Z] and hence the Characteristic Mode calculation weighted eigenvalue equation are modified. The set of Characteristic Modes obtained by the solution of this modified equation are identical to those from the original equation, but now any mode that radiates power below a defined level is suppressed and set to zero.

Pozar (1984) used a similar but simpler empirical method to identify and discard modes with little significance. As before, power radiated by each mode with unit excitation is calculated. Then those that radiate less than 1% of the peak value are discarded.

Since these approaches appear somewhat arbitrary, the problem of modal significance will be addressed further in chapter 6. Essentially the level at which to discard modes is determined by examining the radiation characteristics of both simple and complex structures as the number of modes is increased and comparing the results to the those obtained using the standard Moment Method technique.

It is clear from the above analysis that the accuracy of the synthesis and optimisation routines discussed in the following sections will always be limited by the relative significance of each mode compared to the others. This fact must be considered when implementing the results of the routines because they will only optimise the fields associated with each mode and determine the current which will give the desired effect. The practical difficulty of implementation is

not assessed by the routines and the results must be therefore examined carefully.

4.3.3 Simple Methods of Modal Control

4.3.3.1 Source Situation

When considering electrically small or simple geometrical configurations it is clear that only a few modes will be significant. These usually relate to the natural resonances of a structure and are often clearly recognisable by visual inspection. Hence these few modes will be completely responsible for the radiation characteristics of the structure. In these circumstances the excitation of a particular individual Characteristic Mode is straightforward simply by the correct positioning of a source. Thus a point may be chosen on the structure at which the magnitude of the desired mode current is maximum and the magnitudes of the currents of the other modes are negligible. Hence the substantial value of the $I_n{}^T V$ factor of equation 4.1 for the chosen mode ensures that it is dominant. The resultant radiation characteristics of the structure will therefore be due almost entirely to the chosen Characteristic Mode.

Whilst the inherent simplicity of the above approach is clearly an advantage, many disadvantages exist, which suggest that the method will only be useful in certain restricted circumstances. Firstly the desired radiation characteristic may not be one of the attributes of an individual, significant Characteristic Modes, even though a combination of significant modes could possibly produce it. Also if an individual mode exhibits the desirable characteristics, a source position may not exist that excites it predominantly

without exciting any other modes. The method has however been employed in the literature for the pattern control of simple structures with great success. An example was described by Newman (1979). He examined the Characteristic Modes of a wire cross with the dimensions in figure 4.2. The configuration represents a very simple model of an aircraft frame. At the defined frequency of operation

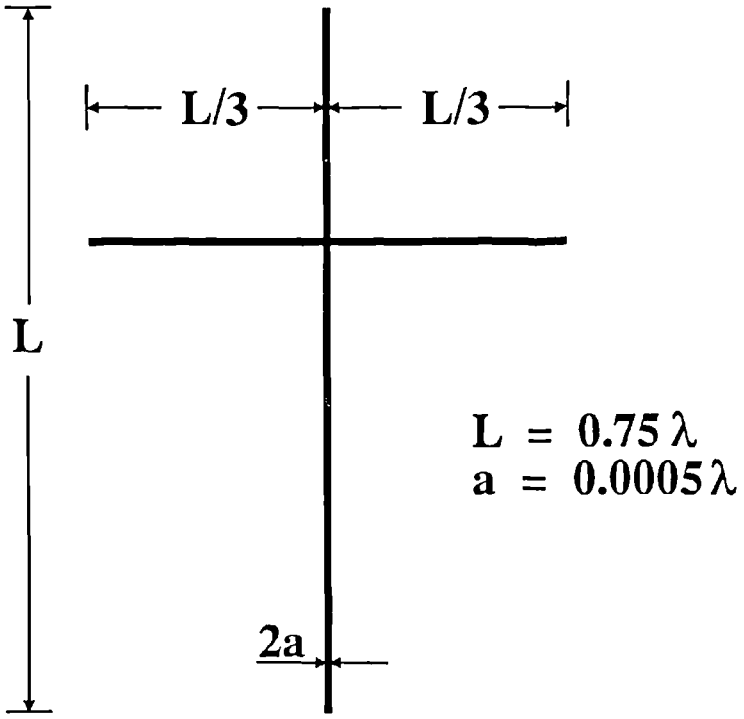

Figure 4.3 Newman's wire cross model

it was found that two Characteristic Modes are significant and each produced a specific radiation pattern. To excite one of these modes in preference to the other required that a point be chosen using the principles outlined above where the current magnitude of the chosen mode was close to its maximum and that of the other mode was minimal. The chosen mode only would therefore be excited by placing a voltage source at that point.

To represent a practical situation Newman (1979) used an electrically small loop antenna at the defined mode current maximum to excite it. As expected, the resultant radiation pattern of the complete system was, to an acceptable degree, the same as that of the chosen Characteristic Mode. This result underlines the fact that an antenna mounted on any structure will excite the Characteristic Modes of the composite system and these will greatly affect the final result. Hence by the correct positioning of an electrically small antenna on such a structure it was shown that it excited a significant, desirable Characteristic Mode of the complete cross. The loop antenna acted as a probe whose purpose was to excite the whole structure.

In essence this simple example demonstrates the underlying philosophy of this thesis. The method of Characteristic Modes identified the radiation properties of a fixed geometrical configuration. Appropriate control of the current distribution allowed these to be excited separately. Although the example was only a simple representation of a complex structure the basic principles are clearly relevant to more complicated, accurate models of such structures, such as those represented by complicated wire grid models. The following sections will therefore describe more sophisticated methods of modal control that do not rely on visual inspection for the positioning or form of the necessary feeding mechanisms.

4.3.3.2 Modal Resonance

Section 4.3.2 demonstrated how the significance of an individual Characteristic Mode is governed by the closeness of its eigenvalue to zero. It was shown that if a mode has a relatively large eigenvalue then it not naturally close to resonance and its contribution to the total radiation characteristics of a structure may be negligible, if other modes exist that are more significant. It is possible though to bring a mode to resonance, with an eigenvalue of zero, by the addition of lumped passive loads as demonstrated by Harrington and Mautz (1972). By adding such loads the generalized impedance matrix $[Z]$ associated with a structure may be divided into two components such that

$$[Z] = [Z_s]+[Z_L] \tag{4.2}$$

where $[Z_s]$ is the standard generalized impedance matrix of the unloaded structure and $[Z_L]$ is a loading matrix. As the loads are passive $[Z_L]$ is a diagonal matrix such that

$$[Z_L] = \begin{bmatrix} Z_1 & 0 & \cdots & 0 \\ 0 & Z_2 & \cdots & 0 \\ \vdots & \vdots & \cdots & \vdots \\ 0 & 0 & \cdots & Z_N \end{bmatrix} = [R_L]+j[X_L] \tag{4.3}$$

where element Z_i (i=1,2,...,N) is the passive load inserted at segment number i and N is the number of segments used in the segmentation scheme. This action clearly redefines the weighted eigenvalue equation 3.33 and a new set of Characteristic Modes are defined for the loaded structure. If the loads are

lossless ($[R_L]$=0) and therefore only reactive, then the orthogonality of the modes is maintained (Harrington and Mautz 1972). Hence equation 3.33 becomes

$$[X_s+X_L]I_n = \lambda_n[R_s]I_n \tag{4.4}$$

with the same definition of Characteristic Mode current I_n and associated eigenvalue λ_n as before.

Then if a certain real mode current is desirable the solely reactive passive loads ($[X_L]$) may be employed to resonate it to ensure that it is highly significant compared to the rest. Hence if a mode current I_n is resonant then its eigenvalue λ_n must be zero. Enforcing this in equation 4.4 yields

$$[X_s]I_n = -[X_L]I_n \tag{4.5}$$

It is then clear that, because of the diagonal nature of the $[X_L]$ matrix, each passive load X_i is the negative of the product of the i th row of $[X_s]$ with the desired current I_n, divided by the desired mode current at point i, I_{ni}. This significant result therefore provides a method of resonating an individual mode current. It is also clear that this technique is not restricted to the actual mode currents of the unloaded structure, but is applicable to any desirable real or equiphase current. However, it is of limited practical use when considering the Characteristic Modes of continuous structures, because a load must be inserted at every defined segmentation point. Clearly this action is impossible, except for the simplest of geometries such as those considered by Harrington and Mautz (1972). They used the method successfully to control the scattering pattern or Radar Cross Section (RCS) of a simple wire triangle.

It is clear that this technique would be particularly effective when used in conjunction with the Characteristic Modes of *N*-port network formulated structures. The method was described in the previous chapter and allows a fixed, manageable number of points to be defined for the situation of sources or loads. Harrington and Mautz (1974a, 1974b) demonstrated the use of the method in this situation, again to control the RCS, for various relatively small *N*-port structures.

4.3.4 Far-Field Pattern Synthesis Techniques

4.3.4.1 Equiphase Current Synthesis

This section discusses how the set of Characteristic Modes associated with a structure may be scaled to produce a far-field pattern that is a least mean squared error approximation to some desired pattern. The procedure involves the development of an algorithm that optimises the far-field of each individual mode, by calculating a factor by which each mode should be scaled. An appropriate current may then be found that, if present on the structure, would physically produce the far-field approximation. The routine described in this section is constrained in that it attempts to find a current that is equiphase over the surface of the structure. Enforcing this restriction simplifies greatly the complexity of the algorithm and hence the required computer resources. The obvious disadvantage is that an equiphase current may not be the most effective method by which an acceptable approximation to the desired pattern can be obtained.

Assuming that E_D is a structure's desired far-field pattern specified in both magnitude and phase, then an approximation to it, E_A, may be specified as a summation of the N Characteristic Modal fields, E_n, associated with it, such that

$$E_D \approx E_A = e^{j\beta} \sum_{n=1}^{N} \alpha_n E_n \tag{4.6}$$

where α_n and β are real constants. Notice that this approximation enforces the equiphase nature of the resultant current I_A which would flow on the structure to realise the approximating field. Using equation 3.38 I_A may be defined as

$$I_A = e^{j\beta} \sum_{n=1}^{N} \alpha_n I_n \tag{4.7}$$

where, as before, I_n are the Characteristic Mode currents.

The synthesis routine needs the desired pattern E_D to be specified at M points on the radiation sphere. If $M \geq N$ then it follows, from the subsequent analysis, that a set of solvable simultaneous equations may be specified. Notice that the N modes used in the synthesis may be less than the total number of modes associated with the structure.

Firstly it is necessary to specify all the appropriate functions required for the synthesis routine in matrix form. $[E_D]$ is therefore defined as a complex M-dimensional column matrix containing the desired field at the defined points. Also $[F]$ may be specified as an M by N dimensional complex matrix. Each column of this matrix contains the corresponding M values of each modal field

at the same defined points as those in $[E_D]$. Next $[A]$ is defined as an N-dimensional column matrix containing the unknown modal scaling factors α_n.

Using the above definitions it follows that for any set of modal scaling factors $[A]$ the absolute mean squared error e_a between the desired field and the approximation is (Harrington and Mautz 1974a),

$$e_a = \left[e^{j\beta}[F][A]-[E_D]\right]^{*T}\left[e^{j\beta}[F][A]-[E_D]\right] \tag{4.8}$$

where * and ^{T} are, as previously specified, complex conjugate and matrix transpose respectively.

Harrington and Mautz (1974a) then showed that, if the $[A]$ matrix is real, it is possible to differentiate equation 4.8. By setting the resulting expression to zero the matrix $[A]$ may be identified that yields a minimum value of e_a for arbitrary β. Hence

$$[A] = [Re([F]^{*T}[F])]^{-1}[Re(e^{-j\beta}[F]^{*T}[E_D])] \tag{4.9}$$

Therefore with an arbitrary β the above expression gives the $[A]$ which will yield the best mean squared error fit to the desired pattern. As the $e^{j\beta}$ factor in equation 4.5 only changes the phase of the approximating pattern this scaling factor obtained with $\beta=0$ gives the best possible equiphase field and current to approximate the magnitude of the desired pattern E_D. Harrington and Mautz also showed how it is possible to find the value of β that gives the best actual mean squared error in terms of both magnitude and phase. Further analysis regarding the phase of a synthesized pattern is presented in section 4.4.6. For the work

described in this thesis, as in many practical situations, the phase of any resultant approximating pattern is unimportant.

4.3.4.2 Complex Current Synthesis

The advantage of the equiphase pattern synthesis method described above is that the Characteristic Modes of a structure may be optimized by considering a user-specified number of points on the radiation sphere. The only restriction is that the number of points specified must equal or exceed the number of modes. Clearly though in many practical situations the specification of a current whose phase does not vary will overly constrain the approximating pattern.

This section discusses how another method of optimization may be developed, based on that of Pozar (1984), which is not limited to equiphase currents. It will be shown however that the computer resources required, compared to the previous technique, are much greater.

Firstly, as with the equiphase current synthesis, a linear summation of the modal fields is specified which represents an approximation to the desired field E_D. Hence if E_A is the approximating pattern then

$$E_D \approx E_A = \sum_{n=1}^{N} \alpha_n E_n \tag{4.10}$$

The difference between this summation and that shown by equation 4.6 is that α_n is now a complex number. The current I_A which must flow on the structure

to generate E_A is therefore

$$I_A = \sum_{n=1}^{N} \alpha_n I_n \tag{4.11}$$

Next for convenience it is desirable to define an inner product of two field functions B and C over the sphere at infinity as

$$\langle B,C \rangle_{S\infty} = \iint_{S\infty} B \cdot C^* \, dS \tag{4.12}$$

The Characteristic Mode field orthogonality condition shown by equation 3.31 may therefore be reexpressed as

$$\langle E_m,E_n \rangle_{S\infty} = Z_0 \delta_{mn} \tag{4.13}$$

Using this relationship the complex number α_n that scales each modal field E_n so that it best approximates the desired pattern E_D in a least mean squared error sense is (Pozar 1984)

$$\alpha_n = \frac{1}{Z_0} \langle E_D,E_n \rangle_{S\infty} \tag{4.14}$$

Thus a set of complex modal scaling factors have been defined. The difference between this synthesis method and that described in the previous section for the equiphase currents is clearly apparent from the examination of the above equation. Using this formulation, where a complex scaling factor is specified for each mode, the pattern variation over the complete sphere at infinity must be considered, not just at a number of user-defined points.

The mean squared error associated with a particular synthesis therefore is also specified as a function of the pattern variation over the complete sphere.

In relative terms the mean squared pattern error e is

$$e = \frac{\left\langle (E_A - E_D), (E_A - E_D) \right\rangle_{S\infty}}{\left\langle E_D, E_D \right\rangle_{S\infty}} \tag{4.15}$$

This technique clearly overcomes the equiphase current constraint of the method discussed in section 4.3.3.1. The major difference between the two techniques, in terms of required computer resources, is that for the latter each modal scaling factor must be calculated over the complete sphere at infinity. This obviously implies a more computer-intensive calculation algorithm, since the previous method could be limited to as few field points as desired. The great advantage of this latter method however is clearly its versatility, because it will find the best possible approximating field, and therefore current, that is available using the specified number of modes.

4.3.5 Source Implementation

The far-field synthesis routines discussed above in section 4.3.4 both calculated a scaling factor for each of the Characteristic Modes used in each routine. The final result of both techniques is the production of a current distribution which, if present on the structure, produces the specified least mean squared error approximation of the far-field. Neither Harrington and Mautz (1972) nor Pozar (1984) considered the implementation of an appropriate feed system to excite the current in their fundamental development of the synthesis algorithms. This section addresses this aspect by relating the final synthesized current to a possible voltage source feed-system capable of exciting it. It relies

on using the same number of sources in the feed-system as modes that were used in the synthesis routine.

If all the modes associated with a geometrical configuration have been employed in the synthesis routine, then every point on the structure, within the limits of the discretization, must be used to excite the appropriate current. In this case the required voltage source column matrix V_A is found by simply using the generalized impedance matrix [Z] such that

$$[Z]I_A = V_A \tag{4.16}$$

This is also the case if an N-port formulation is employed and all modes are used in the synthesis. Here in the above equation [Z] is replaced by [Z_p], the port impedance matrix and I_A and V_A by I_{Ap} and V_{Ap}, the approximating port current and voltage column matrices respectively.

If however, not all of the modes associated with a particular structure are used in the synthesis, then the user may decide on the position of each of the sources, provided the appropriate number are used. In this case it is necessary to relate the synthesized current to the modal summation equations discussed in the previous chapter. Hence to realise the approximating pattern the factor by which each mode must be scaled α_n must equal the total modal scale shown by equation 4.1 such that

$$\alpha_n = \frac{I_n^T V}{1+j\lambda_n} \tag{4.17}$$

Upon choosing the necessary number of points on the structure it is then necessary to define a so-called current source matrix [I_S], which is a square

matrix whose order is the same the number of modes used in the synthesis. Each column of this matrix contains the values of each mode current at the specified feed-points. A further diagonal matrix [Λ] may then be specified which contains the natural orthogonal scaling of each mode by the associated eigenvalue such that

$$[\Lambda] = \begin{bmatrix} \frac{1}{1+j\lambda_1} & 0 & \cdots & 0 \\ 0 & \frac{1}{1+j\lambda_2} & \cdots & 0 \\ \vdots & \vdots & \cdots & \vdots \\ 0 & 0 & \cdots & \frac{1}{1+j\lambda_N} \end{bmatrix} \tag{4.18}$$

Now the elements of $[I_S]$ may be pre-scaled to take into account this natural scaling. Therefore

$$[I_S'] = [I_S][\Lambda] \tag{4.19}$$

The voltage source column matrix V_S containing the necessary feed-point voltages to produce the synthesized pattern is therefore

$$V_S = ([I_S']^T)^{-1}[A] \tag{4.20}$$

where $[A]$ is a column matrix containing modal scaling factors α_n.

Although the above method defines a voltage feed-system that would produce the desired current, no consideration has been given to the actual values of input impedance that this would yield. These, of course, may be unreasonable in terms of feed-system complexity and therefore may be difficult to implement practically . Also, in using this method, the contribution of any mode that was

not used in the synthesis routine must be considered to be negligible. This may clearly not be the case, although in most situations only the modes with the largest eigenvalues would not be used in the synthesis routine. The greatest control that the user has in selecting which point to use to feed the structure is the magnitude of the appropriate mode currents. As discussed in section 4.3.2.1 this factor directly affects the extent by which a mode will be excited.

4.3.6 Synthesis Constraints

4.3.6.1 Phase

The pattern synthesis routines described in section 4.3.4 calculate a least mean squared error approximation to a desired pattern. The desired pattern is specified in terms of a real and imaginary component, the phase therefore being fixed. In many practical situations however, the phase of the resultant approximating pattern would be unimportant. A reduction in the resultant error may therefore be achieved by allowing the phase of the approximating pattern to vary in an iterative method as outlined by Harrington and Mautz (1974a). The flow chart shown by figure 4.4 summarises the technique as applied to both of the synthesis routines considered.

The action shown by steps 2 and 3 of figure 4.4 cannot increase the mean squared error. The final result therefore converges as the number of iterations increases. It should be noted however that this procedure finds the phase values corresponding to a local minimum. The converged result may therefore not be the best possible least mean squared error result. To investigate the relative merit of the converged result compared to other local minima the synthesis

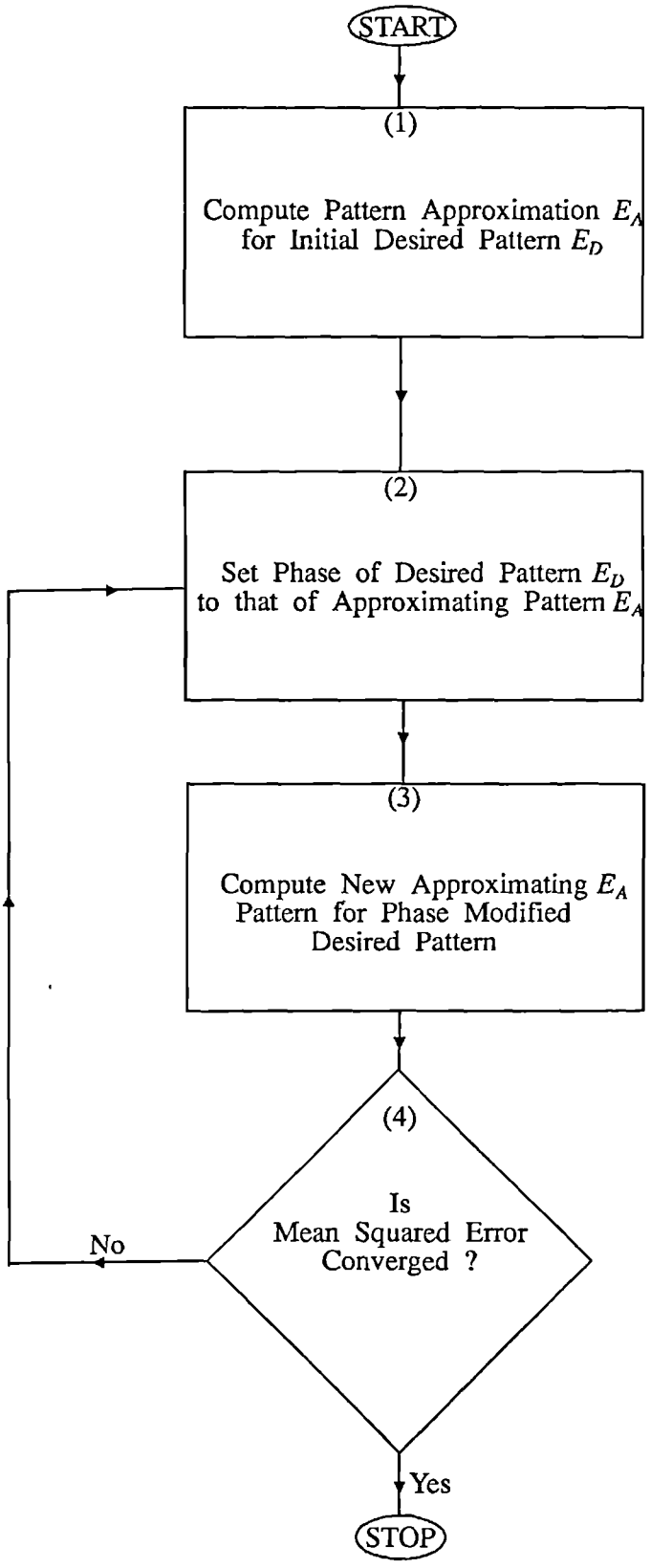

Figure 4.4 Phase modification technique flow chart

should be repeated using a number of different starting points. This involves setting the initial phase of the desired pattern to various different values, possibly using a random number generator.

4.3.6.2 Polarization

In certain practical situations both the phase and the polarization of the final synthesized far-field are unimportant. One such case, which will be considered here, is the antenna configuration for so-called Near Vertical Incidence Skywave (NVIS) propagation (eg. Maslin 1987 pp.81-87). The technique, which is described in greater detail in chapter 7, utilises the ionosphere for propagation. The polarization of the field incident upon the ionosphere may be altered dramatically upon exit. The polarization of the far-field patterns of antennas used for this purpose is therefore of little importance. Again, as with the synthesis example where the desired pattern phase is fixed, a fixed polarization desired pattern specification may also overly constrain the approximating pattern.

The technique outlined here overcomes this constraint. Firstly it is necessary to specify both the desired field, E_D, and the modal fields of the geometrical configuration,E_n, in terms of their theta and phi components $E_{D\theta}$, $E_{D\phi}$, $E_{n\theta}$ and $E_{n\phi}$.

It follows then that the required modal scaling factors α_n shown by equation

4.14, for the latter synthesis method, are

$$\alpha_n = \frac{1}{Z_0}(\langle E_{D\theta}, E_{n\theta}\rangle_{S\infty} + \langle E_{D\phi}, E_{n\phi}\rangle_{S\infty}) \tag{4.21}$$

If the polarization of the final synthesized pattern is unimportant then an iterative technique may be used, at the same time as the phase adjustment technique described in section 4.3.5.1, to reduce the mean squared error.

Firstly, it is necessary to specify the modulus of a total electric field, E_T, in the usual manner as the square root of the sum of the squares of the individual components such that

$$|E_T| = \sqrt{|E_\theta|^2 + |E_\phi|^2} \tag{4.22}$$

A real number K is also defined as the ratio

$$K = \frac{|E_\theta|}{|E_\phi|} \tag{4.23}$$

The modulus of each component may then be specified in terms of K such that

$$|E_\theta| = \frac{K}{\sqrt{K^2+1}}|E_T| \tag{4.24}$$

$$|E_\phi| = \frac{1}{\sqrt{K^2+1}}|E_T| \tag{4.25}$$

If therefore, the initial desired field specification is in terms of a total electric field magnitude and phase then initial values for $E_{D\theta}$ and $E_{D\phi}$ may be found from equations 4.24 and 4.25 with K set at unity. The basic iteration technique is then similar to that above for correcting the phase of the approximating pattern and is outlined in the flow chart of figure 4.5.

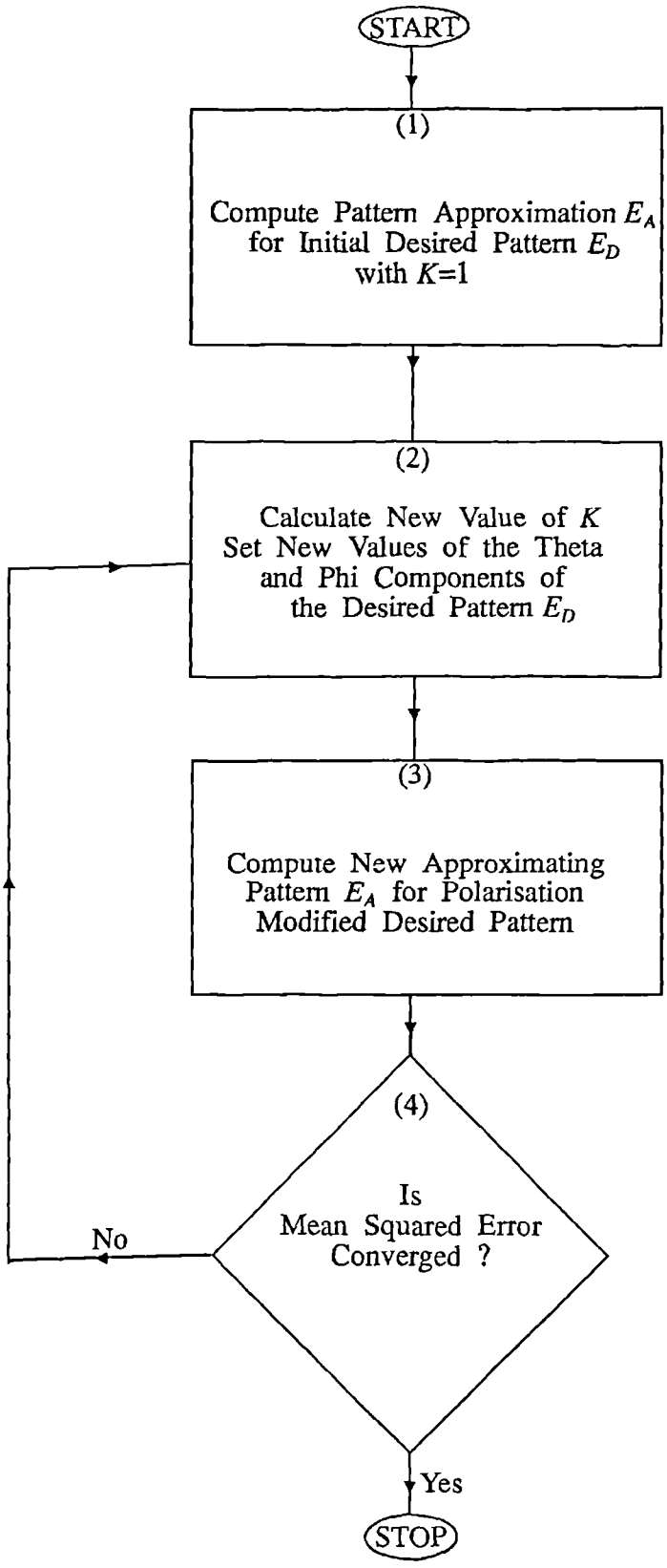

Figure 4.5 **Polarisation modification routine flow chart**

Hence by modifying the ratio of the theta and phi components of the desired field after each synthesis calculation the error reduces with each iteration. Clearly if both the phase and polarization of the final synthesized pattern are unimportant then both this routine and the phase modification routine described in section 4.3.5.1 may be used together to obtain the best possible approximation.

4.4 Summary

This chapter has shown how the set of Characteristic Modes that were defined for any conducting structure by the analysis shown in chapters 2 and 3 may be used in pattern synthesis routines.

Section 4.2 examined many of the existing techniques that are available in the literature such as pattern multiplication and the use of a mathematical series that exhibits the desired properties. The basic principles of such techniques were assessed along with the difficulties of applying them to complex, irregular radiating structures. Also discussed in section 4.2 were the advantages of utilising the orthogonal properties of Characteristic Mode sets for synthesis routines. The attractive nature of using a modal set that could be directly related to the generalized impedance matrix of a structure was also clearly evident.

Section 4.3 went on to develop various methods of controlling the far-field patterns of structures using Characteristic Modes. These included simple techniques, as described in section 4.3.3, where the properties of individual

modes may be made dominant by source positioning or passive loading. More sophisticated numerical optimization algorithms were developed in section 4.3.4 that involve finding factors by which modes may be scaled to produce least mean squared error approximations to desired patterns. The methods considered are general and do not rely on the visual inspection of all the modes themselves, as is the case with the simplistic techniques described in section 4.3.3. They are therefore suitable for optimizing the Characteristic Modes of complex structures which may be numerous and complicated.

A further aspect of Characteristic Mode pattern synthesis was investigated in section 4.3.5, where the problem of the practical implementation of a feed system to physically realise a synthesized current was examined. A straightforward technique was developed to solve this by using the orthogonality conditions associated with each mode current to calculate the appropriate voltage sources.

Finally in section 4.3.6 methods of reducing the mean squared error associated with a particular synthesis example were described. If the phase or the polarization of the synthesized field are unimportant then the iterative methods described may be employed to find the least mean squared error approximation of a desired field specified in magnitude only. Either or both of the routines may be used, depending on the application.

CHAPTER 5

VALIDATION OF THE MODIFIED MININEC3 CODE

5.1 Introduction

In this chapter the accuracy of the MININEC3 Method of Moment computer code, as modified for this research programme, will be assessed. This is a vital aspect of the work of this thesis because of the extreme difficulties associated with making experimental measurements from the type of structures that will be considered. All of the numerical results in future sections will be related to the generalized impedance matrices of the structures that are calculated using this code. To a great extent the accuracy of the final pattern synthesis results will therefore depend upon its ability to model complex structure antenna configurations accurately.

Three different approaches will be used in the assessment of accuracy. Firstly, in section 5.2, MININEC3 will be used to calculate the input impedance of a number of simple wire dipole antennas. The results will be compared to those obtained using the widely accepted analytical techniques of King and Harrison (1969). The level of agreement obtained firstly proves the successful conversion of the code from BASIC to FORTRAN. Secondly the results are used to assess the validity of the general segmentation scheme rules defined by Logan and Rockway (1986), as discussed in chapter 2. Further recommendations are

then made regarding the importance of modelling the area around the feed-point carefully, particulary when wishing to model input impedance accurately.

Section 5.3 describes the use of MININEC3 to calculate the radiation characteristics of a number of complex wire grid models representing continuous surfaces. These are compared to the results obtained using the Numerical Electromagnetics Code (NEC). Although this is also a Method of Moment code it uses entirely different expansion and test functions to represent the current distribution. Also the code is not Galerkin based, as discussed in chapter 2. Chapter 3 showed that it is therefore not possible to calculate Characteristic Modes using its impedance matrix. It is however one of the most widely used codes with its accuracy being extensively studied in the literature. For the application of analyzing complex radiating structures the results obtained with NEC are generally the most highly regarded. Comparing MININEC3 results with those obtained with NEC is therefore an important validation exercise. The generally good agreement obtained shows that MININEC3 is able to emulate, to the same degree of accuracy as NEC, complex structure current distributions.

Finally in section 5.4 relevant experimental data that are available in the literature are used to assess the accuracy of MININEC3. These include a V-dipole antenna. This type of geometrical configuration, with an acute angle between two conductors, has been reported to produce erroneous impedance results with Method of Moment codes (Austin 1993). Wire grid models of complex structures though frequently contain acute angles. It is therefore important that the ability of MININEC3 to model the situation is considered. Also considered are various

complex radiating platforms including a conducting box and a motor vehicle with monopole antennas mounted at various locations on the body. These geometrical configurations are typical of those whose Characteristic Modes the work of this thesis is aiming to exploit. It is therefore vitally important that MININEC3 can analyze such structures accurately.

5.2 Analytical Results

Amongst the most widely accepted analytical data for certain antenna characteristics are those due to King and Harrison (1969). Their results however are limited to centre fed dipoles and loops. The ability of the BASIC based MININEC software to model such geometrical configurations accurately has previously been assessed by Logan and Rockway (1986, 1988). It is the purpose of this section to show the results obtained using the FORTRAN version of MININEC. These are compared to the results of King and Harrison. Further recommendations are then made regarding segmentation schemes which add to those from the literature described in chapter 2. Particular attention is given to the area around the feed-point which is of vital importance for the accurate determination of input impedance.

In figure 5.1 a centre fed dipole is shown with its dimensions. The free space input impedance of this particular example was calculated by MININEC3 as the frequency was varied. To compare with the analysis of King and Harrison this is specified in terms of the factor $k_0 h$, the wave number, which is varied

from 0.50 to 2.20, with k_0 defined in the usual manner as

$$k_0 = \frac{2\pi}{\lambda} \tag{5.1}$$

This frequency range is such that the first natural resonance is approximately in the centre of the band of frequencies tested.

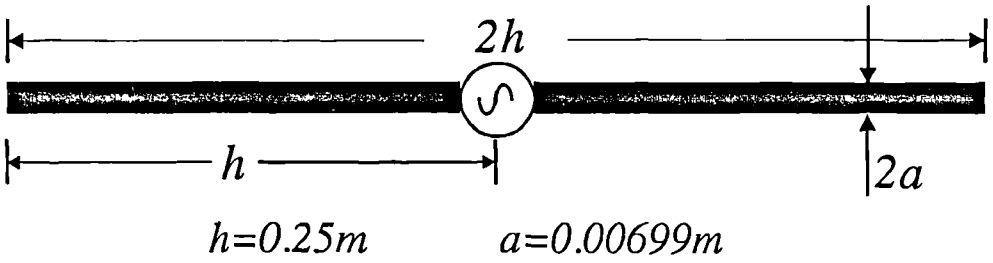

Figure 5.1 Centre fed dipole antenna with dimensions

Two uniform segmentation schemes were initially employed and are shown in table 5.1 along with the segmentation density at the upper and lower frequencies.

Table 5.1 Initial Segmentation Schemes for the Dipole Antenna

Segmentation	Scheme 1 10 Segments	Scheme 2 20 Segments
Electrical Length k_0h	Nominal Segments per wavelength	
0.50	63	126
2.20	14	28

Notice that at the upper frequency, the number of segments used in scheme 1 is below the general recommendation of 20 defined by Logan and Rockway (1986), whereas that used in scheme 2 is substantially above it.

Firstly, considering the predicted far-field, both segmentation schemes gave nearly identical MININEC3 far-field pattern plots with less than 0.1dB difference at any point for all the frequencies considered. Figures 5.2 and 5.3 show the variation with wave number of the input resistance and reactance of each configuration. Also shown are the results due to King and Harrison.

From initial inspection it is clear that both segmentation schemes yield resistance and reactance results indistinguishable from those of King and Harrison for $k_0h<1.6$. For $k_0h>1.6$ the denser segmentation scheme gives the more accurate results. The reactive component though differs from that of King and Harrison for $k_0h>1.9$.

It is clear that the sparser segmentation scheme is adequate for $k_0h<1.6$. In the worst case this corresponds to nominally 20 segments per wavelength of wire, confirming the previous recommendations of Logan and Rockway (1986). Beyond the first resonance however this segmentation density is inadequate. As described above, the results for input reactance obtained even with the denser second segmentation scheme differ somewhat from King and Harrison for $k_0h>1.9$. This is when approximately 30 segments per wavelength are employed, contradicting Logan and Rockway's general guidelines. Other authors (eg. Najm 1992) have illustrated the difficulties in evaluating input impedance accurately using the Method of Moments. The input impedance depends on the near field which must be simulated to a high degree of accuracy in the local area of the feed-point to obtain reliable results. Kubina (1989) suggested that when computing the input impedance the segmentation density around the feed-point

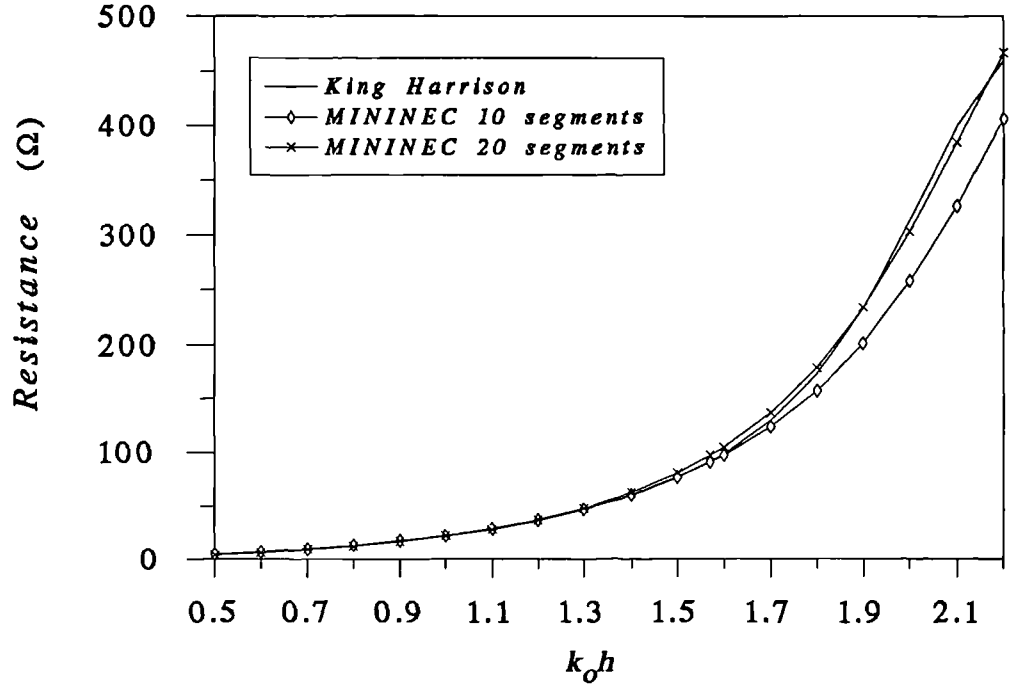

Figure 5.2 Variation of the dipole input resistance with wave number for the segmentation schemes in table 5.1

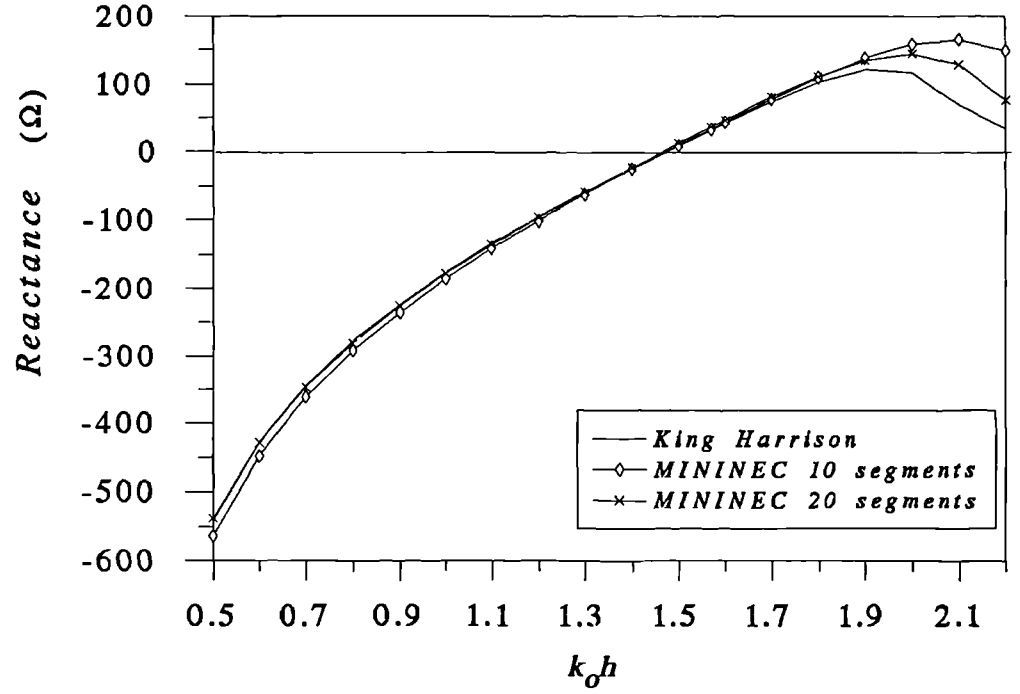

Figure 5.3 Variation of the dipole input reactance with wave number for the segmentation schemes in table 5.1

should be increased. No specific value was quoted but clearly it should be increased beyond that which is normally considered acceptable for far-field accuracy. To investigate this the dipole shown in figure 5.1 was divided into three regions ,as shown in figure 5.4. A graded segmentation scheme was then employed as shown in table 5.2. Notice that the same total number of segments are used as in scheme 2 above.

Table 5.2 Graded Segmentation Scheme for the Dipole Antenna

Segmentation	Regions 1 and 3 5 Segments	Region 2 10 Segments
Electrical Length $k_0 h$	Nominal Segments per wavelength	
0.50	91	236
2.20	20	54

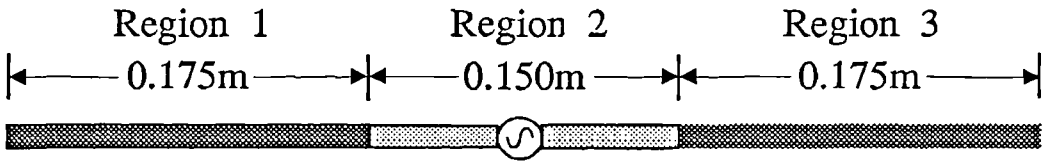

Figure 5.4 Dipole antenna with regions for different segmentation densities

The input impedance of this configuration was then computed over the same frequency range. The results are shown in figures 5.5 and 5.6.

It is clear that the graded segmentation scheme gives the most accurate approximation of the three schemes considered, with negligible difference from the results of King and Harrison. This shows the importance of modelling the feed-point accurately. Both the previous scheme with uniform segmentation and

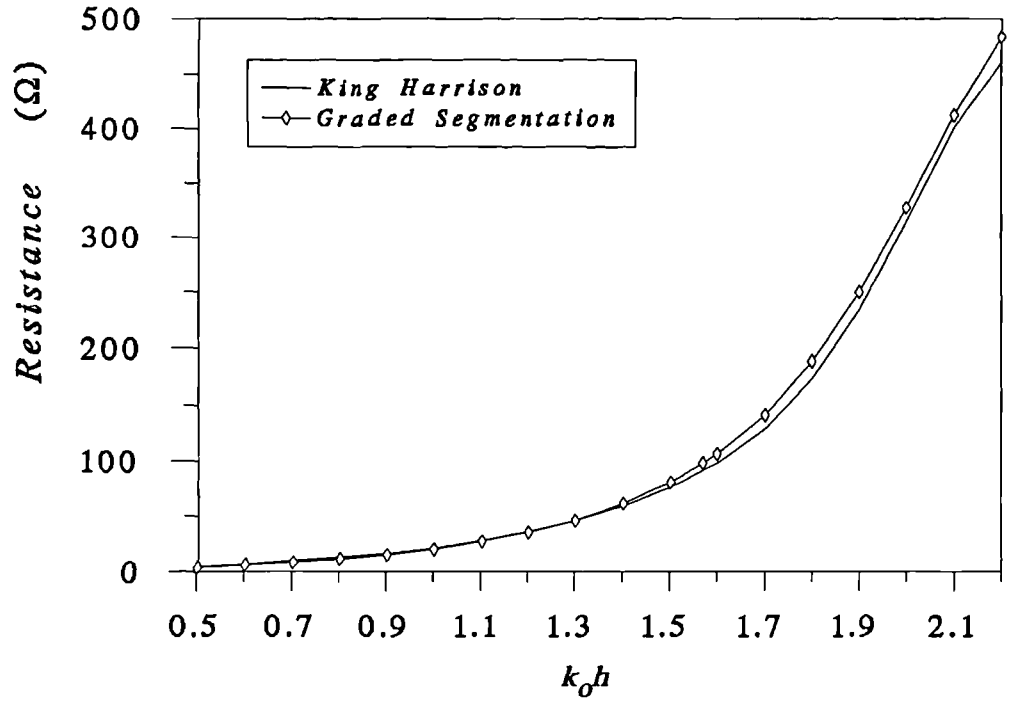

Figure 5.5 Variation of the dipole input resistance with wave number for the graded segmentation scheme in table 5.2

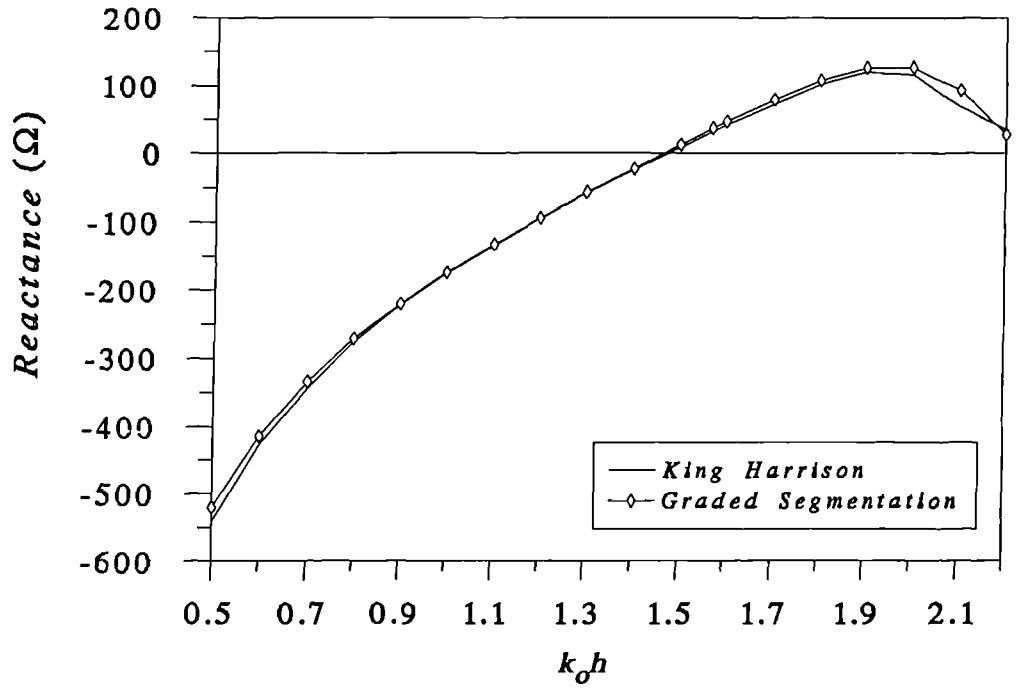

Figure 5.6 Variation of the dipole input reactance with wave number for the graded segmentation scheme in table 5.2

the graded segmentation scheme employed the same number of segments but the graded scheme produced the more accurate result.

This result enforces the general "rule of thumb", discussed in chapter 2, of 20 segments per wavelength of wire which was adequate in this case for the determination of pattern and of the basic shape and trend of the input impedance plots. It is concluded however that a segmentation density of 50 per wavelength be employed in the local area around the feed-point. This produces a more accurate result with a smaller absolute error. Section 5.4.1 describes further beneficial effects of using graded segmentation schemes when computing input impedance.

5.3 Comparison with NEC

5.3.1 Structure Definition

In the previous section the ability of the MININEC code to model, with a high degree of accuracy, the characteristics of a simple centre-fed dipole antenna was demonstrated. The ultimate aim of this thesis however requires the determination of the Characteristic Modes of considerably more complex structures such as motor vehicles. To the knowledge of the author MININEC3 has not previously been employed to model such structures. More commonly the NEC code is used. For the Characteristic Mode analysis of this thesis however, a code is required that generates a symmetrical generalized impedance matrix, as discussed in chapter 3. This therefore necessitates the use of a Galerkin-based code like MININEC3. However its ability to model such structures accurately is

unknown.

It is the purpose of this section to assess the accuracy of both the input impedance and pattern results obtained using MININEC when modelling a number of complex continuous surfaces represented as wire grid models. The results will be compared to those obtained using the NEC code.

The first geometrical configuration considered was a flat plate with a quarter wave monopole mounted in the centre as shown in figure 5.7. Figure 5.8 shows the second structure. This is more complex, consisting of both parallel and orthogonal plates, somewhat representative of a motor vehicle. A quarter wave monopole is situated in the centre of the upper horizontal plate. The third structure that was analyzed is shown in figure 5.9. This consists of an closed box structure with an aperture. Two quarter wave monopoles were mounted on the box as shown. The electrical dimensions of these three structures were chosen such that induced current flowing on their complete surfaces would produce widely varying far-field patterns. This is clearly the most effective method of validation with the pattern containing numerous peaks and nulls for comparison.

In order to model these geometrical configurations using both NEC and MININEC3 it was required that they were represented as wire grids. The mesh generator of Najm (1991) was therefore employed to produce the wire grid models shown in figures 5.10 to 5.12.

In generating these models the basic wire grid modelling criteria described in chapter 2 were adhered to. The spacing between grid elements was therefore set at 0.1λ and the so-called "twice area rule" was applied to calculate the radii

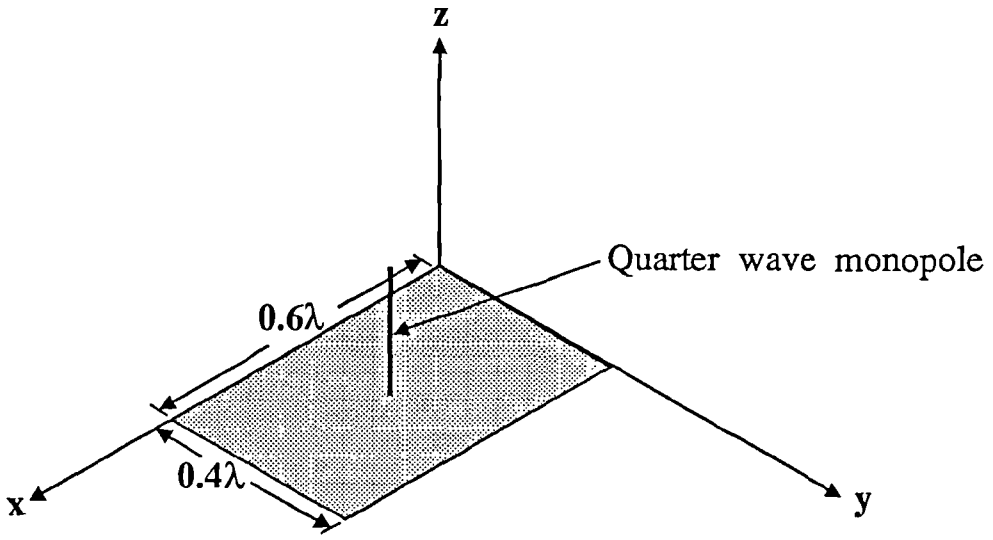

Figure 5.7 Thin flat horizontal plate with centre mounted quarter wave monopole

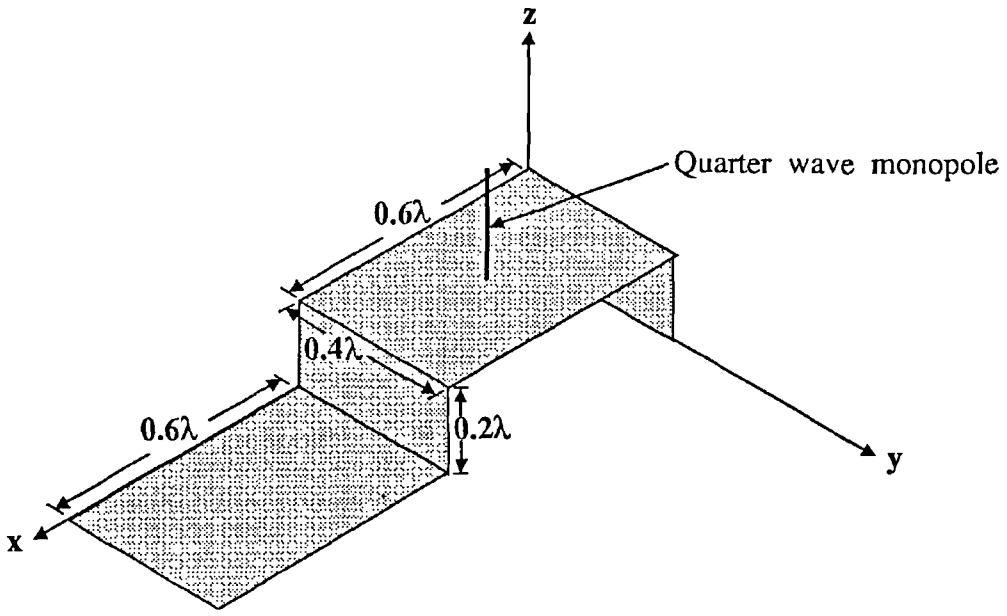

Figure 5.8 Thin flat plates with vertical quarter wave monopole

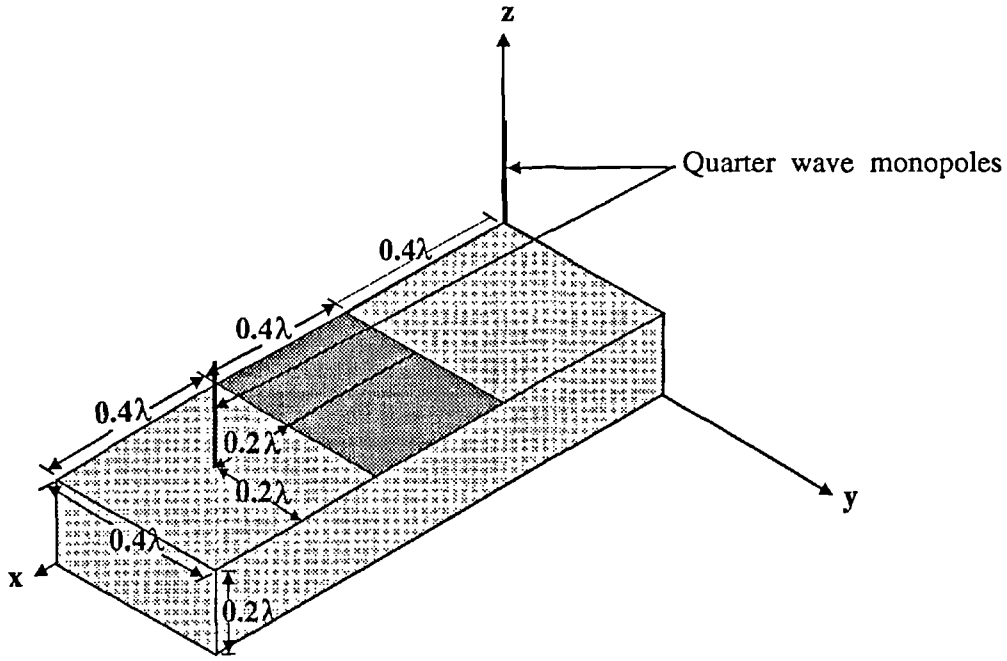

Figure 5.9 Box with aperture and two vertically mounted quarter-wave monopoles

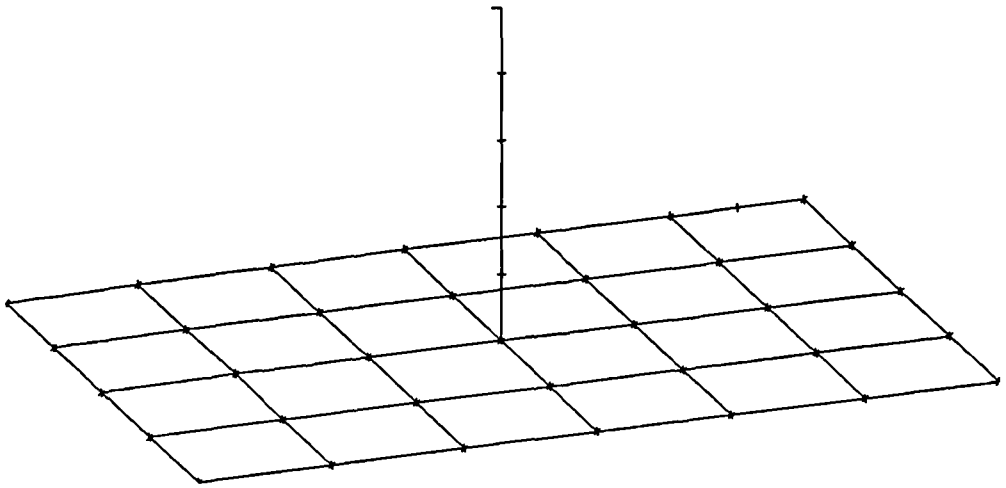

Viewing angles: θ=70°, ϕ=60°

Figure 5.10 Wire grid model of the configuration shown in figure 5.7

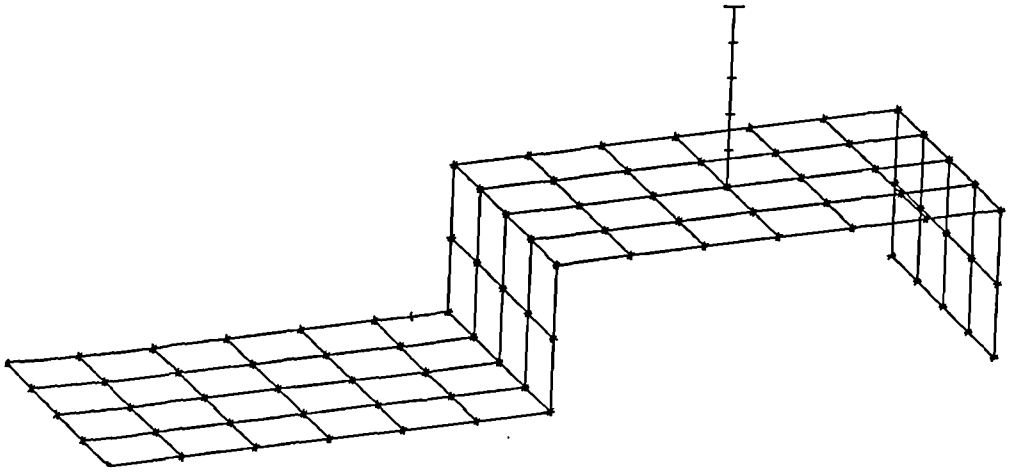

Viewing angles: θ=70, ϕ=50°

Figure 5.11 Wire grid model of the configuration shown in figure 5.8

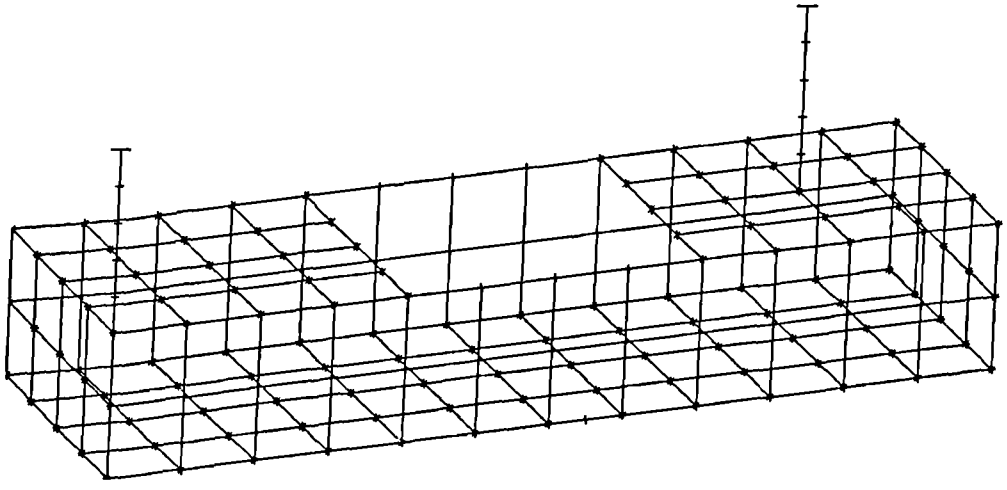

Viewing angles: θ=70°, ϕ=50°

Figure 5.12 Wire grid model of the configuration shown in figure 5.10

of the wires. Also Trueman and Kubina (1990) have defined a set of wire grid modelling guidelines. These empirically derived rules set limits on the characteristics of each individual segment and also on multi-segment junctions. Rules regarding overall segment proximity are also addressed. The MNCHECK software of Shaw (1991), based on their work, automatically verifies that all of the guidelines have been complied with and was employed with all wire grid models described here.

5.3.2 Predicted Results

For the two simpler models, shown by figures 5.10 and 5.11, the vertical monopole was base-fed with a single voltage source. The more complex two monopole configuration shown in figure 5.12 allowed the employment of numerous, different feed configurations by varying the magnitudes and phases of the voltages at each base. Two feed configurations are discussed here using equal magnitude voltages fed firstly in phase and secondly in anti-phase. As expected, these two feed configurations produced significantly different input impedance and pattern results. It is therefore a useful verification exercise as the geometrical configuration is fixed but the current imposed on the structure differs substantially in each case.

Free space conditions were used for the analysis and the input impedance of each configuration was calculated using both codes. Also three pattern sweeps were examined. Sweep 1 was for a varying azimuth angle with θ=90°. In sweeps 2 and 3 the elevation angle was varied with ϕ fixed at 0° and 90° respectively. In this section the results obtained using both codes are compared for the three

defined structures. Input impedance is examined and also a number of the relevant pattern plots described above. Appendix A then contains the complete set of predicted patterns.

5.3.2.1 Radiation Patterns

Firstly considering the predicted far-fields, configuration 1 exhibited an overall pattern similar to that of a vertical monopole over an infinite, perfect ground plane. Figure 5.13 shows the variation in elevation with ϕ=0° of the vertical component of the electric field. Figure 5.14 then shows the azimuthal variation of the horizontal component, demonstrating the effect of current flowing on the horizontal plate. Both plots show that there is excellent agreement between the results of the two codes. In both cases the position of the predicted peaks and nulls coincide exactly and there is maximum difference at any point of 1.5dB.

For the far-fields of configuration 2 both codes predicted a substantial horizontal component of the electric field, suggesting significant current flow on the complete structure. Figure 5.15 shows its resulting azimuth variation predicted by both codes. Figures 5.16 then shows the variation with in elevation with ϕ=0° of the vertical component of the predicted electric field.

The pattern results of both codes again show excellent overall agreement for this configuration. The positions of the peaks and nulls again coincide exactly, as with configuration 1. At the peaks the difference between the two codes is again no more than 1.5dB. For this configuration however there is

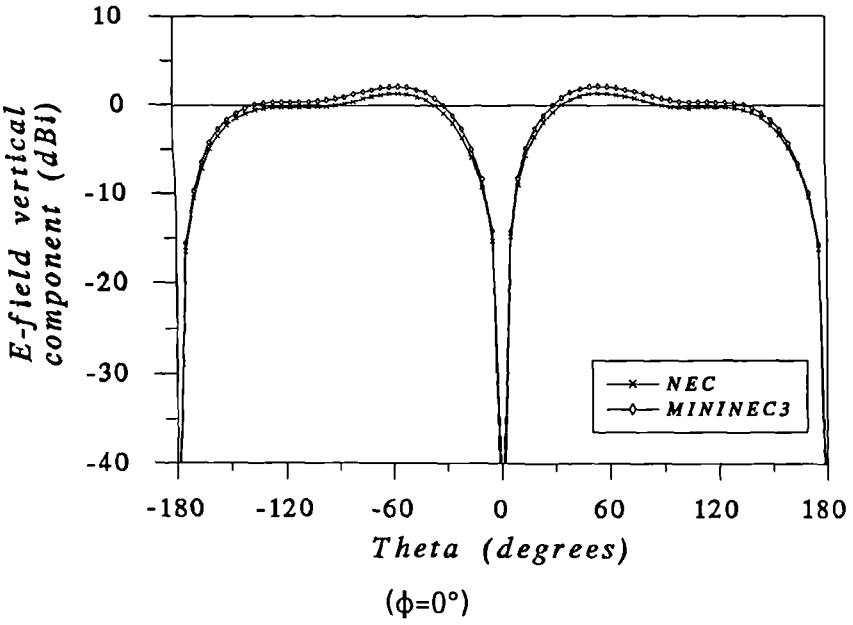

Figure 5.13 Variation in elevation of the *E*-field vertical component of the far-field for geometrical configuration 1

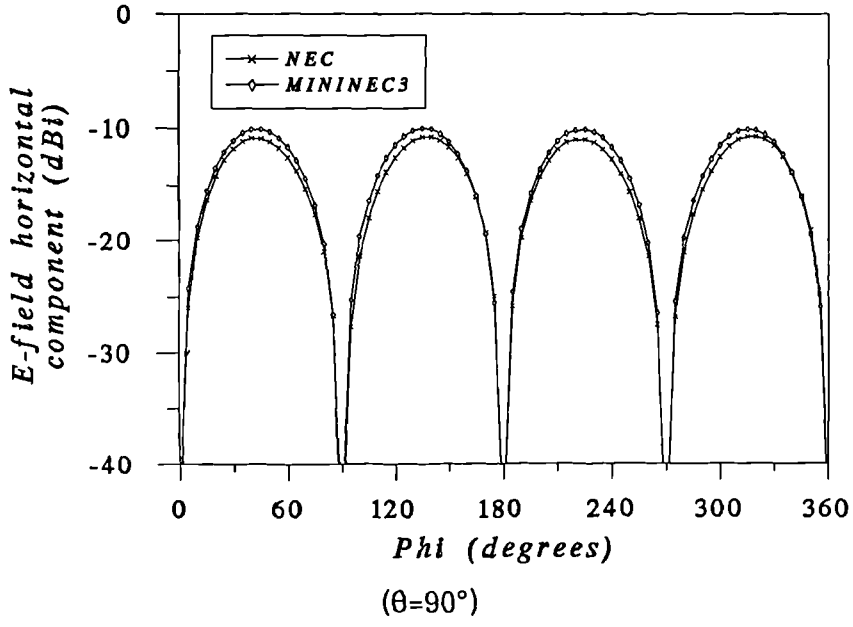

Figure 5.14 Azimuthal variation of the *E*-field horizontal component of the far-field for geometrical configuration 1

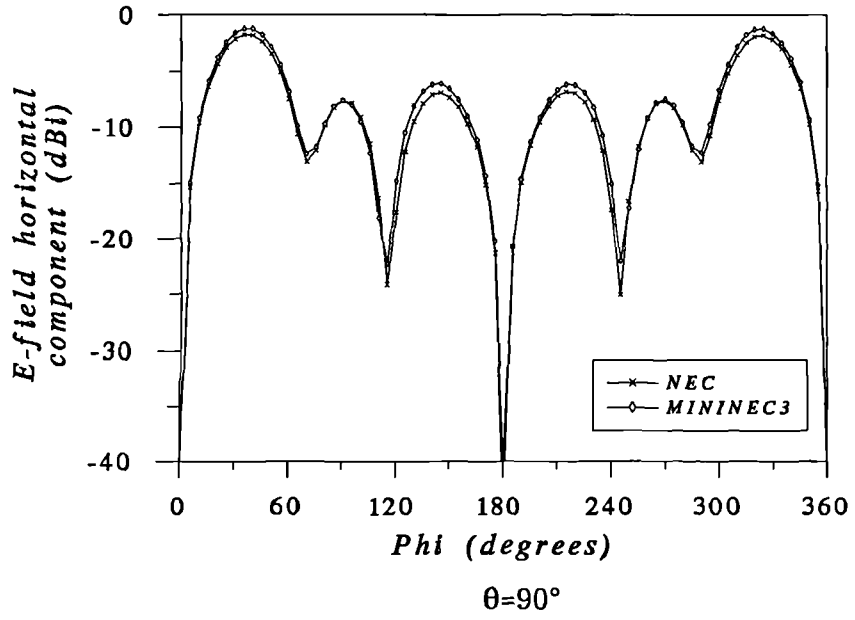

Figure 5.15 Azimuthal variation of the *E*-field horizontal component of the far-field for geometrical configuration 2

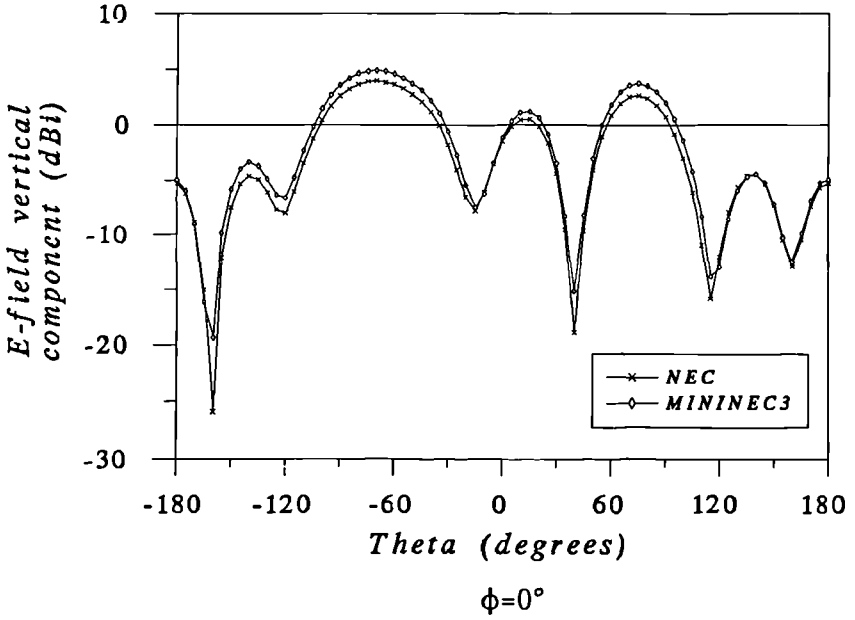

Figure 5.16 Variation in elevation of the *E*-field horizontal component of the far-field for geometrical configuration 2

sometimes a larger difference between the depths of the nulls. Figure 5.16, for example, shows a null where the difference between the two codes is around 5dB. The depth of the null though is around -20dBi and clearly there is negligible difference between the spatial far-field distribution of power predicted by both codes.

The pattern results of the third configuration yielded the largest difference between the two codes. Figures 5.17 and 5.18 show the azimuthal variation of the vertical component of the electric field for the in phase and anti-phase feed systems respectively. Further considering the horizontal component figures 5.19 and 5.20 show its variation in elevation with ϕ=90° for the same feed configurations.

Overall the agreement shown on the plots is good with the position of the numerous peaks and nulls, in general, coinciding. At the peaks the difference is again no more than 1.5dB. The greatest disagreement is in the depth of the nulls where differences of up to 5dB exist. Also noticeable is a slight spatial shift in the position of some nulls. Figure 5.20 shows the worst case.

Figures 5.13 to 5.20 show pattern sweeps that are typical of the complete set shown in appendix A. Overall, both codes show excellent general agreement for all of the configurations considered. Because of the general complexity of the resultant far-fields, both codes clearly predicted similar current distributions over the complete surfaces of the structures considered. The closeness of the results is confirmed in section 5.3.3 by the definition of a mean squared difference between the two codes over the complete sphere at infinity.

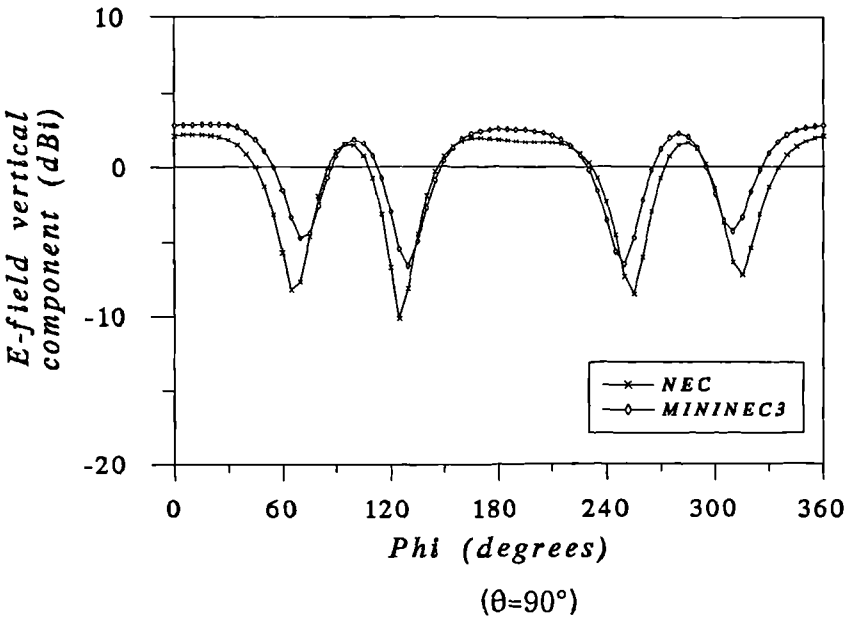

Figure 5.17 Azimuthal variation of the *E*-field vertical component of the far-field for geometrical configuration 3 with the monopoles fed in phase

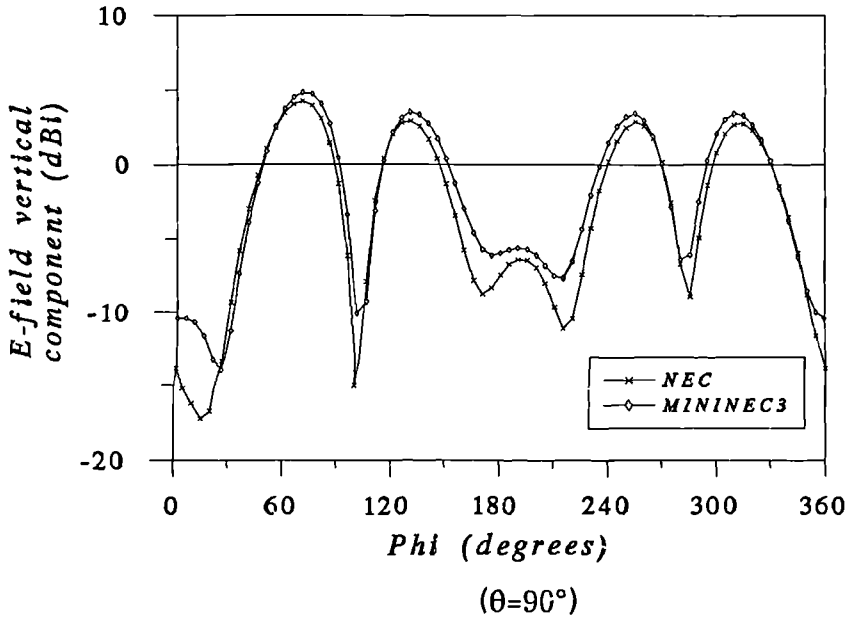

Figure 5.18 Azimuthal variation of the *E*-field horizontal component of the far-field for geometrical configuration 3 with the monopoles fed in anti-phase

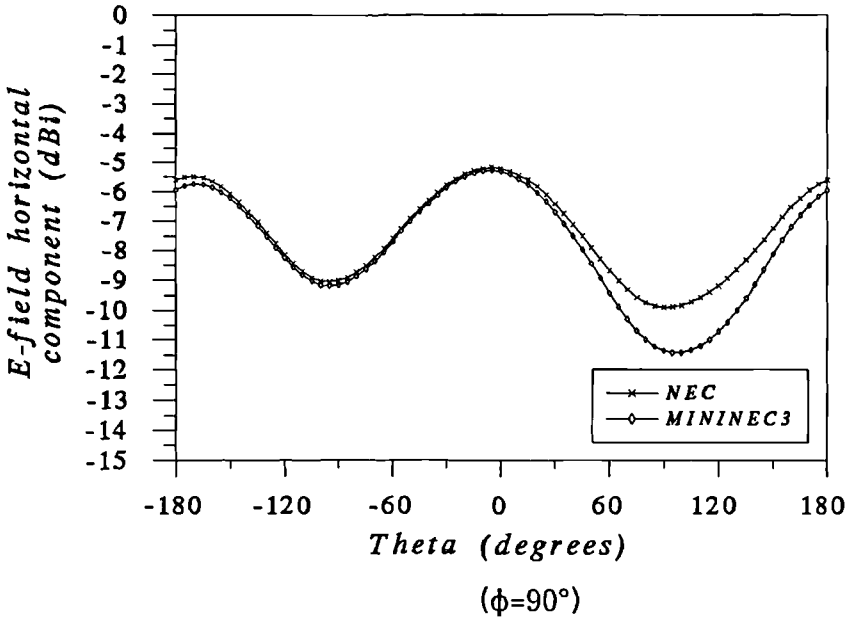

Figure 5.19 Variation in elevation of the *E*-field horizontal component of the far-field for geometrical configuration 3 with the monopoles fed in phase

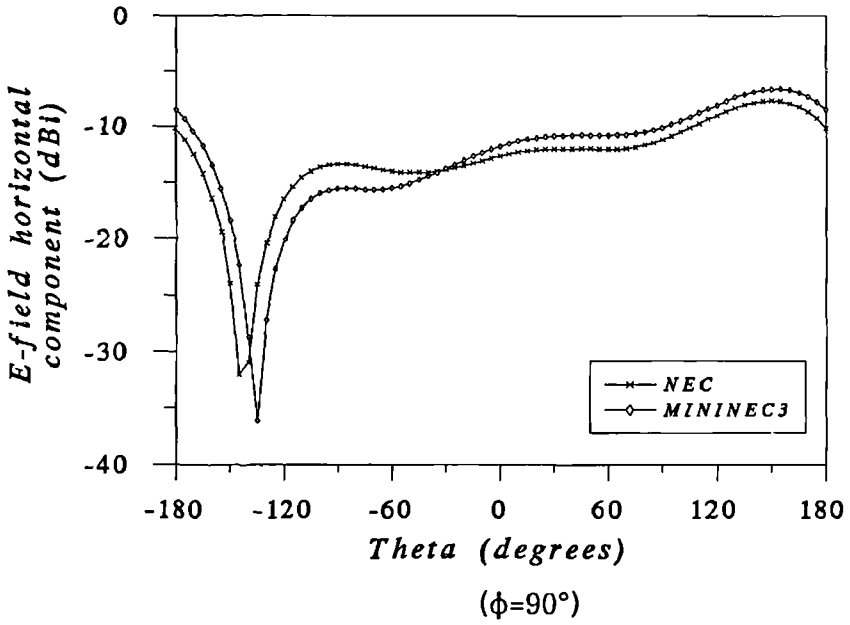

Figure 5.20 Variation in elevation of the *E*-field horizontal component of the far-field for geometrical configuration 3 with the monopoles fed in anti-phase

5.3.2.2 Input Impedance

Next considering the predicted input impedance table 5.3 shows the results obtained for the three structures using both codes.

Table 5.3 Calculated input impedance for Configuration 1 using NEC and MININEC3

Geometrical Configuration	NEC	MININEC3
1	43.34+j42.43	37.66+j18.08
2	43.12+j23.41	32.18 +j6.91
3 - fed in phase		
Monopole 1	151.64+j25.55	148.88 +j7.14
Monopole 2	57.10+j22.26	39.80 -j1.73
3 - fed in anti-phase		
Monopole 1	66.46+j21.87	54.64 +j1.28
Monopole 2	36.59+j15.21	27.45 -j4.98

Notice that the largest difference between the two results is in the reactive component. MININEC3 consistently predicted an input reactance that is substantially more capacitive than those of NEC, whereas the difference in the NEC predicted input resistance from the MININEC3 is never greater than 30%. Section 5.3.3 shows how this difference is explained by the identification of a frequency shift between the results of the two codes. Clearly as the structures considered here are close the resonance the effect is most noticeable because of the rapidly changing reactive component in this region.

5.3.3 Analysis of the Results

The field plots of the previous three sections have clearly shown that the MININEC3 code is capable of producing pattern results similar to those from NEC for complex structures represented as wire grid models. Although the level of agreement is clearly apparent by examination of figures 5.13 to 5.20, a more rigorous technique for describing the difference is sometimes more useful. Hence the method for describing the mean squared error of a synthesized pattern outlined in chapter 4 is employed here. Thus equation 4.12 which defines an inner product between two field functions A and B on the sphere at infinity may be restated as

$$\langle B,C\rangle_{S\infty} = \iint_{S\infty} B\cdot C \; dS \tag{5.2}$$

If E_{NEC} and E_{MN} are the pattern functions of NEC and MININEC3 respectively then the difference between the results of the two codes may be expressed as a relative mean squared error e. Hence assuming that the NEC results are correct the error associated with the MININEC3 results may be defined from equation 4.15 as

$$e = \frac{\left\langle (E_{MN}-E_{NEC}),(E_{MN}-E_{NEC})\right\rangle_{S\infty}}{\left\langle E_{NEC},E_{NEC}\right\rangle_{S\infty}} \tag{5.3}$$

where $0 \le e \le 1$.

Thus normalizing the patterns to radiate the same power yields the mean squared MININEC3 pattern errors shown in table 5.4.

Clearly these results confirm excellent overall agreement between the

Table 5.4 **Mean squared errors between the predicted NEC and MININEC3 radiation patterns with the structures normalised to radiated the same power**

Geometrical Configuration	E_θ Mean Squared Error	E_ϕ Mean Squared Error
1	0.0076	0.0125
2	0.0182	0.0054
3 - Feed 1	0.0228	0.0182
3 - Feed 2	0.0189	0.0087

two codes. In the worst case, obtained for the vertical component of configuration 3 with the monopoles fed in phase, the mean squared error is below 3%. These results confirm that, as previously suggested, both codes predict a closely similar overall current distribution on the complete defined wire grid of each configuration.

The greatest discrepancy between the two sets of results is clearly the input impedances and particularly the reactive component. Although there is an average difference between the resistive components of no more than 30%, MININEC3 consistently predicts a reactance that is substantially more capacitive than the NEC results. Other authors (eg.Lewallen 1991) have identified that MININEC3 introduces a frequency shift in the results. The overall dimensions of the structures considered here are around the first natural fundamental resonance at the defined frequency, where generally the reactive component of the input impedance is changing rapidly. Table 5.5 shows the results of the NEC simulations for each configuration with an empirically determined reduction in

frequency of 5%. The initial MININEC3 impedances are also shown for comparison.

Table 5.5 Comparison of calculated MININEC3 and frequency shifted NEC input impedance results

Geometrical Configuration	NEC Frequency = $0.95f_0$	MININEC3 Frequency = f_0
1	34.46+j23.21	37.66+j18.08
2	42.40 +j9.76	32.18 +j6.91
3 - fed in phase		
Monopole 1	150.70 +j9.21	148.88 +j7.14
Monopole 2	52.15 +j7.26	39.80 -j1.73
3 - fed in anti-phase		
Monopole 1	64.39 -j1.42	54.64 +j1.28
Monopole 2	35.12 -j1.34	27.45 -j4.98

This negative frequency shift of 5% clearly reduces the difference between the two sets of impedance results. Whereas the resistive component changes negligibly, the input reactance of each feed-point is reduced considerably.

The MININEC3 code has been shown to be capable of the comparable emulation of the current distribution compared to NEC. This is confirmed by the good agreement obtained between pattern and impedance results. The codes use different methods of segmentation and dissimilar expansion and testing functions to model the current distribution and minor differences in results would therefore be expected. The level of agreement obtained though, especially with the far-fields, proves the validity of using the MININEC3 code to model complex

structures represented as wire grid models. The results of this section also concur with those of other authors who have found a frequency shift between different codes. The 5% reduction in frequency employed in the NEC analysis greatly reduced the difference form the MININEC3 input reactance results, although there was negligible change in both the input resistance and far-field pattern. The following section further validates the MININEC3 code by using relevant experimental data. The practical significance of the frequency shift is also investigated.

5.4 Experimental Data

The previous section has demonstrated that there is excellent overall agreement between the NEC and MININEC3 codes when modelling wire grid structures appropriate to the work of this thesis. This section shows further validation of MININEC3 by the modelling of a number of practical antenna configurations that have been investigated experimentally in the literature. The types of structures chosen as before, are particularly relevant to the geometrical configurations that are analyzed in future chapters. It was also thought beneficial that MININEC3 data was compared to experimentally determined results as well as those from another Method of Moment code. The work described in this section further addresses the previously identified modelling issues such as the accurate determination of input impedance and overall segmentation density. Also 5.4.3 illustrates the difficulties associated with making practical measurements by the comparison of the MININEC3 determined

input impedance of a cubical box with the experimental results.

5.4.1 The V Dipole Antenna

The input impedance of a centre fed V dipole antenna in free space was determined analytically by Jones (1976). His results showed excellent agreement with experimental data. The antenna configuration used is as shown in figure 5.21. Jones varied the angle ψ between the two wires from 30° to 180° in 30° increments.

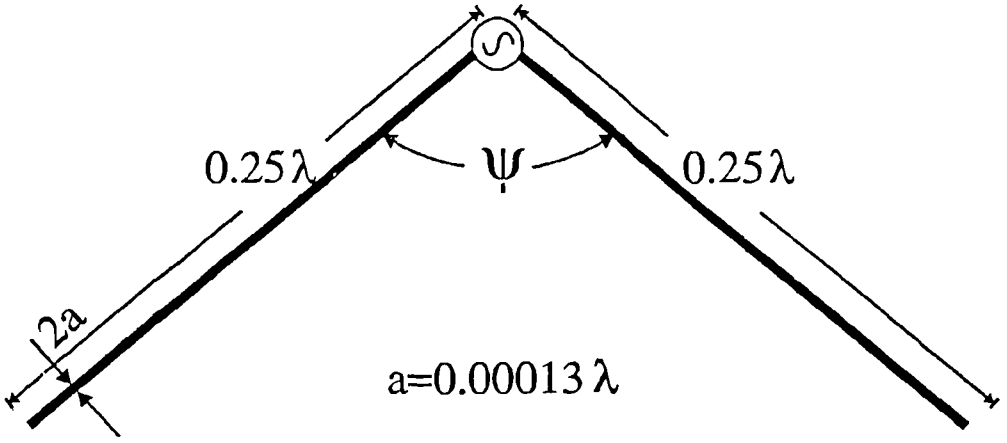

Figure 5.21 V dipole antenna with dimensions

In using a Method of Moment code to model this configuration it should be noted that acute angles between wires have been shown to produce erroneous impedance results (eg. Austin 1993). This may be attributed to the complex nature of the near field at the local area around the junction. Also Trueman and Kubina (1990) have associated such modelling errors in NEC to the close proximity of match points between adjacent segments.

For the MININEC3 model three uniform density segmentation schemes

were initially employed as shown in table 5.6. Schemes 2 and 3 give higher densities than those recommended in chapter 2. A graded segmentation scheme was also considered each wire was divided into two equal sections. For the section including the feed-point a higher segmentation density was employed. This is also detailed in table 5.6. Figures 5.22 and 5.23 then show the resulting predicted input resistances and reactances and compares them to those of Jones.

Table 5.6 Segmentation schemes for the V dipole antenna

Scheme	1	2	3	4
Total number of segments	12	20	40	30 (20 Region 1) (10 Region 2)
Segments per wavelength	24	40	80	80 - Region 1 40 - Region 2

Figure 5.22 shows that the MININEC input resistances obtained with all of the segmentation schemes are indistinguishable from the experimental data. For the input reactance however it is noticeable that as ψ is reduced the difference between the MININEC3 and the experimental results is substantial for the lower density segmentation schemes. Clearly the results obtained with segmentation schemes 1 and 2 give a substantially larger error than those of schemes 3 and 4.

The results show that the MININEC3 code is capable of the reliable representation of geometrical configurations with acute angles. This is an important aspect of the work of this thesis. Many of the structures that are

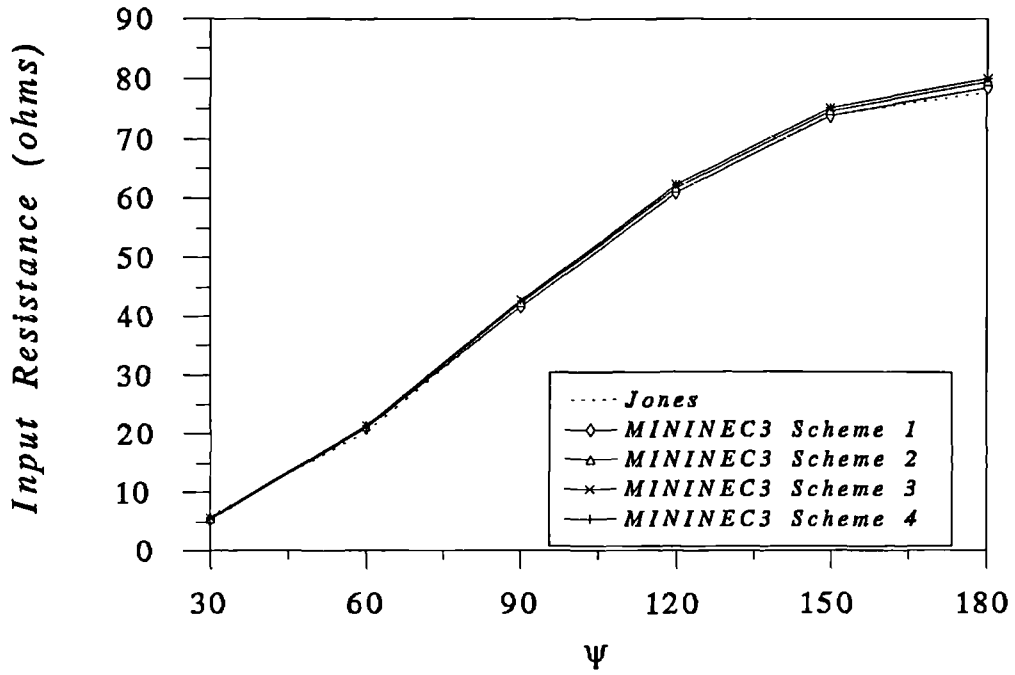

Figure 5.22 V dipole input resistance variation for different segmentation schemes

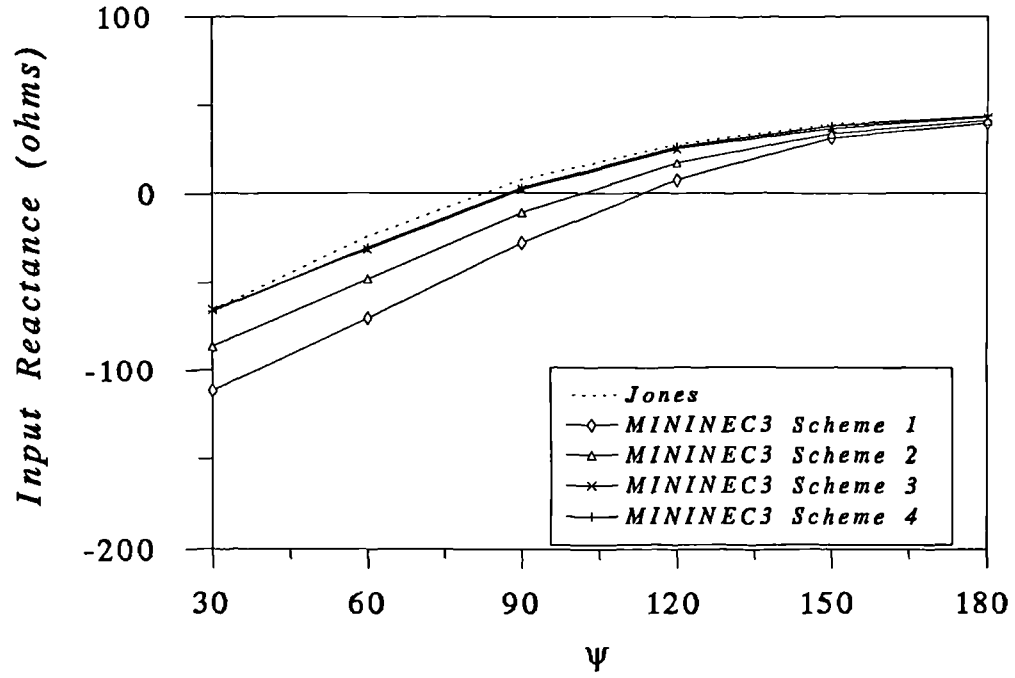

Figure 5.23 V dipole input reactance variation for different segmentation schemes

analyzed in future chapters contain conductors orientated in this way. It is apparent that to model the wire junction accurately a relatively dense segmentation scheme must be employed for $\psi<90°$. Here 80 segments per wavelength were found to be satisfactory. Comparing the results of schemes 3 and 4 it is clear that they have similar accuracy. It is concluded therefore that only in the local area around the junction including the feed-point is it necessary to use this relatively high density. The advantage of employing scheme 4 compared to scheme 3 is the reduction of the total number of segments by 25%, thereby reducing both the required computer memory and CPU time.

5.4.2 Analysis of Vehicle Mounted Antennas

The far-field patterns of a vertical monopole antenna mounted on a motor vehicle have been experimentally investigated by Jesch (1985). Various different antenna positions were examined at a number of frequencies. Najm (1992), used NEC to model some of these configurations in order to assess the validity of that code. For his application he concentrated upon the 40MHz results. At this frequency, where the wavelength is 7.495m, the largest dimension of the vehicle is approximately the first natural resonant length. It is therefore expected that current flow on the body of the vehicle will produce an azimuthal pattern that is considerably different from that of a base fed monopole alone.

In constructing a wire grid model to verify the MININEC3 code a similar procedure to that of Najm (1992) was followed. He found that many of the vehicle's styling features such as small indentations on the body could be ignored.

Hence a simplified box model of the vehicle is shown in figure 5.24. Also shown are the three positions at which a vertical monopole was mounted by Jesch. Figure 5.25 then shows the resulting grid model with the monopole mounted in the centre of the roof. For the grid the same modelling criteria as before were employed. Hence a maximum grid spacing of $\lambda/10$ was enforced and the so-called "twice area" rule was applied to determine the appropriate wire radius. Notice also that in the area around the feed-point the mesh density has been doubled compared to the remainder of the vehicle. This is to address the feed-point modelling issues identified in previous sections. This action was also repeated for both the front and rear wing mounted monopoles.

The measurement test range used by Jesch is shown schematically in figure 5.26. This yields a zenith measurement angle of θ=88.48°. In the MININEC3 model the metal turntable was assumed to be perfectly conducting. Also the characteristics of the surrounding ground were not specified by Jesch. Here the typical values for the conductivity and permittivity of clay soil listed by Kraus (1988 p851) were employed in the MININEC3 Fresnel integral determination of the far field, where ϵ_r=14 and $\sigma=5.0\times10^{-3}$ Sm^{-1}.

It should be noted that in Jesch's experimental measurements only the vertical component of the far field was measured. Also no absolute values of field strength were stated. The following field plots which compare experimental with MININEC3 predicted data are therefore normalized to the maximum value in both cases.

Figures 5.27 to 5.29 show the normalized and MININEC3 predicted vertical

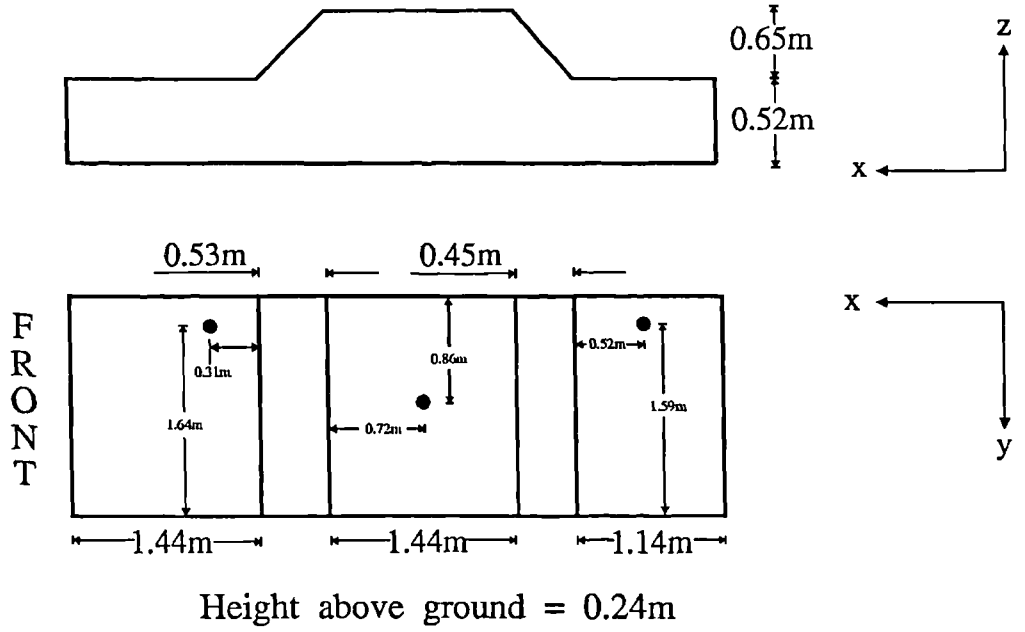

Figure 5.24 Simplified motor car box model

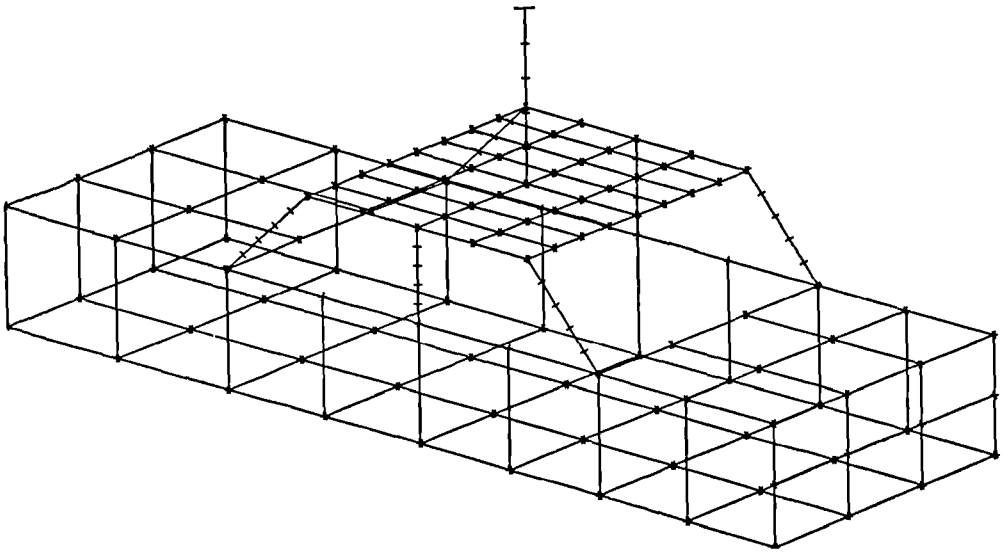

Viewing angles θ=70° ϕ=130°

Figure 5.25 Motor car wire grid model with centre roof mounted vertical monopole antenna

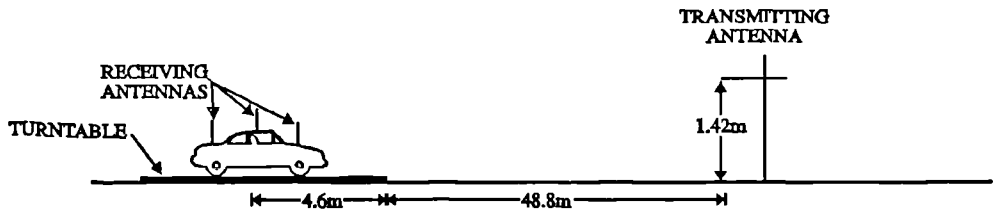

Figure 5.26 Schematic representation of the far-field measurement test range.

far-fields for the three vehicle monopole antenna configurations. The plots show that satisfactory agreement is obtained in all three cases. For the centrally mounted roof antenna the pattern is predominantly circular, although a reduction of around 1dB from the maximum is present in the direction of the sides of the vehicle (ie. ϕ=90° and 270°). For the wing mounted antennas both experimental and predicted results show the maximum field lying along the diagonal from the antenna to the opposite corner of the vehicle, although for the front wing antenna a spatial shift of around 20° is noticeable between the two results. Table 5.11 shows both the maximum difference and mean absolute difference between the experimental and predicted results. The roof mounted monopole with its circular azimuthal pattern clearly gives the best agreement with a mean absolute difference of less than 0.5dB. Good agreement between predicted and experimental data is also obtained for both of the wing mounted monopoles with a mean absolute difference of around 1.5dB. In both cases the predicted position of the maximum field is in the diagonal direction away from the monopole clearly shows that an appropriate current distribution is enforced on the structure.

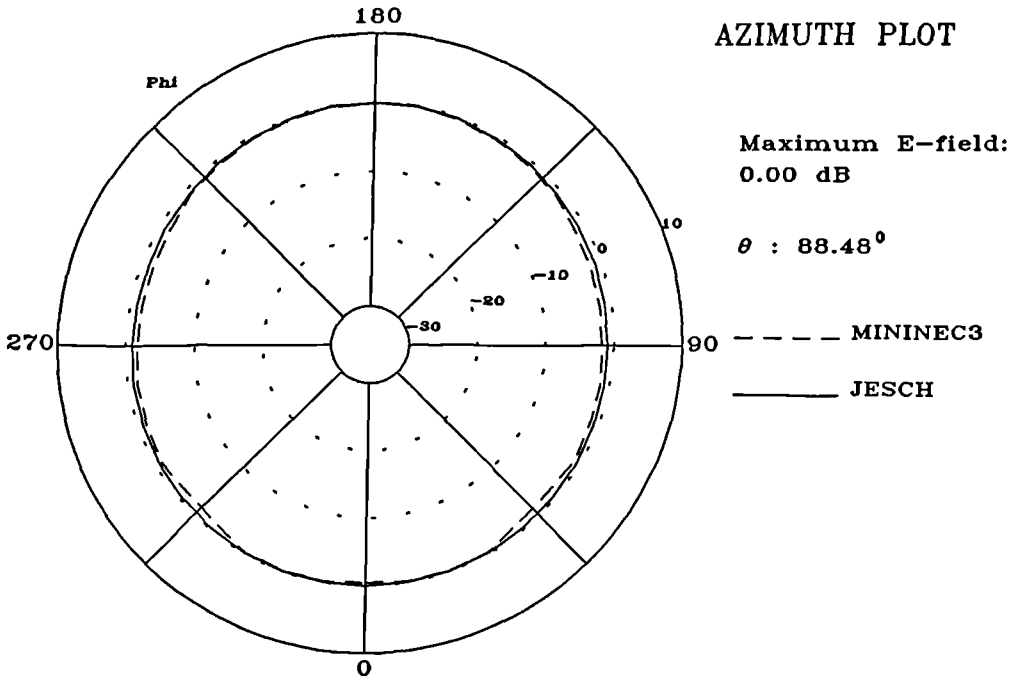

Figure 5.27 Comparison of Jesch's experimental and the MININEC3 predicted results for the motor vehicle with the centrally mounted roof monopole.

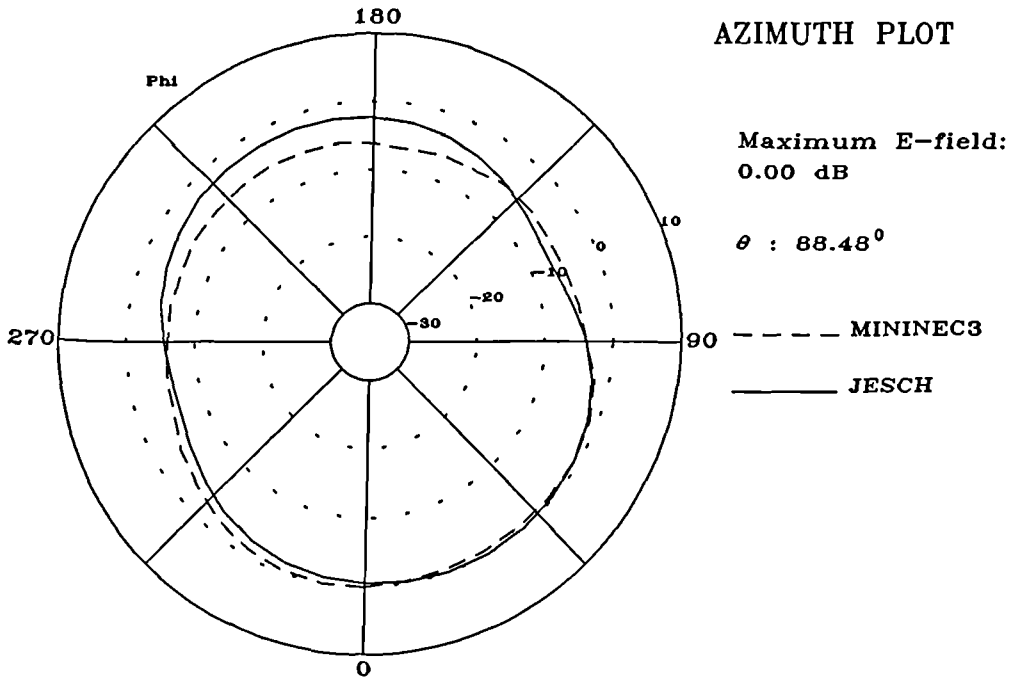

Figure 5.28 Comparison of Jesch's experimental and the MININEC3 predicted results for the motor vehicle with right rear wing mounted monopole.

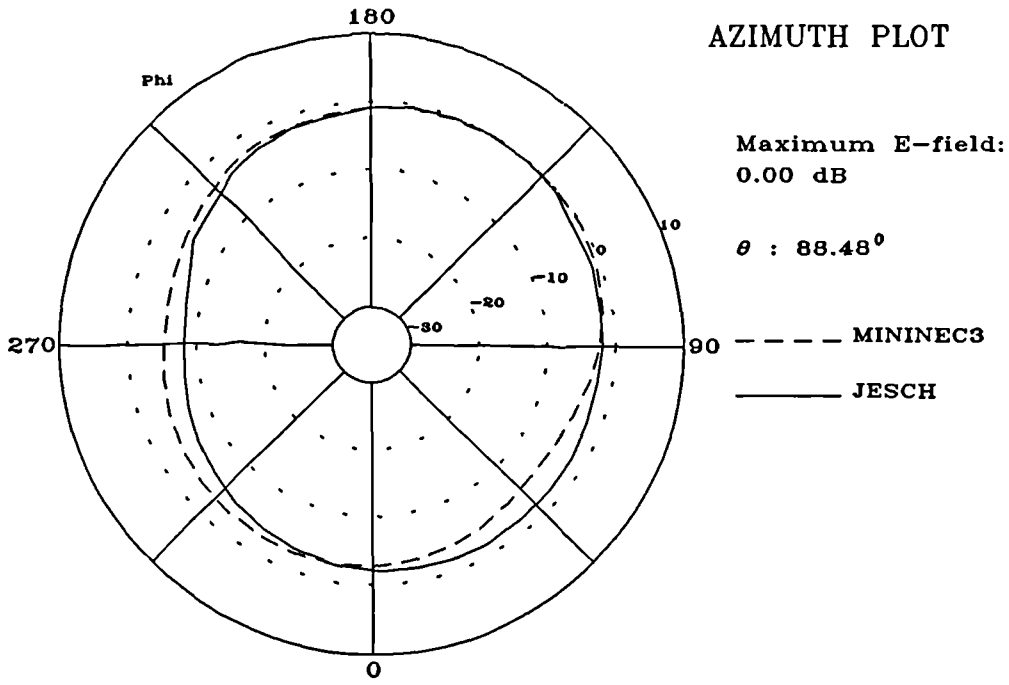

Figure 5.29 Comparison of Jesch's experimental and the MININEC3 predicted results for the motor vehicle with the right front wing mounted monopole.

Table 5.7 Maximum and mean absolute difference between Jesch's experimental and the MININEC3 predicted far-field pattern results

Monopole antenna mounting position	Maximum difference (dB)	Mean absolute difference (dB)
Roof	1.047	0.446
Rear wing	3.833	1.456
Front wing	3.371	1.363

5.4.3 Monopole antenna mounted on a conducting box

Bhattacharya *et al* (1987) measured the input impedance of a monopole antenna mounted on a conducting metal box. The structure was a five sided 10cm cube centrally attached to a 105cm square conducting ground plane. A base fed 6cm vertical monopole antenna was mounted at various positions on the upper face of the cube. The radiation patterns of the same configurations were later measured by Chu *et al* (1990). The configuration is shown in figure 5.30 along with two typical monopole positions which were used for a MININEC3 simulation. The frequency range considered was 1-2GHz.

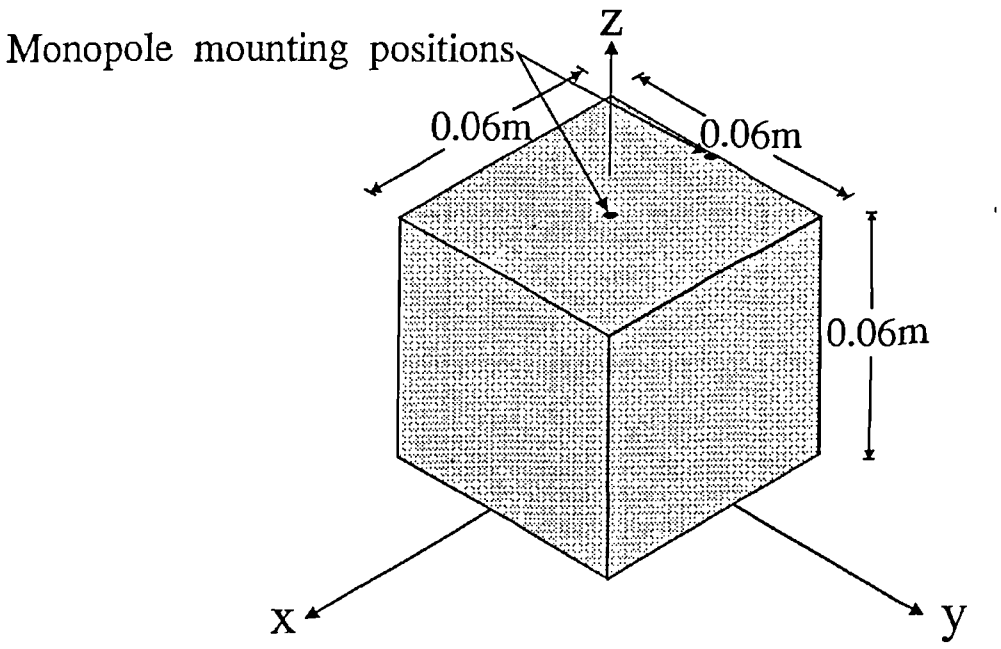

Figure 5.30 Conducting box configuration with monopole mounting positions

As before, a wire grid model was set up for the MININEC3 analysis. Each surface of the box was divided into a 6x6 mesh, corresponding to a grid spacing of 0.0556λ and 0.1111λ at 1GHz and 2GHz respectively. The so called "twice

area" rule was again applied and yielded a uniform wire radius of 0.027m. Figures 5.31 and 5.32 show the resulting wire grid models for the two chosen monopole positions. In the MININEC3 simulation it was assumed that the wires were perfectly conducting. It was also assumed that the finite dimensional conducting ground plane used in the experimental investigation was large enough, in terms of wavelengths, to be replaced by an infinite perfectly conducting ground plane in the computer simulation. This approximation dramatically reduces the amount of required computer time.

Figures 5.33 to 5.36 compare the results obtained with MININEC3 for the input admittance of both configurations to the experimental data. This G and B representation was chosen rather than input impedance by Bhattacharya *et al* to more easily illustrate the resonances associated with each structure.

The computed and experimental results for both monopole configurations show a similar trend with a clear well defined resonance. In all cases the peak values differ somewhat and a frequency shift of around 5% is noticeable in the position of the resonances. To understand the reason for these differences the ability of the wire grid box to accurately model the continuous surface was investigated. Thus the model was changed by incorporating the critical modelling guidelines that have been examined in previous sections. The centre-mounted monopole case only was considered. Firstly, to increase the accuracy of the feed-point near field the density of the mesh on the upper surface was doubled as shown in figure 5.37. Secondly the overall area factor of this denser model was doubled. Figures 5.38 and 5.39 show the resultant calculated input admittances

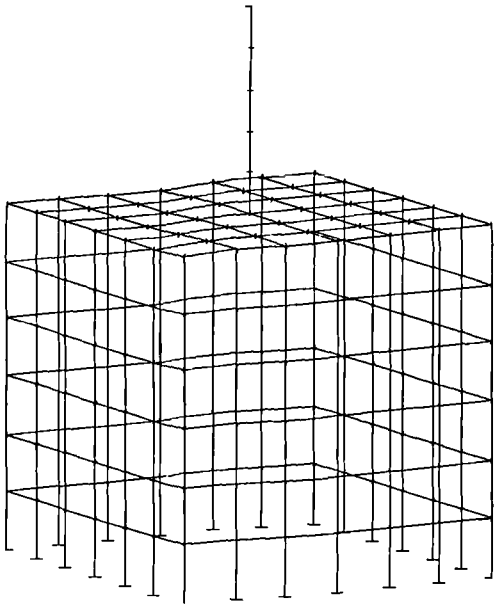

Viewing angles θ=70° ϕ=50°

Figure 5.31 Wire grid representation of the conducting box with centre mounted vertical monopole

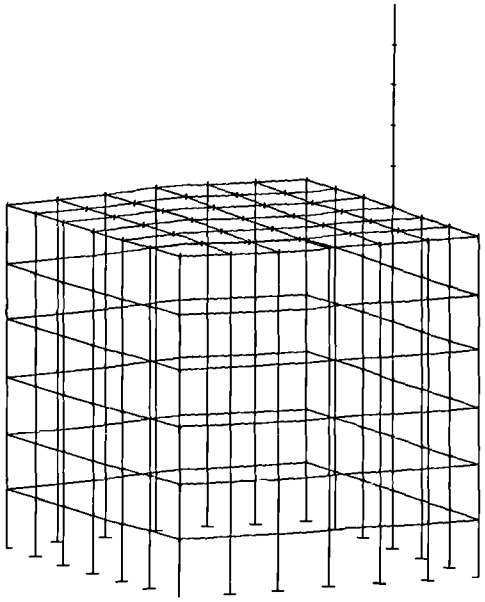

Viewing angles θ=70° ϕ=50°

Figure 5.32 Wire grid representation of the conducting box with edge mounted vertical monopole

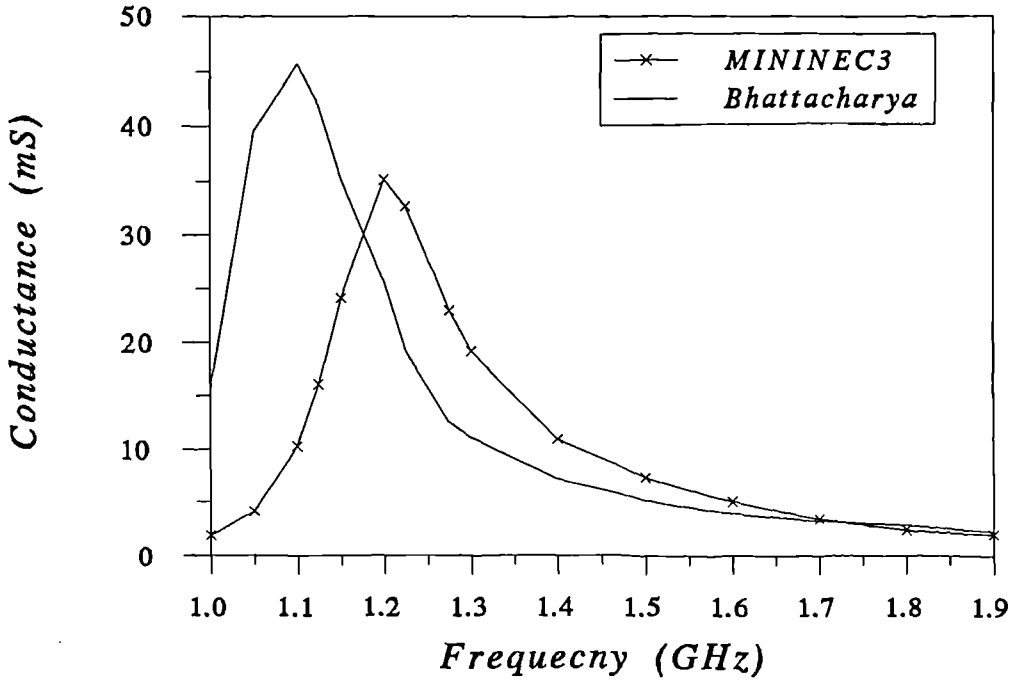

Figure 5.33 Comparison of experimental and MININEC3 predicted input susceptance with the monopole in the centre

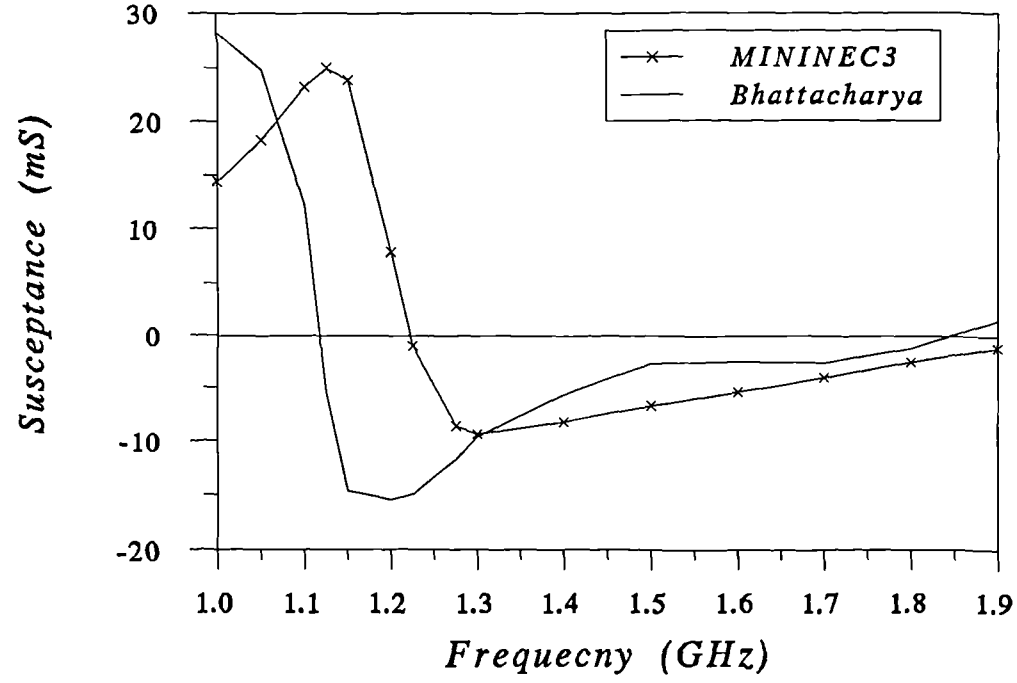

Figure 5.34 Comparison of experimental and MININEC3 predicted input conductance with the monopole in the centre

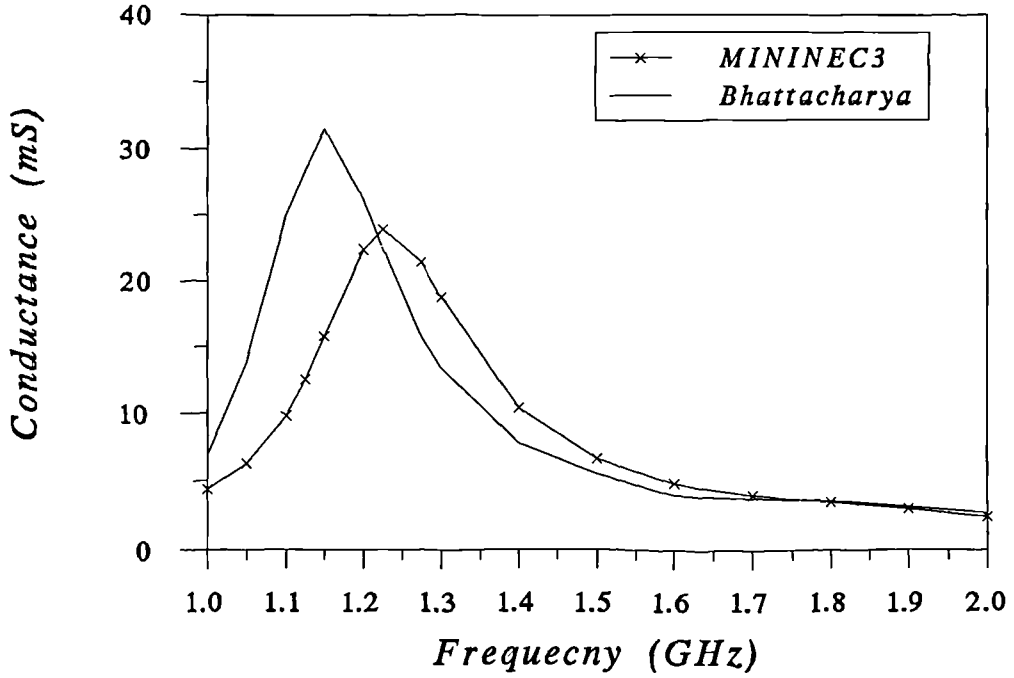

Figure 5.35 Comparison of experimental and MININEC3 predicted input conductance with an edge mounted monopole

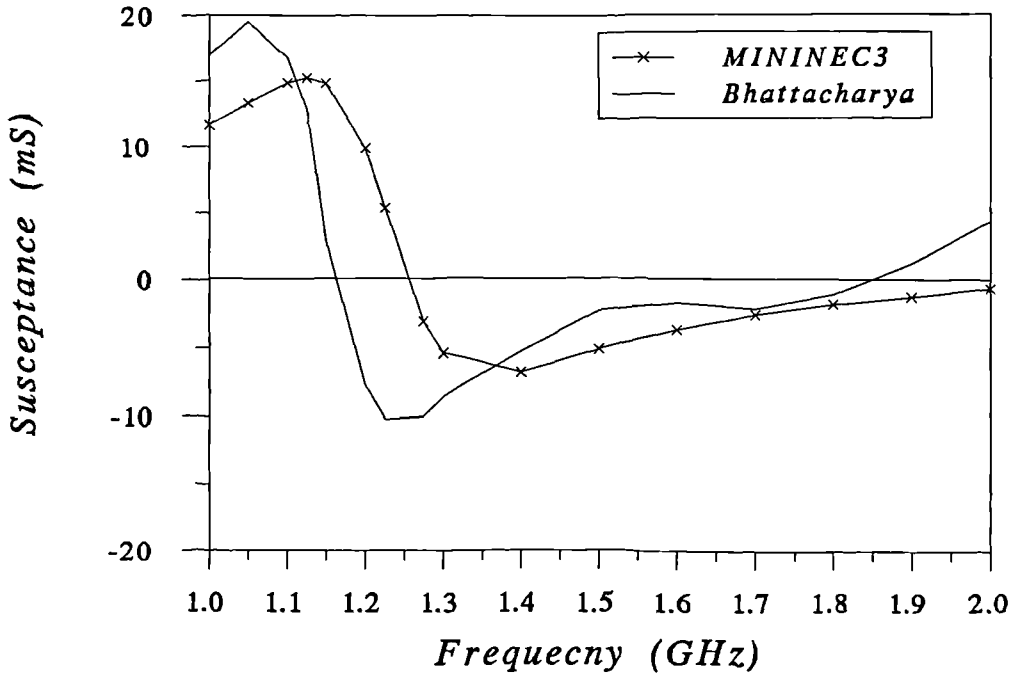

Figure 5.36 Comparison of experimental and MININEC3 predicted input susceptance with an edge mounted monopole

for the same frequency range as before.

It is noticeable that the results obtained with both of the latter models are only marginally more accurate than those of the original. The second model with both the denser upper face and the increased area factor does shift the position of the resonance but only by less than 1%.

The above results show that the original MININEC3 wire grid model had converged in terms of the necessary grid density and area factor. It therefore yielded the best possible representation of the defined geometrical configuration using this code. The discrepancy between predicted and experimental results is therefore likely due to a factor introduced by the measurement system. Cox (1989) compared experimental and NEC-predicted input impedance of a number of HF antennas on aircraft. He attributed differences which existed between predicted and experimental input impedance to dissimilarities in the modelled and actual feed-point. He also showed how differences in the position of the actual point of measurement introduced a predominantly reactive differential between the results. Considering the MININEC3 model of the centre mounted monopole the difference between the predicted and experimental reactance at each frequency corresponded, within ±5%, to an inductive offset in the MININEC results of L=2.938nH. Introducing this inductance in series with the MININEC3 predicted impedance yields the *G* and *B* plots shown in figures 54 and 55.

Clearly this action reduces both the frequency offset and the difference in the magnitude of each component. These results now show markedly better agreement, with the position of the resonance coinciding and the peak absolute

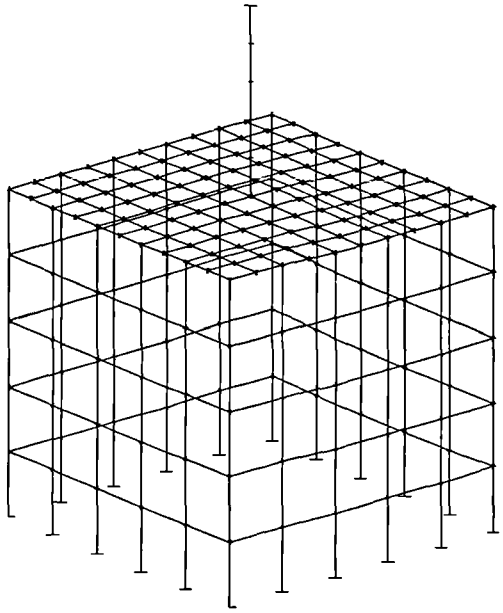

Viewing angles θ=50°, ϕ=50°

Figure 5.37 Wire grid model of the conducting box with centre mounted vertical monopole and denser top

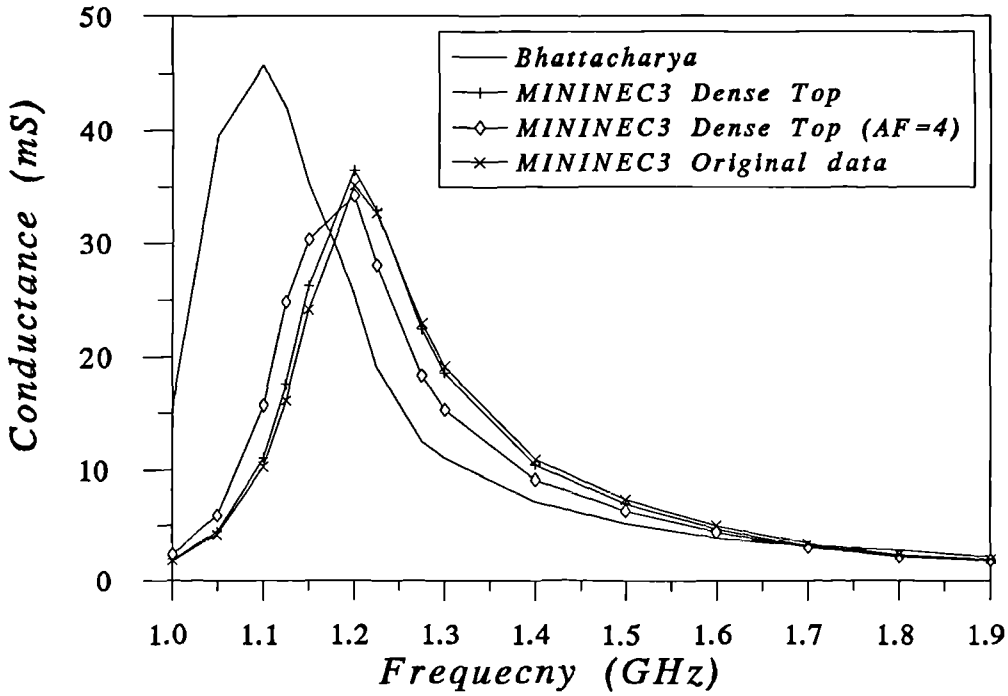

Figure 5.38 Comparison of experimental and MININEC3 predicted input conductance for the centrally mounted monopole and different box configurations

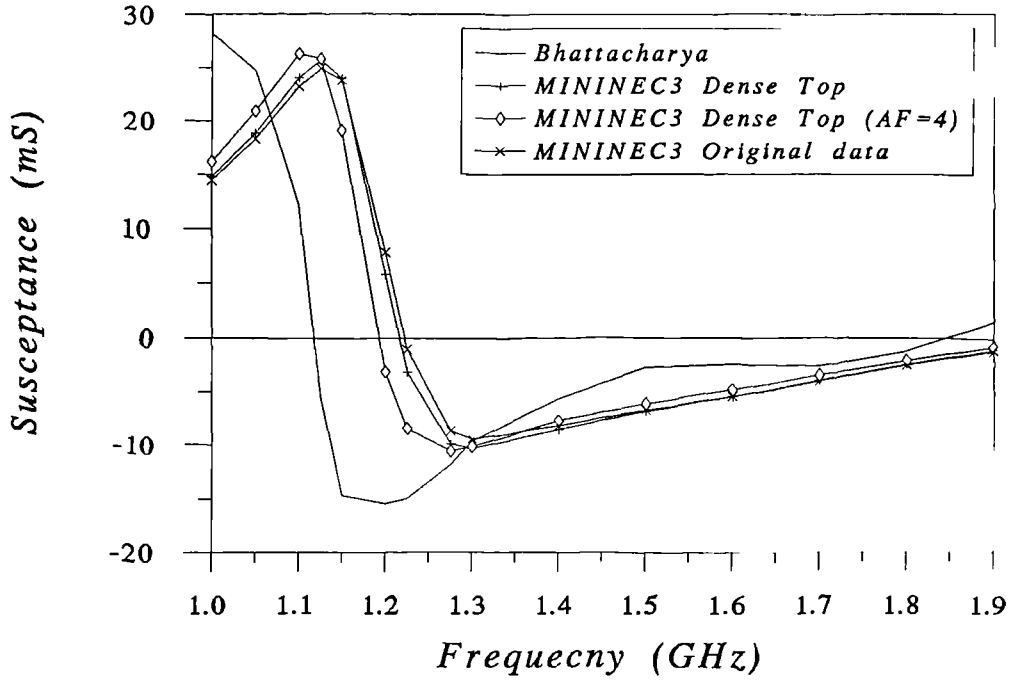

Figure 5.39 **Comparison of experimental and MININEC3 predicted input susceptance for the centrally mounted monopole for various box configurations.**

values of both G and B concurring within 10%.

5.5 Summary

This chapter has addressed the validation of the modified MININEC3 code. This was necessary both to check that the conversion from the BASIC language to FORTRAN was correct and also because of BASIC compiler constraints which limited the number of available segments. The code has not previously been used to model complex structures represented as wire grid models.

Section 5.2 proved the validity of the FORTRAN implementation by comparison with the analytical results of King and Harrison (1969) for straight wire, centre-fed dipoles. In that section the general segmentation rules expressed by Logan and Rockway (1986) were also examined. The results show that their

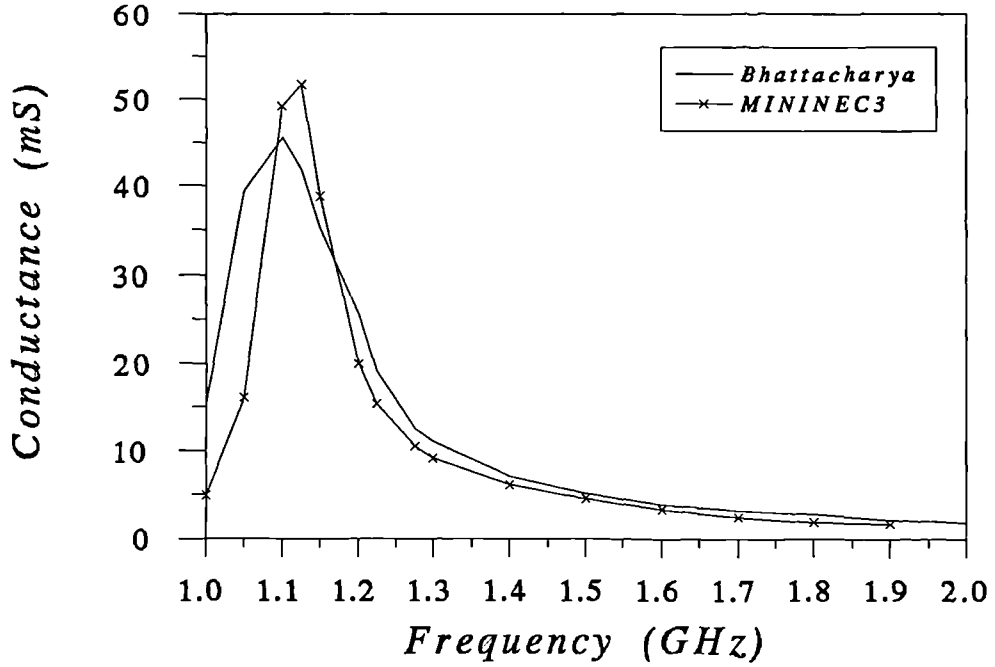

Figure 5.40 Comparison of experimental and MININEC3 predicted input conductance for the centrally mounted monopole with a shunt inductance introduced into the predicted results

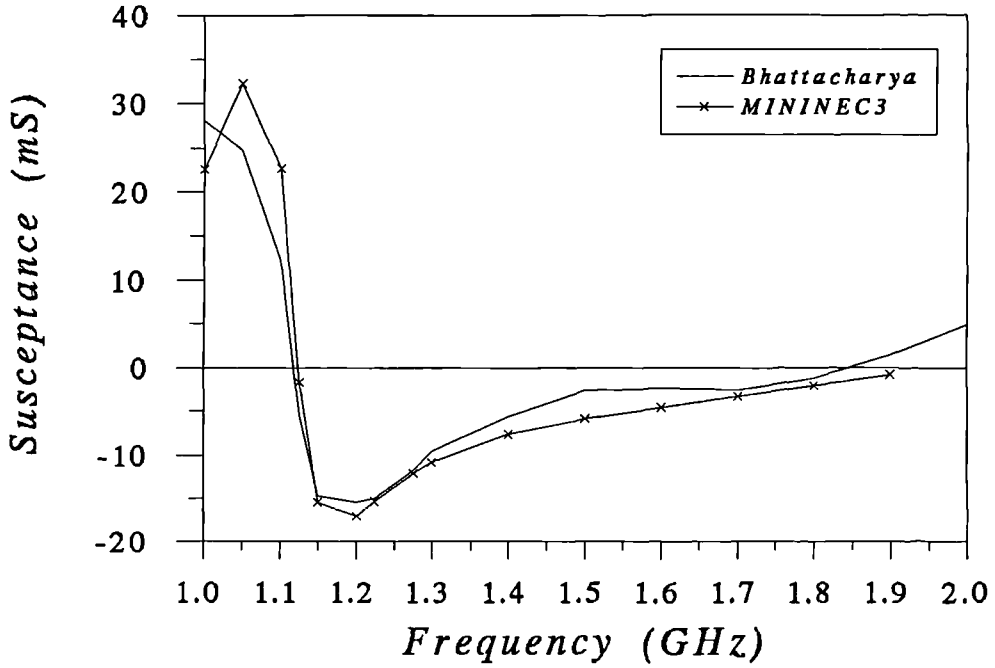

Figure 5.41 Comparison of the experimental and MININEC3 predicted input susceptance for the centrally mounted monopole with a shunt inductance introduced into the predicted results

general rule of 20 segments per wavelength of wire is adequate for the determination of far-fields. In the critical area around the feed region however a more accurate representation of the near-field is necessary for the accurate determination of input impedance. For the geometrical configuration considered, 50 segments per wavelength of wire were required to yield accurate input impedance. This density was employed within approximately 0.2λ of the feed-point.

In section 5.3 the ability of the modified MININEC3 code to model complex structures represented as wire grids was investigated. Three structures were considered consisting of various plate and box configurations on which vertical base-fed, quarter-wave monopoles were mounted. The results obtained were compared to the NEC code. The dimensions were chosen such that the structures were in the vicinity of their first natural resonance. This ensured that substantial currents were induced not just on the monopole but also on the mounting structure thus producing complex far-fields. Numerous peaks and nulls were obtained to compare the two codes. The overall agreement between them was excellent. In the worst case there was a 3% mean squared error between the far-field patterns of the most complex structure. The analysis also confirmed the existence of a frequency shift between the results of the two codes. Excellent agreement between the input impedance predicted by the codes was achieved if an empirically derived 5% differential in the frequency of operation was defined.

Section 5.4 demonstrated the ability of the MININEC3 code to accurately simulate various antenna configurations that have been studied experimentally.

In section 5.4.1 the recognised modelling problem of acute angles between wires was investigated. Excellent agreement between experimentally confirmed analytical results and MININEC3 was shown. In the local area around the junction of the wires a denser than normal segmentation scheme was required for V angles of 90° or less. The most accurate results were obtained when 80 segments per wavelength were used within 0.125λ of any acute angled junction.

In sections 5.4.2 and 5.4.3 the experimentally derived results of a motor vehicle and a conducting box were used to validate MININEC3. The motor vehicle's measured far-fields were compared to those predicted with MININEC3. Excellent overall agreement was obtained for a vertical monopole mounted at three different positions with an average absolute difference of no more than 1.5dB. Section 5.4.3 described the use of the MININEC3 code to simulate the input admittance of an monopole antenna mounted at various positions on a conducting cube. This section highlighted the difficulties of making practical measurements. Initially the code predicted the basic trend of the experimental G and B plots but with a frequency offset and a difference in the peak values. Adding a shunt inductance to the MININEC3 results improved the accuracy markedly such that the position of the resonance coincided exactly with the experimental data and the difference in the peak values was less than 10%.

In conclusion this chapter has demonstrated the ability of the modified MININEC3 code to accurately model complex structure antenna characteristics. For the geometrical configurations considered it is clear that the results obtained are as accurate as those possible using other codes, such as NEC, but

with the advantage in this application that it generates a symmetrical generalised impedance matrix. Overall the results show that when modelling for far-field the general segmentation rule of 20 segments per wavelength of wire is adequate. Considering wire grid modelling using a grid spacing of $\lambda/10$ and the "twice area" rule for determining the radius yielded excellent overall pattern agreement for a number of dissimilar complex geometrical configurations. The most important aspect of all the results is the importance of modelling critical regions accurately for the determination of input impedance. For two of the configurations considered it was necessary to use a segmentation density of up to 80 segments per wavelength of wire to obtain accurate predictions of input impedance.

CHAPTER 6

THE APPLICATION OF CHARACTERISTIC MODES FOR ANTENNA ANALYSIS AND FAR-FIELD SYNTHESIS

6.1 Introduction

The previous chapter examined the ability of the modified MININEC3 Method of Moments code to accurately predict the radiation characteristics of complex conducting structures and their antennas. Excellent overall agreement was obtained with various NEC-predicted data and also with available analytical and experimental data. Chapters 3 and 4 demonstrated how the technique of Characteristic Modes presented an alternative formulation of the Method of Moments. Whilst identical results, compared to conventional implementations, are obtained for antenna radiation characteristics, many clear advantages of a modal approach have been illustrated.

The purpose of this chapter therefore, is to demonstrate the practical considerations of using the modified MININEC3 code as the basis of a suite of general purpose computer programs for Characteristic Modal antenna analysis and far-field pattern synthesis. Thus in section 6.2 the implementation of the software necessary firstly to calculate the Characteristic Modes and then to optimise them to produce desirable far-fields is described. These routines are general purpose and are applicable to both the modes of complete, continuous structures or for the constrained port modes described in chapter 3. Flow charts

are included to illustrate the features of each routine.

Section 6.3 begins with an analysis of the Characteristic Modal sets of a number of relatively simple antenna configurations. The results demonstrate how each individual mode current is related to a natural resonances of a structure. Also the significance of both the modal eigenvalue and the feed-point position in controlling a mode's contribution to the overall radiation from a structure is investigated. The results also clearly show how greater insight is obtained into the radiation characteristics of structures compared to the conventional Moment Method technique.

In section 6.4 far-field pattern synthesis using Characteristic Modes is demonstrated. The suitability of using these modes compared to the other sets of functions described in chapter 4 is clearly evident. Unlike the latter, Characteristic Modes are related to the generalised impedance matrix of the structure with the ease by which each may be excited clearly specified by the associated eigenvalue. This section also shows how a trade-off between the accuracy of the synthesized far-field and the relative complexity of the feed-system necessary to physically realise it may be achieved.

6.2 Code Implementation

6.2.1 Modal Calculation Routine

Chapter 3 has discussed the necessity of using a Galerkin based Method of Moments code for the calculation of Characteristic Modes. In chapter 5 the accuracy of the MININEC3 code which is Galerkin, using pulses for both

expansion and testing, was verified. This code was therefore used as the basis of a general purpose a Characteristic Mode calculation routine for arbitrary conducting structures.

The Characteristic Modes of any structure are defined by equation 3.33, which is repeated here for convenience:

$$[X]I_n = \lambda_n[R]I_n \tag{6.1}$$

where $[R]$ and $[X]$ are the resistive and reactive components of the generalized impedance matrix $[Z]$. This equation defines a set of modal currents I_n and associated eigenvalues λ_n for any continuous structure. Section 3.3.3 showed how this equation could be modified for N-port structures where only a certain number of points on a configuration are viable for feed-points. The defining equation is identical to that of 6.1 but uses the port impedance matrices $[R_p]$ and $[X_p]$, which are defined from the original generalized impedance matrix.

To solve a weighted eigenvalue equation of this type a number of commercially available routines may be used. Harrington and Mautz (1971b) employed an IBM routine using the Jacobbi method. Hilbert *et al* (1985, 1989) used a similar IMSL routine in their Characteristic Mode analysis of log-periodic arrays. In the work described in this thesis routines from the NAG FORTRAN library (1981) were used. The accuracy of the chosen routines will be discussed in later sections by the comparison of the conventional Moment Method matrix inversion results for input impedance and far-field to those obtained by summing the appropriate Characteristic Modes.

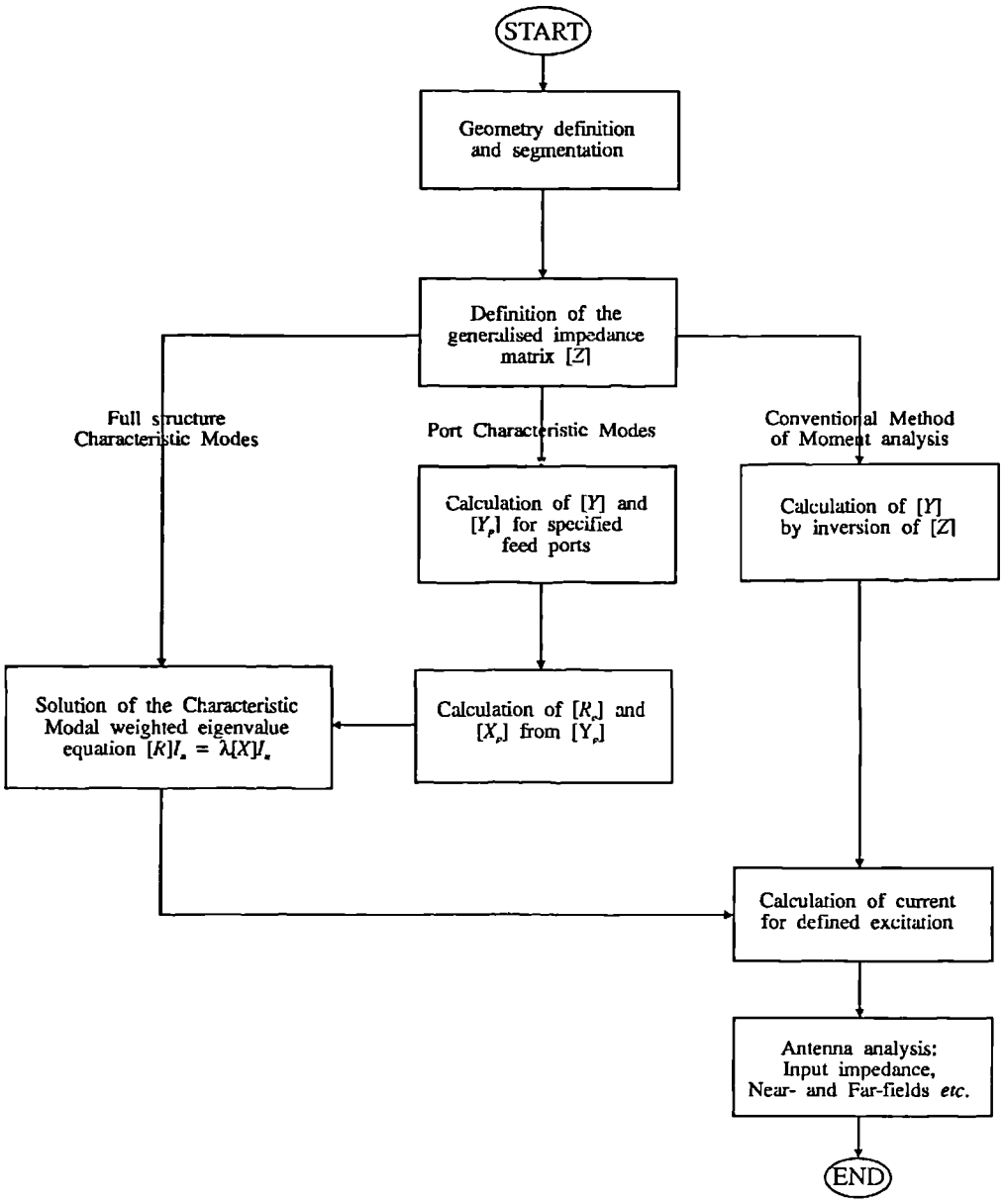

Figure 6.1 Flow Chart of the Characteristic Mode calculation routine

Figure 6.1 shows a flow chart of the resulting Characteristic Mode calculation routine. It uses the same menu-driven format as the original MININEC3 code. Notice that also included in the routine is the ability to use the conventional format of the Method of Moments by matrix inversion. This code is therefore a complete version of the MININEC3 code with all the same features

as the original. It also has the additional advantage however of being able to use Characteristic Modes for antenna analysis. Hence linearly summing the modes allows the rapid determination of identical results to those obtained using the conventional Moment Method.

6.2.2 Far-field Pattern Synthesis Routines

A suite of three pattern synthesis computer programs were implemented using the optimization principles formulated in chapter 4. These were designed to use the Characteristic Mode data calculated by the routine described in the previous section.

The first routine uses the technique of individual modal resonance described in section 4.3.3.2. This finds an entirely reactive loading scheme which resonates any desired mode current by setting the eigenvalue associated with it to zero. Equation 4.5 shows the resulting relationship which is repeated here:

$$[X]I_n = -[X_L]I_n \tag{6.2}$$

where $[X]$ is the reactive component of the generalized impedance matrix and $[X_L]$ is the loading scheme required to resonate the mode current I_n.

The next two routines allow the optimization of the complete modal set of currents to obtain the most appropriate overall current distribution. The basic calculation algorithms are those described in section 4.3.4. The technique due to Harrington and Mautz (1972) determines an equi-phase current which produces a desired far-field at any number of defined points on the sphere at infinity. The second procedure following Pozar (1984) is less constrained in that there is no

restriction on the phase of the approximating current, although the calculation must be carried out over a complete continuous region on the sphere at infinity. Both routines therefore find a factor by which each mode must be scaled to yield the best approximation to the desired field. Figure 6.2 shows a flow chart that applies to both routines. Notice that the two iterative phase and polarization modification routines are also included. These may be invoked if the phase or polarization of the final synthesized pattern are unimportant as discussed in section 4.3.6.

6.3 Antenna Analysis

6.3.1 Analysis Principles

The purpose of this section is to demonstrate the basic principles of antenna analysis using Characteristic Modes. This is achieved by the examination of a number of practical antenna configurations. Firstly, in section 6.3.2, the relationship between the modal currents of a straight wire dipole and its natural resonances are examined. Also illustrated is the importance of the eigenvalue and feed-point position in controlling a mode's contribution to the overall radiation characteristics of the antenna.

Section 6.3.3 demonstrates the usefulness of a Characteristic Modal approach to antenna analysis by examining the experimentally determined input impedance data of a centre fed dipole antenna. The antenna was fed with a coaxial transmission line without a balun which resulted in a number of spurious responses on the Smith Chart. A Characteristic Mode model of both the antenna

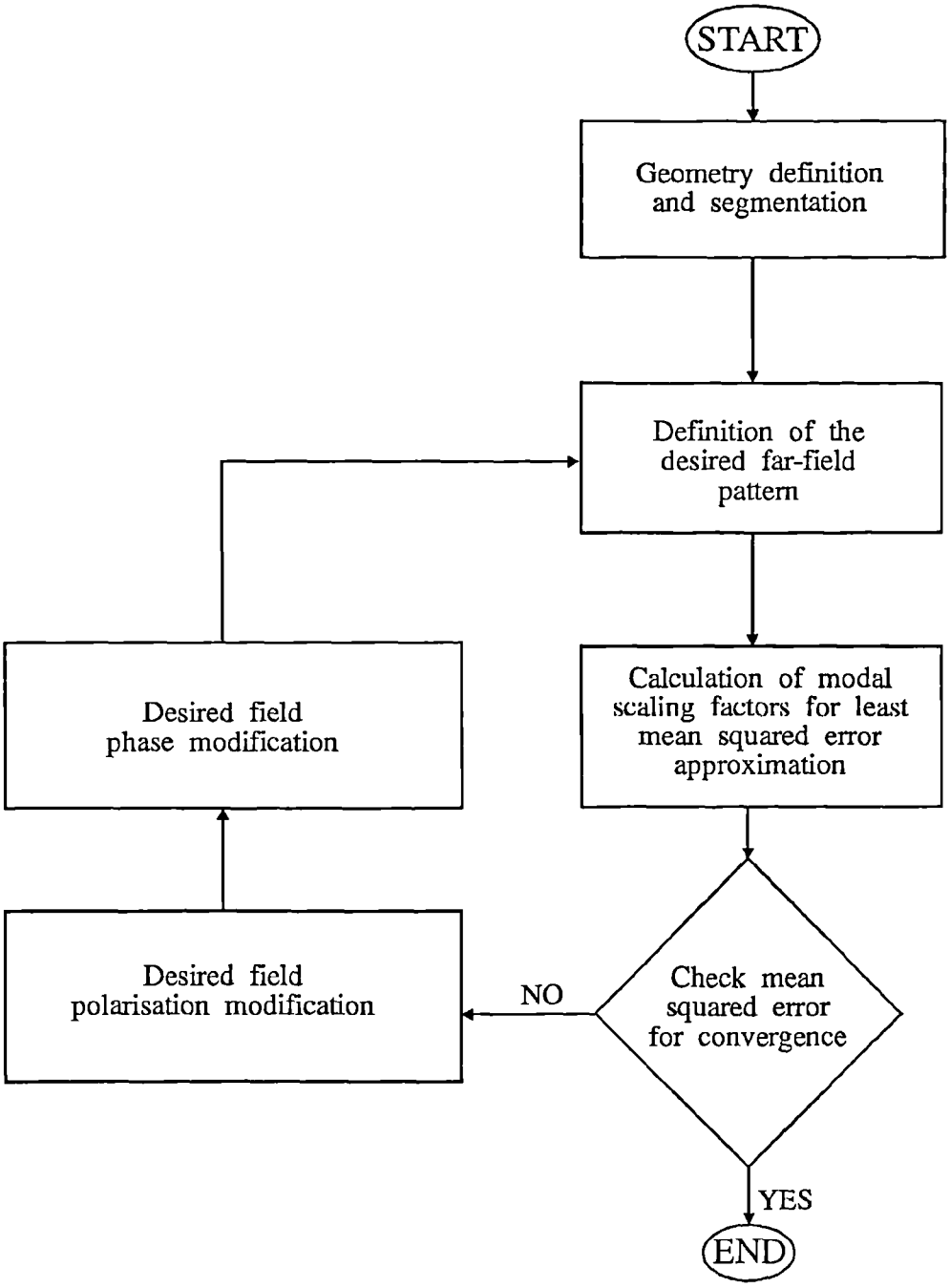

Figure 6.2 Flow Chart of the Characteristic Mode far-field pattern synthesis routines

and radiating transmission line allows greater insight into the radiation properties of the combination compared to the conventional Moment Method technique. Thus the various features of the Smith chart plot of the measured driving-point impedance are explained.

The ultimate aim of this thesis is to use Characteristic Modes for designing antenna systems on complex structures. In section 6.3.4 a corner reflector antenna is used as a simple example of such a structure. Although this geometrical configuration is a complete, purpose designed antenna, modal analysis demonstrates how only relatively few of the modes associated with the structure are utilised with it fed conventionally. This enforces the view that a wide range of far-field patterns are possible from complex structures by the appropriate excitation of the wide range of available modes.

6.3.2 The Characteristic Modes of a Straight Wire

6.3.2.1 Modal Structure

Figure 6.3 shows the dimensions of a straight cylindrical wire. Although this is a relatively simple structure, it perfectly illustrates the basic principles of a Characteristic modal analysis. Similar simple geometrical configurations such as a 2-element linear halfwave array have also been studied by Austin and Murray (1991). Modal analysis is independent of excitation and therefore no feed-point is initially specified.

Chapter 3 showed that the smaller the modulus of an eigenvalue, then the more naturally significant a mode will be compared to others. Using this criterion, table 6.1 shows the eigenvalues of the four most significant modes of

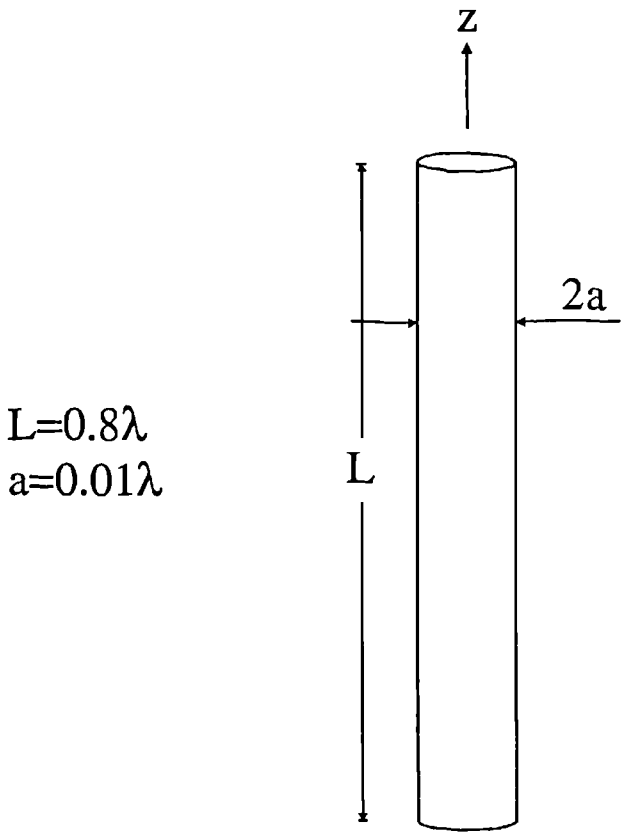

Figure 6.3 Straight cylindrical wire with dimensions

the straight wire. Mode 1 has a positive eigenvalue and is therefore inductive. The eigenvalues of the other three modes are negative and thus they are capacitive. It is clear from the relatively small eigenvalue of modes 1 and 2 that in this case they will dominate the radiation characteristics of this structure if properly excited.

These results were obtained using a 32 segment model of the wire in the Method of Moment evaluation of the generalised impedance matrix. This segmentation scheme was chosen after consideration of the MININEC3 validation data in the previous chapter and the other modelling guidelines discussed in chapter 2. As a final check of the segmentation scheme the variation of modal

Table 6.1 Eigenvalues of the 4 most significant modes of the straight wire

Mode	Eigenvalue
1	3.03
2	-7.39
3	-312.64
4	-13207.70

eigenvalue scaling, expressed as the modulus of the factor $1/(1+j\lambda_n)$, with total number of segments used was investigated. Figure 6.4 shows the resulting plot for mode 1 only. Clearly rapid convergence of the eigenvalue is achieved when more than 20 segments are employed. A similar result was achieved for the other modes of the system. This result shows that, as expected, stability of the calculated Characteristic Modes is achieved by adherence to the antenna modelling and segmentation guidelines outlined in the previous chapter.

Next figure 6.5 shows the equi-phase current distributions associated with modes 1 and 2. These are approximately the half- and full- sinusoid current distributions usually associated with the first and second resonances of a straight wire respectively. This phenomenon is repeated with the current distributions of the higher order modes with each corresponding to that associated with a natural resonance of the wire.

This result illustrates one of the useful attributes of a Characteristic Modal analysis, with each mode corresponding to a natural resonance of the structure. Although, for this simple structure, they are easily identified by

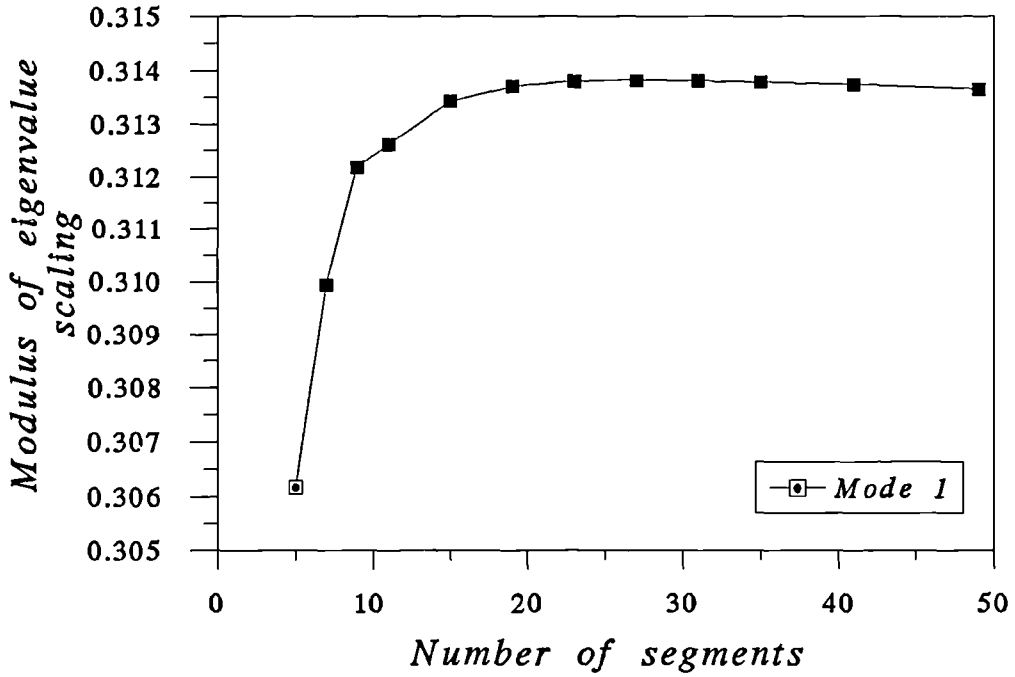

Figure 6.4 Variation of the eigenvalue associated with mode 1 with the total number of segments used

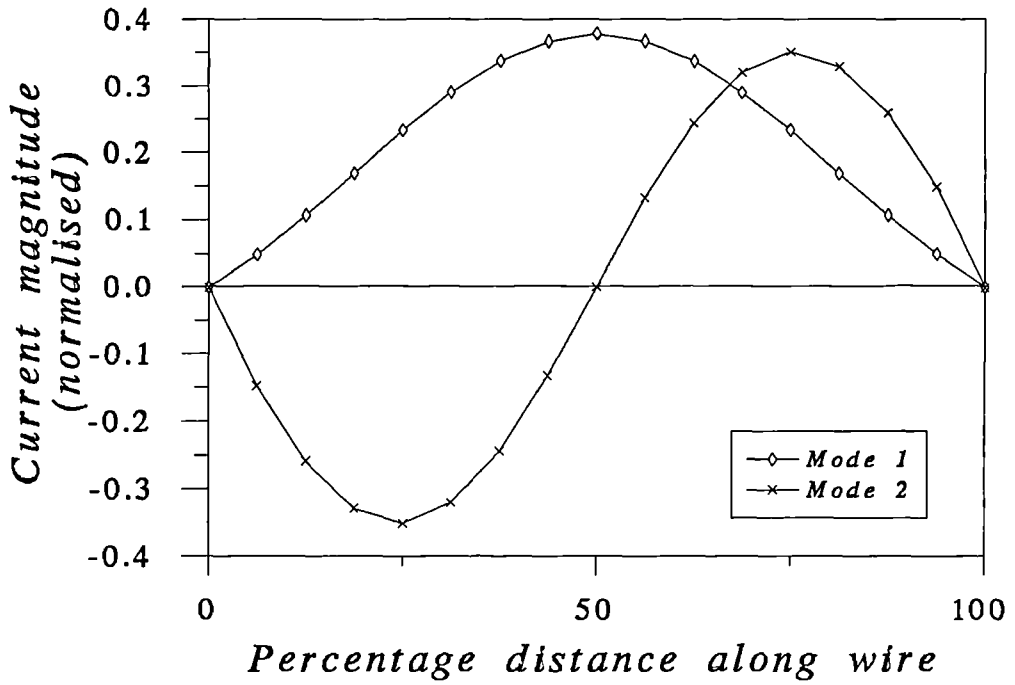

Figure 6.5 Current distributions of modes 1 and 2 of the straight 0.8λ wire

inspection, for complex geometrical configurations they may not be as apparent. Hence the technique expands a structure's current distribution into a set of functions that are naturally related to its generalised impedance matrix. As these functions are related to the inherent resonances of the structure they are therefore ideal for optimization purposes. Identification of these resonances is also useful in explaining certain features of a radiation characteristic. This application is further investigated in section 6.3.3.

6.3.2.2 Input Admittance and Pattern Convergence

It has been previously suggested that in general the higher order modes associated with a particular structure contribute less to the radiation from it. Thus for this configuration it has been reasoned that modes 3 and 4, as shown in table 6.1, will contribute little because of their eigenvalues relative to modes 1 and 2. To examine this effect the input admittance and radiation patterns of the straight wire antenna were calculated using increasing numbers of less significant modes. A single feed-point was used to excite the structure. Its position was chosen such that it did not coincide with any mode current nulls. This ensured that all modes would be substantially excited. The modes were then summed consecutively with them ordered as in table 6.1, in terms of decreasing significance. Figure 6.6 shows how the input admittance of the structure converges as the number of modes used in the summation increases. The converged result agrees exactly with that predicted by MININEC3 using conventional matrix inversion.

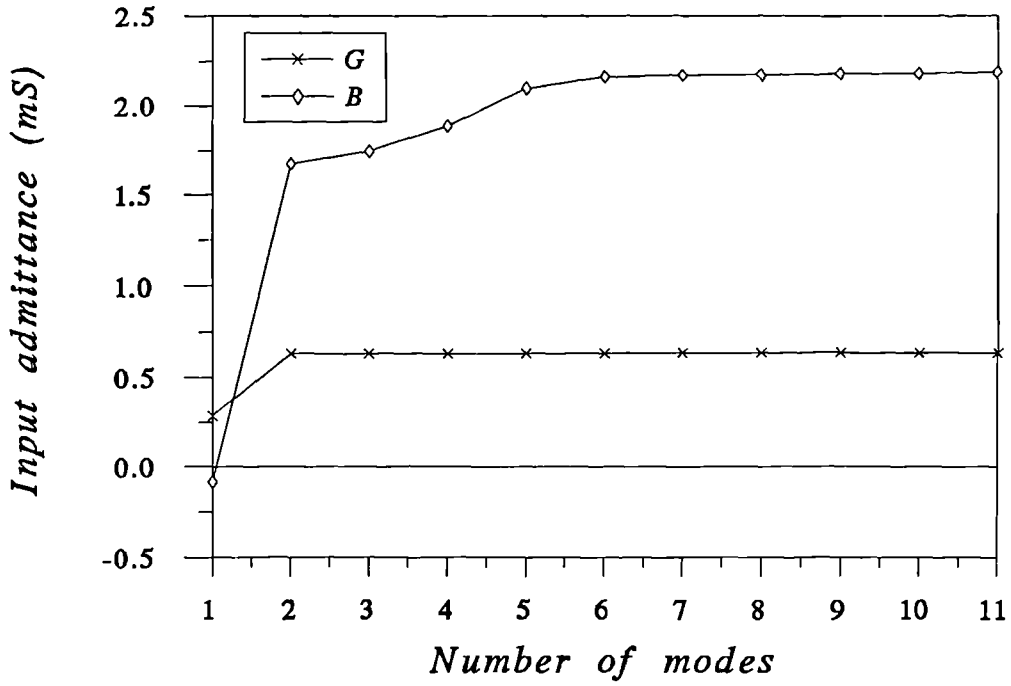

Figure 6.6 Variation of the Characteristic Modal predicted input admittance with the number of mode used in the summation

It is noticeable that the input conductance is convergent after including only the first two most significant modes. The input susceptance however converges after six modes are used in the summation. This would be expected due to the $1/(1+j\lambda_n)$ scaling of each mode. Clearly the real part of the current, the conductance component, is scaled by $1/(1+\lambda_n^2)$ whereas the imaginary part, the susceptance component, is scaled by $-\lambda/(1+\lambda_n^2)$. This is confirmed in figure 6.7 which shows the variation of the percentage difference from the matrix inversion result of the input susceptance obtained with increasing numbers of modes. Whereas using the two most significant modes gave an input conductance identical to that using matrix inversion, the input susceptance is still 25% in error although it is dramatically reduced compared to using just one mode. The error does however decrease steadily as more modes are added and is less than

2% when six modes are employed.

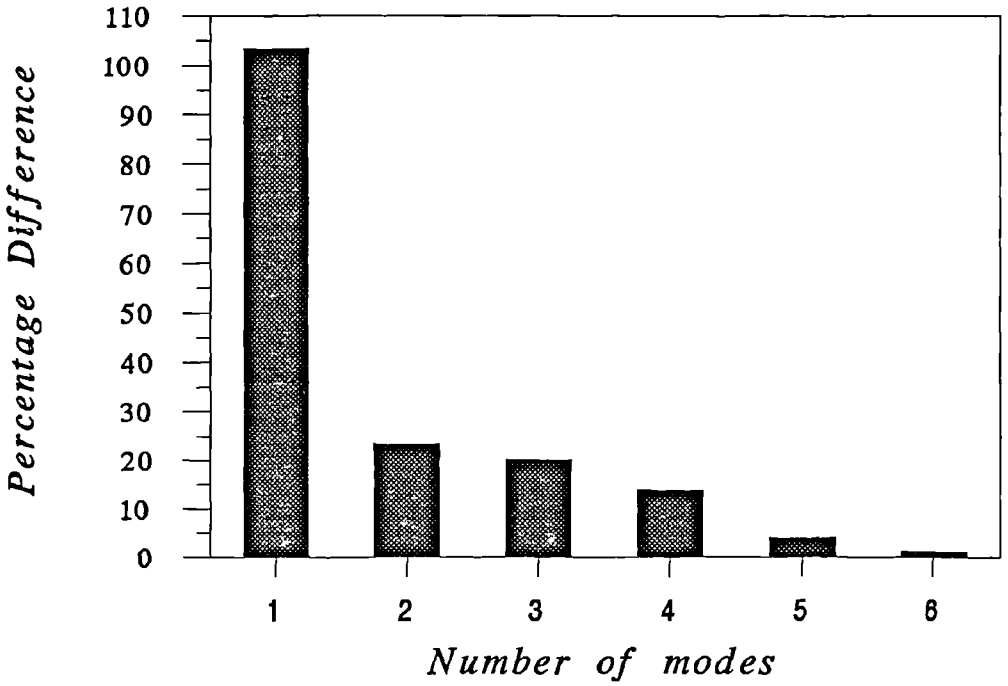

Figure 6.7 **Variation of the percentage difference in the summed modal input susceptance with the number of modes used**

Next, figure 6.8 shows how the radiated far-field of the same antenna is affected as the number of modes used in the summation is increased from one to two. Also shown is the field calculated using the conventional Moment Method with matrix inversion.

Clearly the result obtained using the two most significant modes is nearly identical to that using the conventional Moment Method. This is confirmed in table 6.2 which shows both the maximum percentage difference and the mean absolute difference of the modal summed patterns from that predicted using matrix inversion.

The analysis shown in this section has illustrated the features and some of the advantages of using a Characteristic Modal approach. An important

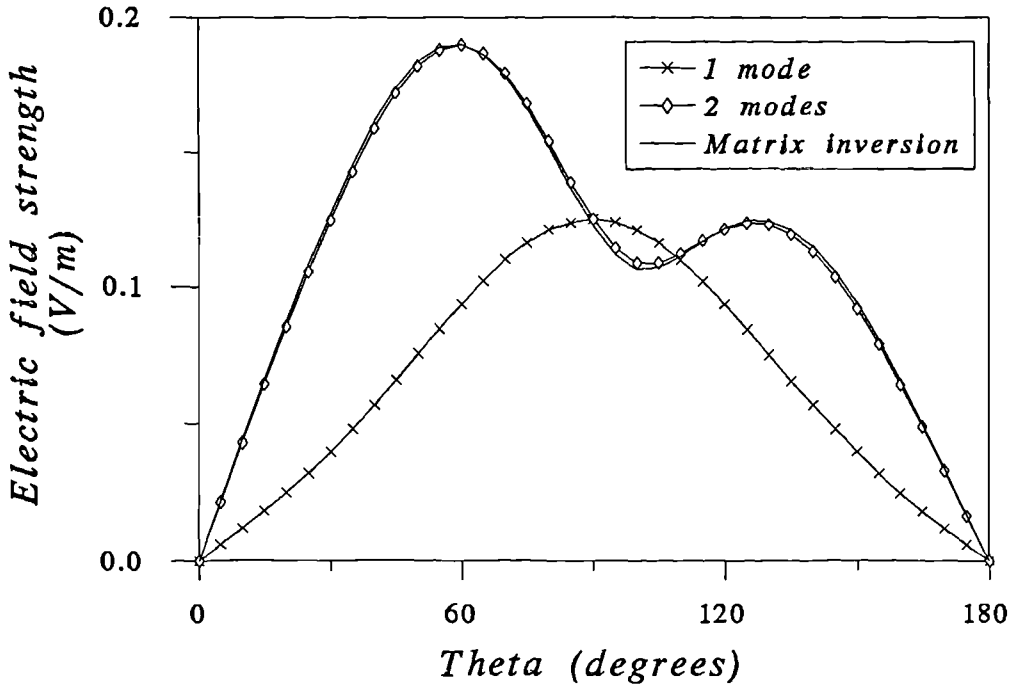

Figure 6.8 Variation of the predicted *E*-field of the 0.8λ straight wire with the number of modes used in the summation

Table 6.2 Variation with number of modes of the maximum percentage difference and the percentage mean absolute difference of the modal summed *E*-field from the conventional Method of Moment result

Number of modes used in the summation	Maximum percentage difference	Percentage mean absolute difference
1	73.43	46.35
2	2.93	1.68
3	1.80	0.63
4	0.11	0.04

finding, especially for complex structure analysis, is the ability to identify a structure's natural resonances. Off resonance it has been shown that these currents still contribute to a structure's radiation characteristics, but are

inherently scaled by the associated modal eigenvalue. This was demonstrated for the 0.8λ wire by only two of its associated total modes significantly contributing to its radiation characteristics. This result generally confirms the mode cut-off criterion outlined in chapter 3 by both Harrington and Mautz(1971b) and Pozar (1984). In later sections therefore, a general "rule of thumb" will be enforced , based on this, whereby only modes whose eigenvalue modulus is no more than 30dB larger than that of the most significant will be considered as useful. It is clear that generally, even if a mode has a desirable characteristic, if its eigenvalue is outside this range it will be extremely difficult to excite. Also the contribution of the other more significant modes of the system will usually dominate.

6.3.3 The Balun problem

Experimental data were available (Leather, 1991) for a horizontal wire antenna, centre fed with a coaxial transmission line without a balun. This configuration is expected to produce unwanted radiated fields and hence peculiarities in the input impedance characteristic due to the excitation of the outer braid current on the coaxial cable as described by Monteath and Knight (1960). The input impedance at the antenna feed-point did indeed exhibit a number of spurious responses on the Smith Chart. To analyze this situation figure 6.9 shows a simple equivalent Method of Moments representation. The model consists of a 26m horizontal dipole with a 56m vertical radiating transmission line.

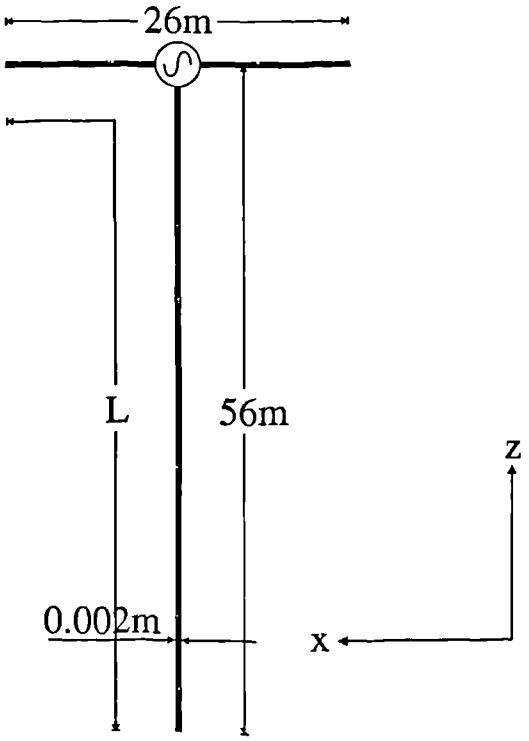

Figure 6.9 **Simple model of a horizontal dipole with vertical transmission line without a balun**

Using a simple physical argument, the currents due to the transmission line would be expected to be most pronounced when the dimension L is a multiple of half a wavelength. Here L=69m, hence critical frequencies (calculated using $f=nc/2L$, n=1, 2, 3,...) are typically 2.1, 4.3, 6.5 MHz *etc.*, while the 26m dipole antenna would resonate at typically 5.5, 11.3, 17.0 MHz *etc.*

A Characteristic Mode approach was used to confirm the existence of these predicted resonances and to verify their exact frequencies. Useful engineering insight is also provided by the examination of the mode current distributions. Figure 6.10 shows the variation of the characteristic angles of the most significant modes in the frequency range 1-20MHz. A characteristic angle of 180° is indicative of modal resonance (λ_n=0) and hence modal dominance, as

described in chapter 3. Using the mode cut-off criterion of the previous section it can be concluded that these ten modes will completely control the radiation from the configuration in the defined frequency range. Their resonant frequencies are thus shown in table 6.3.

Modes 3, 6 and 9 clearly correspond to the 26m dipole antenna's resonances. This is confirmed by the examination of their current distributions shown in figure 6.11. Negligible current flows on the vertical transmission line section and the dipole currents only are shown. As with the 0.8λ wire described in section 6.3.2, these are comparable to the natural resonant dipole sinusoidal current distributions. The other modal resonances were then attributed to half of the antenna plus the transmission line. Figure 6.12 confirms this by showing the current distribution of mode 7 on this section of the structure which consists of approximately 3 sinusoids. The resonant frequency of this mode corresponds approximately with that predicted using the simple physical model $f=nc/2L$ with $n=6$ and $L=69m$.

Figure 6.13 next shows the extent to which of these defined modes will be excited with the source position shown in figure 6.9. This is expressed in terms of a modal excitation factor defined as the ratio of the mode current at the source position to that of the mode current maximum. This is directly proportional to the factor $I_n{}^T V$ in equation 3.45. Although this is for a fixed frequency (11MHz), the mode currents remained substantially the same over the complete range. Thus the diagram is relevant for all frequencies considered.

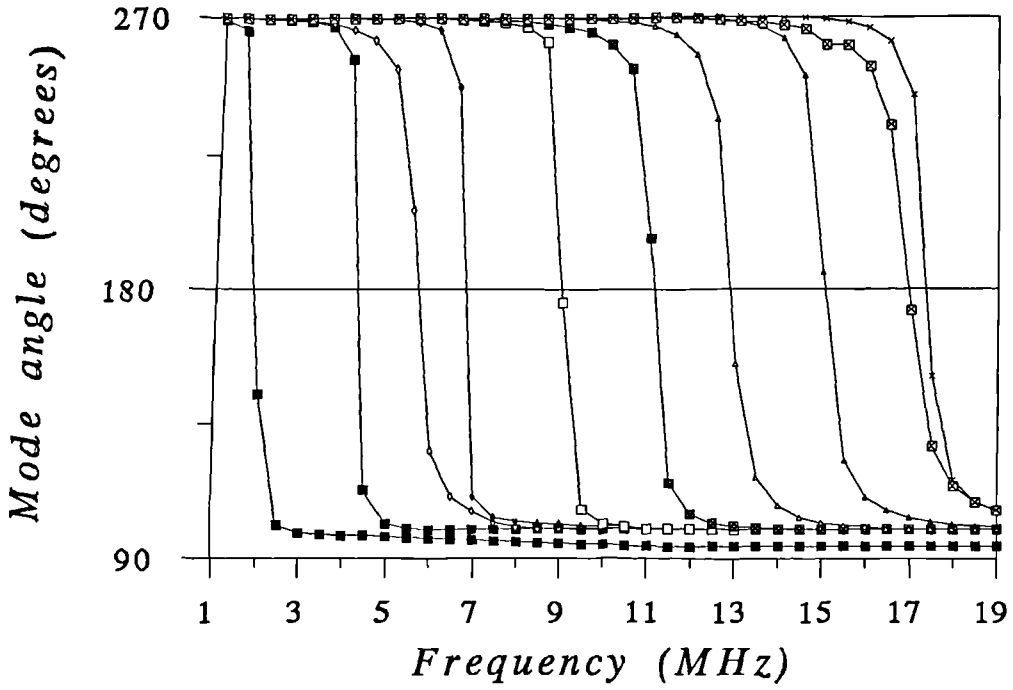

Figure 6.10 Variation with frequency of the characteristic angle of the ten most significant modes of the dipole and transmission line combination

Table 6.3 Resonant frequencies of the ten most significant modes of the dipole and transmission line combination

Mode	Resonant Frequency (MHz)	Mode	Resonant Frequency (MHz)
1	1.8	6	11.2
2	4.3	7	12.9
3	5.6	8	15.1
4	6.5	9	17.0
5	9.0	10	17.3

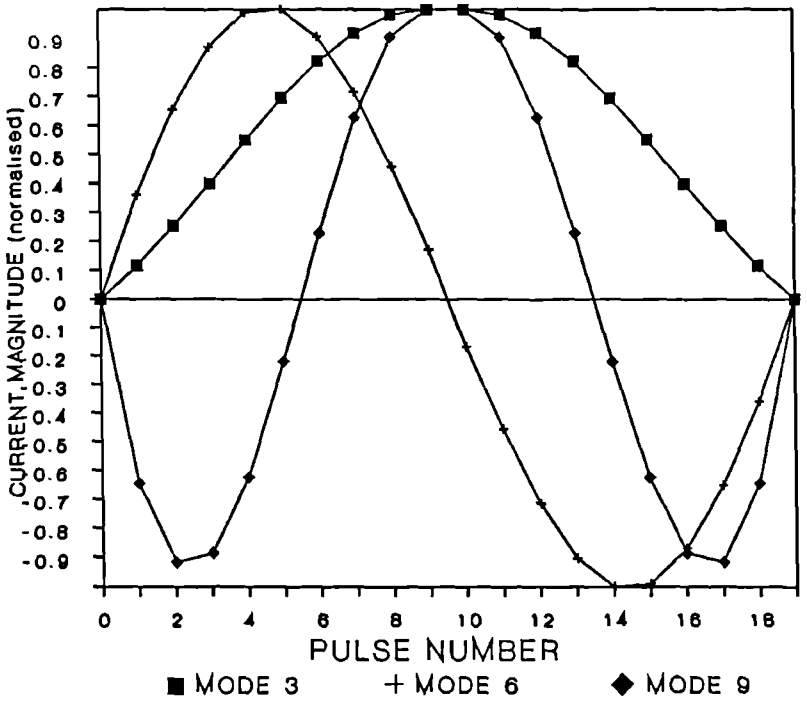

Figure 6.11 Current distribution along the horizontal dipole of modes 3, 6 and 9

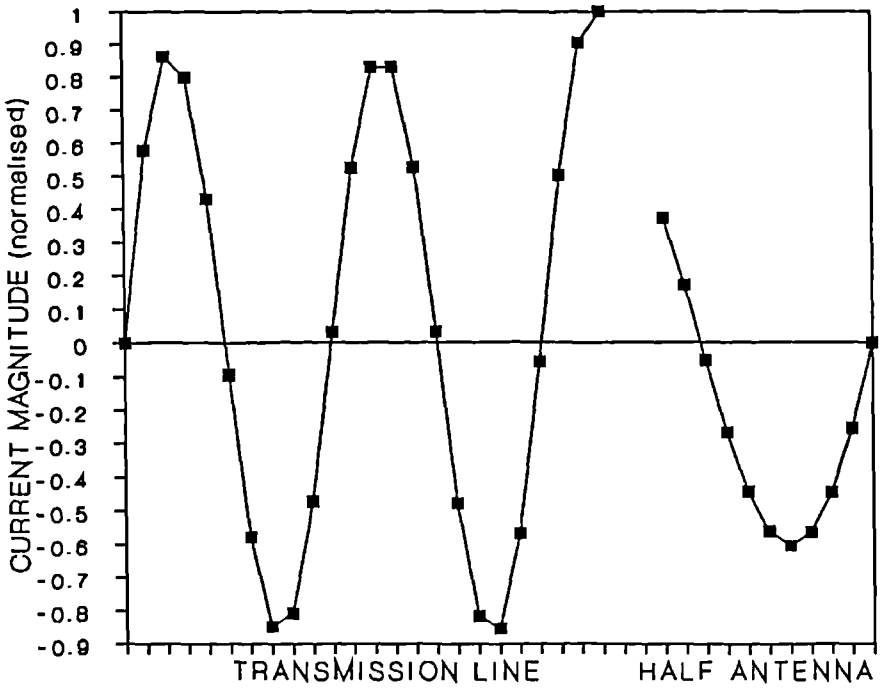

Figure 6.12 Current distribution of mode 7 along the vertical transmission line and half of the horizontal dipole

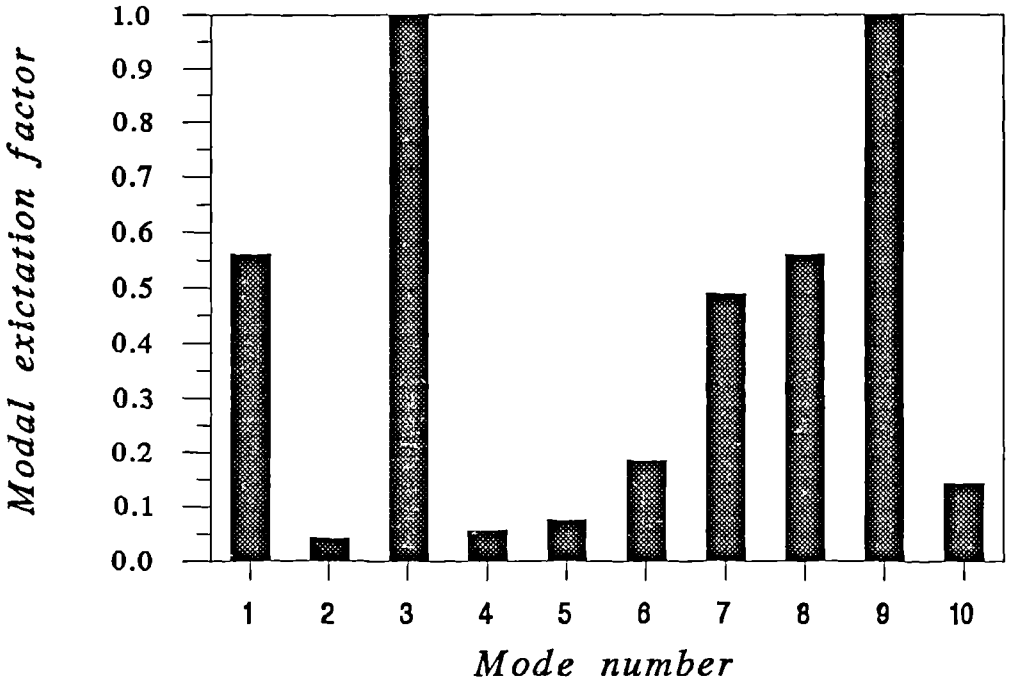

Figure 6.13 Modal excitation factors of the modes of the dipole antenna and transmission line model

As expected modes 3 and 9 are excited maximally. Also modes 1, 7 and 8, due to the half antenna plus transmission line, are also excited significantly. The resonance effects due to these substantially stimulated modes will clearly be evident in the experimental data plotted on the Smith Chart of Leather (1991) which is shown in figure 6.14 for the frequency range 1-18MHz. Also shown are the positions of the resonant frequencies of these five strongly stimulated modes.

Firstly the resonant frequencies of modes 3, 8 and 9 correspond exactly with resonances on the Smith Chart. This suggest that at each these frequencies the radiation characteristics of the structure are due solely to those of each of these modes. Also apparent however are the clear disturbances on the Smith Chart due to modes 1 and 7. The resonant frequency of mode 1 corresponds to a noticeable loop in the capacitive half of the chart whereas the mode 7 resonant

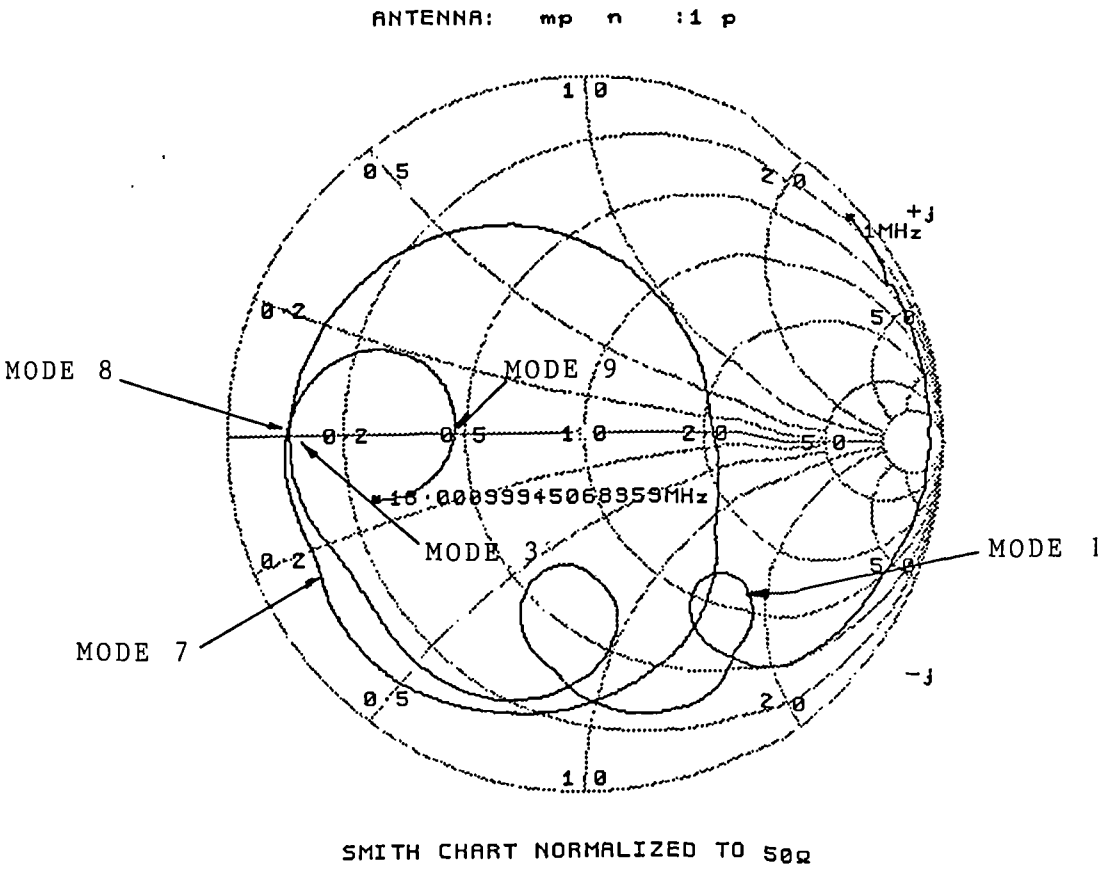

Figure 6.14 Smith chart normalised to 50Ω of the experimental dipole input impedance data of Leather (1990)

frequency is coincident with an unexpected kink.

This above analysis has further illustrated the usefulness of a Characteristic Mode approach. Although the approximate resonant frequencies of the above antenna were initially identified using a simple physical model, Characteristic Modes allowed their exact determination. The technique further showed that by examining the extent to which each mode associated is excited, its probable contribution to the overall radiation can be assessed. In the above example there were ten significant modes in the defined frequency range but the chosen source position only substantially excited five of them. The effect of these five modes was then apparent on the Smith Chart. Although the simple representation used didn't identify all of the unexpected responses an advantage of a modal technique compared to conventional Moment Methods is clearly an insight into the mechanisms responsible for an antenna's characteristics.

6.3.4 The Characteristic Modes of a Corner Reflector

The previous two sections have described the composition of the Characteristic Modal sets of two relatively simple antenna structures. The usefulness of the approach is clearly apparent with each mode corresponding to a natural resonance of the structure. Also illustrated was the dependence of the contribution of a mode to radiation on both the inherent significance of a mode, denoted by its eigenvalue, and the scaling effect of the chosen source configuration. The purpose of this section is extend these techniques and

demonstrate their application to more complex structures, whose modal composition will clearly be of a more complicated nature.

Figure 6.15 shows a plan view of a corner reflector antenna. The width of the reflector is 0.6λ and the driven element is a centrally-fed halfwave dipole. For Moment Method analysis a wire grid was implemented using the previously investigated modelling rules and is shown in figure 6.16. Although this antenna is purpose designed for a particular application it is a useful example of a relatively complex, electrically large configuration. It differs form the two previous simpler antennas in that the resonances associated with it are not identifiable merely by inspection.

The Characteristic Modal analysis of the configuration yielded 30 modes, the moduli of whose eigenvalues were less than 10^6. This is a wider modal spread than would normally be identified using the 30dB cut-off "rule of thumb" suggested in the two previous sections. Considering all these modes though allows a reassessment of this rule for complex structures. Figure 6.17 shows the extent to which each these 30 modes are excited with a single voltage source positioned at the centre of the halfwave dipole. This is again expressed in terms of the modal excitation factor as described in section 6.3.3. As before the modes are ordered in terms of decreasing significance, mode 1 exhibiting the smallest eigenvalue.

This diagram shows that only 12 out of the 30 modes shown are excited at all by the defined voltage source. Also the inherent inverse proportionality of each modes' contribution to its eigenvalue suggests that only a few of these

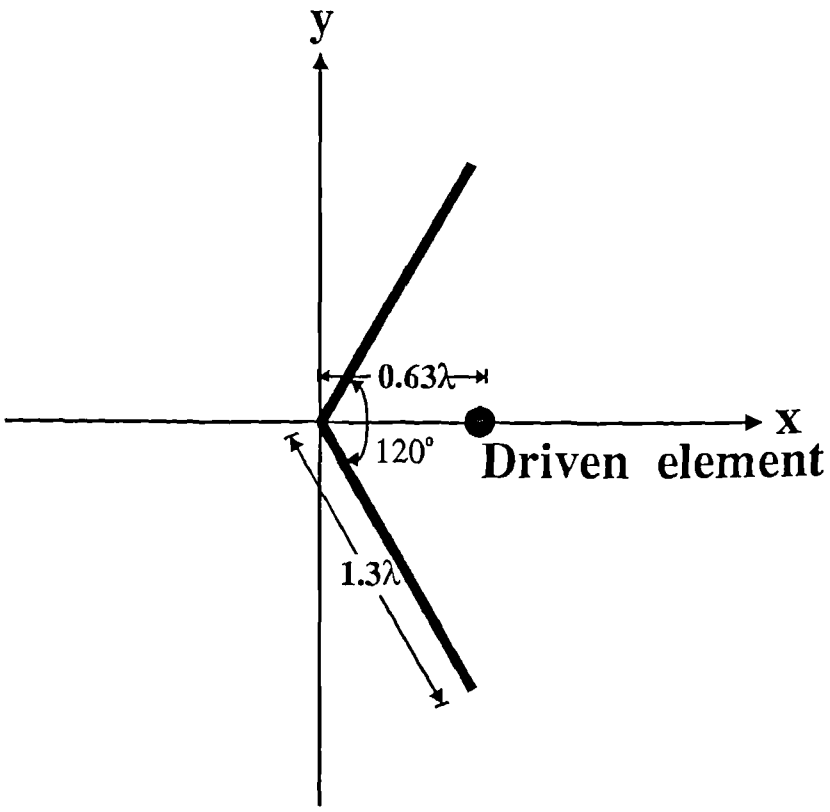

Figure 6.15 Corner reflector plan view with dimensions

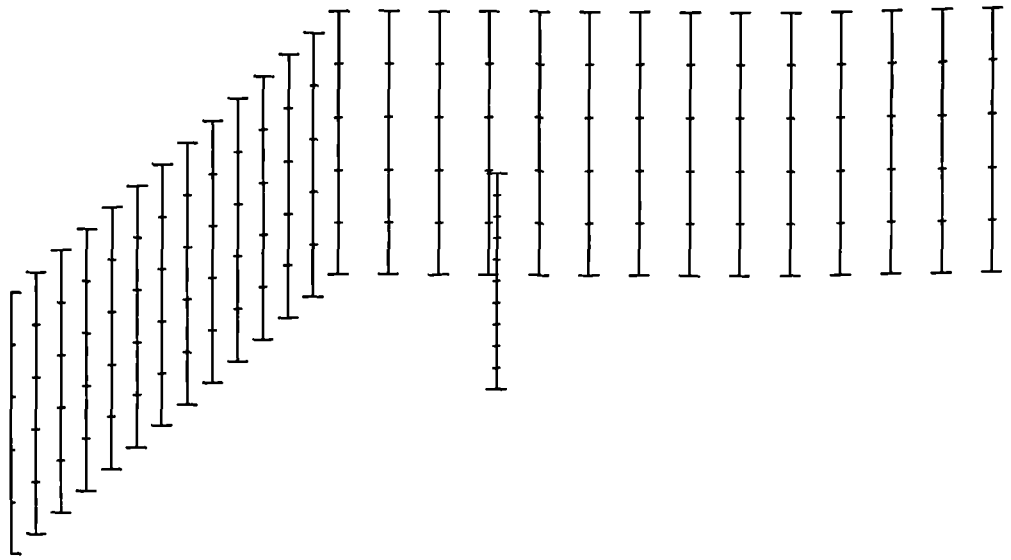

Viewing angles: θ=70°, ϕ=150°

Figure 6.16 Corner reflector wire grid model

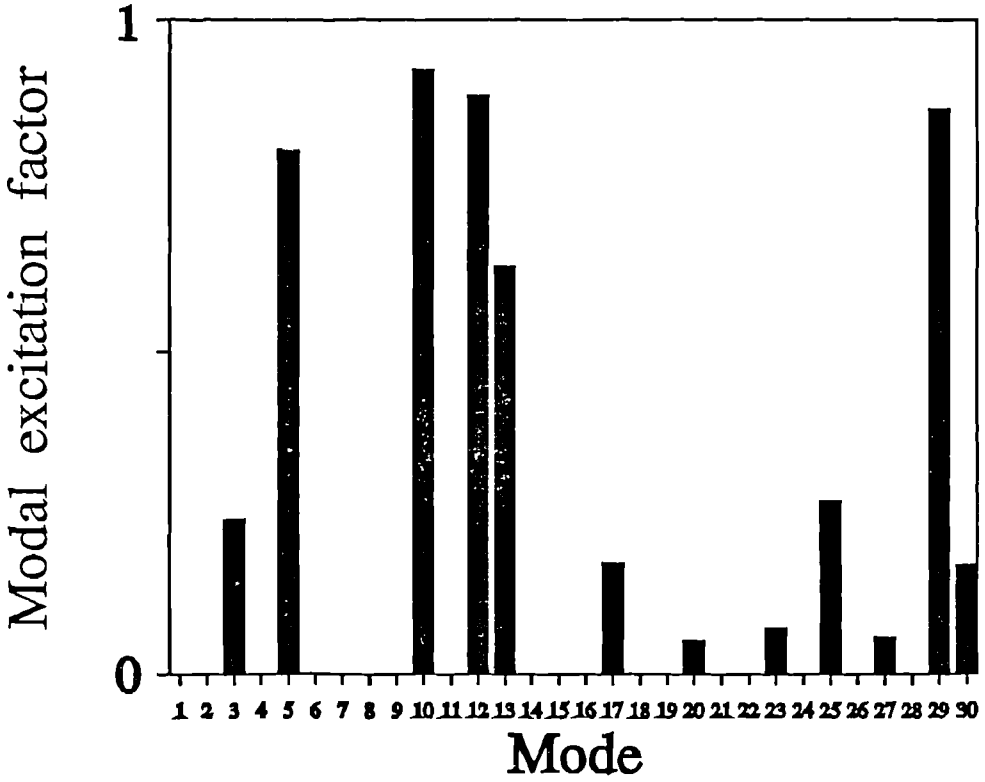

Figure 6.17 Modal excitation factors of the 30 most significant modes of the corner reflector

excited modes will be predominantly responsible for the radiation. This is confirmed by figure 6.18 which shows the resultant far-field pattern obtained by consecutively summing modes 3, 5, 10 and 12, the four most significant modes that are excited substantially. Also shown is the far-field obtained using conventional Moment Method matrix inversion.

The field obtained when using modes 3, 5, 10 and 12 is nearly identical, with less than 1% difference at any point, to that obtained using conventional Moment Method matrix inversion. This result again shows the importance of the eigenvalue associated with a mode in governing its contribution to the overall radiation characteristics. Also the analysis of this geometrical configuration has shown the significance of the position of any feeding mechanism. Considering the

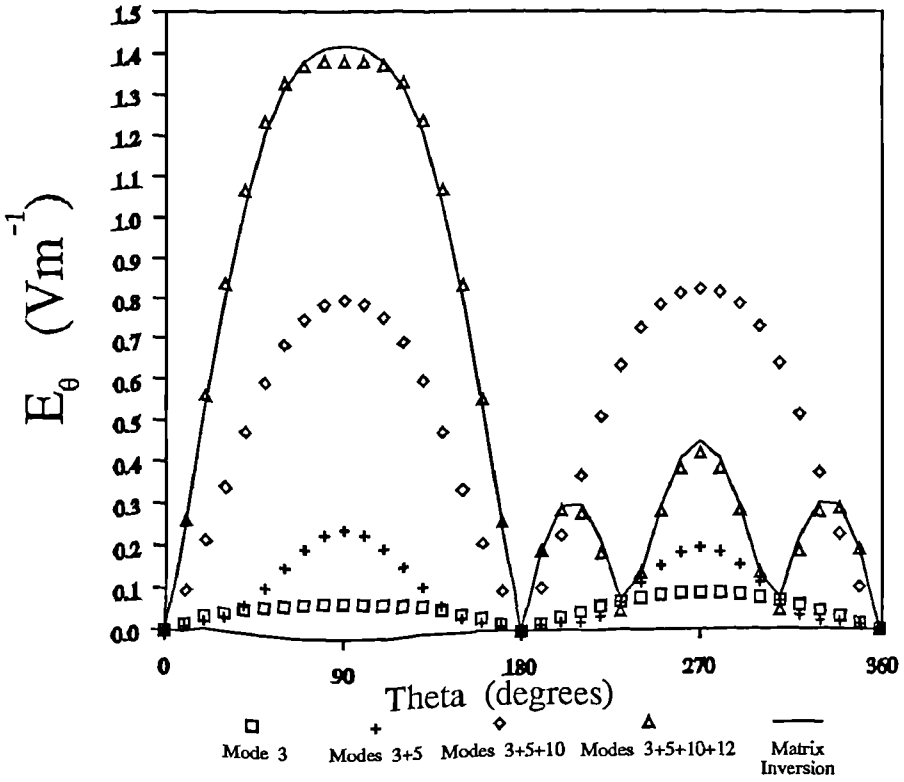

Figure 6.18 Convergence of the elevation far-field of the corner reflector with the number of modes summed

first 12 most significant modes of this structure, only 4 of them contribute substantially to the radiation characteristics. Although for the corner reflector this excitation probably produces optimum current flow for its application, the result has important implications for the complex vehicular structures whose antenna systems this thesis addresses. Previously the Method of Moments has always been used for analysis of such configurations. The method of Characteristic Modes however allows the extension of this theory enabling the definition of an orthogonal set of currents. For a vehicle these modes will clearly be numerous with many diverse far-fields. Analysis of this corner reflector, fed conventionally, has demonstrated that usually the modes associated with it are not exploited for radiation. This is also clearly the case with vehicular antenna

systems, where spurious current flow on the structure is only considered in terms of its modifying effect on the performance of the mounted antenna. The following section demonstrates the principles of using this previously spurious current flow to beneficial effect by modal optimization to produce desirable far-field patterns. Simple antenna configurations are initially used to investigate the various pattern synthesis issues that must be addressed, with chapter 7 then applying the same techniques to complex vehicular antenna systems.

6.4 Pattern Synthesis

6.4.1 Straight Wire Far-field Synthesis

The analysis described in this section follows the initial Characteristic Mode synthesis work of Pozar (1984). He used a straight wire and demonstrated how its modes could be optimised to generate a current that produces a least mean squared error approximation to a desired far-field pattern. An important issue in using Characteristic Modes for pattern synthesis, which was not addressed to any extent by Pozar, is an assessment of the practical implications of using voltage sources to physically realise the current distribution that produces the approximating far-field. In his work, Pozar used a 1.91λ straight wire orientated as illustrated in figure 6.19.

The eigenvalues of this geometrical configuration are shown in table 6.4. The first eight modes are listed and are shown in decreasing order of significance as denoted by the modulus of each eigenvalue.

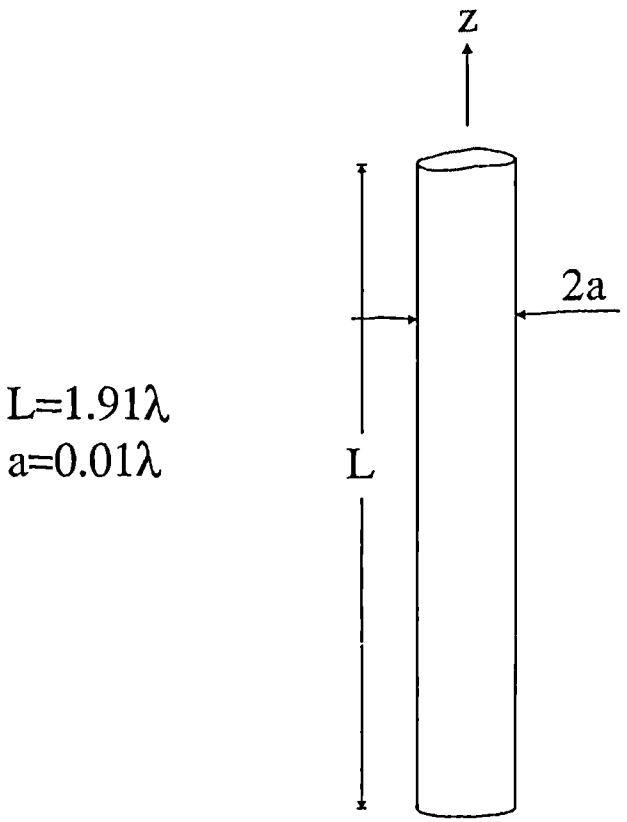

Figure 6.19 Straight 1.91λ wire as used in the pattern synthesis work of Pozar (1984)

Table 6.4 Characteristic modal eigenvalues of the 1.91λ straight wire

Mode	Predicted modal eigenvalue
1	-1.210
2	3.152
3	3.34
4	3.39
5	-63.20
6	-1122.45
7	-24794.08
8	-627280.65

In Pozar's work he concluded that only the first six modes would contribute to the overall radiation characteristics of the structure. This is clearly the case with the moduli of the eigenvalues of modes 7 and 8 being relatively very large compared to those associated with the other modes and outside the 30dB "rule of thumb" discussed earlier. Practically, this suggests that to completely control the radiation pattern of this configuration requires six voltage sources.

To investigate, a target far field pattern for the above configuration was specified as:

$$|E_\theta| = \begin{cases} 1: & 100° < \theta < 150° \\ 0: & \textit{otherwise} \end{cases} \qquad (6.3)$$

This pattern is clearly physically unrealizable but was thought adequate to demonstrate the basic features of the pattern synthesis routine. The phase of the resultant synthesized pattern was assumed unimportant which allowed the iterative modification routine described earlier to be invoked. Figure 6.20 shows how the relative mean squared error of the approximating field reduced with each synthesis iteration, using increasing numbers of modes. The final converged results are then shown in table 6.5.

There is less than 2% total difference between the results obtained using 3,4,5 or 6 modes. This suggests that modes 4, 5 and 6 are contributing little to the synthesized pattern. It is possible to obtain the required excitation of the first three modes using three voltage sources. However, this action would produce an unspecified excitation of the other three significant modes, which

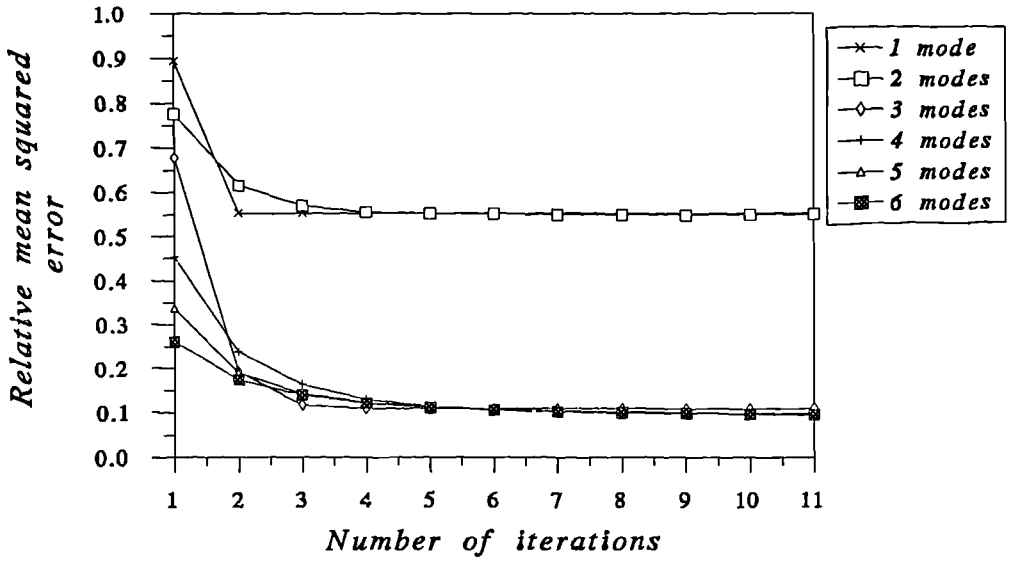

Figure 6.20 Variation with number of iterations of the relative mean squared error of the synthesized far-field pattern with increasing numbers of modes

Table 6.5 Converged results for the relative mean squared error of the synthesized patterns of the 1.91λ wire using increasing numbers of modes

Number of modes	Converged relative mean squared error
1	0.5534
2	0.5510
3	0.1089
4	0.0998
5	0.0962
6	0.0954

would possibly upset the overall synthesized pattern. A simplistic technique to overcome this is to position the voltage sources at the mode current minima of modes 4, 5 and 6. This, of course, may not be practically possible as the minima of the unwanted modes may not coincide. A more effective method of reducing the number of required voltage sources is to use the technique of port Characteristic Modes.

Four ports were therefore defined on the 1.91λ wire described above. They were chosen, as much as possible, to coincide with positions where the currents of modes 1, 2 and 3 were substantial. Their positions are shown in table 6.6, with the eigenvalues of this new modal set then shown in table 6.7.

Table 6.6 Positions of the four ports defined as a vertical distance along the z-axis from the bottom of the wire

Port number	Vertical distance form bottom of wire
1	0.7346λ
2	0.9550λ
3	1.1019λ
4	1.4692λ

This modified modal set was then used in the synthesis routine for the same target pattern as before. Table 6.8 show the resulting converged relative mean squared errors obtained using increasing numbers of these modes.

The relative mean squared error of the synthesized pattern reduces steadily as the number of modes is increased. Interestingly the error obtained

Table 6.7 Eigenvalues of the port Characteristic Modal system of the 1.91λ wire

Mode	Eigenvalue
1	0.59
2	-1.42
3	2.24
4	-133.92

Table 6.8 Converged relative mean squared error results obtained using the 4-port representation of the 1.91λ wire

Number of modes	Converged relative mean squared error
1	0.9895
2	0.4724
3	0.3268
4	0.1158

using all four modes is only around 2% greater than the best result obtained using the modes of the complete structure. Figure 6.21 confirms this similarity by comparing the far-fields obtained in each case.

The plots show that clearly the main lobe predicted by each system is nearly identical, with substantial power radiated in the idealized target pulse. Only in the minor lobes positioned at $\theta<90°$ is there a noticeable difference.

The purpose of this section has been twofold. Firstly the correct operation of the modal synthesis routine has been confirmed. Secondly aspects associated

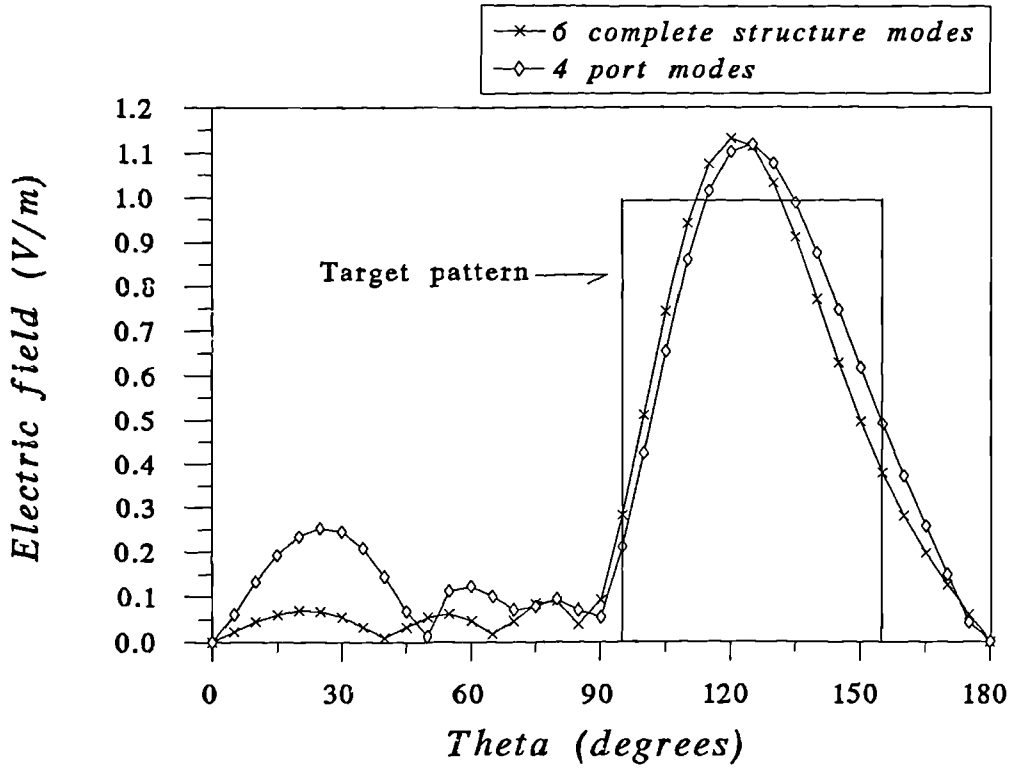

Figure 6.21 Far-field obtained using the six complete structure modes and the 4-port system

with the practical realisation of the synthesized far-fields have been investigated. An important finding has been the ability of using the method of port Characteristic Modes to reduce the number of voltage sources that are required to physically realise the approximating pattern. In the case illustrated nearly identical far-field patterns were obtained using six and four voltage sources. Clearly from a practical standpoint the latter case is preferable. Judicial examination of the currents associated with each is therefore an important aspect of using Characteristic Modes for pattern synthesis.

6.4.2 Pattern Synthesis for Linear Arrays

This section shows the application of Characteristic Mode pattern synthesis to multi-element linear arrays. Figure 6.22 shows a typical geometrical configuration with 6 halfwave equi-spaced elements positioned horizontally over a infinite perfectly conducting ground plane.

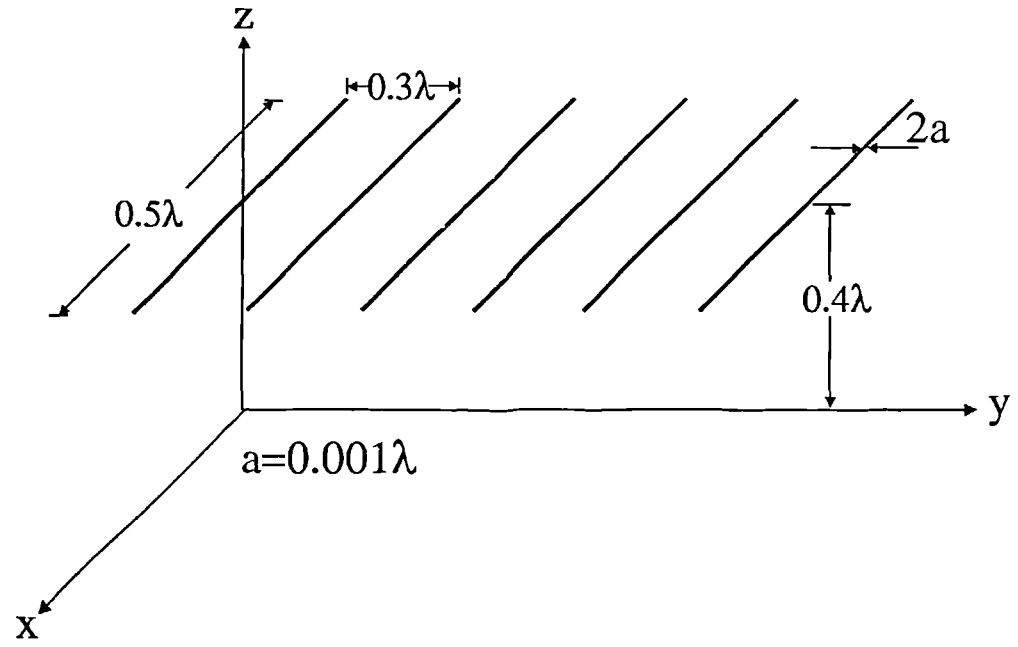

Figure 6.22 Typical six element halfwave linear array

The Characteristic Modes of this structure were calculated and figure 6.23 demonstrates an interesting attribute of its modal composition. It graphically shows the significance of each mode. This, as before, is in terms of the modulus of $1/(1+j\lambda_n)$, the inherent modal scaling factor.

It is noticeable that the modes are clustered in groups of six with similar significance. Examination of these modes showed that each group exhibited a current distribution on each element of approximately the same shape. Modes 1-6 had approximate half-sinusoids on each element, modes 7-12 exhibited full-

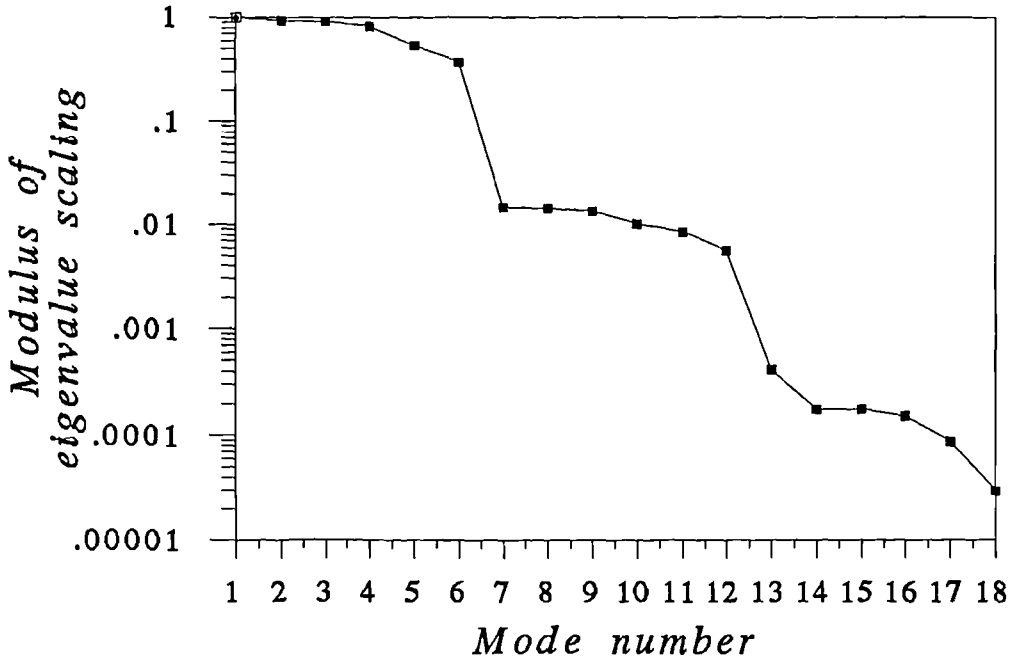

Figure 6.23 Eigenvalue scaling of the Characteristic Modes of the 6 element array shown in figure 6.22

sinusoids and modes 13-18 one and a half-sinusoids. The only difference between the mode currents of each of these groups therefore is the magnitude of the common distribution on each element.

This form of modal composition was found to be standard for a wide range of linear halfwave arrays. Independent of element spacing or height above the ground plane, the modes of these structures generally were in groups numbering the same as the elements of the array. The modes of each of these groups were always of similar significance with current distributions of the same shape on each element. This is a useful attribute for pattern synthesis. Each group of modes will clearly be more suitable for synthesizing different types of patterns. For example, if the desired pattern for the above six element array is symmetric about y-z plane then it is clearly undesirable to excite modes 7-12 which will

introduce an unsymmetrical far-field component. However, as the shape of the current distributions of each modal group are identical it is straightforward to choose source positions that only excite the desired group.

To demonstrate this effect an idealised target pattern for the six element array was specified as:

$$|E_\phi| = \begin{cases} 1: & 35° \le \phi \le 145° \ \textit{and} \ 30° \le \theta \le 90° \\ 0: & \textit{otherwise} \end{cases} \qquad (6.4)$$

and is shown in figure 6.24.

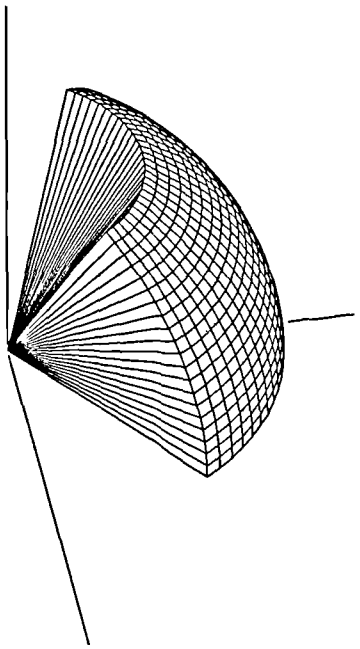

Viewing angles: θ=70°, ϕ=20°

Figure 6.24 Six element array target pattern

Using the first group of six modes yielded an approximating far-field pattern with a relative mean squared error of 0.2516. Then defining 6 voltage sources centrally placed on each element yields the approximating pattern shown in figure 6.25 predicted using the NEC code with conventional Moment Method

matrix inversion. The required driving voltages and the resultant input impedances are further shown in table 6.9 with the elements numbered consecutively from the origin.

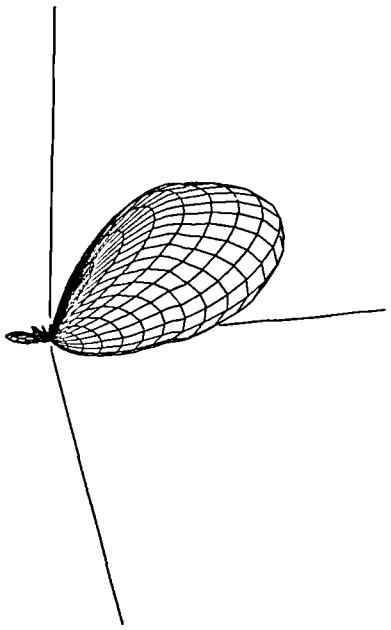

Viewing angles: θ=70°, ϕ=20°

Figure 6.25 Synthesized far-field pattern of the six element array using six voltage sources

This example has shown the importance of carefully examining the composition of a structure's modal set. The unique grouping of modes with similar significance and coincident modal current maxima and minima meant that it was not necessary to use the method of port Characteristic Modes, thus saving computer resources. Hence employing centrally positioned voltage sources only excited the required modes. This is apparent in figure 6.26 which shows the total scaling of each mode by the voltage sources in table 6.9. This factor takes into account both the inherent eigenvalue scaling of $1/(1+j\lambda_n)$ and the that due to the voltages sources $I_n{}^T V$. The correct excitation of modes 1-6 is clearly achieved.

Table 6.9 Feed-point driving voltages and resultant input impedances for the six element array

Element	Feed-point voltage		Input impedance	
	Magnitude (volts)	Phase (degrees)	Resistance (ohms)	Reactance (ohms)
1	0.1047	-93.12	18.22	20.51
2	0.6187	135.71	63.73	71.64
3	1.0000	0.00	102.11	129.56
4	0.9243	-135.49	122.59	279.31
5	0.4984	92.80	-342.70	96.45
6	0.1433	-8.41	-54.60	-59.72

Modes 7-12 are not excited at all by the defined voltages sources and the eigenvalues of modes 13-18 assure that they are negligibly stimulated.

6.5 Summary

This chapter has shown the application of the theoretical principles of Characteristic Modal analysis and far-field pattern synthesis that were discussed in chapters 2, 3 and 4 to a number of practical antenna configurations.

Firstly, section 6.2 described the implementation of various necessary software routines. This included the enhancement of the original MININEC3 code to enable the calculation of the Characteristic Modes of any arbitrary antenna configuration. Further routines then allowed the employment of the calculated modal data for analysis and far-field pattern synthesis.

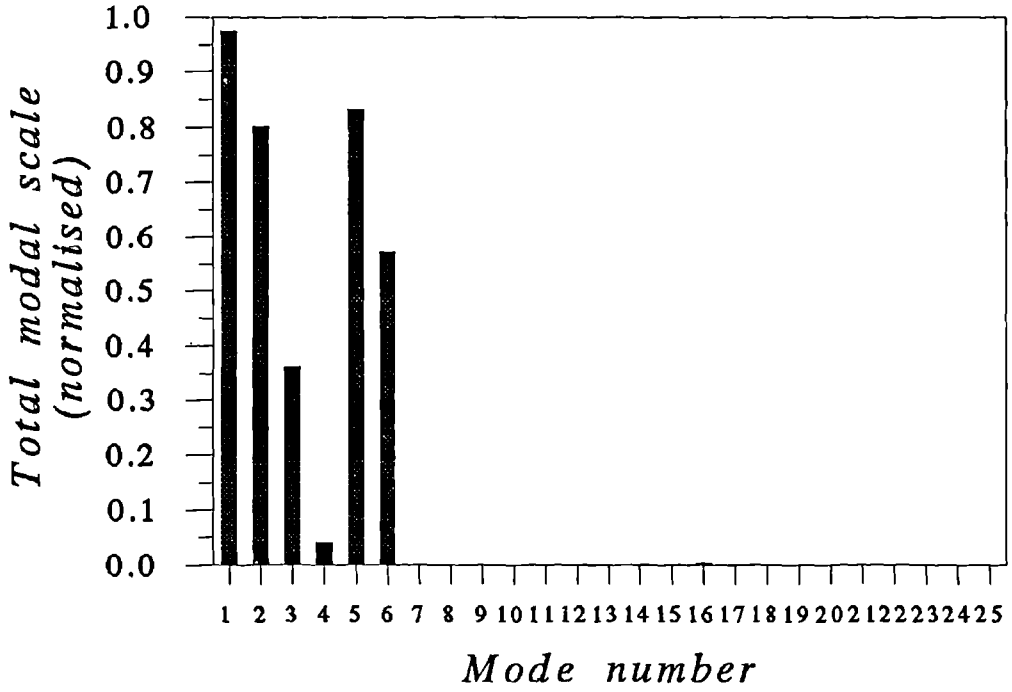

Figure 6.26 **Total modal scale of the 25 most significant modes of the 6 element array introduced by the six centrally positioned voltage sources shown in table 6.9**

In section 6.3 the methodology of using a Characteristic Modal approach to antenna analysis was illustrated. In the first instance this was facilitated, in section 6.3.2, by the analysis of a simple 0.8λ straight wire in free space. The unique relationship between its modal currents and the well-known sinusoidal resonant currents associated with a straight wire showed the ability of the technique to identify the inherent resonances associated with any general radiating system. Also investigated was the dependence of the calculated modal eigenvalues of this system on the segmentation scheme used in the Moment Method representation. The importance of employing the previously determined modelling guidelines to obtain a stable modal set was clearly apparent.

An important aspect of using the method of Characteristic Modes is an assessment of each modes probable contribution to radiation. This was shown to be reliant on two factors. Firstly, the eigenvalue, relative to those of the other modes of the system and secondly the effectiveness of any applied feed-system. For the 0.8λ straight wire, the modes were summed consecutively to give the input impedance and far-field for a defined excitation. These results were compared to those obtained using the conventional Moment Method with matrix inversion. The analysis showed that as a general "rule of thumb" the effect of a mode will only be noticeable if the modulus of its eigenvalue is no more than 30dB greater than that of the most significant.

In section 6.3.3 further modal analysis was illustrated by simulating an experimental dipole antenna centrally fed by a coaxial cable without a balun. The experimental results showed a number of spurious resonances on the Smith Chart and these were attributed to so-called "antenna currents" flowing on the outer surface of the transmission line. Characteristic Modal analysis enabled the determination of a set of modes, some associated with the antenna and some associated with the line and half antenna combination. The extent to which the defined voltage source excited each of these modes was easily assessed. The resonant frequencies of the strongly excited transmission line and half antenna modes then helped explain the positions of the spurious loops on the Smith Chart. This demonstrated a useful feature of a modal approach compared to conventional Moment Method techniques. With relatively simple structures it is

possible to remove the effect of an unwanted mode, merely by altering the feed-point position.

In section 6.3.4 the Characteristic Modes of a corner reflector antenna were analyzed. It was demonstrated that usually, for complex or electrically large radiating structures, only a few of their significant modes contribute to the overall radiation. Although for the corner reflector these few excited significant modes produce optimal current flow for the desired application, this result has important implications for the next chapter. There, the Characteristic Modes of a number of vehicular structures are examined. These configurations will clearly exhibit numerous modes with many diverse far-field patterns. It is the intention to utilize these modes for pattern synthesis. Thus the once spurious current flow on an entire vehicular structure may be employed to realise desirable far-fields.

Section 6.4 addressed far-field pattern synthesis using Characteristic Modes. In section 6.4.1 the basic principles of the technique were demonstrated using a straight 1.91λ wire in free space. An important result of the analysis was that the method of port Characteristic Modes may be employed to reduce the total modes of the system without dramatically increasing the relative mean squared error of the synthesized far-fields. For the configuration considered there were six significant modes, thus requiring six voltage sources to completely control the radiated far-field pattern. Using a 4-port system however allowed the synthesis of particular target pattern whose relative mean squared error was only 0.0204 greater than that obtained using all six of the modes of the full structure. An important aspect of using the port mode technique however, was shown to be

the judicious choice of the ports taking into account the positions of the mode current maxima and minima of the modes of the full structure.

In section 6.4.2 the far-field pattern of a linear halfwave array was synthesized. The general-purpose nature of a Characteristic Modal approach was clearly shown. In this case a standard modal configuration for arbitrary linear arrays was formulated. It was shown that the modes of such structures could be arranged in groups with similar significance, the members of each group numbering the same as the elements in the array. More interestingly, the shape of the current distribution of the modes of each group on each element was nearly identical. This enabled a set of voltage sources to be defined to only excite one of these groups. This example again showed the importance of source positioning in determining the extent to which each mode is excited as well as its appropriate eigenvalue.

CHAPTER 7

ANTENNA SYSTEM DESIGN FOR COMPLEX STRUCTURES

7.1 Introduction

The preceding chapter described the principles of using Characteristic Modes for antenna analysis and far-field synthesis. Previously these techniques have only been applied to simple structures (eg. Yee and Garbacz 1973, Garbacz and Newman 1980), but in this chapter the principles developed in chapter 6 are applied to more complex vehicular structures. The aim of the analysis is to demonstrate how the current flow on the complete surface of such configurations may be utilized to realise desirable far-field patterns.

Initially in section 7.2 the general form and composition of the modes of simplistic box models of vehicular structures are investigated. Each geometrical configuration, in wire grid form, is initially analyzed without any antenna. This illustrates the modes inherently associated with complex structures alone and further how their composition is affected by mounting particular antennas in various positions.

In section 7.3 the problem of HF vehicular antenna design is addressed. This involves the development of antenna systems for the application of Near Vertical Incidence Skywave (NVIS). This is a particular difficult situation where an antenna is required that radiates power at a high elevation angle.

Conventional vehicle antennas are examined and modelled in section 7.3.1 and are shown to be inherently unsuitable for this purpose. Optimization of the Characteristic Modes of the composite structure of vehicle plus antenna however, allow the realization of desirable NVIS far-field patterns. Section 7.3.2 describes the Characteristic modes of a typical motor vehicle and applies the principles of Characteristic Modal analysis. Also a manageable number of modes is obtained by treating the vehicle as an *N*-port network. With this representation the choice of the position of the ports is clearly of vital importance. This is addressed in section 7.3.3 which shows how the current distributions of the modes of the complete vehicle may be used to assist in deciding on their positions.

In section 7.3.4 the Characteristic Modes of the vehicle are optimized to produce a number of appropriate NVIS far-field patterns. The practical implications of using multi-port feed-systems to excite these desirable currents are examined. Unconventional methods of feeding such structures are suggested and the overall radiation efficiency of typical systems is also assessed.

7.2 Complex Structures

7.2.1 Vehicle Structures

This section examines the Characteristic Modes of a simple box representation of a land based motor vehicle. The frequency of operation used in the analysis is such that the structure is below its first natural resonance. Antenna system design in this region presents a particular difficult situation. When the antenna and vehicle are of comparable electrical size, the specified

far-field of the antenna may be significantly altered by current flow on the mounting structure. Examination of the modes of the vehicle alone however allow insight to be gained into their probable effect on the performance of any mounted antenna. Also, it is shown that the modes of the vehicle alone exhibit numerous diverse far-field patterns. This suggests that a wide range of patterns may be synthesized by optimizing particular modes.

Figure 7.1 show a closed perfectly conducting box structure, somewhat representative of a motor vehicle, situated 0.5m over an infinite, perfectly conducting ground plane. A corresponding wire grid model of the structure is then shown in figure 7.2. No antenna is initially specified.

The modes of this structure were examined at 15MHz, where the wavelength is 20m and the largest dimension of the box is below the first fundamental resonance. Using the significance criterion discussed in the previous chapter, four modes were found to control the overall radiation characteristics. Their eigenvalues are shown in table 7.1. All other modes exhibited eigenvalues that were at least two orders of magnitude larger than mode 4 and their effect was considered entirely negligible based on the 30dB cut-off.

Considering the radiated far-fields of these four modes, figure 7.3 shows firstly the percentage of power radiated in each electric field polarisation, either vertical or horizontal. Figure 7.4 then shows the 3-dimensional far-fields patterns of the modes in each of these polarizations.

The far-field of mode 1 is predominantly vertically polarised with a horizontally omni-directional pattern. Modes 2 and 3 give both horizontally and

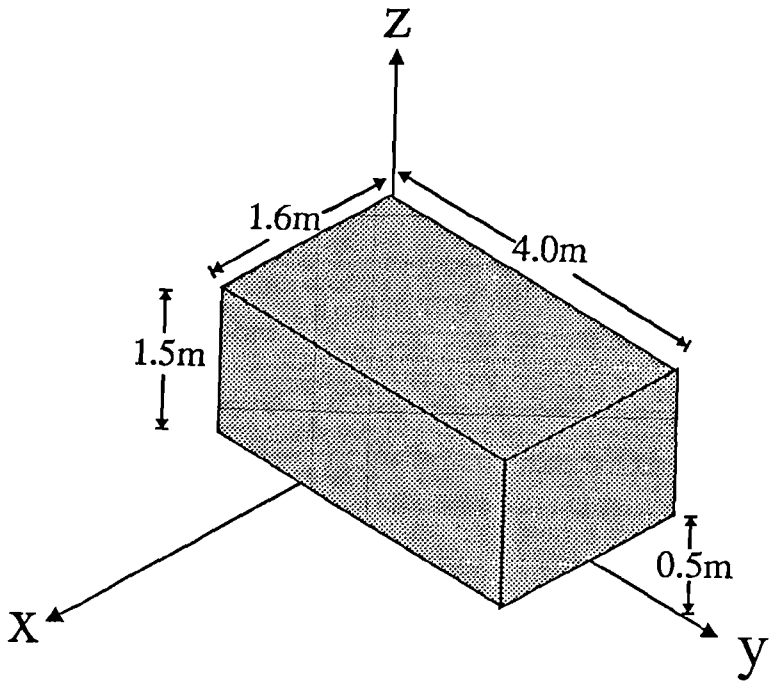

Figure 7.1 Conducting box with dimensions

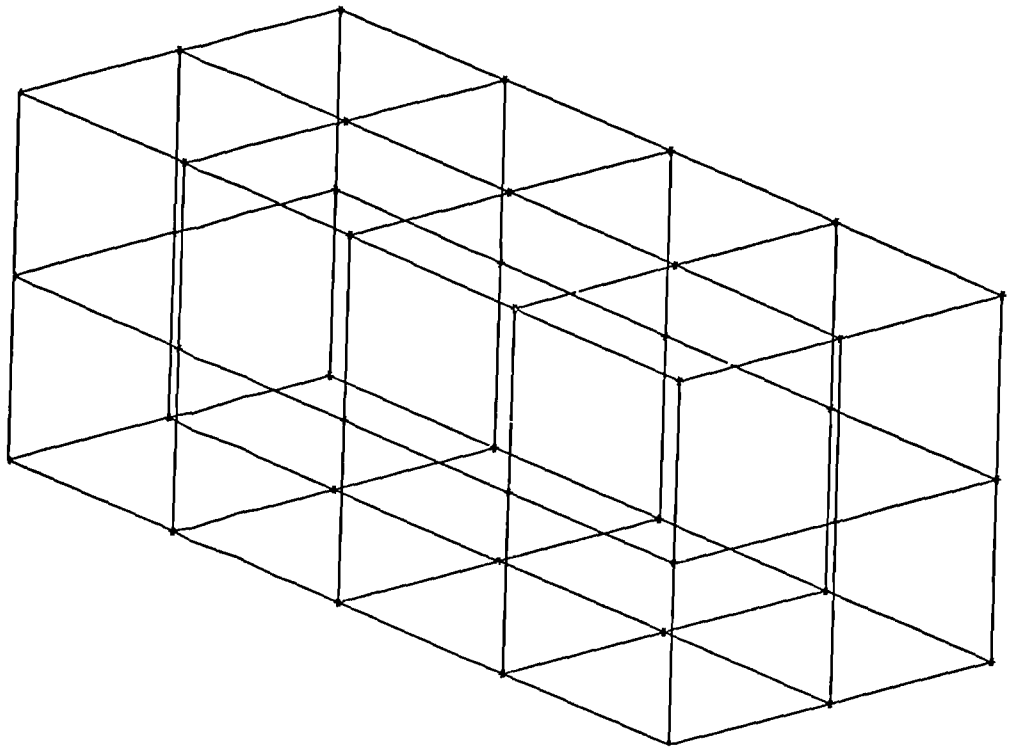

Viewing angles: θ=70°, ϕ=50°

Figure 7.2 Wire grid model of the conducting box shown in figure 7.1

Table 7.1 Modal eigenvalues of the four most significant modes of the conducting box

Mode	Eigenvalue
1	-8.493
2	21.539
3	30.659
4	-69.688

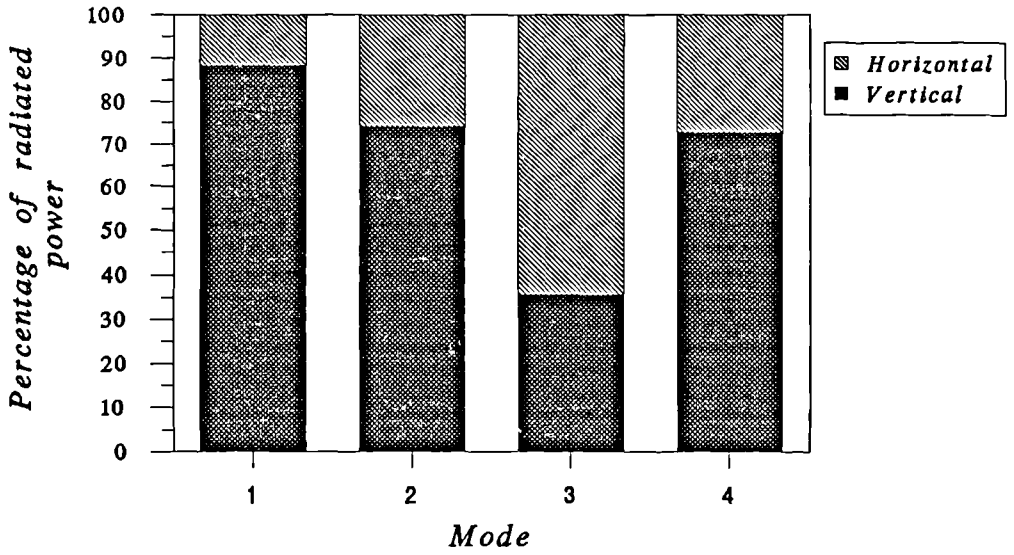

Figure 7.3 Percentage power of the electric far-field of each Characteristic Mode of the conducting box in each linear polarization

vertically polarized far-field patterns of nearly identical shape, but with different orientations. The percentage of power radiated in each polarization also differs markedly for these two modes. Mode 4 gives the most complex vertically polarised pattern. Whereas the horizontally polarized pattern is nearly identical to that of mode 2, the vertically polarized pattern consists of a vertically directed lobe and two other horizontal lobes whose maxima are directed along the largest dimension of the vehicle.

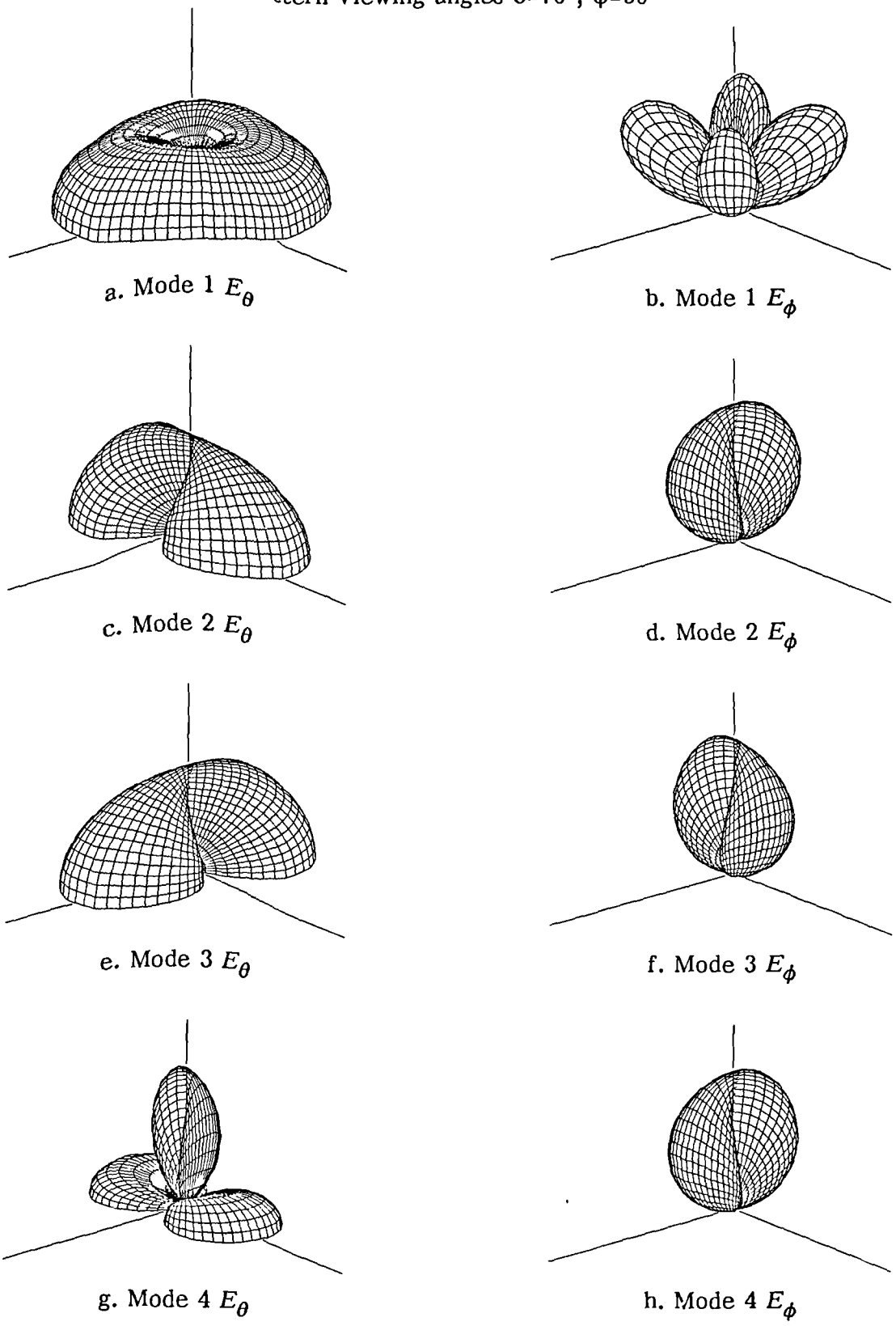

Figure 7.4 Far-field patterns of the four most significant modes of the conducting box shown in figure 7.1

These four modes were found to be specific to numerous wire grid representations of boxes below their first fundamental resonance. Changing the electrical dimensions of the box analyzed above, or its height above the ground plane, did not alter, to any noticeable extent, the shape of the far-fields of these four significant modes. Their patterns always remained nearly identical to those illustrated in figure 7.4. Only the eigenvalue associated with each mode, and thus the ease by which it is excited, was affected by changes in the box dimensions.

Using a simple representation of a vehicle, the above analysis suggests that a standard 4-mode composition exists for such structures. Below resonance these four modes are dominant and they will therefore completely control the radiation or scattering characteristics of such structures. Thus the effect of mounting an antenna that electrically couples the structure is the excitation of these four specific modes. Clearly though, the type and mounting position of the antenna will directly affect the extent to which each of the modes are stimulated. A further concern is also the modifying effect of the mounted antenna on the far-fields patterns of the standard modal composition. This is discussed below in section 7.2.2.

7.2.2 Vehicular Antennas

This section describes the Characteristic Modes of the box structure shown in figure 7.1 with two typical conventional antennas attached. The first is a vertical 2m monopole (a=0.01m) that was mounted at the centre of the upper surface of the box. Figure 7.5 shows the wire grid model of the configuration.

Secondly a vertical loop was added. Figure 7.6 shows the resulting wire grid model with a 4.0m x 1.5m (a=0.01m) loop centrally positioned on the box and spanning its complete length.

The Characteristic Modes of these complete, composite structures were calculated at 15MHz. It was noted that both configurations, as before, yielded four significant modes. The far-field patterns of these modes corresponded almost identically (within 1% at any point) with those of the four modes associated with the box alone shown in figure 7.4. Table 7.2 shows the eigenvalues of these two newly defined modal systems.

Table 7.2 Eigenvalues of the four most significant modes of the box shown in figure 7.1 with a monopole and a loop antenna

Mode	Monopole antenna	Loop antenna
1	-7.256	-6.939
2	21.534	18.882
3	30.456	30.658
4	-69.235	-69.408

It is interesting to compare the modal eigenvalues of these two systems with those of the box alone without any antenna. For the vertical whip configuration only the eigenvalue of mode 1 is changed to any extent. Those of modes 2, 3 and 4 are nearly identical to those of the structure alone. For the loop antenna however the eigenvalues of both modes 1 and 2 are changed compared to the box alone, with those of mode 3 and 4 staying the same. Hence the effect of mounting an antenna on the box is only to increase the significance

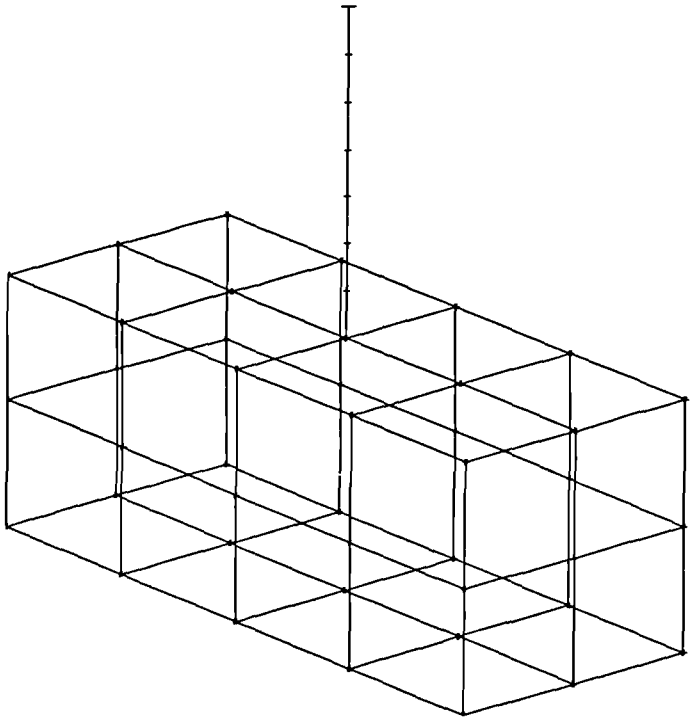

Viewing angles: θ=70°, ϕ=50°

Figure 7.5 Wire grid model of the conducting box shown in figure 7.1 with a centrally mounted vertical monopole

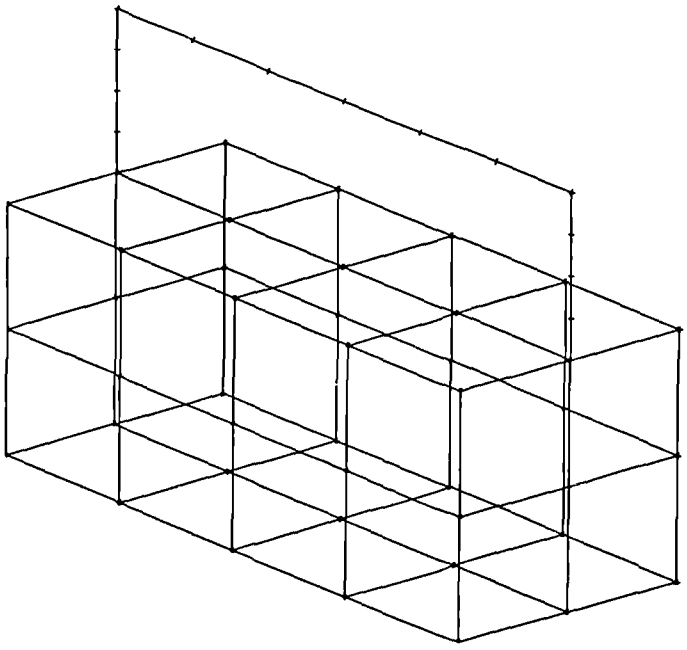

Viewing angles: θ=70°, ϕ=50°

Figure 7.6 Wire grid model of the conducting box shown in figure 7.1 with a vertical loop attached

of certain of the modes associated with the structure alone. The modal composition, in terms of far-field patterns, remains the same. This effect was found to be independent of altering the electrical dimensions or mounting position of the monopole or loop antennas. Only as their electrical dimensions became comparable to those of the box did the far-field patterns of the four begin to change.

Generally then, for a vertical monopole of length less than 0.25λ mounted on a box below its first fundamental resonance, four significant modes are apparent. Their far-field patterns are nearly identical to those above in figure 7.4. Three of these modes are unaffected by changes in the length of the monopole and are inherently controlled by the overall dimensions of the box. The significance of the other mode however is controlled by both the length of the monopole and the dimensions of the box. Similarly any loop mounted on a box structure below its first resonance exhibits four significant modes with far-field patterns as above. This is provided that the largest dimension of the loop is no larger than that of the box. In this case the significance of two of the four modes is controlled by the size of the loop.

It can be concluded therefore that, below resonance, the radiation characteristics of vehicle antenna systems are significantly reliant upon the shape and dimensions of the complete, composite structure. For a wide range of boxes below their first fundamental resonance a standard four mode composition is defined. The far-fields of these four modes are substantially independent of the electrical dimensions of the box. Only the eigenvalues, which govern each

mode's significance in the overall radiation, are affected by the dimensions of the box. The far-fields of these modes are also substantially unaffected by mounting a conventional monopole or loop antenna. Provided the antenna is no larger than the maximum dimension of the box the same standard four-mode composition is obtained. Mounting an antenna though does affect the eigenvalues of the four modes. It can therefore be considered as a device which increases modal significance. Interestingly the monopole antenna above only increased the significance of one of the standard modes, whereas the loop increased that of two. Hence a particular antenna is more effective at enhancing certain, individual modes. Thus, in using the method of Characteristic Modes for vehicle antenna system pattern synthesis, the choice of antenna is clearly important, as it acts as a probe which enables the varying excitation of the standard vehicular modal configuration. With the level of excitation governed by the antenna, this is clearly an vital aspect in enabling the utilization of these complete structure modes.

The following section extends the principles discussed here to a practical application by addressing the problem of mobile HF antenna design. Further to the simplistic representation of vehicular structures described above, the Characteristic Modes of a realistic wire grid model of a Land Rover are identified. These modes are then optimised to produce a far-field suitable for the so-called Near Vertical Incidence Skywave (NVIS) mode of propagation.

7.3 HF Mobile antennas

7.3.1 Near Vertical Incidence Skywave (NVIS)

For certain applications there is a need to communicate within the HF skip zone which falls between the first skywave return and the boundary of the ground-wave. The region is usually always beyond the line of sight (BLOS) and is frequently obscured by terrain features. Hence in the absence of man-made relay facilities or satellites, radio communication is only possible using the so-called Near Vertical Incidence Skywave (NVIS) (eg.Goodman 1992 pp.217-224, Maslin 1987 pp.81-85). Figure 7.7 shows a typical application of this mode of propagation, where it is clearly necessary to use an antenna that radiates substantial power at angles close to zenith.

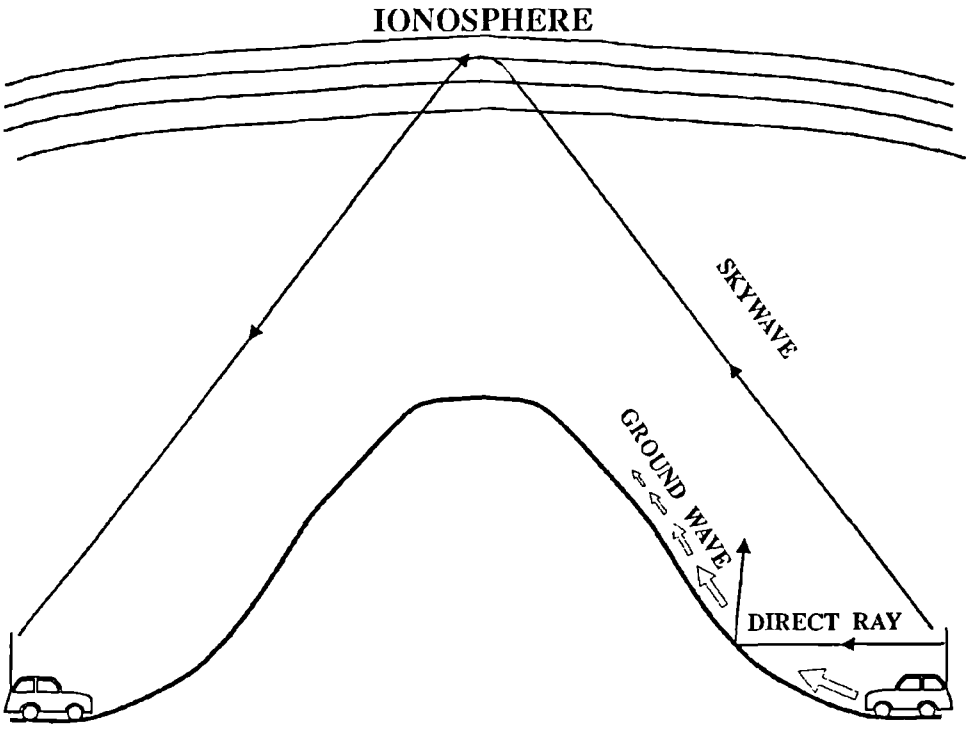

Figure 7.7 The Near Vertical Incidence Skywave (NVIS) mode of propagation.

The necessity for this form of relatively short-range radio link is most apparent in military situations. Herbstreit and Crichlow's (1964) World War II experimental field trials of the performance of various military mobile antennas demonstrated the difficulty in propagating radio signals using the ground-wave through dense jungles. This is a clear application for NVIS. Hagn *et al* (1970, 1973 and 1974) described how NVIS was successfully used in the Vietnam conflict. Most recently in the Middle East, Wallace (1992) described the American Army's reliance upon NVIS for short-range radio links.

A significant constraint on NVIS antenna systems is the frequency of operation. Because of the need for vertical incidence of the radiated signal upon the ionosphere, the frequency of operation must be close to the prevailing critical frequency f_c. This varies with the time of day, season and also the level of sunspot activity. For the F2 layer, which is usually employed for NVIS, the critical frequency will be in the range 1.5-12.0 MHz. At the lower end of this band, where the wavelength is nominally 200m, feeding power into any vehicular antenna system will clearly present difficulties. For typical geometrical configurations, comparable in size to those described in section 7.2.1, the input impedance will generally be highly reactive with a relatively small resistive component.

7.3.2 NVIS Antennas

7.3.2.1 Whip Antennas

The conventional, most widely used HF vehicle antenna is a vertical whip. This antenna though is clearly unsuitable for NVIS applications because of the

inherent null that exists at $\theta=0°$. Figure 7.8 shows the dimensions of a box model of a Land Rover. This is typical of the type of vehicle from which NVIS communications are required. Figure 7.9 then shows its implemented wire grid model with a 2m vertical whip antenna mounted on the rear left corner of the roof.

Figure 7.10 confirms the inherent unsuitability of this antenna system for NVIS communications, showing the predicted three-dimensional total electric far-field pattern with the antenna base fed at 10MHz. Defining a figure of merit for NVIS antenna systems as the percentage of total radiated power in the cone specified by $\theta<45°$, it amounts to just 13.21% for this antenna.

One approach used to overcome the NVIS antenna problem is to tilt the whip antenna. Eley *et al* (1991) proved the viability of this procedure by using the

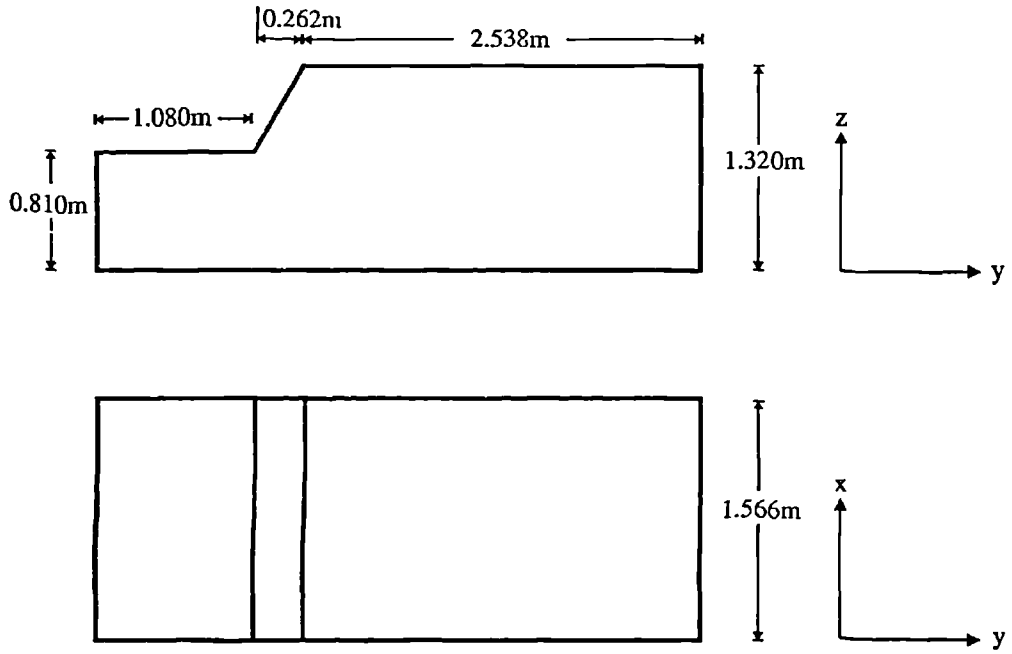

Figure 7.8 Simple box model of a Land Rover vehicle

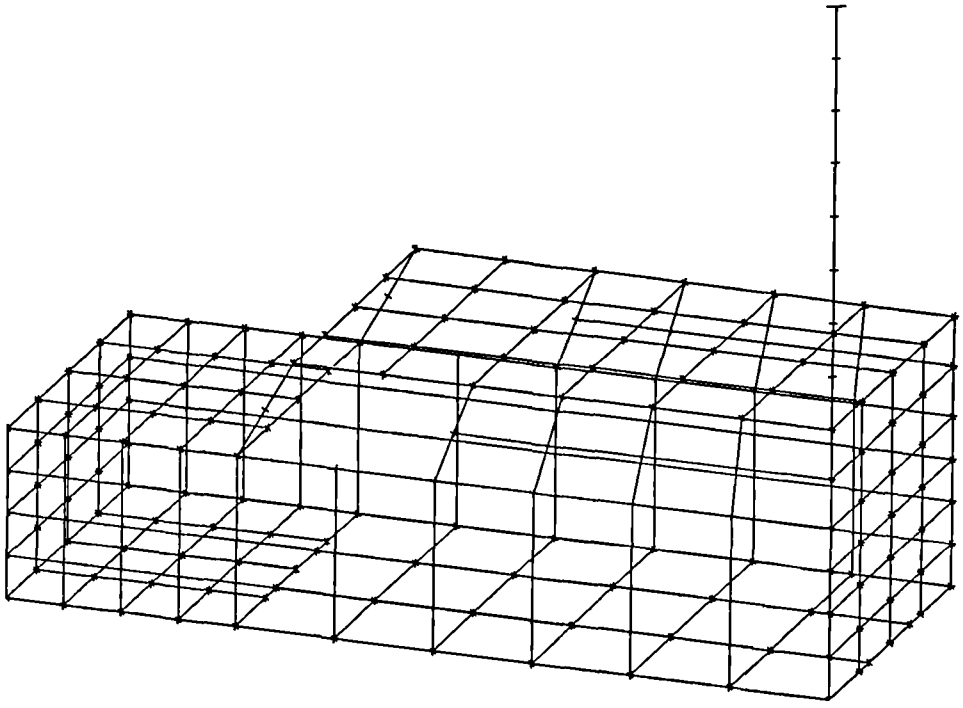

Viewing angles: θ=70°, ϕ=20°

Figure 7.9 Wire grid model of the Land Rover of figure 7.8 with a 2m vertical whip antenna mounted at the left rear corner

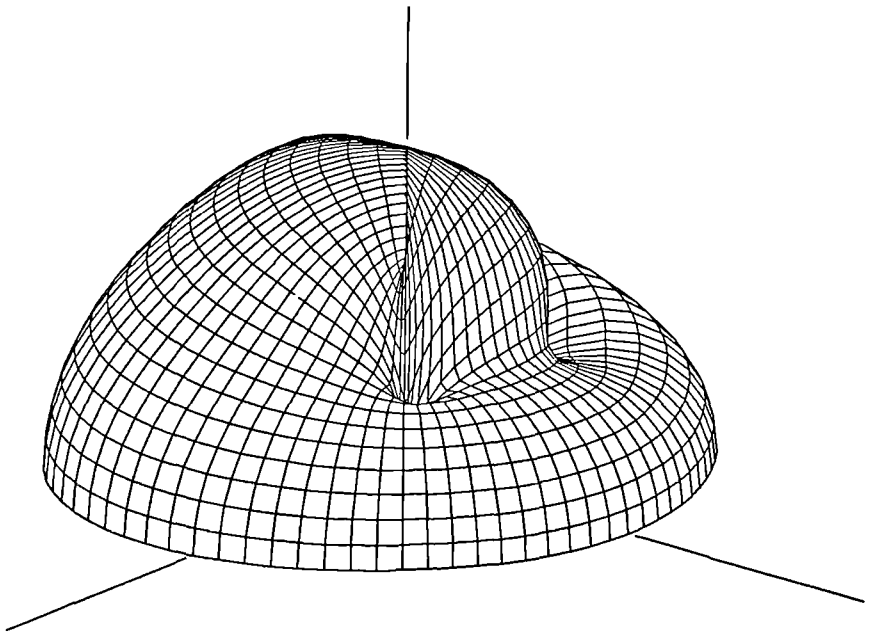

Viewing angles: θ=70°, ϕ=40° (Origin=-20dBi)

Figure 7.10 Predicted total far-field pattern in dBi of the Land Rover with vertical whip antenna base fed at 10MHz

NEC code to predict the far-fields of a tilted whip mounted on a land based HMMWV vehicle. Antelme and Straub (1990) also designed a horizontal dipole antenna system for mobile HF communications. Figure 7.11 demonstrates the effect of tilting the whip antenna mounted on the Land Rover described above. It shows the calculated variation in the percentage power radiated in $\theta<45°$ as the whip is tilted both toward and away from the vehicle at a frequency of 10MHz.

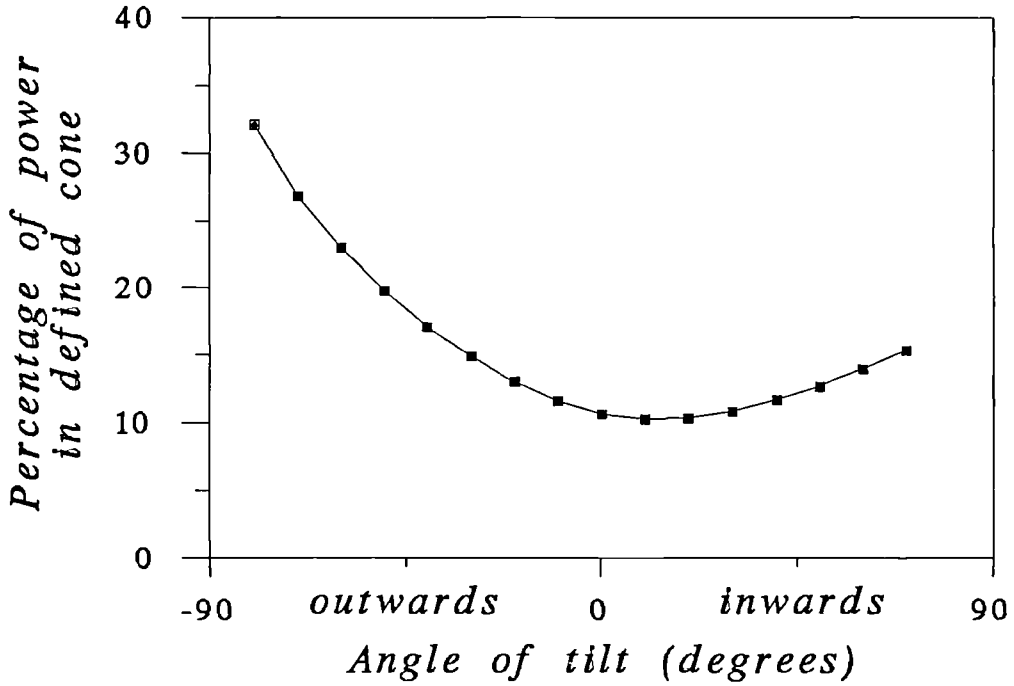

Figure 7.11 Variation in the percentage of total power radiated in $\theta<45°$ with whip tilt angle

The best improvement is clearly obtained with the whip tilted away from the vehicle. With a tilt angle of 80° more than 30% of the total radiated power is in the defined figure of merit cone. Tilting the whip inwards produces only negligible improvement with at best around only 5% more of the total radiated power in $\theta<45°$than with the whip vertical. These results agree broadly with the

HMMWV simulations of Eley *et al* (1991).

The above analysis shows that the titled whip is suitable for NVIS antenna vehicular systems. The major disadvantage however is practical difficulties associated with the whip protruding, at a near horizontal angle, from the rear of the vehicle. A further concern is the input resistance associated with the system. Figure 7.12 shows how this quantity varies with the tilt angle.

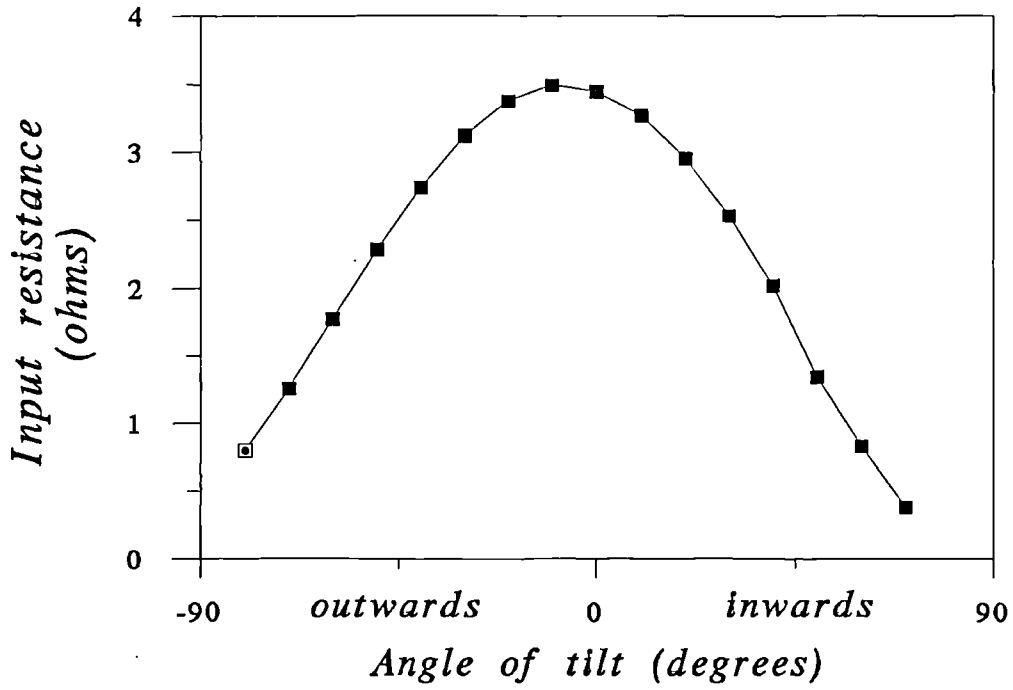

Figure 7.12 Variation with tilt angle of the input resistance of a 2m whip antenna mounted at the rear of a Land Rover

Clearly for effective NVIS communications the relevant input resistance is less than 1Ω, around a quarter of the value with the antenna vertically orientated.

7.3.2.2 Loop Antennas

Another conventional technique for overcoming the NVIS problem is the use of loop antennas. Burberry (1982) recognised the inherent unsuitability for NVIS of existing mobile antennas and developed a range of loop antennas for mounting on various air, land and sea mobile structures. Baker (1991) measured the performance of a scale model helicopter with a loop antenna and found it suitable for NVIS. Griffiths and Baker (1990) further developed a portable loop antenna for NVIS.

Figure 7.13 shows a wire grid model of the Land Rover described above with a mounted loop similar to that described by Burberry (1982). Figure 7.14 then shows the predicted total far-field pattern obtained with the loop excited at its front base at a frequency of 10MHz, although the pattern remained substantially unaltered over the complete frequency range 2-12MHz.

This geometrical configuration is inherently more suitable than the vertical whip antenna for NVIS applications with 30.45% of the total radiated in power in $\theta<45°$ at 10MHz. This figure remained consistent throughout the frequency band. It is clearly a more robust configuration than the tilted whip with the percentage of radiated power in $\theta<45°$ comparable to the best obtainable with the tilted whip. This is obtained however without the practical constraints associated with tilting the whip nearly horizontally away from the vehicle.

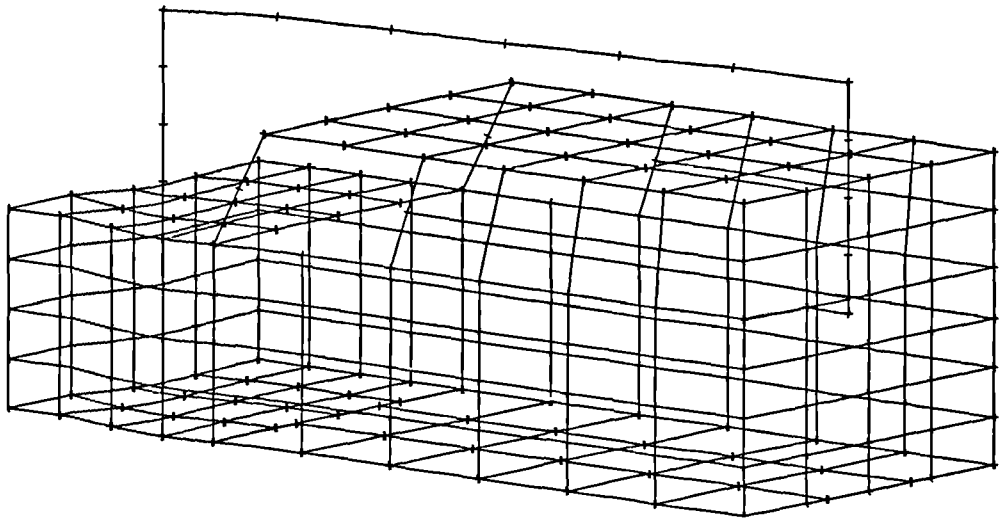

Viewing angles: θ=80°, ϕ=40°

Figure 7.13 Wire grid model of the Land Rover of figure 7.8 with a mounted loop antenna for NVIS communications

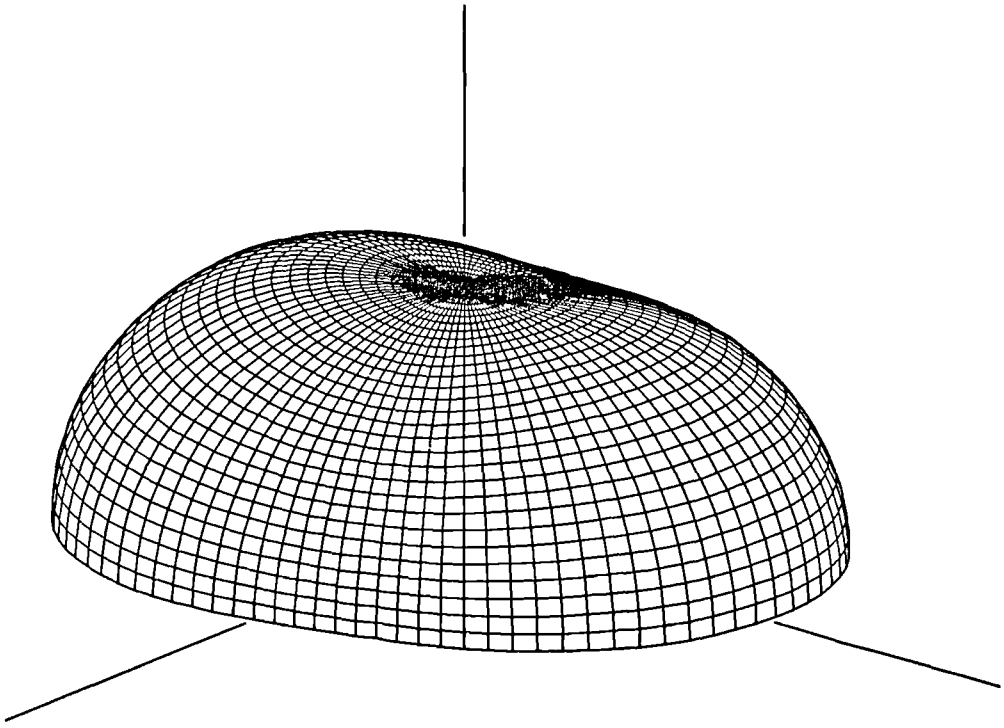

Viewing angles: θ=70°, ϕ=40°

Figure 7.14 Far-field pattern of the loop antenna fed at the front base at 10MHz

7.3.2.3 Antenna Design

The previous two sections have demonstrated existing antenna systems that are employed for NVIS communications. Both configurations, the tilted whip and the loop, have been designed without attempting to utilize current flow on the vehicle. It is the philosophy of this thesis that the method of Characteristic Modes allows such utilization. Section 7.2.2 proved that for vehicular structures below their first resonance four specific modes exist. The far-field patterns of these modes remain substantially unaffected by wire antennas mounted on the structure. The relative significance of each mode and the ease by which it can be excited is though reliant on the type and position of any mounted antenna. The following section uses the method of Characteristic Modes as a tool for the design of antenna systems for complex structures and shows how, with the choice of a suitable antenna, this standard modal configuration for vehicles may be exploited to yield desirable radiation characteristics.

7.3.3 Vehicle Characteristic Modes

7.3.3.1 Land Rover without Antenna

The Characteristic Modes of the Land Rover described in the previous section were calculated in the NVIS frequency band 2-12MHz. Initially, with no antenna specified, the wire grid was assumed perfectly conducting and was situated over a infinite, perfectly conducting ground plane.

The modal composition of this configuration was similar to that of the previous simple box model. Using the 30dB cut-off four modes could be classed as completely controlling the radiation from the structure. Figure 7.14 shows

how the significance of each these modes varied in the defined NVIS frequency band. As before, this is specified in terms of the inherent modal significance, expressed as the modulus of $1/(1+j\lambda_n)$.

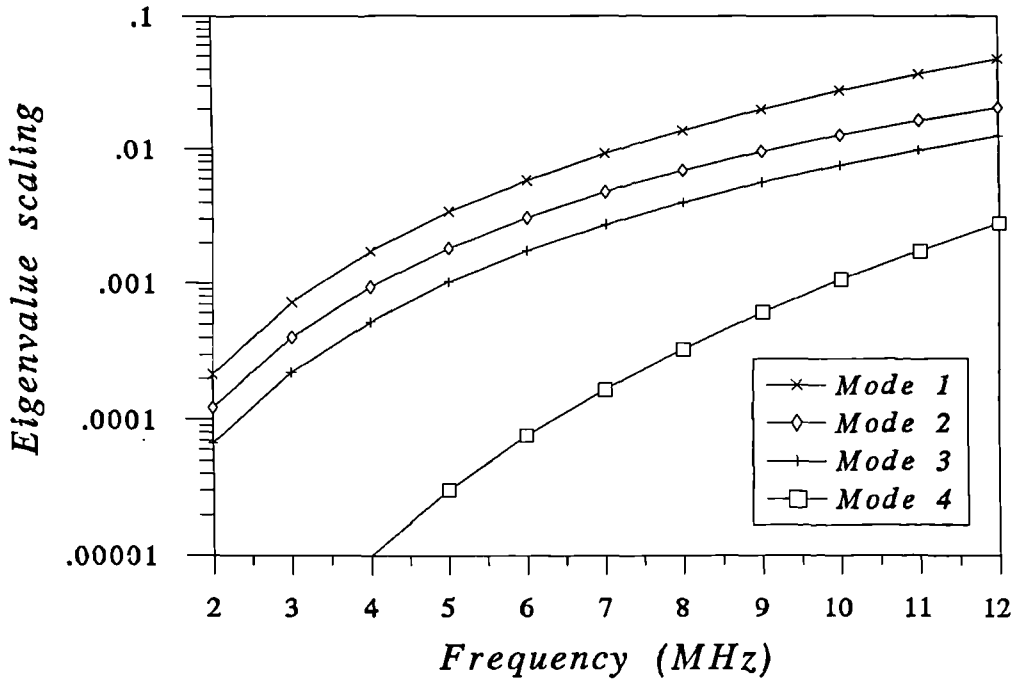

Figure 7.15 Variation with frequency of inherent eigenvalue scaling of the significant modes of the Land Rover without any antenna

Interestingly, the significance of the first three modes decreases at approximately the same rate as the frequency is reduced. For mode 4 however, its significance decreases at a rate substantially greater than the other three. At the lower end of the frequency band therefore the effect of this mode will be entirely negligible.

Another important finding is that the far-field patterns of these four modes are nearly identical to those of the simple conducting box. This confirms the previous conclusion that a standard modal composition exists for vehicular structure below their first fundamental resonance. This is further affirmed by

the examination of the eigenvalues associated with each mode, which are shown in table 7.3 for a frequency of 12MHz. Also presented, for comparison, are the eigenvalues of the simple conducting box at 15MHz from table 7.1.

Table 7.3 **Comparison of the modal eigenvalue spreads of the conducting box at 15MHz and the Land Rover at 12MHz**

Mode	Modal eigenvalue (conducting box at 15MHz)	Modal eigenvalue (Land Rover at 12MHz)
1	-8.493	-26.602
2	21.539	59.180
3	30.659	80.795
4	-69.688	-435.441

The similarity in each of these eigenvalue spreads is clearly apparent. Firstly, due to the lower frequency and smaller electrical size, the moduli of the eigenvalues of the Land Rover are generally larger. Secondly though, each mode from one set directly corresponds with the same mode from the other set. Each pair of modes have nearly identical far-fields. Also the sign of each eigenvalue pair is the same inferring the same form of current flow. Pavey (1980) used a simplistic modal representation of loops and dipoles to represent the current flow on aircraft frames. A similar approach may be applied here. Hence a mode with a negative eigenvalue whose modulus increases as the frequency is reduced may be termed as a "dipole mode". Its behaviour is similar to that of the modes associated with a straight wire as described section 6.3.2. Thus this type of mode

has an eigenvalue that goes from negative through resonance to positive as the frequency is increased. Modes 1 and 4 thus exhibit the characteristics of "dipole modes" in this case. Modes 2 and 3 however may be termed "loop modes". Their modal characteristics are similar to those associated with a simple loop and thus circulating current. These modes are initially inductive with a positive eigenvalue which reduces goes through zero and becomes negative as the frequency is increased. This simplistic approach also helps explain the far-field patterns of the standard four mode configuration.

7.3.3.2 Land Rover with Antenna

In section 7.2.2 it was suggested that the effect on the composition of the Characteristic Modes of a vehicle structure of mounting a simple wire antenna was minimal. It was found that only the significance of each mode was changed and that the far-field patterns remained substantially unaltered. This property was investigated for the Land Rover by comparing the previously defined modal set, specified without any mounted antenna, with that obtained with the loop antenna configuration mounted as shown in figure 7.13.

The results obtained confirmed the initial conclusion. Across the entire frequency range the far-field patterns of the modes remained significantly the same as those associated with the Land Rover without any antenna. The loop though did though change the modal significance, reducing the modulus of the eigenvalue associated with each mode. This increase remained approximately the same for each mode across the complete frequency range 2-12MHz. Table 7.4

shows the mean absolute increase across the frequency band of the modulus of the factor $1/(1+j\lambda_n)$ associated with each mode, although the increase in significance of any mode at any frequency never differed from these figures by more than 2%.

Table 7.4 Percentage mean absolute increase in modal significance due to mounting a loop antenna on the Land Rover

Mode	Percentage mean absolute increase in modal significance
1	25.30
2	20.94
3	0.29
4	19.77

With this antenna configuration, which is more complex than the initial loop configuration mounted on the simple conducting box in section 7.2.2, the significance of three of the four standard vehicular modes is increased. Mode 3 is unique for this configuration in that its significance is virtually unaffected by the presence of the antenna.

In the next section the Characteristic Modes of this antenna configuration are employed in the pattern synthesis routines that were developed and described in chapter 6. This vehicular antenna was chosen as the basis of the work because alone it is inherently more suitable for NVIS than the others that have been considered. Secondly, this antenna increases the significance of three of the four modes of the standard modal composition. This suggests their probable easier

stimulation by direct excitation of the loop.

7.3.4 Pattern Synthesis for NVIS

7.3.4.1 Target Pattern Definition

In using the Characteristic Modes of the Land Rover described above for far-field pattern synthesis, an important aspect is the choice of target pattern. For the work described here two approaches were used. In both cases total electric field was specified as the polarization of the final result is unimportant for NVIS propagation because of the modifying effect of the ionosphere. The first pattern specified that all of the power radiated should be in $\theta<45°$ as shown in figure 7.16.

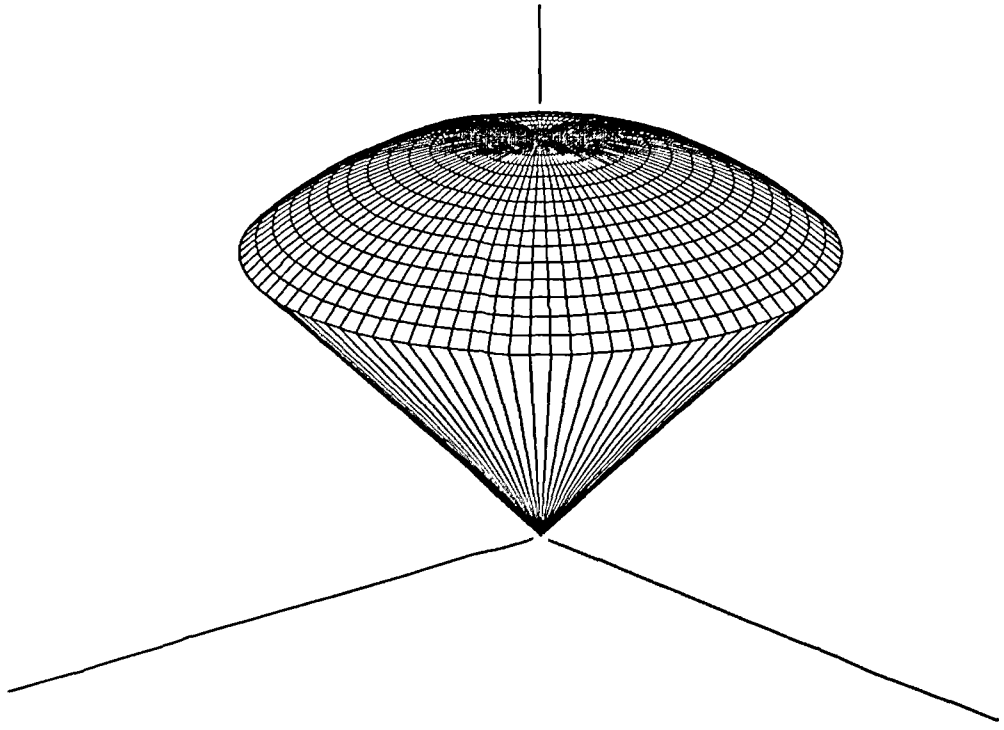

Viewing angles: $\theta=70°$, $\phi=50°$

Figure 7.16 Initial target far-field pattern used for NVIS synthesis.

Although this target pattern was successful in determining modal scaling factors that yielded approximating patterns suitable for NVIS, it was found that the abrupt change in target field sometimes overly constrained the approximation. Thus a fourth order polynomial function was defined for the target pattern. Constant for all ϕ and with θ expressed in radians the target total far-field pattern E_T was defined as:

$$E_T = \begin{cases} 1.008 - 0.694\theta + 2.657\theta^2 - 4.252\theta^3 + 1.659\theta^4 & : \theta \leq 75° \\ 0 & : \theta > 75° \end{cases} \qquad (7.1)$$

and is shown in figure 7.17.

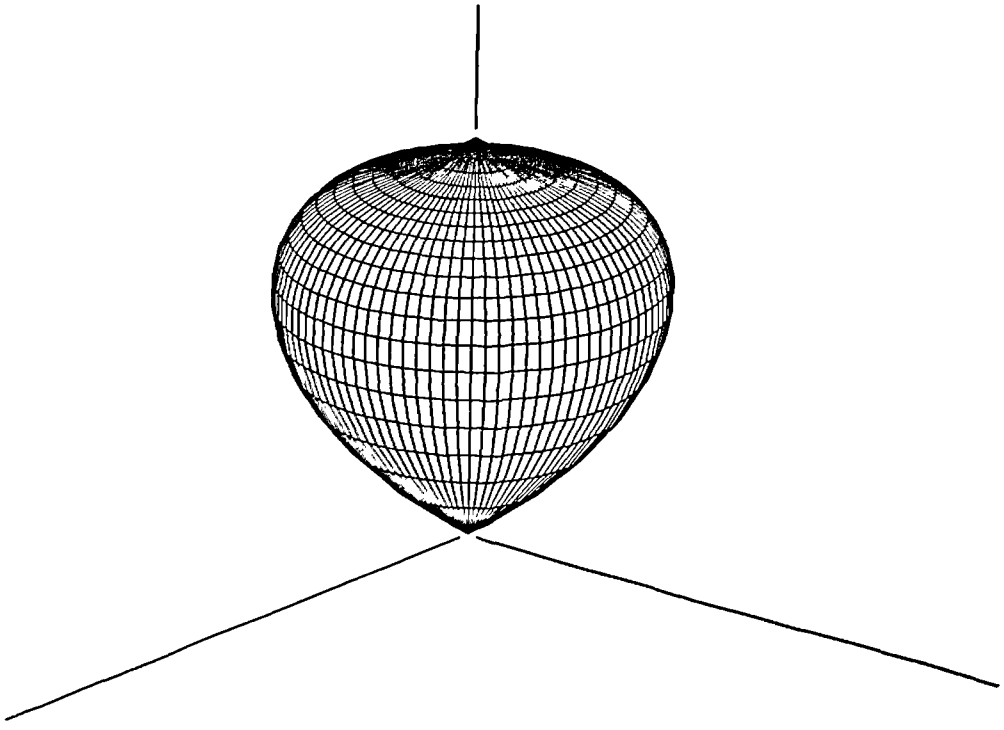

Viewing angles: θ=70°, ϕ=40°

Figure 7.17 Modified target far-field pattern used for NVIS synthesis

This target pattern was found to much better fully utilize each of the modes. Although some power is radiated below θ=45°, nearly 90% of the total is in θ<45°.

7.3.4.2 Modal Optimization

Section 6.4 showed that examination of the current distributions of the modes associated with a structure is important in choosing the best place at which to position voltage sources. Also shown, in section 7.2.2, was how mounting an antenna on the structure presented a method by which certain modes could be more effectively excited. This was evident by the change in modal significance introduced by the antenna and also the appropriate mode current distribution along its surface.

In order to assess the most appropriate positions for sources to best excite the 4 modes associated with the Land Rover and loop configuration their current distributions were examined. It was found that there was substantial power coupling into the ground shown by relatively large mode currents on the underside of the structure. Assuming that it would be impractical to position voltage sources here these mode current maxima were ignored. Figure 7.18 though shows a number of mode current maxima that were thought possible suitable locations for an as yet unspecified feeding mechanism.

These points were a number of a range of points which consistently exhibited a mode current within 95% of the maximum for at least two of the modes. They are therefore the most effective positions at which to excite the

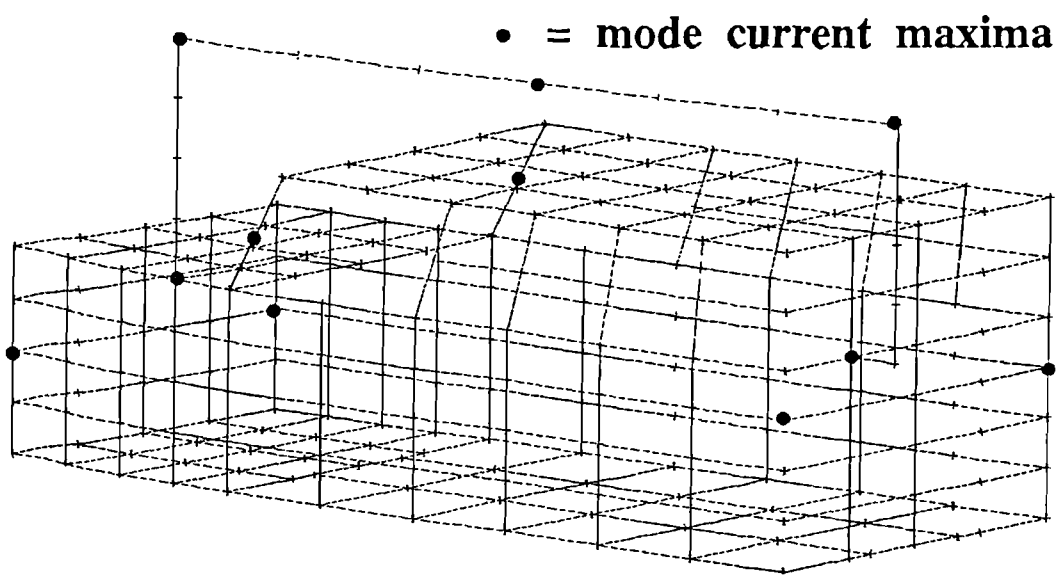

Figure 7.18 Land Rover and loop configuration with a number of mode current maxima

structure and stimulate all modes strongly. Four of these points were thus chosen to use in a 4-port mode representation of the Land Rover. They were chosen as being the most practically accessible in terms of the later positioning of voltage sources to physically realise the synthesized far-field patterns. Although in the initial analysis these feed-points were defined using the Method of Moment delta-gap model, the practicality of their implementation will addressed in section 7.3.4.4. Table 7.5 thus specifies the positions of each of these four chosen ports.

Hence a new Characteristic Modes scheme was defined, specific to these four feed-points. These port positions ensured that this new composition exhibited the same four standard modal far-field patterns. These modes were then used in the unrestricted phase pattern synthesis routine with the polynomial function shown in equation 7.1 employed as the target pattern. Figure 7.19 shows

Table 7.5 Positions of the four chosen feed-ports associated with the Land Rover

Port Number	Position on Land Rover
1	Right-hand side roof pillar
2	Left-hand side roof pillar
3	Loop antenna - front base
4	Loop antenna - rear base

how the mean squared error of the resulting approximating pattern varied with the number of modes used. As usual the modes were ordered in terms of decreasing significance. This result is for an operating frequency of 10MHz but the error remained substantially unaltered throughout the NVIS band.

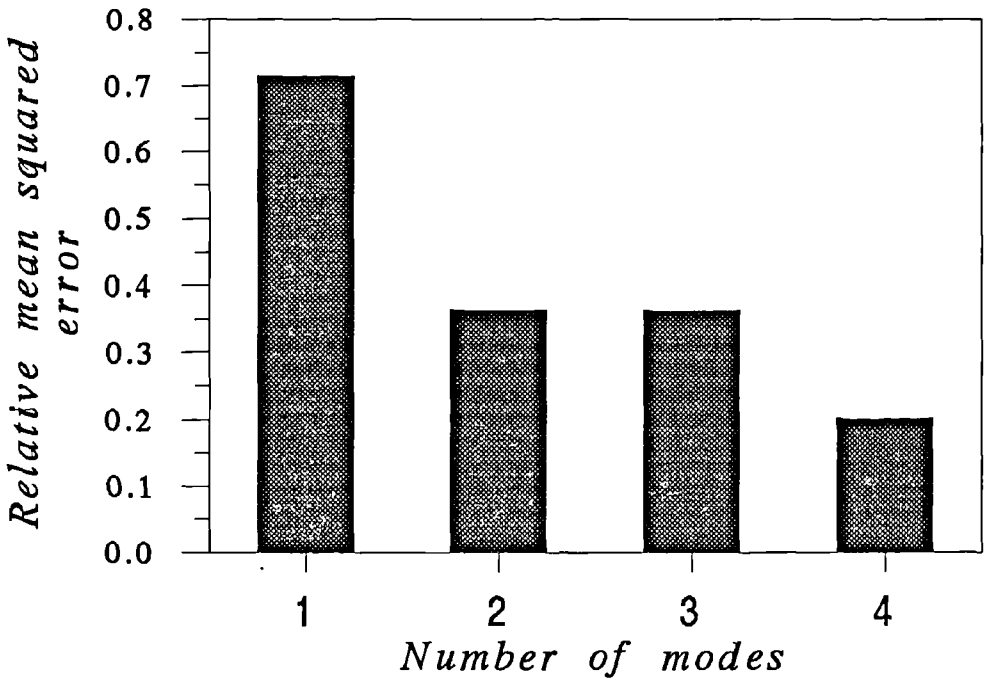

Figure 7.19 Variation of the mean squared error of the approximating pattern using the 4 port mode representation of the Land Rover

As expected, there is a clear improvement in the accuracy of the approximating pattern as the number of modes used is increased. The result using three modes however is only marginally better than with two modes.

To assess the importance of exciting current flow on both the antenna and on the vehicle surface two alternative 2-port representations of the Land Rover were examined. The first was specified using only the front and rear bases of the loop whilst the second defined only the two roof pillars as feed-ports. The variation of the relative mean squared error of these two simpler configurations, using either one or two of their resulting modes, is shown in figure 7.20.

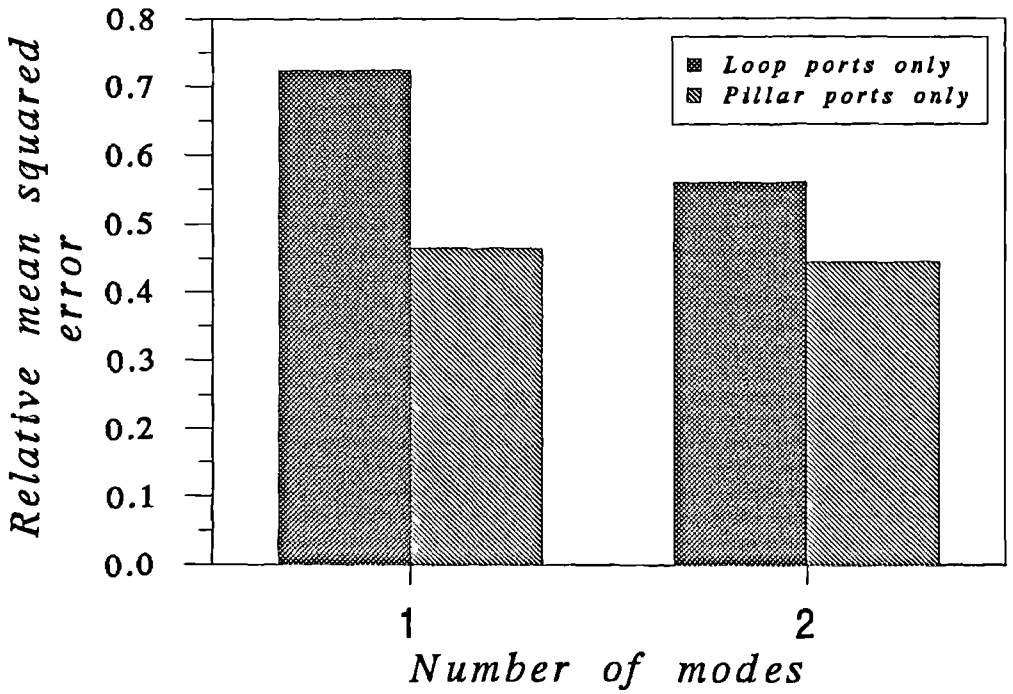

Figure 7.20 Variation of the relative mean squared error of the two simpler 2-port representations of the Land Rover

Clearly this plot demonstrates the importance of exciting substantial current flow on both the vehicle structure and the antenna. Using only the loop mode feed-points the lowest possible relative mean squared error is 176% greater

than that obtainable using the 4-port configuration. Similarly using only the 2 pillar mode feed-points the best mean squared error is 159% greater. This is further illustrated by figure 7.21 which shows the percentage of total power radiated in $\theta<45°$ for each of the modal compositions shown here. Also shown are the figures of merit for the conventional vertical whip and for the loop fed conventionally as discussed in section 7.3.2.

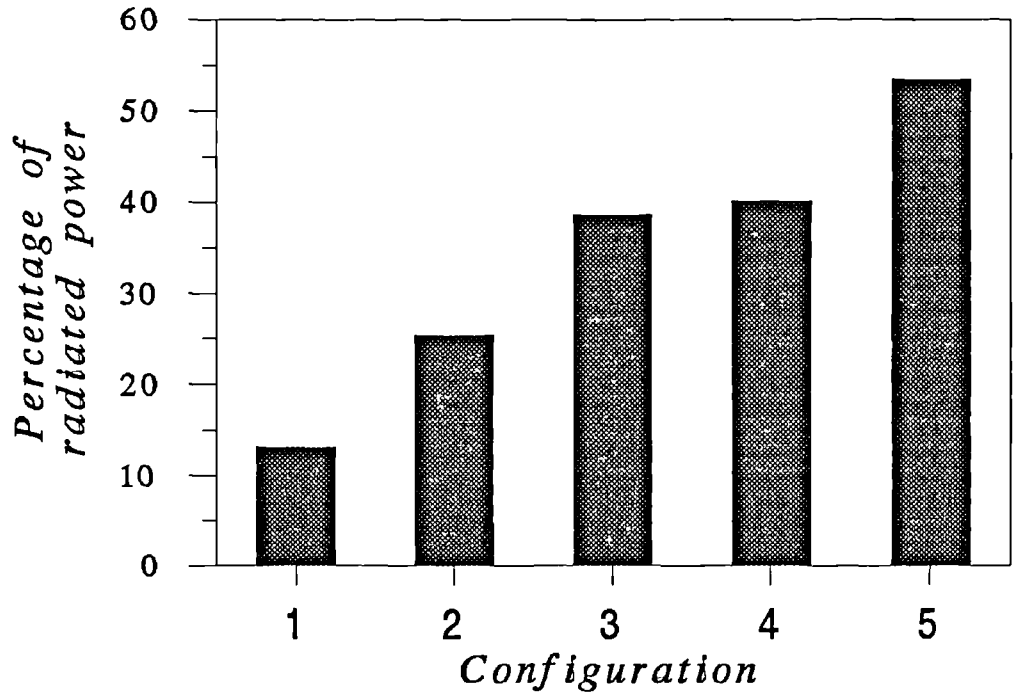

Key:
1 - Vertical 2m whip antenna
2 - Loop antenna fed conventionally
3 - 2-port loop modes
4 - 2-port pillar modes
5 - Full 4-port representation

Figure 7.21 Percentage of the total radiated power in $\theta<45°$ for various Land Rover antenna configurations

7.3.4.3 Feed System Implementation

The previous section has demonstrated that the optimization of the Characteristic Modes of a complex structure and its antenna enables the definition of a current that if present would yield an approximation to a desirable far-field pattern. The results have shown the clear relationship between the number of modes and the accuracy of the synthesized pattern. The obvious disadvantage of utilising a relatively large number of modes is that the required feed-system will increase in complexity. This section will demonstrate how a trade-off may be achieved between the accuracy of the overall approximating pattern and complexity of the required feed-system.

To demonstrate this effect two specific examples are considered. Figure 7.19 showed the variation of the relative mean squared error of the approximating pattern of the 4-port system as the number of modes used was increased. Firstly, a dramatic reduction in the error is noticeable when the modes used is increased from 1 to 2. This suggests that the individual attributes of mode 2 are substantially more suitable for NVIS than mode 1, the more significant mode. To investigate this a 4-port loading scheme was defined using the software described in section 6.2.2. The loads were specified such that they made mode 2 dominant with an eigenvalue of zero. If it is then assumed that the effect of all other modes will be negligible compared to this, then a single voltage source may be used to excite the structure and thus make its radiation characteristics predominantly those of mode 2 only.

Two factors are important in the choice of which port to use for the single feed-point. Firstly substantial mode 2 current must exist at the port. Secondly if a number of ports exhibit similar mode 2 current then the port should be chosen that least excites the other modes of the system. Using this procedure with a single voltage source positioned at port 2, the left hand side roof pillar, the far-field pattern shown in figure 7.22 was obtained with 40.12% of the total radiated power in $\theta<45°$.

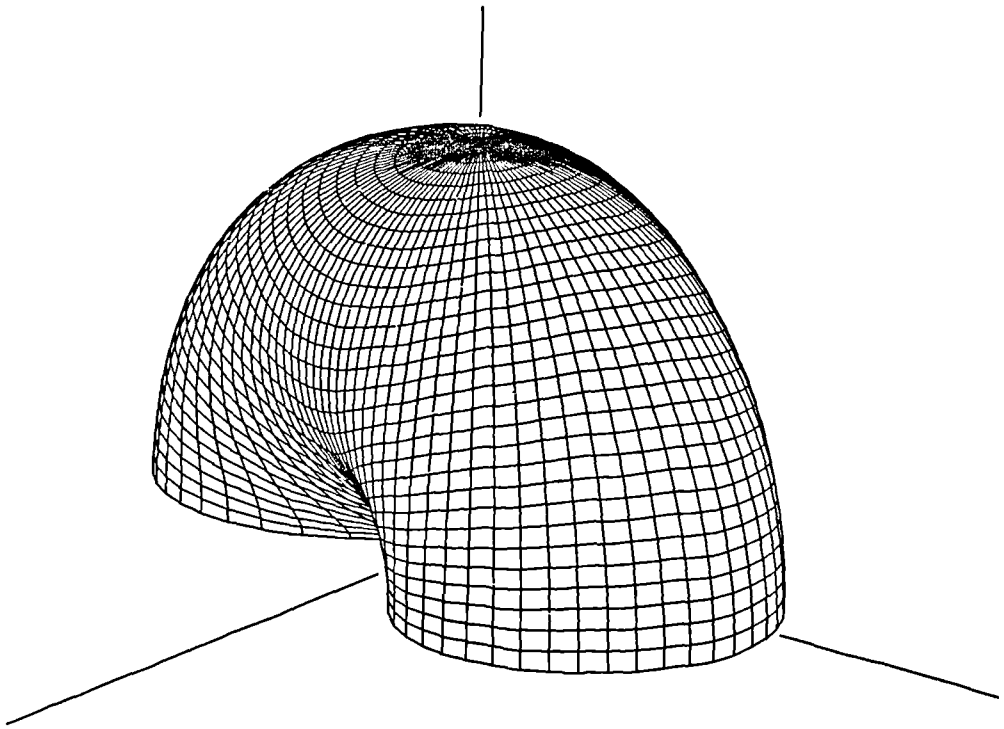

Viewing angles: $\theta=70°$, $\phi=40°$

Figure 7.22 Far-field pattern of the Land Rover with loop antenna using a 4 port loading scheme with a single voltage source

Next, the most accurate approximating pattern shown in figure 7.19 is with the complete, optimal excitation of all four defined modes. To physically realise this requires the use of four voltage sources, which results in the far-field

pattern shown in figure 7.23. For this configuration 53.52% of the total radiated power is in $\theta<45°$.

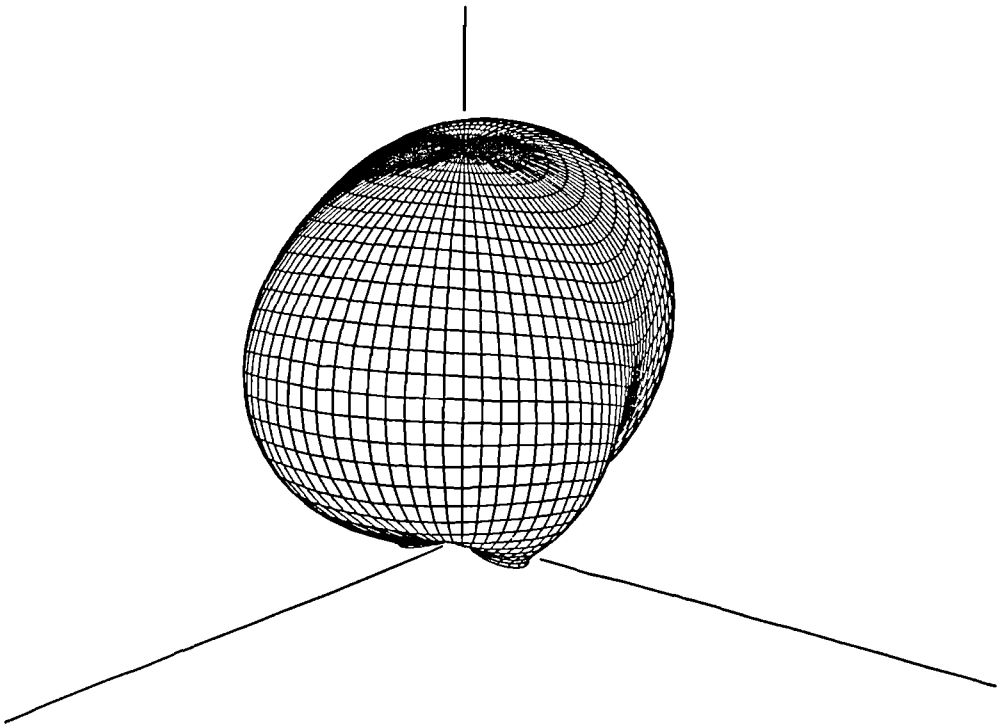

Viewing angles: $\theta=70°$, $\phi=40°$

Figure 7.23 Synthesized far-field pattern obtained using 4 voltage source on the Land Rover and loop antenna configuration

An important aspect of the two above feed-systems is clearly the input impedance presented at each of the defined ports. These are shown in table 7.6 with the voltages required to initially produce the approximating patterns. Also presented is the input impedance of the loop fed conventionally at its front base.

The complexity of the 4 voltage source system is clearly apparent with power transfer between ports as signified by the negative input resistances of ports 1 and 4. One interesting aspect of this system however is the inductive reactance presented to all ports. Practically, this necessitates the use of a

Table 7.6 Synthesized patterns feed-system data

Feed-port	Feed voltage		R_{in}	X_{in}
	Magnitude (volts)	Phase (degrees)		
4-port feed-system Port 1	0.6845	178.60	-1.54	39.95
Port 2	0.8174	-178.27	1.13	29.94
Port 3	1.0000	0.00	1.87	124.94
Port 4	0.6860	0.95	-1.45	65.19
Loaded port feed-system Port 2 only	1.0000	0.00	4.53	0.47
Unloaded port feed-system Port 3 only	1.0000	0.00	7.55	307.91

capacitive loading scheme to yield a solely resistive input characteristic, which is clearly preferable to using inductors.

Considering the loaded feed-system an input resistance comparable to that of the loop fed conventionally is obtained. Hence a marked improvement in the power radiated into $\theta<45°$ may be obtained without substantial degradation of the real component of the input impedance. This has important implications for the overall radiation efficiency of any practical implementation of these systems which is discussed in the next section. The relatively small reactive component of this system's input impedance is introduced by the excitation of the other less significant modes. It value suggests that, because of the loading scheme and the chosen source position, their effect is entirely negligible.

7.3.4.4 Antenna Efficiency

An vitally important aspect of any practical antenna system is the overall radiation efficiency. The input impedances shown in table 7.6 have been calculated assuming that the Land Rover's surface is perfectly conducting. Clearly this is not the case. This section investigates how the electrical resistance associated with the vehicle's surface will affect the feasibility of the synthesized feed-systems. Hence the wires in the grid model of the Land Rover were specified as aluminium with conductance $\sigma=3.96\text{x}10^{7}\text{Sm}^{-1}$. The radiation efficiency of the three feed configurations shown in table 7.6 was then assessed. This was investigated using the pattern synthesis results obtained throughout the complete NVIS frequency band 2-12MHz. Hence, figure 7.24 shows their resulting variation.

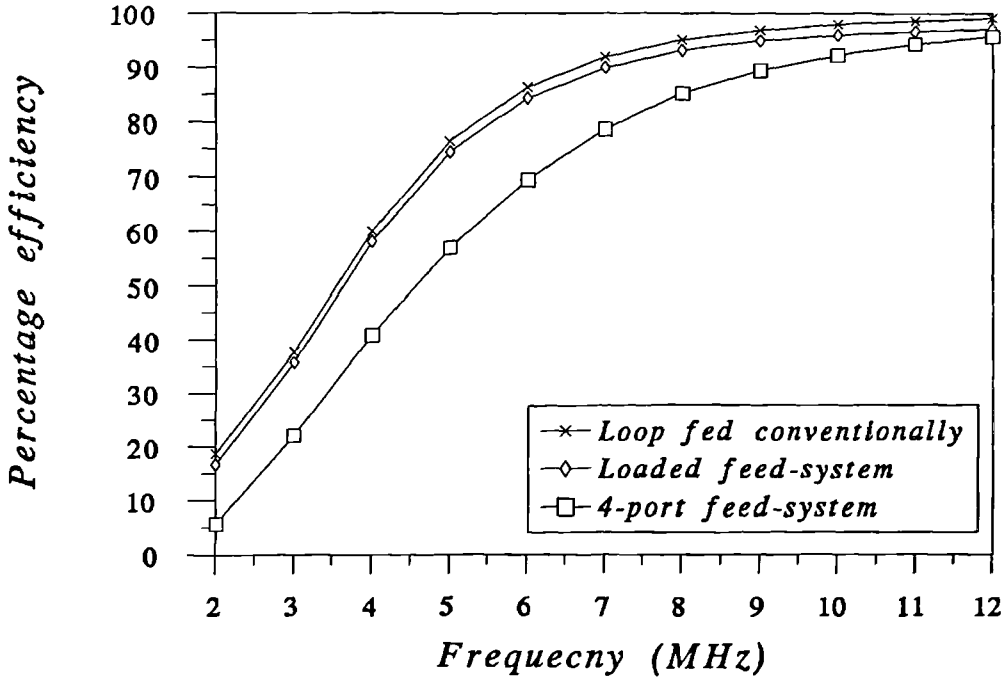

Figure 7.24 Variation of the radiation efficiency of three Land Rover NVIS antenna systems with frequency

The plot shows that the result for the conventionally fed loop antenna and the 4-load system is substantially similar over the complete frequency band with a maximum difference at any point of around 2%. The plot for the 4-port feed-system is also similar to that of the loop fed conventionally at the top of the frequency band. As the frequency is reduced however, the efficiency of the 4-port system reduces at a greater rate than the other two. This would be expected because of the relatively small values of resistive component associated with this feed-system.

This result stresses how practically a trade-off can be achieved between the various modal optimization results. At the top of the defined frequency range using the 4-port feed system is clearly feasible. Even at intermediate frequencies where its efficiency is markedly less than the conventionally fed loop this configuration may still radiate more total power in $\theta<45°$. The intermediate case of the loaded ports however is clearly feasible over the complete frequency band as its efficiency always remains similar to that of the conventional loop.

Another important aspect of the illustrated synthesized vehicular antenna systems is the feeding mechanisms. At the front and rear bases of the loop antenna, the conventional delta-gap model used in the Method of Moments formulation is a realistic representation of how it would be excited in practise. It is possibly unfeasible though to use a similar model for the roof pillar feed-ports. One possible solution to this problem, which warrants further investigation, is the well-known technique of using a toroidal coil to induce current flow on a conducting surface. This has been used applied successfully in many other

applications including that of exciting a wire rope as described by Hill and Wait (1973, 1978). This technique would clearly alleviate the problem of having to intersect a supporting component of the vehicle's structure. In his work on vehicular antennas, Lindenmeier (1989) has also suggested the use of unconventional couplers to induce desired current flow.

7.4 Summary

This chapter has shown the novel application of the method of Characteristic Modes for the analysis and far-field pattern synthesis of complex vehicular antenna systems.

In section 7.2 the Characteristic Modes of a number of simple representations of vehicles were examined. It was shown that if the structures were below their first fundamental resonance, then four specific modes completely control the overall radiation characteristics. The far-field patterns of these modes were unaffected by changes in the electrical dimensions of the structure. Thus, this may be thought of as a standard modal composition for vehicular structures, with their electrical dimensions controlling only the significance of each of these four standard modes. The interesting finding in section 7.2.2 was that the far-field patterns of this composition were also unaffected by the addition of a conventional monopole or loop antenna to the structure. They do though effect modal significance, with each configuration changing the eigenvalue of a number of the standard modes. Thus an antenna

presents a means by which certain of the modes associated with a vehicle may be more easily excited.

In section 7.3 the technique of Characteristic Modal far-field synthesis was employed as a design tool for a specific HF antenna system. The application was that of a vehicular antenna for use with the so-called NVIS mode of propagation. This is a particular problematic situation as an antenna must be employed which radiates substantial power at a high elevation angle. Conventional vehicular antenna systems were found inherently unsuitable for this purpose as shown in section 7.3.2. In section 7.3.3 it was shown how the Characteristic Modes of a composite vehicle and antenna configuration could be optimized to produce a desirable NVIS far-field pattern. This was a novel application as it allowed the utilization of previously spurious current on the vehicle's surface. Various factors were then shown to affect the practical feasibility of the synthesized antenna systems. Clearly the greater the number of modes employed, the more closely the resultant far-field approximates the target. Section 7.3.4 though demonstrated how the complexity of the feed-system associated with the best approximation could present practical implementation difficulties, especially at the lower end of the defined frequency band. Comparison of this case with another using less modes showed that overall there is a necessity to achieve a trade-off between the accuracy of the synthesized far-field and its physical realizability.

Although the techniques described in this chapter have been applied only to below resonance vehicular structures, the general methodology is clearly

applicable to any complex radiating structure. Thus in the next chapter, the work of this thesis is summarized and a number of overall conclusions are made.

CHAPTER 8

SUMMARY AND CONCLUSIONS

This study has investigated an alternative method for the design of antenna systems on complex structures. This was achieved using the method of Characteristic Modes which defines a unique set of orthogonal current and far-field functions for any structure. Software for their calculation was developed from a widely available Method of Moments Galerkin based computer code, which was expanded to cater for the modal analysis and far-field pattern synthesis of any arbitrary antenna structure.

An important aspect of the study was the validation of this enhanced software. This was vitally important as the MININEC code, which formed the basis of this work, had not previously been used to model such complex radiating platforms. One significant finding was that the algorithm used in the MININEC code is capable of accurately modelling the radiation characteristics of such structures. This was proved in chapter 5 by the comparison of its predicted radiation patterns and input impedances with those from a wide range of analytical, experimental and computed data. The latter were obtained by using the Numerical Electromagnetics Code (NEC) which has been tested extensively in similar applications. It was shown that the types of structures used in the validation exhibited substantial current flow on all of the conducting surface of the geometrical configuration, not just on the mounted antenna. The agreement obtained with both radiation pattern and input impedance showed that the

MININEC code was predicting the current distribution accurately. This was a particularly important consideration as the ultimate aim of the research was the utilization of these structure currents. This would clearly involve the use of unconventional feed-mechanisms positioned at various points on the complete radiating structure. Accurate prediction of the complete structure current was therefore crucial.

The usefulness of a Characteristic Modal approach to antenna design was clearly illustrated in this thesis. Initially in chapter 6 the relationship between the modes of a number of simple antennas and the fundamental resonances that are definable by elementary inspection was shown. The advantage of a modal approach though is that these resonances and an associated current are exactly identified. Their probable effect due to a particular voltage feed configuration is then easily assessed. This was demonstrated in chapter 6 with the analysis of a horizontal dipole fed centrally with a coaxial transmission line without a balun. Using Characteristic Modes the resonant currents were identified and the extent by which each was excited evaluated.

There is evidence in this thesis that the Characteristic Modes of complex structures are numerous and exhibit many diverse far-field patterns. It has been proved however, that many complex structure antenna systems only exploit a few of these modes. Hence the overall radiation characteristics of such structures are governed by the attributes of only a few of its associated modes. This was most apparent in chapter 6 where a corner reflector antenna was analyzed. It was shown that, out of the first 12 most significant modes, only 4 governed the

overall radiation pattern, although in this case optimally for the defined application. The result though shows that the full potential of many radiating structures is not taken advantage of. This is especially true where the antenna is not an integral part of the structure's design. For example, the radiation pattern of a vertical monopole mounted on a motor vehicle, was shown in chapter 5, to be substantially changed by current flow on the vehicle surface. This modification of the radiation pattern is due to a random, unspecified excitation of the numerous modes associated with the complete composite structure. Clearly Characteristic Modal analysis allows the better understanding of such effects.

Another important finding of this thesis is the determination of a standard modal configuration for vehicular structures below their first fundamental resonance. Using a simple wire grid box model to simulate numerous vehicles, a system consisting of four significant Characteristic Modes was always apparent. The four distinct far-field modal patterns were found to be significantly independent of the dimensions of the box, provided it remained below its first resonance. Changes in the dimensions of the box only altered the relative significance of each mode.

Another important finding was the effect that any mounted conventional antenna had on this standard modal composition. Chapter 7 showed that mounting a monopole or loop antenna on the vehicle had a negligible effect on the far-field patterns of the four modes which are inherently a function of the vehicle dimensions. The antenna does though change the modal significance which

considerably affects the ease with which these four modes may be excited. The change in each mode's significance is governed by the type and mounting position of the antenna. For example, in chapter 7 a vertical monopole altered the significance of only one of the four modes to any extent. Later though it was shown that a loop mounted on a particular vehicle substantially altered the significance of three of the four modes. This result is important as it demonstrates that the vehicle surface is predominantly responsible for the radiation characteristics of such systems. The antenna only presents a means of exciting these four specific modes.

There is therefore evidence to prove that the method of Characteristic Modes is a viable design tool for complex antenna systems. The results in chapter 7 show how the currents flowing on the complete surface of such structures may be utilised. Hence previously spurious current, if adequately controlled, can contribute usefully to the overall radiation characteristics. One great advantage of the technique is orthogonality of the modal fields. This allows them to considered either independently or as useful set of functions for optimization. This was most apparent in chapter 7 where approximations to a desirable far-field were realizable either by the exploitation of one particular mode or by optimally exciting the four most significant. This demonstrated how, by carefully considering all possible modal excitation schemes, a trade-off between the accuracy of the synthesized pattern and the associated complexity of the resultant feed-system is possible.

A further useful feature of a modal approach, compared to other synthesis techniques, is the ability to examine the individual orthogonal mode currents. This allows the most appropriate position of voltage sources that fully exploit the full radiation potential of a structure to be easily assessed. For example, in chapter 7 the pillars supporting a vehicle's roof were found to exhibit substantial mode current and were therefore effective source locations.

There are a number of important aspects that were not considered in this thesis. These are presented below and are suggestions for future research in this area.

In using the method of wire gird modelling to represent actual vehicle structures such as the Land Rover, the conducting surface was considered as a continuous conducting skin. No account was taken of any imperfections that may exist. These will clearly include obvious discontinuities such as doors and the bonnet and possibly to a lesser extent welded or riveted joints at adjacent panels. Corrosion may also be a problem, introducing a difference between the modelled and actual current paths. An important advancement to the accuracy of the numerical analysis would therefore be a more precise representation of the structure under test, taking into account the above effects.

In using the method of Characteristic Modes for far-field pattern synthesis it is apparent that it is necessary to excite currents on the complete surface of structures. For example, in the work here the most appropriate position at which to optimally excite a particular mode was at the pillars supporting the roof. Clearly it is impractical to insert a delta-gap voltage source, as used in the

Moment Method software. This research programme did not address to any great extent the practicality of these unconventional feed-mechanisms. This is a clear area for future research. As discussed in chapter 7 the author sees one possibly worthwhile area as the use of some form of toroidal coupler. An investigation into the characteristics and efficiency of such devices is therefore necessary.

The results in this thesis have been based on the numerical analysis of complex vehicular structures using the Method of Moments. The ability of this enhanced MININEC code to model complex antenna configurations was proved conclusively in chapter 5. Clearly though a further research programme would be the experimental verification of the principles that have been outlined here.

APPENDIX A

ADDITIONAL MININEC3 VALIDATION DATA

In this appendix additional plots comparing the far-fields predicted by NEC and the modified MININEC3 code are shown. These are in addition to those shown in chapter 5. Three geometrical configurations were considered labelled 1,2 and 3 which correspond to those shown in figures 5.7, 5.8 and 5.9 respectively.

Configuration 1 results

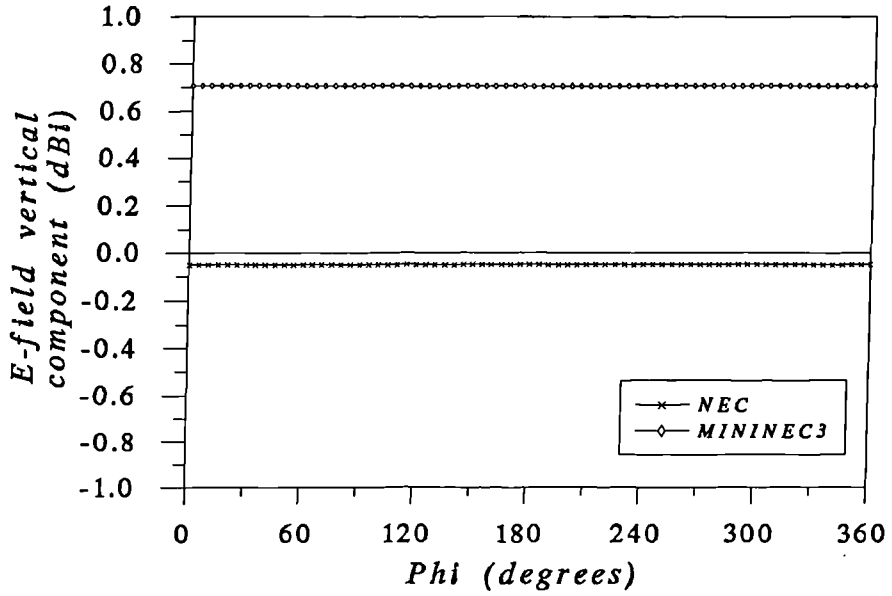

Figure A.1 Azimuthal variation of the E-field vertical component of the far field for geometrical configuration 1

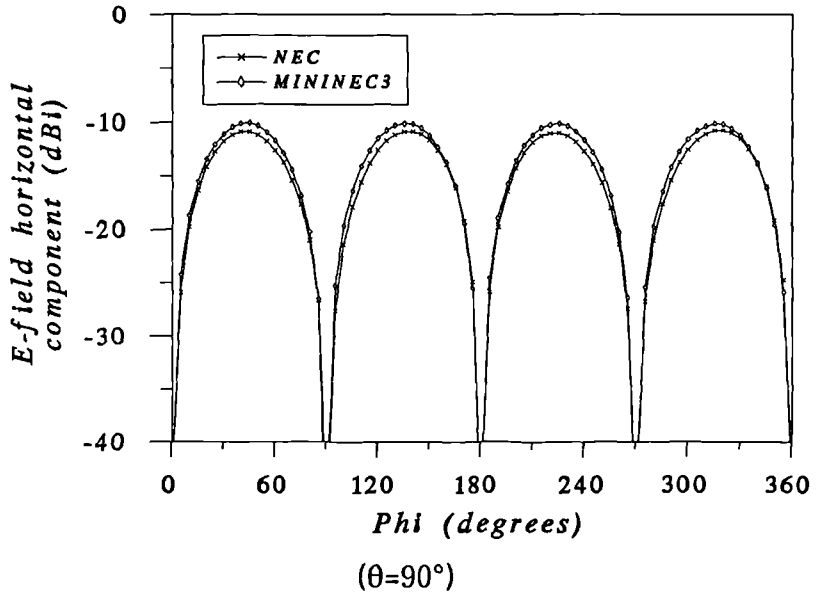

Figure A.2 Azimuthal variation of the E-field horizontal component of the far field for geometrical configuration 1

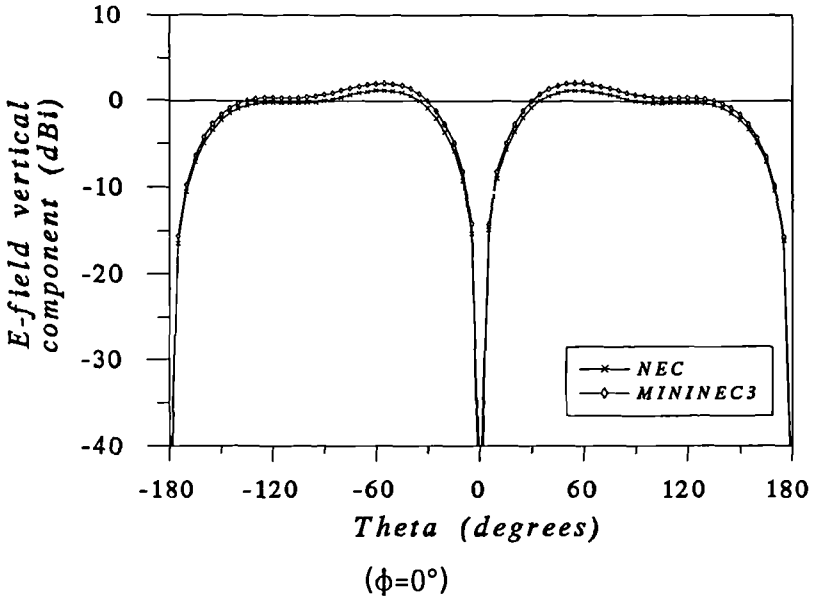

Figure A.3 Variation in elevation Azimuthal of the E-field vertical component of the far field for geometrical configuration 1

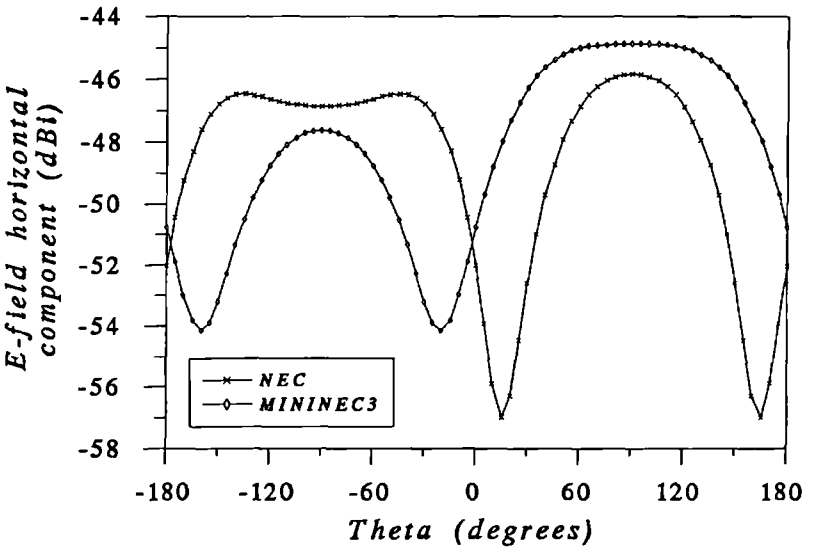

Figure A.4 Azimuthal variation of the E-field vertical component of the far field for geometrical configuration 1

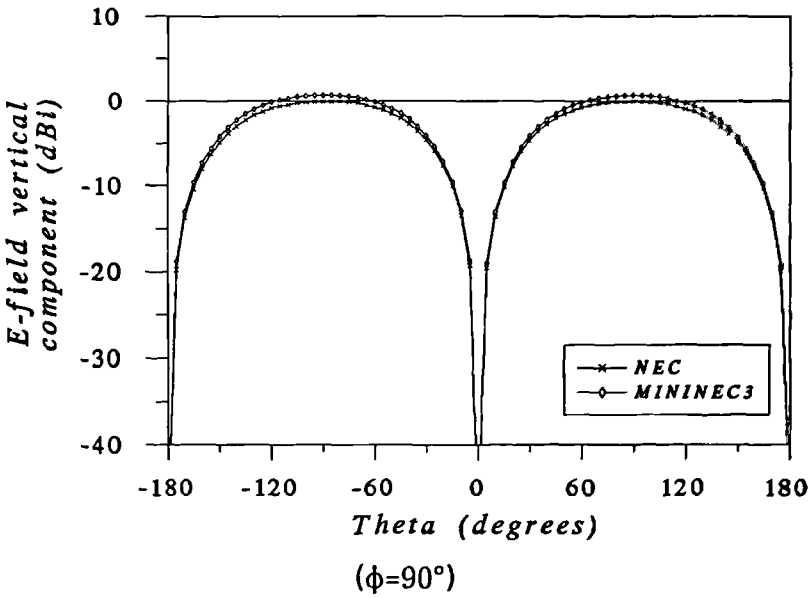

Figure A.5 Variation in elevation of the E-field vertical component of the far field for geometrical configuration 1

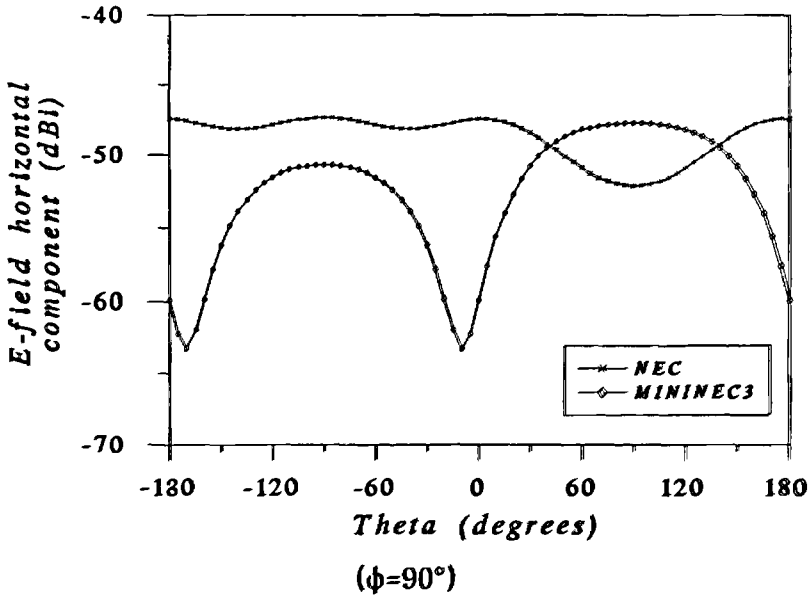

Figure A.6 Variation in elevation of the E-field horizontal component of the far field for geometrical configuration 1

Configuration 2 results

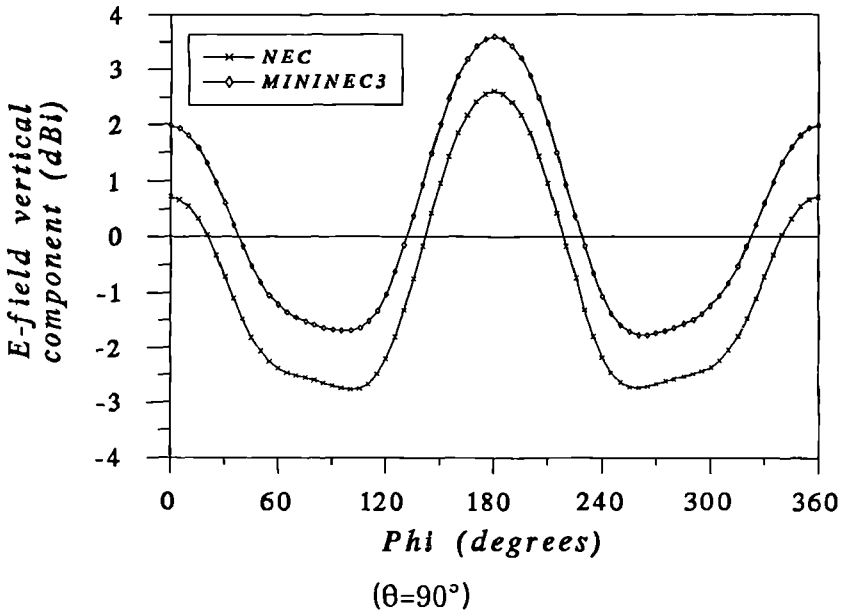

Figure A.7 Azimuthal variation of the *E*-field vertical component of the far-field for geometrical configuration 2

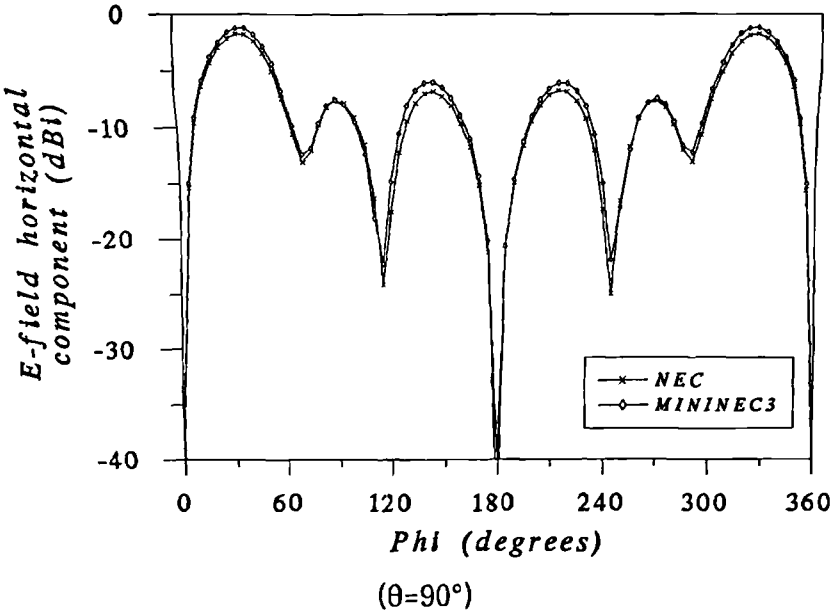

Figure A.8 Azimuthal variation of the *E*-field horizontal component of the far-field for geometrical configuration 2

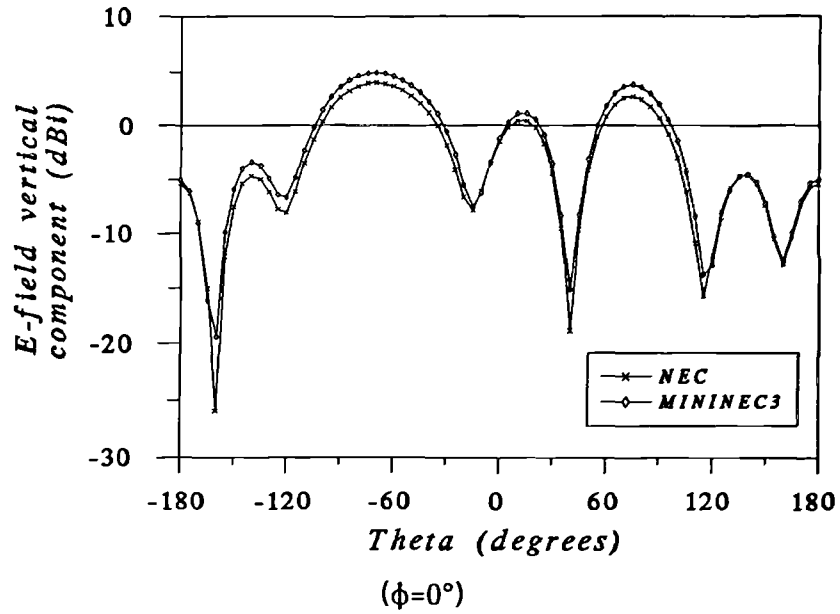

Figure A.9 Variation in elevation of the *E*-field vertical component of the far-field for geometrical configuration 2

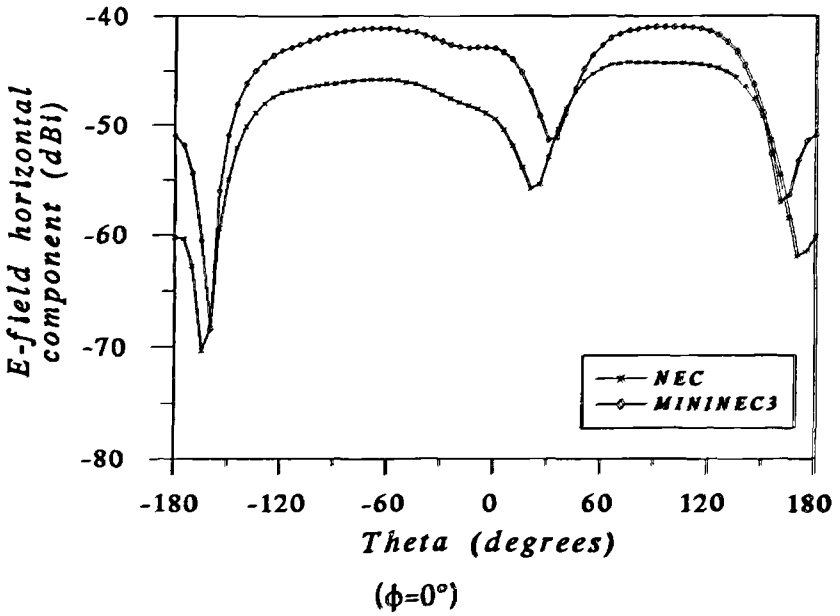

Figure A.10 Variation in elevation of the *E*-field horizontal component of the far-field for geometrical configuration 2

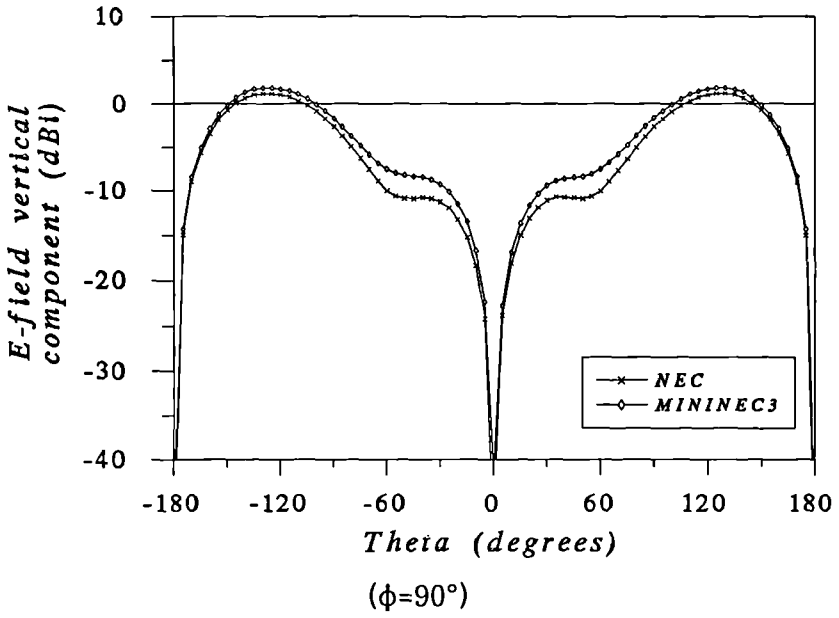

Figure A.11 Variation in elevation of the *E*-field vertical component of the far-field for geometrical configuration 2

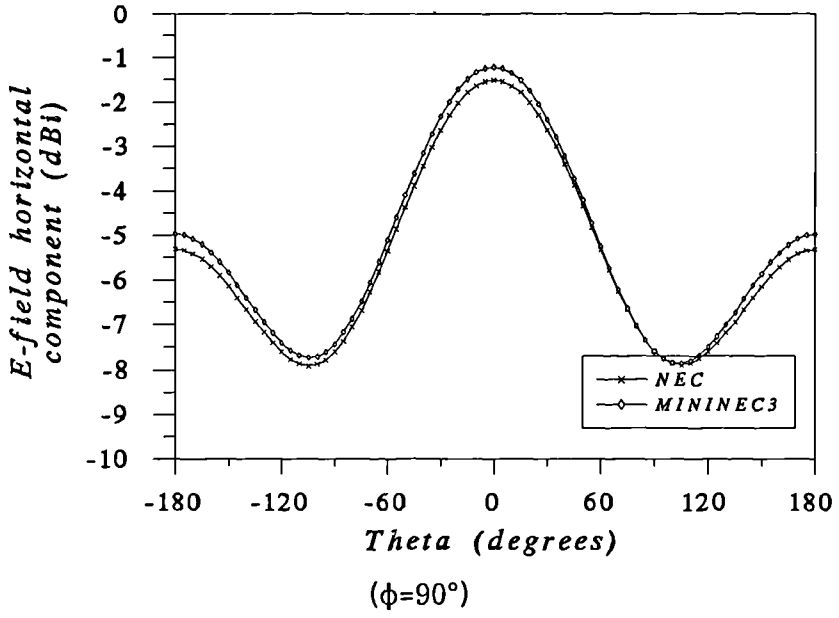

Figure A.12 Variation in elevation of the *E*-field horizontal component of the far-field for geometrical configuration 2

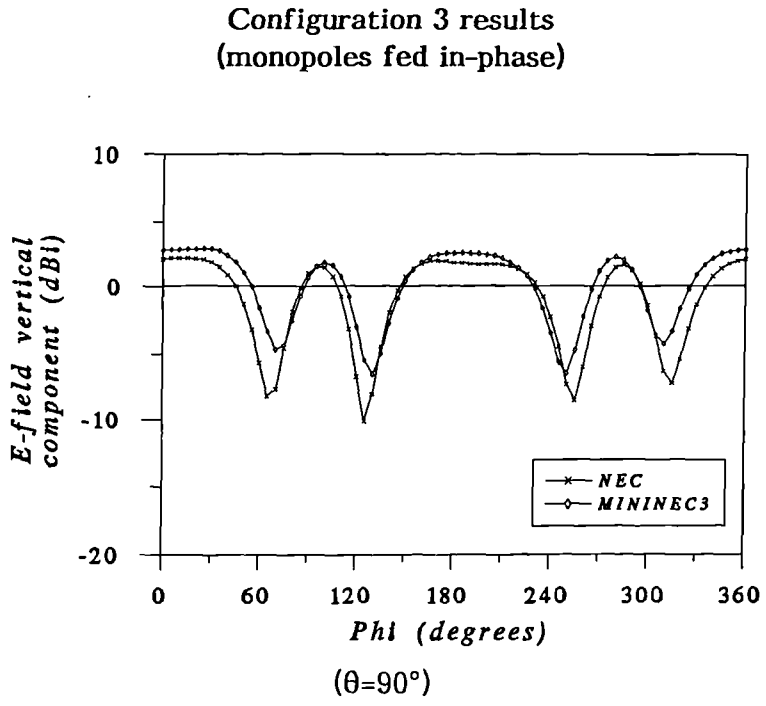

Figure A.13 Azimuthal variation of the *E*-field vertical component of the far-field for geometrical configuration 3 with the monopoles fed in-phase

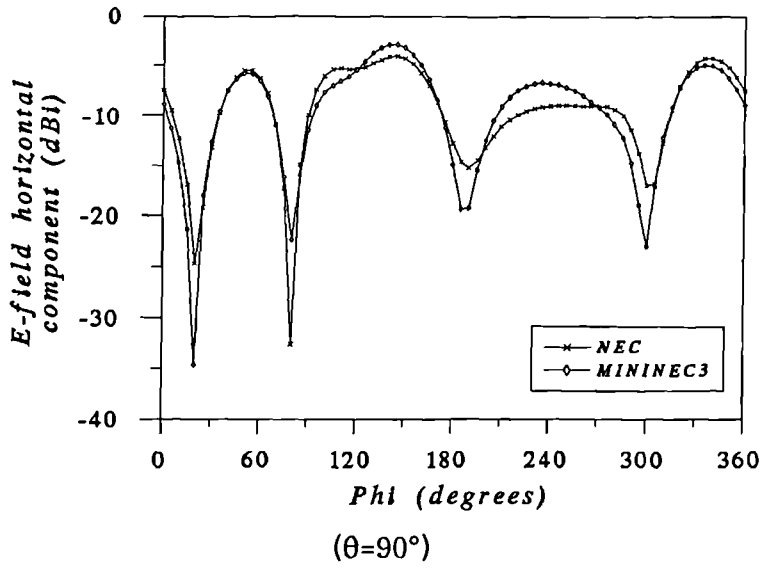

Figure A.14 Azimuthal variation of the *E*-field horizontal component of the far-field for geometrical configuration 3 with the monopoles fed in-phase

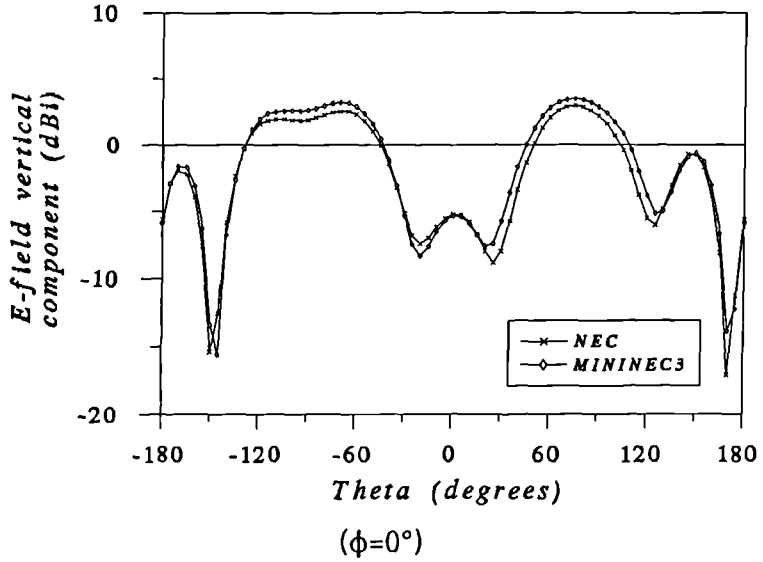

Figure A.15 Variation in elevation of the *E*-field vertical component of the far-field for geometrical configuration 3 with the monopoles fed in-phase

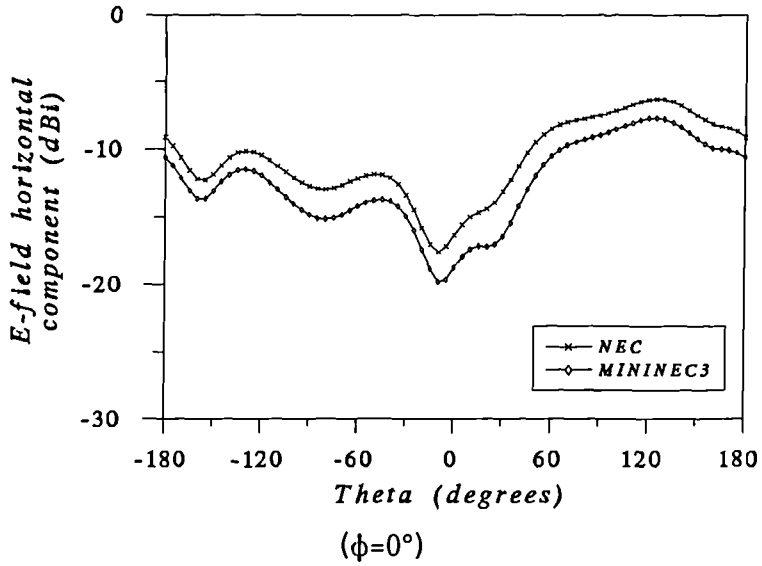

Figure A.16 Variation in elevation of the *E*-field horizontal component of the far-field for geometrical configuration 3 with the monopoles fed in-phase

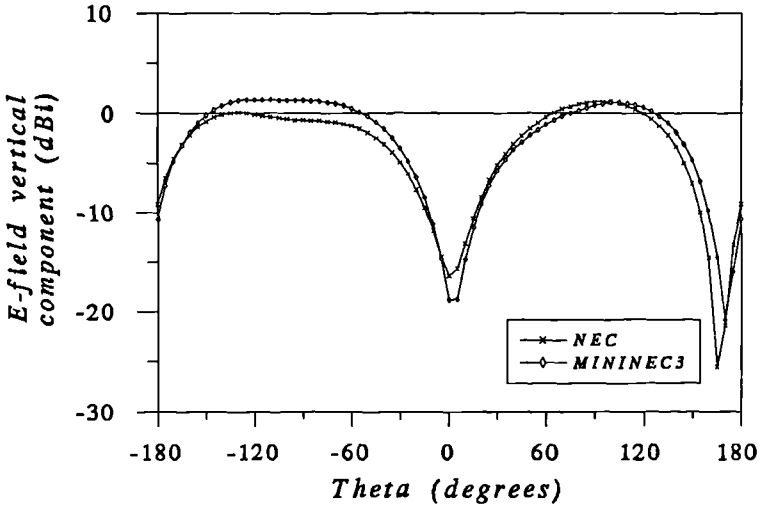

Figure A.17 Variation in elevation of the *E*-field vertical component of the far-field for geometrical configuration 3 with the monopoles fed in-phase

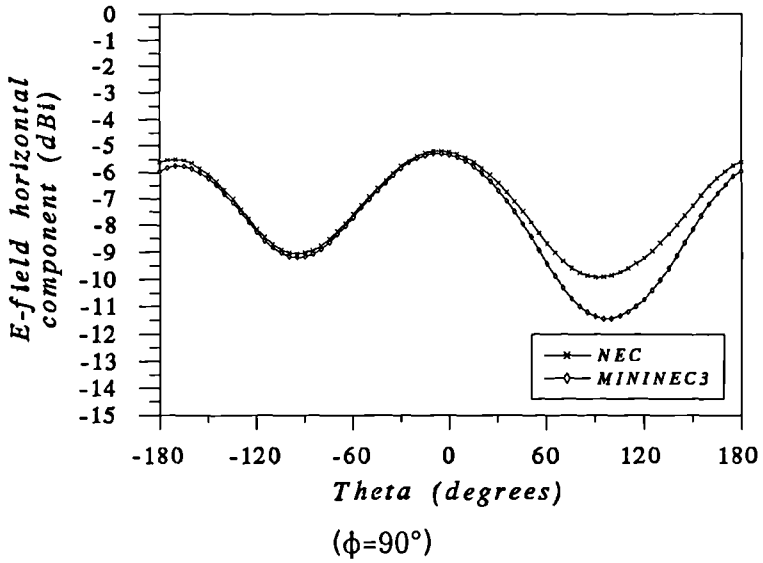

Figure A.18 Variation in elevation of the *E*-field horizontal component of the far-field for geometrical configuration 3 with the monopoles fed in-phase

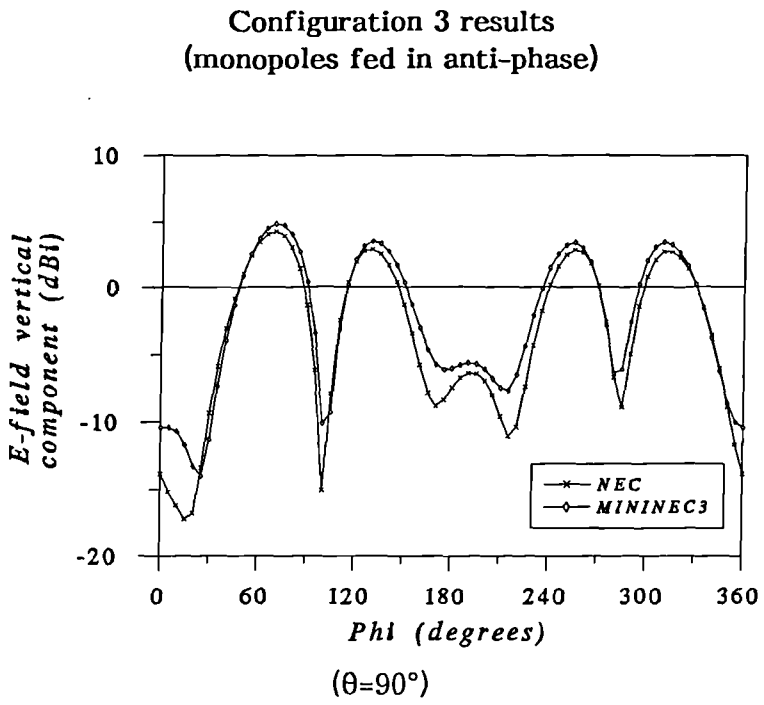

Figure A.19 Azimuthal variation of the *E*-field vertical component of the far-field for geometrical configuration 3 with the monopoles fed in anti-phase

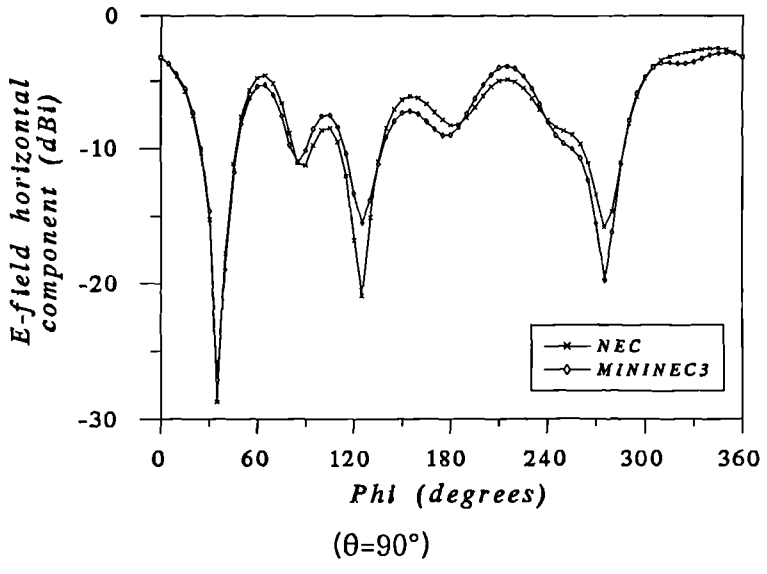

Figure A.20 Azimuthal variation of the *E*-field horizontal component of the far-field for geometrical configuration 3 with the monopoles fed in anti-phase

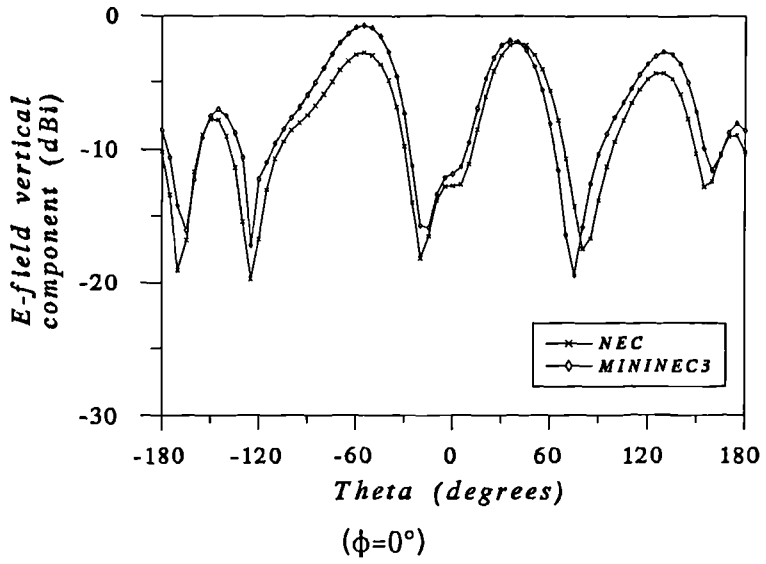

Figure A.21 Variation in elevation of the *E*-field vertical component of the far-field for geometrical configuration 3 with the monopoles fed in anti-phase

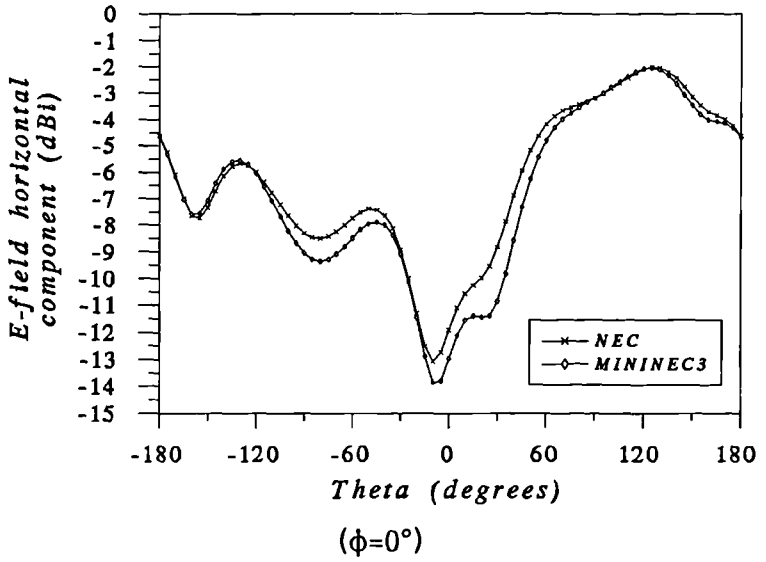

Figure A.22 Variation in elevation of the *E*-field horizontal component of the far-field for geometrical configuration 3 with the monopoles fed in anti-phase

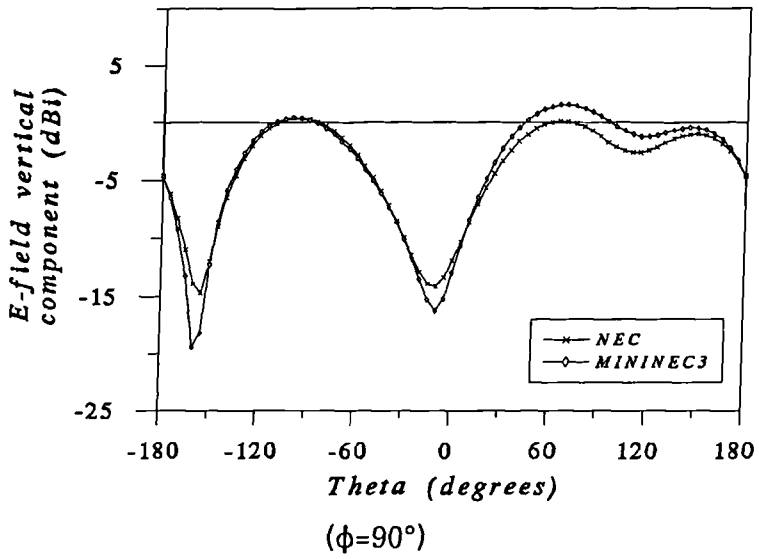

Figure A.23 Variation in elevation of the *E*-field vertical component of the far-field for geometrical configuration 3 with the monopoles fed in anti-phase

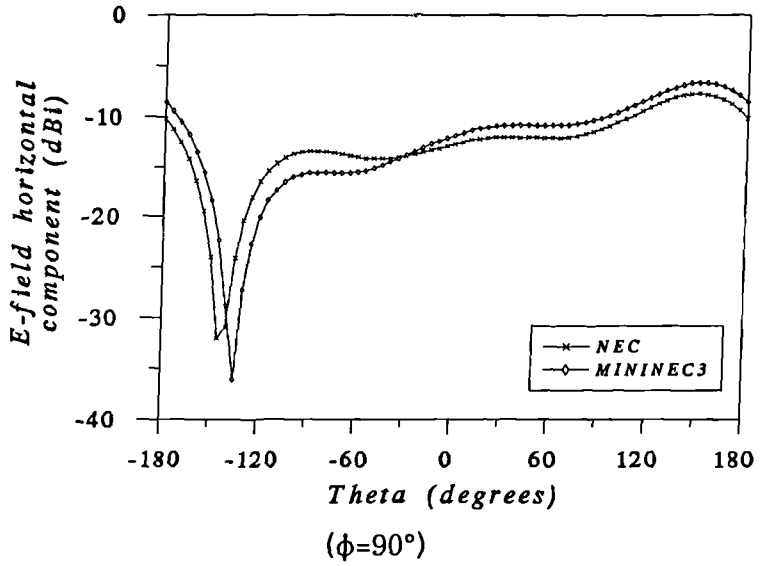

Figure A.24 Variation in elevation of the *E*-field horizontal component of the far-field for geometrical configuration 3 with the monopoles fed in anti-phase

APPENDIX B

LIST OF PUBLICATIONS

1. Austin, B.A. and Murray, K.P., (1991). "The Generation of Antenna Characteristic Modes from the Impedance matrix using the Moment Method", Proceedings of the Seventh International Conference on Antennas and Propagation (ICAP-91), IEE Conference Publication No. 333, vol.2, pp.713-716.

2. Murray, K.P. and Austin, B.A., (1992). "The use of Characteristic Modes for Pattern Synthesis with Wire Antennas on Complex Structures", Proceedings of the 18th Queen Mary and Westfield College Antenna Symposium.

3. Austin, B.A., Murray, K.P. and Najm, R.K., (1992). "Analysis and synthesis of vehicular antennas using Moment Methods and Characteristic Modes", The 9th National Radio Science Colloquium, Bradford, UK.

4. Murray, K.P. and Austin, B.A., (1992). "The use of Characteristic Modes for Antenna Analysis and Far Field Pattern Synthesis", ACES-UK Chapter Group Newsletter, No.1, pp.2-10.

5. Murray, K.P. and Austin, B.A., (1992). "HF antennas on vehicles - a characteristic modal approach", IEE Colloquium on HF Antenna Systems, Digest no. 1992/225.

6. Murray, K.P. and Austin, B.A., (1993). "Synthesis of radiation patterns for HF mobile communications using the method of Characteristic Modes" accepted for publication at the Eighth International Conference on Antennas and Propagation (ICAP-93), Edinburgh, UK.

THE GENERATION OF ANTENNA CHARACTERISTIC MODES FROM THE IMPEDANCE MATRIX USING THE MOMENT METHOD

B A Austin and K P Murray

University of Liverpool, UK.

1. INTRODUCTION

The theory of Characteristic Modes enables the current distribution and hence the radiation characteristics of structures to be expressed as an infinite set of mathematical basis functions. This set of functions is uniquely defined by the structure's dimensions and frequency of operation and it is independent of any particular excitation. This paper describes a procedure for the computation of the Characteristic Modes of arbitrary antenna geometries using a readily available Moment Method code. The reliance of the Characteristic Modes on the wire segmentation scheme used is investigated along with the number of significant modes that need to be summed to obtain accurate pattern and impedance data. Finally Characteristic Modes are used as an aid to understand the experimental impedance data from a particular antenna and transmission line configuration.

2. CHARACTERISTIC MODE THEORY

2.1. Background and Computation

Characteristic Modes have been used to solve electromagnetic boundary value problems when the boundaries coincide with co-ordinate surfaces in which the Helmholtz equation is separable. Garbacz [1] showed that, given a body's geometrical dimensions, a set of Characteristic Modes could be defined. The theory was developed further by Harrington and Mautz [2, 3], who presented a relatively straight-forward method for their calculation.

Beginning with the so-called generalised impedance matrix [Z] of a body, a weighted eigenvalue equation may be set up,

$$[X]\ I_n = \lambda_n\ [R]\ I_n \qquad (1)$$

where [R] and [X] are the real and imaginary parts of the generalised impedance matrix [Z]=[R+jX]. Solution of (1) yields a set of eigenvectors or characteristic mode currents, I_n, each with associated eigenvalue λ_n. Provided a Galerkin method, which involves the same functions for both expansion and testing, is used in the determination of the generalised impedance matrix [Z], then this matrix will be symmetric. This is an important feature because the calculated eigenvalues and hence associated mode currents are real and have a physical meaning which is easily understood.

With the mode currents scaled to unit norm the following orthogonality relationships may now be stated:

$$I_m^T\ [R] I_n = \delta_{mn}\ P_n \qquad (2)$$

$$I_m^T\ [X] I_n = \lambda_n \delta_{mn}\ P_n \qquad (3)$$

$$I_m^T\ [Z] I_n = (1 + j\ \lambda_n)\delta_{mn}\ P_n \qquad (4)$$

The eigenvalue associated with each mode therefore shows how much power is stored by that particular mode. Also the scaling factor P_n associated with each mode shows how much power the mode radiates under unit excitation compared to the other modes. The total current flow on a body due to a particular excitation may now be shown to be

$$I_T = \sum_{n=1}^{N} I_n^T [V_i] I_n / (1+j\lambda_n)\ P_n \qquad (5)$$

where N is the order of the Moment Method matrix and $[V_i]$ is the column matrix representing the segmentation excitation voltages or electric fields.

2.2 Advantages of a modal approach

The usefulness of a Characteristic Mode approach is clearly demonstrated by consideration of the above properties. The Characteristic Mode currents of a structure are orthogonal and therefore radiate power independently of each other. The far fields too, exhibit orthogonality over the sphere at infinity, which is another useful property.

It is clear therefore from these properties that insight may be gained into the radiation and scattering characteristics of complex bodies by considering the current distributions and patterns of the individual modes. Also the dominance of each mode, signified by eigenvalue λ_n, or normalisation factor P_n, may be examined. Whereas such performance features can also be found more conventionally from a knowledge of the current distribution obtained by inverting the impedance matrix, such computationally expensive procedures are not required when using the Characteristic Mode approach. This is a significant aspect when analysing structurally complex configurations at high frequencies. The possibility too for implementing synthesis procedures for the generation or suppression of certain modes by appropriate source positioning and loading is also attractive.

2.3 Moment Method Implementation

A widely used Method of Moments computer code was modified in order to produce the required generalised impedance matrices of various geometries. The code used was MININEC3 [4], a personal computer-based program for the analysis of arbitrary wire antennas. The code uses current pulses for both the expansion and testing functions and is thereicre Galerkin, which ensures symmetric impedance matrices. Considerable user experience with this code provided some confidence in the validity of the results obtained but one drawback is the 125 segment limit imposed by the BASIC language compiler.

The NAG mathematical subroutines [5] were used to solve the resulting eigenvalue equation (1). This software uses the so called QZ algorithm [5], whereby the matrices are reduced to upper Hessenberg and triangular forms to enable eigenvalue extraction.

3. CHARACTERISTIC MODE CALCULATIONS AND RESULTS

3.1 Verification

Specific validation of the software used to calculate the various Characteristic Modes was done by comparing our results with those published in the literature. For example the characteristic angles and radar cross section were computed for a symmetrical wire cross [6] of length to diameter ratio 42.42. Both results were indistinguishable from those in [6].

3.2 Segmentation convergence

The dependence of the Characteristic Modes of various geometries on the Moment Method segmentation scheme used was investigated. Fig. 1 shows how the eigenvalues of the six most significant modes of a two element halfwave dipole array with quarterwave spacing varied as the number of segments per wavelength was increased. The graph shows convergence for all six cases. It is noticeable that eigenvalue stability is achieved when using 15 to 20 segments per wavelength. Similar agreement was found for other structural shapes too so this segmentation scheme was enforced for all further analysis.

3.3 Input admittance and pattern convergence

In general, the higher order modes contribute less to the radiation from a structure. To examine this effect, the input admittance and radiation patterns were calculated for the two element array described above using different numbers of modes for the current summation of equation (5). The modes were first numbered in ascending modulus of eigenvalue order with the eigenvalue closest to zero being dominant. By examination of the mode current distributions a feed position was chosen that was not at any modal current null thereby ensuring that all modes would be excited to a certain extent. It is worth noting here that even if a mode is dominant certain source positions may still not excite it if they coincide with mode current-nulls.

Fig. 2 shows the spread in Characteristic Mode eigenvalue and power normalisation factors for the twelve most dominant modes of this two element array. Both are normalised to 0dB and were calculated using:

$$\text{Eigenvalue level} = 10 \log \left(\left| \frac{\lambda_1}{\lambda_n} \right| \right) \text{ dB} \qquad (6)$$

$$\text{Power normalisation level} = 10 \log \left(\left| \frac{P_1}{P_n} \right| \right) \text{ dB} \qquad (7)$$

These factors give an indication of the relative dominance of the modes compared to each other, assuming equal modal excitation.

Fig. 3 shows how the input admittance of the structure converges as the number of modes in the summation is increased. It is noticeable that the input conductance is convergent after including only the first two most significant modes whereas the input susceptance converges when the six most significant modes are included in the summation. This would be expected due to the $1/(1+j\lambda_n)$ scaling factor in equation (5). Multiplication of each mode current by this factor produces the real and imaginary components. The real part of the current, the conductance component, is scaled by $1/(1+\lambda_n^2)$, whereas the imaginary part, the susceptance component, is scaled by $-\lambda_n/(1+\lambda_n^2)$. The effect on the imaginary part of the total current and the input susceptance is more apparent for relatively large eigenvalues than for the real component. Input admittance is therefore relatively easily calculated using only a few of the most significant modes.

Fig 4 shows how the radiated far field of the same antenna is affected by the number of modes used in the summation. The magnitude of the radiated E-field is shown as the number of modes used in the summation is increased. The same field, calculated using the Conventional Moment Method approach, is shown for comparison. Acceptable agreement is obtained when using only two modes while three modes yield an indistinguishable field plot from the Moment Method result. Similar agreement is also achieved for the phase of the E-field.

3.4 The BALUN problem; Characteristic Mode analysis

Experimental data were available [7] for a horizontal wire antenna, centre fed with a coaxial transmission line without a balun. The input impedance at the antenna feedpoint exhibited a number of spurious responses on the Smith Chart which were attributed to the existence of "antenna currents" on the outer surface of the coaxial cable [8].

The insert in Fig. 5a shows how such a situation could be modelled for a 26 metre dipole with a 56 metre radiating transmission line. The currents due to the transmission line would be expected to be most pronounced when the dimension L is a multiple of half a wavelength. Here L=69m, hence critical frequencies (calculated using f=nc/2L, n=1, 2, 3, ...) are typically 2.1, 4.3, 6.5 MHz etc., while the 26 metre antenna would resonate at typically 5.5, 11.3, 17.0 MHz etc. The Characteristic Mode approach was used to analyse this configuration in order to confirm the existence of these resonances and to provide useful engineering insight by examination of the modal current distributions.

The variation of the characteristic angles of the most significant Characteristic Modes is shown in Fig. 5 for the frequency range 1-20 MHz. A characteristic angle of 180 degrees is indicative of resonance and hence Characteristic Mode dominance, as it is the angle between the mode current and its associated voltage or field. There are 10 modes which exhibit a mode angle of 180 degrees over this range and their frequencies are given below in Table 1.

TABLE 1: CHARACTERISTIC MODE RESONANT FREQUENCIES

MODE	fr (MHz)	MODE	fr (MHz)
1	1.8	6	11.2
2	4.3	7	12.9
3	5.6	8	15.1
4	6.5	9	17.0
5	9.0	10	17.3

Modes 3, 6 and 9 clearly correspond to the 26m dipole antenna resonances and this is confirmed by examination of the current distributions shown in Fig. 6. The other modal resonances are due to the combination of half the antenna plus the transmission line. This is again confirmed by the modal current distributions as in Fig. 7 which show the currents for mode 7, for example.

Finally Fig. 8 shows the extent to which each mode will be excited with a source in the feed position shown in Fig. 7. Although this is for a fixed frequency (11MHz), the modal currents remained substantially the same over the complete range. Thus this diagram is relevant for all frequencies considered. In this case the excitation factor was defined as the ratio of the mode current at the source position to that of the mode current maximum. As expected, modes 3 and 9 are excited maximally. Also modes 1, 7 and 8, due to the "half antenna plus transmission line" mechanism, are also excited significantly. This confirms that these resonance effects will be evident in the experimental data [7].

4. CONCLUSIONS

An analytical procedure, based on Characteristic Modes, has been tested and then used to determine the performance of some simple antenna configurations. The required generalised impedance matrix was obtained from a modified version of the MININEC software and readily available library routines were used to solve the resulting eigenvalue equation for the Characteristic Modes. The optimum segmentation scheme yielding converged results was found to be 15 to 20 segments per wavelength. Good agreement was found

with results obtained with the conventional, but slower, matrix inversion procedure as embodied in the Moment Method approach.

5. ACKNOWLEDGEMENT

The authors gratefully acknowledge the support given for this work by the Science and Engineering Research Council.

6. REFERENCES

1. Garbacz, R.J., "A generalised expansion for radiated and scattered fields", Ph.D. dissertation - The Ohio State University, 1968.

2. Harrington, R.F. and Mautz, J.R., "Theory of characteristic modes for conducting bodies", IEEE Trans. on Antennas and Propagation, vol. AP-19, 1971, pp 622-628.

3. Harrington, R.F. and Mautz, J.R., "Computation of characteristic modes for conducting bodies", ibid., pp 629-639.

4. Logan, J.C. and Rockway, J.W., "The new MININEC (version 3): A mini-numerical electromagnetics code", NOSC Technical Document 938, Sept. 1986.

5. NAG FORTRAN Library Manual, Routines F02, "Eigenvalues and Eigenvectors", Mark 8, Volume 4, 1981.

6. Garbacz, R.J. and Newman, E.H., "Characteristic modes of a symmetric wire cross", IEEE Trans. on Antennas and Propagation, vol. AP-28, 1979, pp 712-715.

7. Leather, P.S.H., (Personal Communication)

8. Monteath, G.D. and Knight, P., "The performance of a balanced aerial when connected directly to a coaxial cable", Proc. IEE , vol. 107, Pt. B, 1960, pp 21-25

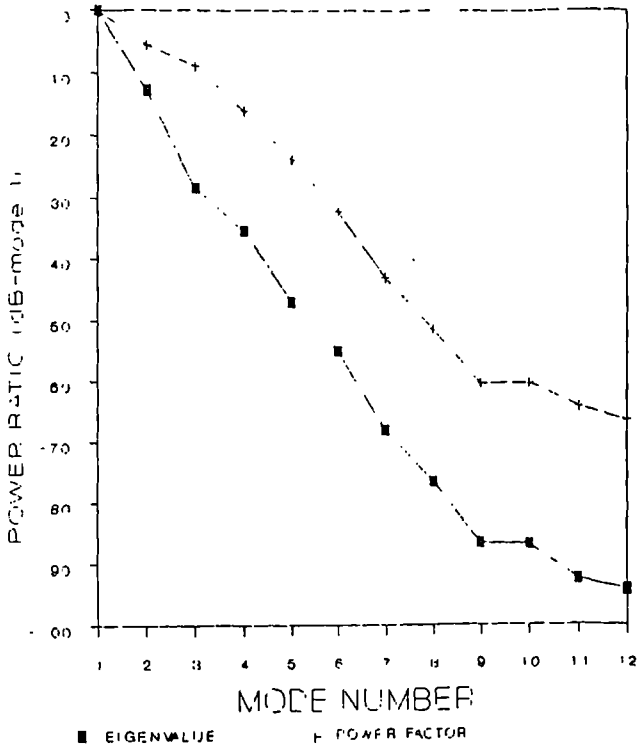

Figure 2. Eigenvalues and power normalisation factors for a two element halfwave array.

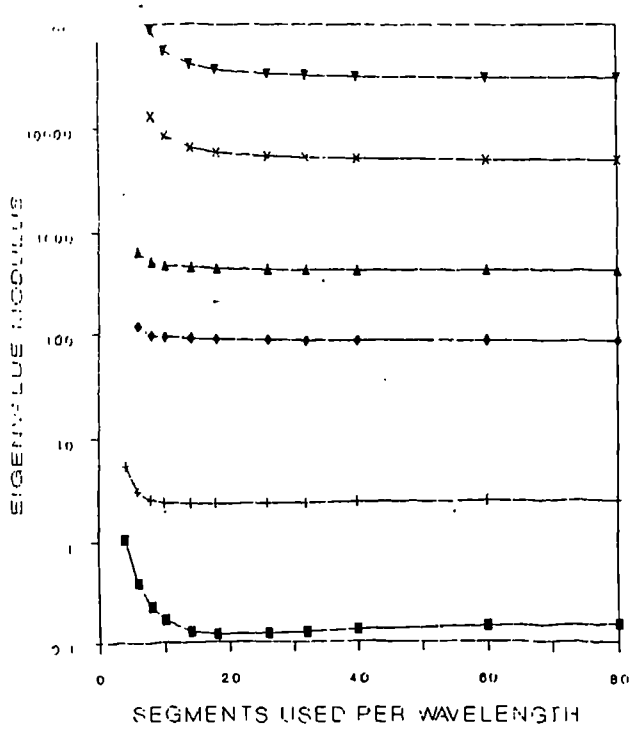

Figure 1. Convergence of the eigenvalues of a two element halfwave array.

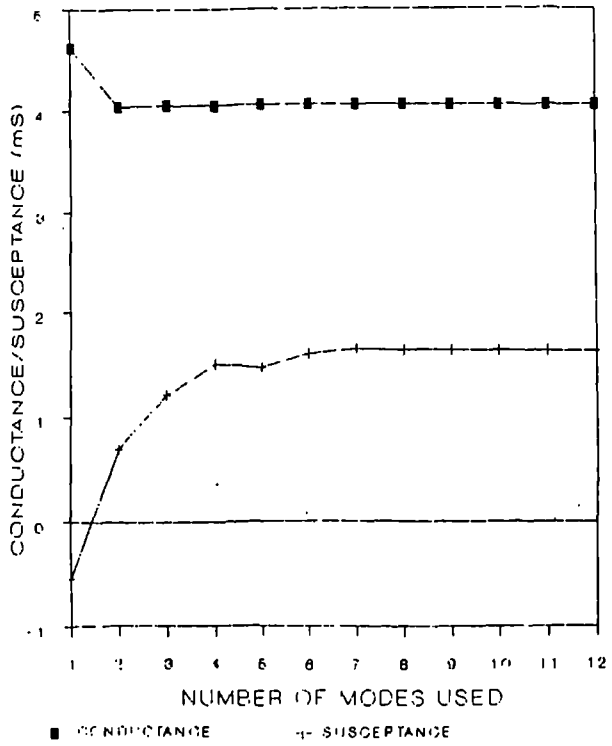

Figure 3. Convergence of the input admittance of a two element halfwave array.

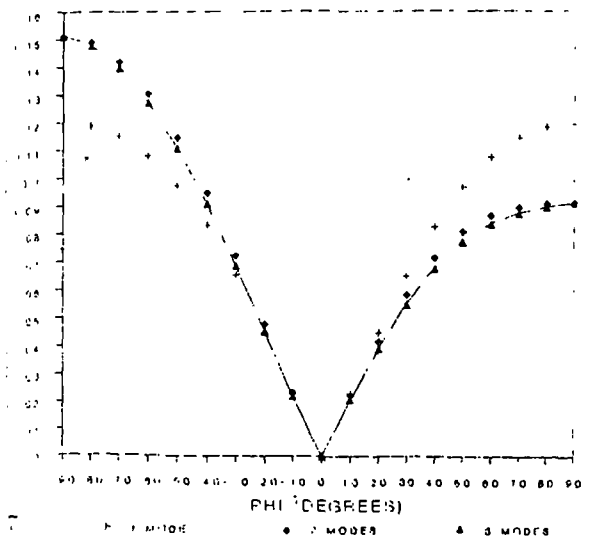

ure 4. Far-field pattern of a two element
lwave array.

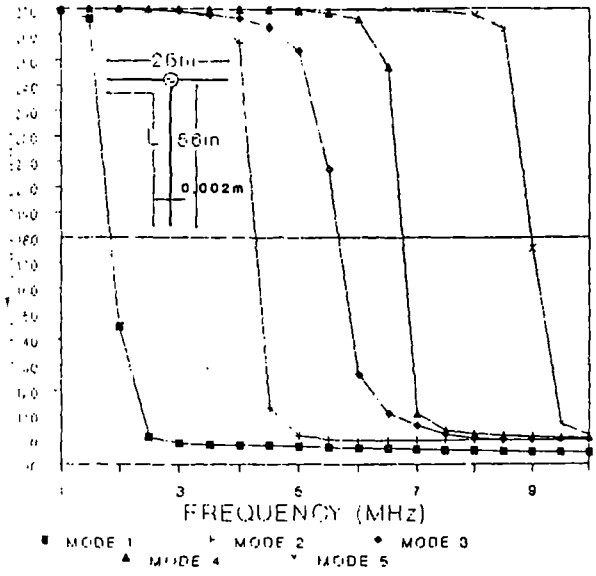

ure 5a. Characteristic angles of the dipole
enna and radiating line (1-10MHz).

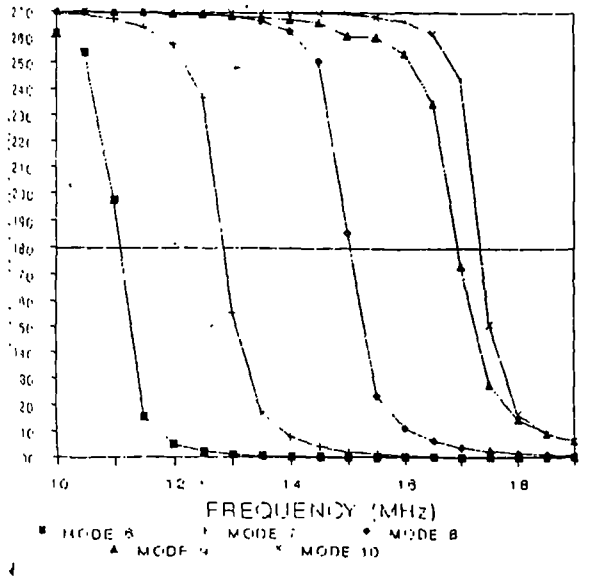

re 5b. Characteristic angles of the dipole
nna and radiating line (10-20MHz).

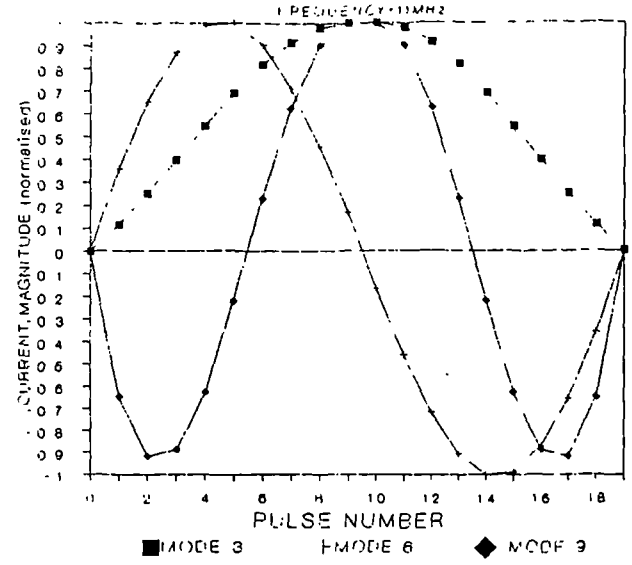

Figure 6. Current distributions (26m dipole).

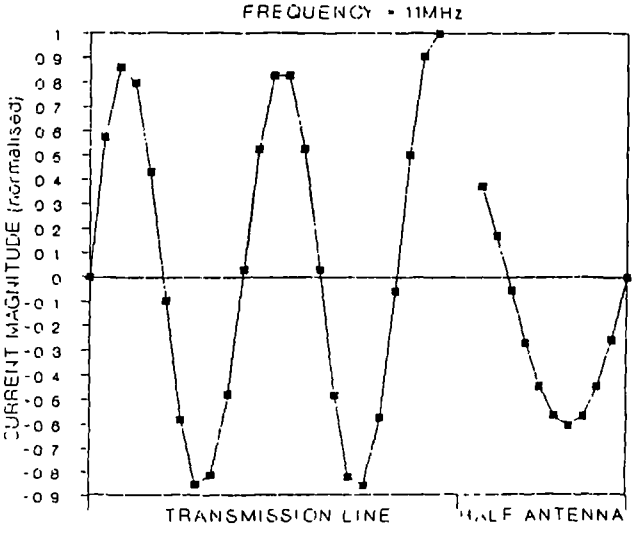

Figure 7. Mode 7 currents on section L.

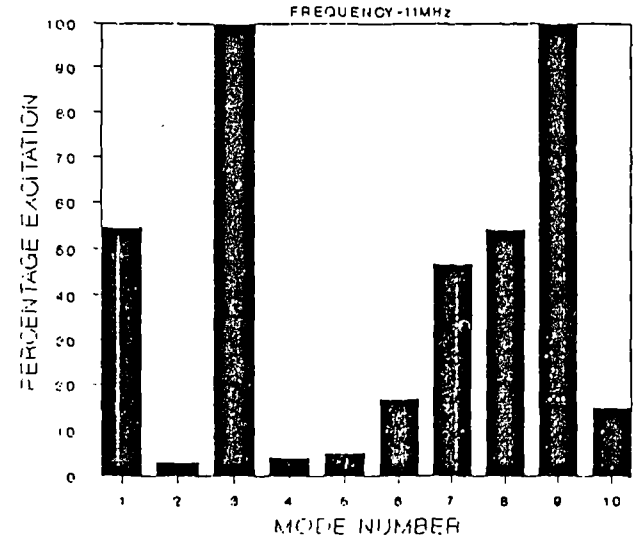

Figure 8. Modal excitation factors of the dipole antenna with radiating line

The use of Characteristic Modes for Pattern Synthesis with wire antennas on complex structures

K.P.Murray and B.A.Austin
Department of Electrical Engineering and Electronics
University of Liverpool
United Kingdom

The relationship between antenna radiation characteristics and the so-called Characteristic Modes which exist on the antenna structure has not been studied extensively. The results to date of an investigation to compute the Characteristic Modes of wire and rod antenna structures is presented here.

The theory of Characteristic Modes was formulated initially by Garbacz [1], who showed that, given a body's geometrical dimensions, it was possible to define an infinite set of basis functions or mode currents to represent the current flow on the body. A relatively straightforward method for their calculation was presented by Harrington and Mautz [2], which involved the manipulation of the impedance matrix of the structure, obtained from a Moment Method Solution of the defining operator equation.

The usefulness of considering the Characteristic Modes of a body, is that the mode currents are orthogonal over the source region. Each mode therefore radiates power independently from the rest. The far field patterns associated with each mode are also orthogonal over the sphere at infinity. Insight may therefore be gained into the radiation and scattering characteristics of bodies by considering the current distributions and patterns of the individual modes and from the relative dominance of each mode.

For simple electrically small geometries only a few modes will contribute to the radiation characteristics of a body at any fixed frequency. It is easy therefore to observe the effect of each mode and to suppress or enhance any feature by source positioning or loading. For complex radiating structures however where many modes may exist with a similar significance, simple observation of individual modal properties is not sufficient. Here optimization routines must be implemented to produce excitation or loading schemes that will generate a desired characteristic.

The work presented here will concentrate on a pattern synthesis routine following Pozar [3]. In this case an approximation to a desired target pattern is specified as a summation of the product of each Characteristic Mode field with a scaling factor. A function relating the mean squared error of the approximation and the modal scaling factors is defined and minimized. It is then possible to implement a feed system to generate the approximating pattern provided that the same number of sources as modes are used.

There are many applications where control of an antenna far field pattern is desirable. One example considered in this work was to look at multi-element linear arrays. Many different directional target patterns were synthesized for a variety of different sized arrays. The improvement in pattern approximations with increased number of modes used in the synthesis was investigated. Another application considered was that of antennas mounted on vehicles. Using a Characteristic Mode approach enables the whole vehicle to be considered as the antenna and multi-port feed networks may be implemented to produce approximations to desired patterns.

[1] Garbacz, R.J., "A generalized expansion for radiated and scattered fields", Ph.D dissertation, The Ohio State University, 1968.

[2] Harrington, R.F. and Mautz, J.R., "Computation of Characteristic Modes for conducting bodies", IEEE Trans. on Antennas and Propagation, vol. AP-19, 1971, pp 629-639.

[3] Pozar, D.M., "Antenna Synthesis and Optimization using weighted Inagaki Modes". IEEE Trans. on Antennas and Propagation, vol. AP-32, 1984, pp 159-165.

Analysis and Synthesis of Vehicular Antennas using Moment Methods and Characteristic Modes

B.A. Austin, K.P. Murray and R.K. Najm,
Department of Electrical Engineering and Electronics,
University of Liverpool.

Wire grid modelling used in conjunction with the moment method for the analysis of antennas on complex structures is now a well established technique. The results obtained for both the resulting radiated fields and the driving point characteristics of antennas on aircraft, ships and vehicles have achieved a significant degree of credibility as a result of intensive code development, refinement, testing and validation. Whereas no fundamental limitation of the method exists as regards frequency, the computer power required to handle such configurations increases significantly with increasing mesh density, which itself must increase with frequency. Hence the moment method has generally been regarded as a low-frequency procedure [1].

This paper will present the results of some work done at VHF (typ. 100 MHz), using the NEC-2 code to model antennas on vehicles, particularly when the antenna is flush-mounted on the glass of the rear window of the vehicle. It has been shown that the method of feeding the antenna and the resulting current distribution on it and on the vehicle have a major effect on the radiation pattern. It has also been found, for these rather unusual antennas, that the radiation pattern cannot be predicted accurately without also considering the dielectric loading of the glass. In addition, there is evidence of a resonant cavity effect which results from the coupling of energy through the window apertures into the vehicle compartment. Because of the size of these apertures this effect is probably most severe in passenger vehicles at VHF.

The synthesis of required radiation patterns from vehicle antennas is also under investigation. Use is made of the impedance matrix of the host vehicle plus its antennas, obtained from a Galerkin moment method code, to calculate the characteristic mode currents existing on the entire structure [2]. A required radiation pattern can be approximated by exciting the most appropriate modes from that set and suppressing others. Preliminary results have been most promising, particularly at HF, where the requirement to increase the radiation towards the zenith for near vertical incidence skywave (NVIS) propagation has been examined.

[1] Miller, E.K. and Burke, G.J., "Low-Frequency Computational Electromagnetics for Antenna Analysis", Proc. IEEE, 80, 1, 1992, 24-43.

[2] Mayhan, J.T., "Characteristic Modes and Wire Grid Modelling", IEEE Trans. Antenna Propagat., 38, 4, 1990, 457-469.

THE USE OF CHARACTERISTIC MODES FOR ANTENNA ANALYSIS AND FAR FIELD PATTERN SYNTHESIS

K.P.Murray and B.A.Austin
Department of Electrical Engineering and Electronics
University of Liverpool

Introduction

The method of Characteristic Modes for antennas and scatterers was pioneered by Harrington [1]. He showed that the current distribution and hence the radiation characteristics of structures could be represented as a set of orthogonal basis functions or modes. Because of the desirable property of orthogonality of the elements of the modal set, the method has found applications in both analysis and synthesis. Initially though this has only been with relatively small structures because of the reliance on Moment Method codes. However with the recent relative increase in computer power, both desktop and mainframe, the method of Characteristic Modes is a viable tool for the analysis and far field pattern synthesis of more complex radiating structures such as motor vehicles or aircraft.

This paper details the development procedure and some results of a study into using Characteristic Modes for the analysis and synthesis of complex radiating structures. This will include a description of the technique used to generate the modes and also the procedure implemented for the synthesis of desirable far field radiation patterns.

Theory

Calculation of Characteristic Modes is achieved using the Method of Moments [1], by manipulation of the so called generalised impedance matrix $[Z]$. Using its real and imaginary parts $[R]$ and $[X]$, a weighted eigenvalue equation may be set up:

$$[X]I_n = \lambda_n[R]I_n \qquad (1)$$

Solution of this equation yields a set of eigenvectors or Characteristic Mode currents, each with an associated eigenvalue.

An important aspect of solving equation 1 is that the $[Z]$ matrix should be symmetrical. This implies that the Moment Method code that calculated it enforced the reciprocity condition between matrix elements. This is only achieved if a Galerkin-based code is used, where the same expansion and testing functions are employed. Enforcing this condition ensures that the calculated eigenvalues and mode currents are real which gives the orthogonality conditions stated below an understandable physical meaning.

Firstly the modes are orthogonal over the source region such that:

$$\tilde{I}_m[Z]I_n = (1+j\lambda_n)\delta_{mn} \qquad (2)$$

where tilde $\tilde{}$ denotes matrix transpose and δ_{mn} is the Kronecker delta. This condition shows clearly the importance of the eigenvalue as it represents the ratio of stored to radiated power and hence how significant the mode is compared to others.

The second orthogonality condition applies to the far fields E_n associated

with each mode current I_n. These too are orthogonal over the sphere at infinity such that:

$$\frac{1}{\eta}\iint_{S_\infty} E^*_m E_n \, ds = \delta_{mn} \qquad (3)$$

where η is the characteristic impedance of freespace. Clearly this condition is highly desirable for pattern synthesis techniques.

Generation

Because of the necessity of using a Galerkin based technique for Characteristic Mode calculation the Numerical Electromagnetics Code (NEC), with its three term expansion functions and delta testing functions, was clearly unsuitable for the purpose. The use of the MININEC code was therefore investigated. Although this code is Galerkin, using pulses for expansion and testing functions, it had the disadvantage of been written in BASIC, which introduces compiler constraints in terms of addressable memory and relative execution time. Also there was little validation data, except for relatively simple geometries, available in the literature.

The first of these constraints was overcome by the translation of MININEC to FORTRAN, initially by the method described by Miller [2]. Here the relatively unstructured nature of the BASIC language was retained by replacing BASIC 'GOSUB' statements with FORTRAN 'ASSIGN' and 'GOTO' statements. This format was eventually replaced by the more usual method of calling subroutines. Also the matrix factorisation routine of MININEC was replaced by a more efficient NAG library routine [3] which reduced the inversion time of typical problems by up to 30%.

To assess the suitability of using MININEC for analyzing complex structures a study was undertaken to compare NEC and MININEC. Structures of the type that have been successfully analyzed using NEC were used and both far field pattern and input impedance were compared. Figure 1 shows an example of a wire grid model of a vehicular type structure with a cavity and two mounted vertical quarter wave monopole antennas. The size of the box representation is $1.2\lambda \times 0.5\lambda \times 0.2\lambda$ and the cavity is 0.4λ wide. The model was situated 0.25λ over perfect ground.

The two monopoles were base fed with various combinations of voltage magnitude and phase. Overall the calculated NEC and MININEC input impedances for all the cases considered varied by no more than 10%. Similarly the far field patterns showed excellent agreement. Figures 2 and 3 show the azimuth patterns for $\theta=80^\circ$ for both the vertical and horizontal components for two different feed combinations labelled Case 1 and Case 2. It can be seen that the patterns vary by no more than 2dB with the exception of the horizontal component of case 1 where the difference in the deepest null is around 5dB. This type of agreement of pattern was encountered for all the cases of feed considered and also with a wide range of other wire grid models examined. These results led to an increased confidence in the modified MININEC code. As the results of NEC and MININEC agreed for a wide range of complex wire grid models it was concluded that the MININEC code was suitable for this type of analysis.

A Characteristic Mode calculation routine was therefore implemented using a NAG library routine to solve the weighted eigenvalue equation 1. It was merged with the body of the modified FORTRAN MININEC and a menu option for Characteristic Mode calculation inserted. Also included was the ability to calculate the Characteristic Modes of an N-port antenna system. Here a continuous structure is reduced to N predefined ports or feedpoints. A port

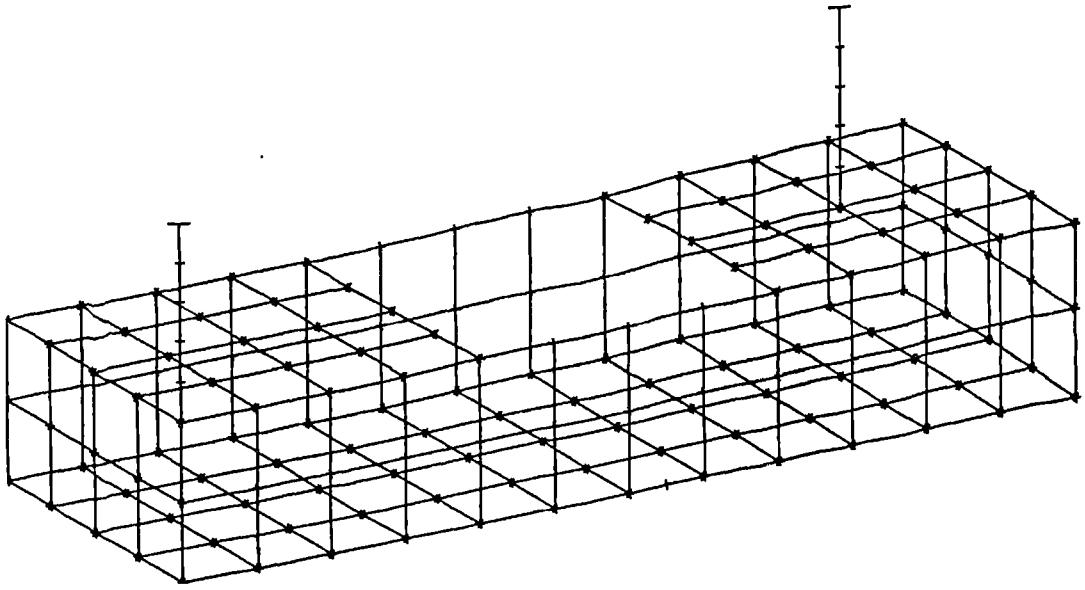

Figure 1 Wire Grid Model of a Typical Vehicular Structure

generalised impedance matrix is defined by manipulation of the generalised admittance matrix of the continuous structure. This formulation is useful if an antenna's feedpoints are fixed, as the generalised impedance matrix of the full, continuous structure is reduced to a smaller matrix, the generalised port impedance matrix, of order N. Full verification of both routines was carried out by comparison with published data.

Antenna Analysis and Pattern Synthesis

For relatively small, simple antenna geometries the method of Characteristic Modes has been applied with great success. Studies, such as that due to Garbacz [4], has enabled greater insight into the radiation properties of radiating structures to be gained. For these small antennas, where only a few modes are significant, the positioning of feedpoints to obtain desirable radiation properties is easily determined by visual examination of the individual mode currents.

For larger, more complex structures such as wire grid models however it is necessary to use numerical algorithms to optimize the scaling of each mode to obtain desirable results. For the work described here a far field pattern synthesis routine based on that due to Pozar [5] was implemented. This routine iteratively optimizes a scaling factor for each modal field producing a least mean squared error approximation to a specified target far field pattern. Upon calculating the modal scaling factors a voltage feed system may be implemented to generate the required current distribution.

The application considered here is that of improving the radiation of energy towards the zenith for antennas mounted on vehicles, specifically for so called Near Vertical Incidence Skywave (NVIS) propagation via the ionosphere. One of the commonest vehicular HF antennas is the conventional vertical whip. The characteristic null at $\theta=0^\circ$ makes this type of antenna ineffective for NVIS applications. Burberry [6] addressed the problem of NVIS communications from a Land Rover. Amongst the solutions suggested was a loop antenna spanning the longest dimension of the vehicle. A wire grid model representation of this situation was implemented and is shown in figure 4. Although feeding this configuration at one feedpoint produced an improved

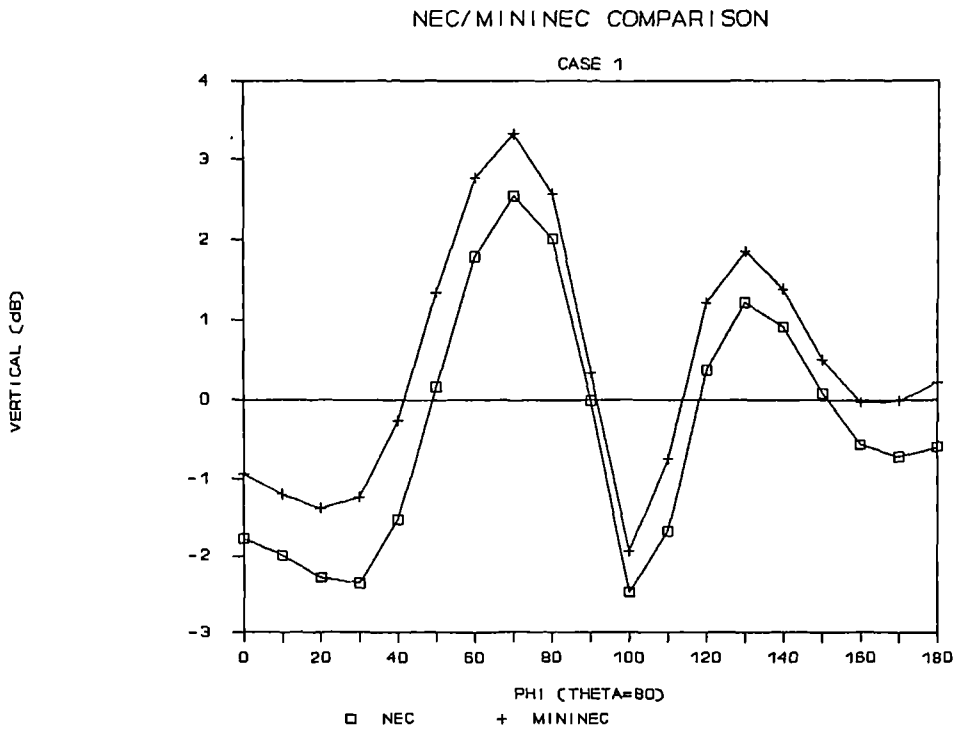

(a) Vertical

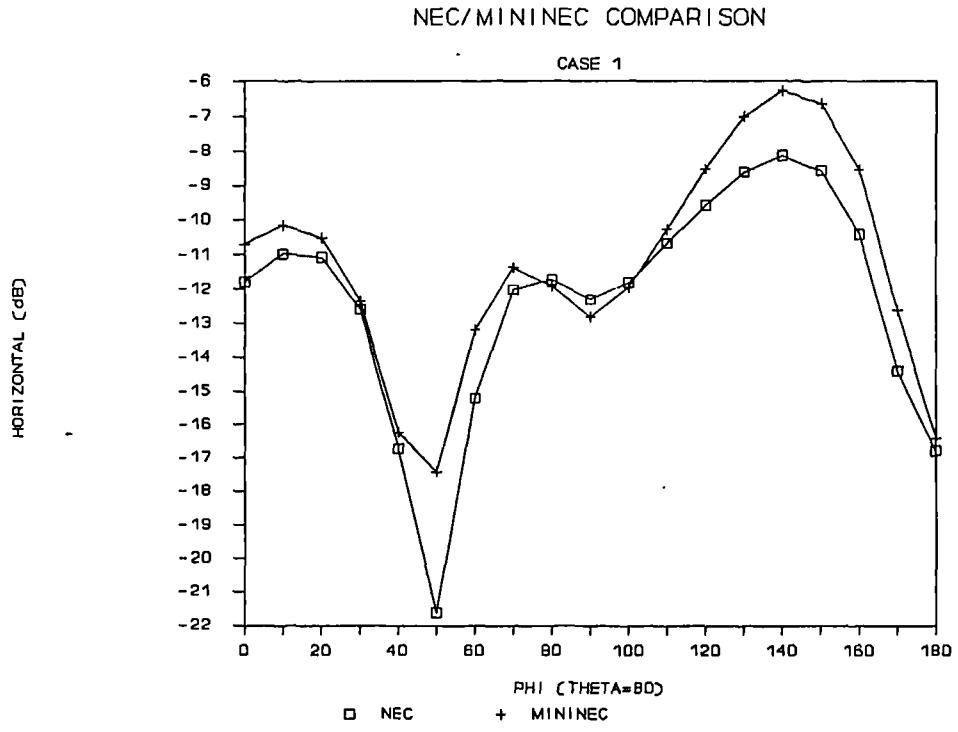

(b) Horizontal

Figure 2 Comparison of NEC and MININEC radiation patterns - Case 1

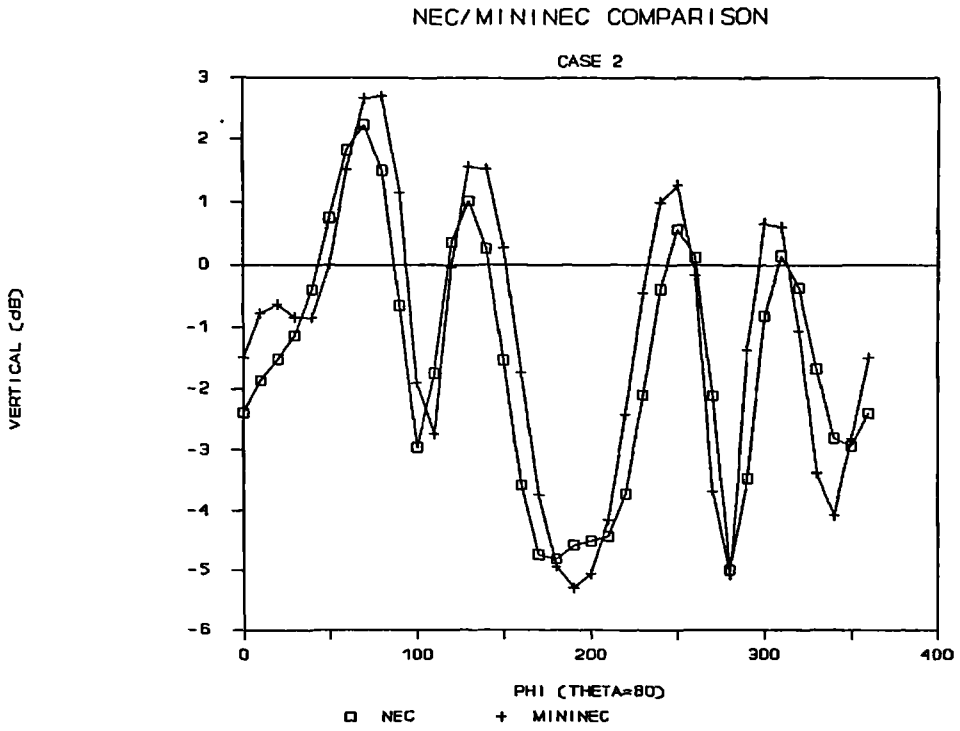

(a) Vertical

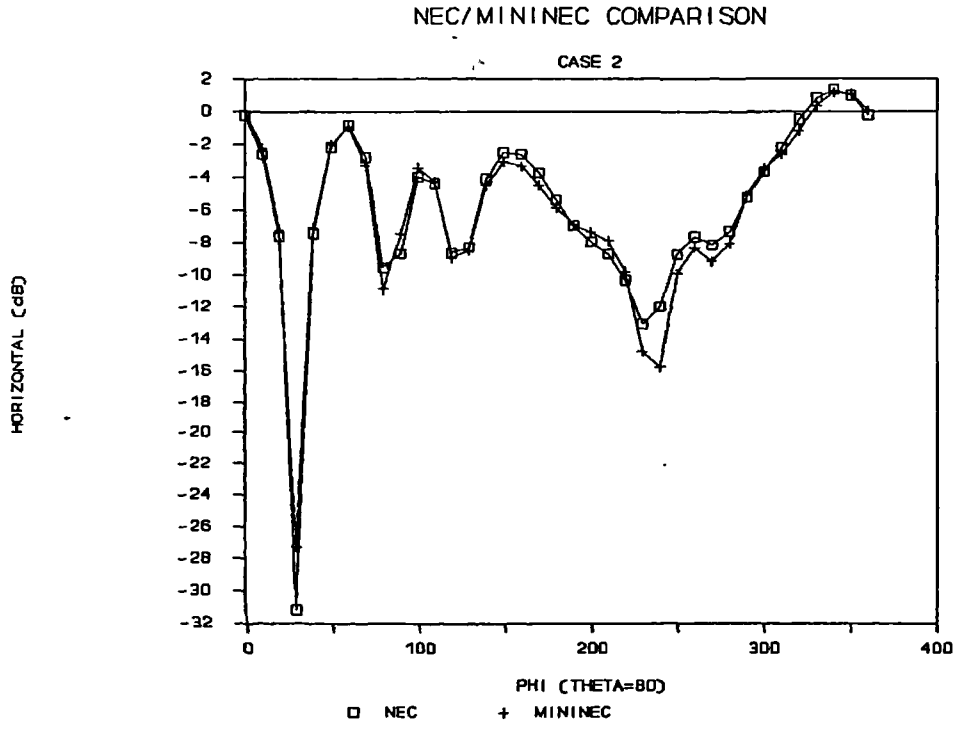

(b) Horizontal

Figure 3 Comparison of NEC and MININEC radiation patterns - Case 2

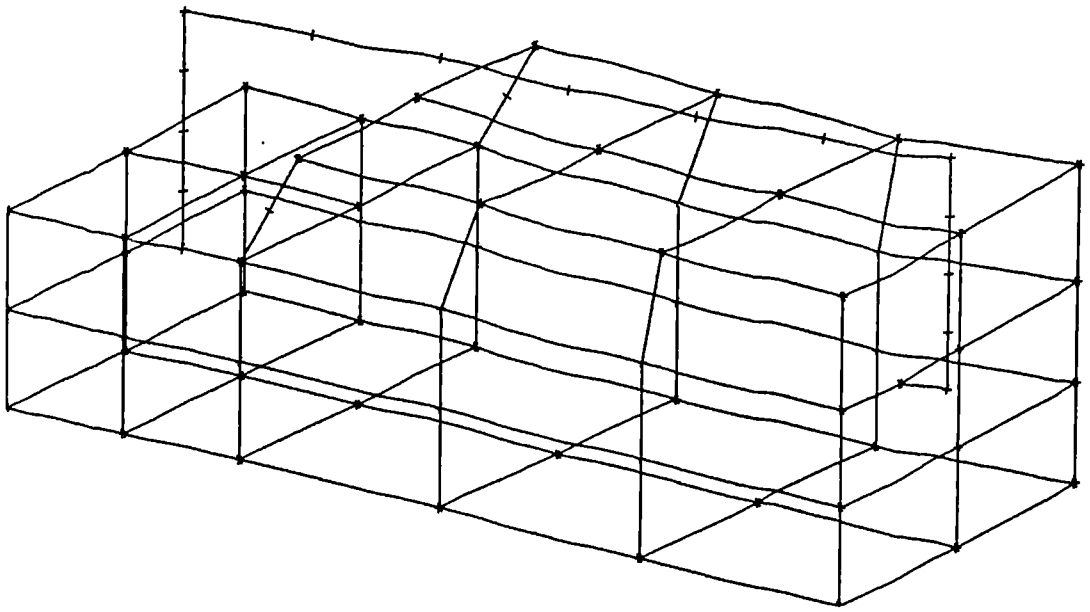

Viewing angles: $\theta=70^\circ, \phi=35^\circ$

Figure 4 Wire grid model of a Land Rover with loop

result compared to the whip, it was thought that the Characteristic Modes of such a complex structure when properly excited could produce an bigger improvement. Four feedpoints were therefore defined, two at the bases of each end of the loop and two others on the front pillars supporting the roof. The modal structure of this port configuration situated over perfect ground at a frequency of 10MHz was calculated using the MININEC Characteristic Mode calculation routine. The modes were ordered in terms of ascending eigenvalue to assess their significance.

In order to use the defined modal structure for pattern synthesis a desired target pattern for total electric field was defined as a polynomial expansion shown graphically in figure 5.

Using this polynomial expansion nearly 90% of the power is radiated in the sector defined by $\theta<45^\circ$, with the advantage of no abrupt changes in the field pattern which may overly constrain the approximating pattern.

Using the four port configuration the synthesized pattern mean squared error was investigated as the number of modes was increased. The results are shown in Table I, along with the mean squared error obtained when feeding the loop alone at the front loop base. Clearly when using all four modes the mean squared error is reduced by over a half compared with feeding the loop alone. Also using only the first two modes reduces the mean squared error by over a third. Interestingly for the two port synthesis the modal scaling factor for mode 2 was an order of magnitude greater than that of mode 1, inferring that the synthesized pattern is due predominantly to the second mode.

The results of three of the cases shown in Table I are considered here. Firstly all four feedpoints were used to excite the appropriate 4 mode current, for a mean squared error of 0.2018. Secondly the four feedpoints were reactively loaded, using the technique described by Harrington [1], to make mode 2 the dominant mode of the system with a eigenvalue of zero. A single voltage source was then used. This second result presumed that due to the loading the contribution of the other modes to the total field would be negligible. To help ensure this the port that exhibited the largest mode 2 current was chosen as the feedpoint. This being the pillar feedpoint on the

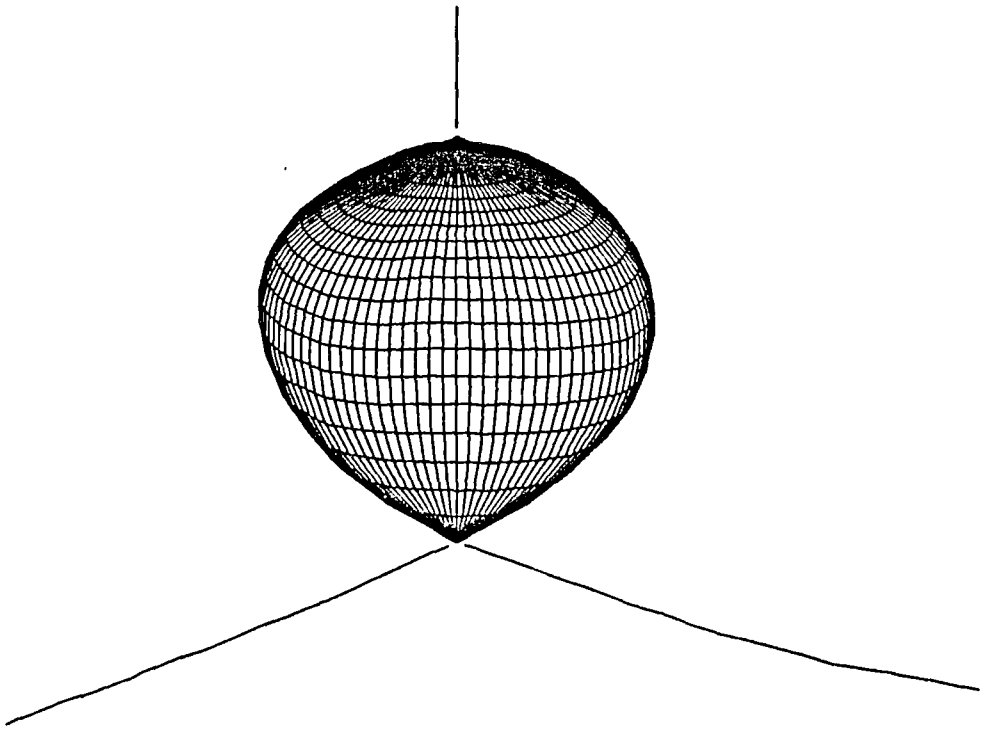

Viewing angles: $\theta=70^{\circ}, \phi=40^{\circ}$
Origin = -20dBi

Figure 5 Target pattern for synthesis

Table I Mean Squared Error Variation

NUMBER OF MODES	MEAN SQUARED ERROR (ϵ)
1	0.7156
2	0.3663
3	0.3656
4	0.2018
LOOP -ALONE	0.5484

left of the vehicle adjacent to the front loop feedpoint. Figure 6 shows the resulting synthesized patterns. The voltages required to generate these patterns and the resulting input impedances are shown in Table II, along with the power radiated into the sector defined by $\theta<45^{\circ}$ by each case. Clearly the best result is obtained using the 4 mode synthesis, although the resulting feedpoint impedances may cause difficulties from practical point of view with small negative resistances. In the case of the loaded feedpoints a substantial improvement in pattern is obtained compared to the unloaded loop fed case, with little degradation to the input resistance.

Table II Voltages and input impedances for the synthesized patterns

PORT	VOLTAGE MAGNITUDE	VOLTAGE PHASE (DEGREES)	R_{in}	X_{in}	% POWER IN $\theta<45°$
4 PORT FEED: PORT 1	0.6845	178.60	-1.54	39.95	53.52
PORT 2	0.8174	-178.27	1.13	29.94	
PORT 3	1.0000	0.00	1.87	124.94	
PORT 4	0.6860	0.95	-1.45	65.19	
LOADED PORTS: FEED PORT 2 ONLY	1.0000	0.00	4.53	0.47	40.12
UNLOADED PORTS: FEED PORT 3 ONLY	1.0000	0.00	7.55	307.91	24.82

Conclusions

This paper has detailed how a Characteristic Mode Calculation routine was implemented using widely available Galerkin based Moment Method software. The advantage of using such an approach, particularly for complex structures is demonstrated.

Clearly for pattern synthesis the method of Characteristic Modes allows the whole of a complex structure to be considered as an antenna. Correct positioning of voltage sources and loading enables beneficial excitation and suppression of modes to produce synthesized approximations to desired far field radiation patterns. Although the efficiency of the implemented feed-systems was not investigated here, it is clear that a balance may be struck between the accuracy of the synthesized pattern and the complexity and physical realizability of the feeding mechanism.

References

1 Harrington, R.F., "Characteristic Modes for antennas and scatterers", in Topics in Applied Physics-Numerical and Asymptotic Techniques in Electromagnetics, vol. 3, pp52-87, Springer-Verlag, 1975.

2 Miller, E.K., "MININEC in FORTRAN", IEEE Antennas and Propagation Society Newsletter, vol.31, no.6, pp28-29, December 1989.

3 The Numerical Algorithms Group (NAG) User Manual, 1979

4 Garbacz, R.J. and Newman, E.H., "Characteristic Modes of a Symmetric Wire Cross", IEEE Trans. on Antennas and Propagation, vol.AP-28, pp712-715, 1980.

5 Pozar, D.M., "Antenna synthesis and optimization using weighted Inagaki modes", IEEE Trans. on Antennas and Propagation, vol.AP-32, pp159-165, 1984.

6 Burberry, R.A., "HF loop antennas for air, land and sea mobiles", Proceedings of the 2nd Conference on HF Communications and Techniques, IEE Conference Publication No.206, pp18-22, 1982.

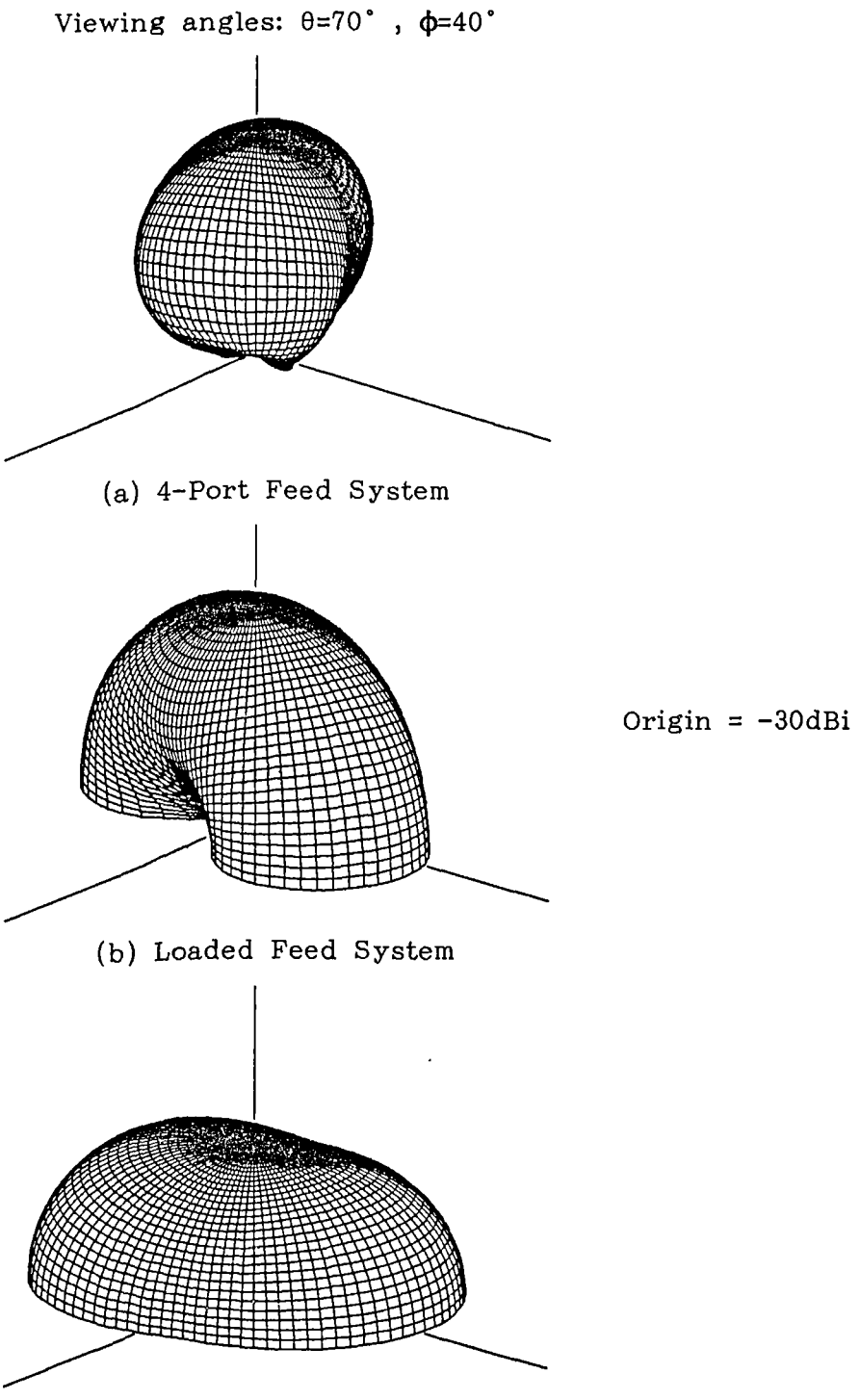

Figure (6). Synthesized Total Far Field Patterns

HF ANTENNAS ON VEHICLES - A CHARACTERISTIC MODAL APPROACH

K.P. Murray and B.A. Austin

Mobile antenna systems have always presented engineers with a challenge. This is particularly true at HF where the physical size and the orientation of the antenna are severely constrained by practical considerations, yet both are key factors in ensuring effective HF communications. In this paper we present an entirely new approach to the analysis and synthesis of HF antennas on vehicles with dimensions much less than a wavelength. Of particular importance is the relationship between the antenna and the propagation mode required for a given service.

Characteristic Modes Garbacz [1] showed that it was possible to define an infinite set of basis functions or mode currents which represented the current distribution on any suitably excited structure. The geometrical dimensions of the structure and the method of current excitation significantly affect this distribution and this, in turn, will determine the radiating properties of the vehicle plus its antennas or sources, considered as one. Calculation of the Characteristic Modes (CM) is facilitated by the use of the Method of Moments [2, 3]. The generalised impedance matrix $[Z] = [R] + j[X]$, for any given configuration, is used to produce a so-called weighted eigenvalue equation

$$[x]\, I_n = \lambda_n [R]\, I_n \qquad (1)$$

where λ_n and I_n are the set of N eigenvalues and eigenvectors or Characteristic Mode currents with N being determined by the order of the [R] and [X] matrices and hence by the segmentation scheme used in the Moment Method solution. From each eigenvalue there exists a characteristic angle which represents the phase difference between the mode current and its associated electric field. This property is significant because modal dominance is indicated by a mode angle of 180 degrees. In order to solve the eigenvalue equation it is necessary that the impedance matrix is symmetrical which then requires that a Galerkin-based Moment Method code be used. This stipulation effectively rules out the use of NEC - the Numerical Electromagnetics Code but not its derivative MININEC. However MININEC, being written in BASIC, is severely limited by the compiler constraints and relative execution time. In the work reported here MININEC has been translated into FORTRAN and its matrix factorisation routine replaced by one that reduced matrix inversion time by 30%. It has been shown [2] to produce accurate results when compared with NEC for a wire-grid model of a vehicle with dimensions of $1.2\lambda \times 0.5\lambda \times 0.2\lambda$.

HF Mobile Antennas Severe constraints exist as regards the size of antennas which can be used on conventional vehicles. This fact seriously affects antenna performance, particularly at the lower end of the HF (1.6-30 MHz) band. A particularly serious problem is the radiation pattern produced by a vertical antenna on a vehicle. Whereas it is nominally "omnidirectional" on the horizon ($\theta = 90°$) there is a significant null (-20 dBi) at the zenith ($\theta = 0°$). Figure 1 shows the computed far-field pattern of a vehicle-mounted whip. It will be noted that the power radiated within the cone angle $\theta \leq 45°$ amounts to just 13% of the total.

For certain applications there is a need to be able to communicate within the HF skip-zone which falls between the point of first skywave return and the boundary of the groundwave. This region is usually always beyond line-of-sight (BLOS) and is frequently obscured by terrain features. Hence, in the absence of man-made relay facilities such as repeaters or satellites, radio communication is only possible by using the near vertical incidence skywave (NVIS) mode [5]. This requires radiation angles towards the zenith which clearly makes the whip configuration inherently unsuitable. Two approaches to overcome this problem, which have been reported, involve either the use of tilted whips [6, 7] or a vertically-mounted loop [8]. The propagation constraints imposed on NVIS are also severe. Because of the need for vertical incidence of the radiated signal upon the ionosphere (usually the F2 layer, [5, p.220]), the operating frequency must be close to the prevailing critical frequency, $f_c = f_0$ F2, at the time and locality in question. This value varies considerably over 24 hours but particularly at night, reaching its nadir just before dawn. Frequencies as low as 1.5 MHz may have to be used to ensure reliable contact over a 50 km path at that hour [5. p.222]. The FOT required can exceed

University of Liverpool, U.K.

10 MHz at mid-day. This wide range of frequencies and the need for zenithal radiation angles makes it obligatory to consider alternative antenna configurations for NVIS applications.

Figure 2 shows the improved radiation within the cone $\theta \leq 45°$ obtained by exciting the computed Characteristic Modes (CM) of a Land Rover plus vertically mounted loop which spans the longest dimension of the vehicle. The loop, when fed conventionally, certainly exhibits an improved pattern compared with a vertical whip. However the CM analysis identified four ports on the vehicle-loop combination which, when suitably excited at 10 MHz would surpass the performance of the loop alone. The method of synthesising the source configuration is based on the technique described in [9]. Nearly 90% of the power is radiated within the $\theta \leq 45°$ cone when the ports at both junctions between the loop and the vehicle plus one in each of the front roof pillars were suitably excited. The driving signals required in this case are shown in the table.

Table 1: Driving requirements for NVIS at 10 MHz

Port	Voltage (V)	Phase (°)	$R_{in}(\Omega)$	$X_{in}(\Omega)$
1	0.6845	178.60	-1.54	39.95
2	0.8174	-178.27	1.13	29.94
3	1.000	0.00	1.87	124.94
4	0.6860	0.95	-1.45	65.19

Conclusion A new technique for the analysis and synthesis of vehicle-mounted HF antenna systems has been presented. An application of the method for NVIS communication is presently under investigation.

Acknowledgement Support from the SERC for the fundamental work on Characteristic Modes and their applications is gratefully acknowledged.

References

1. Garbacz, R.J., "A generalised expansion for radiated and scattered fields", Ph.D. dissertation, The Ohio State University, 1968.

2. Harrington, R.F., "Characteristic modes for antennas and scatterers", in Topics in Applied Physics - Numerical and Asymptopic Techniques in Electromagnetics, Vol.3, pp.52-87, Springer-Verlag, 1975.

3. Austin, B.A. and Murray, K.P., "The generation of antenna characteristic modes from the impedance matrix using the Moment Method", Proc. 7th IEE International Conf. on Antennas and Propat., No.333, York, pp.713-716, 1991.

4. Murray, K.P. and Austin, B.A., "The use of characteristic modes for antenna analysis and far-field pattern synthesis", ACES (UK) Newsletter, No.1, Autumn 1992.

5. Goodman, J.M., "HF Communications-Science and Technology", van Nostrand Reinhold, pp.218-223, 1992.

6. Eley, A.S., Barr, E.E. and Choi, J.H., "Near vertical incidence skywave antenna examination", Proc. 5th IEE International Conf. on HF Radio, No. 339. pp.79-83, July 1991.

7. Wallace, M.A., "HF radio in Southwest Asia", (Operation Desert Storm), IEEE Comms. Magazine, Vol.30, No.1, pp.58-61, Jan. 1992.

8. Burberry, R.A., "HF loop antennas for air, land and sea mobiles", Proc. 2nd IEEInternational IEE Conf. on HF Comms. and Techs., No.206, pp.18-22, 1982.

9. Pozar, D.M., "Antenna synthesis and optimisation using weighted Inagaki modes", IEEE Trans. Antennas and Propagat., Vol. AP-32, pp.159-165 1984.

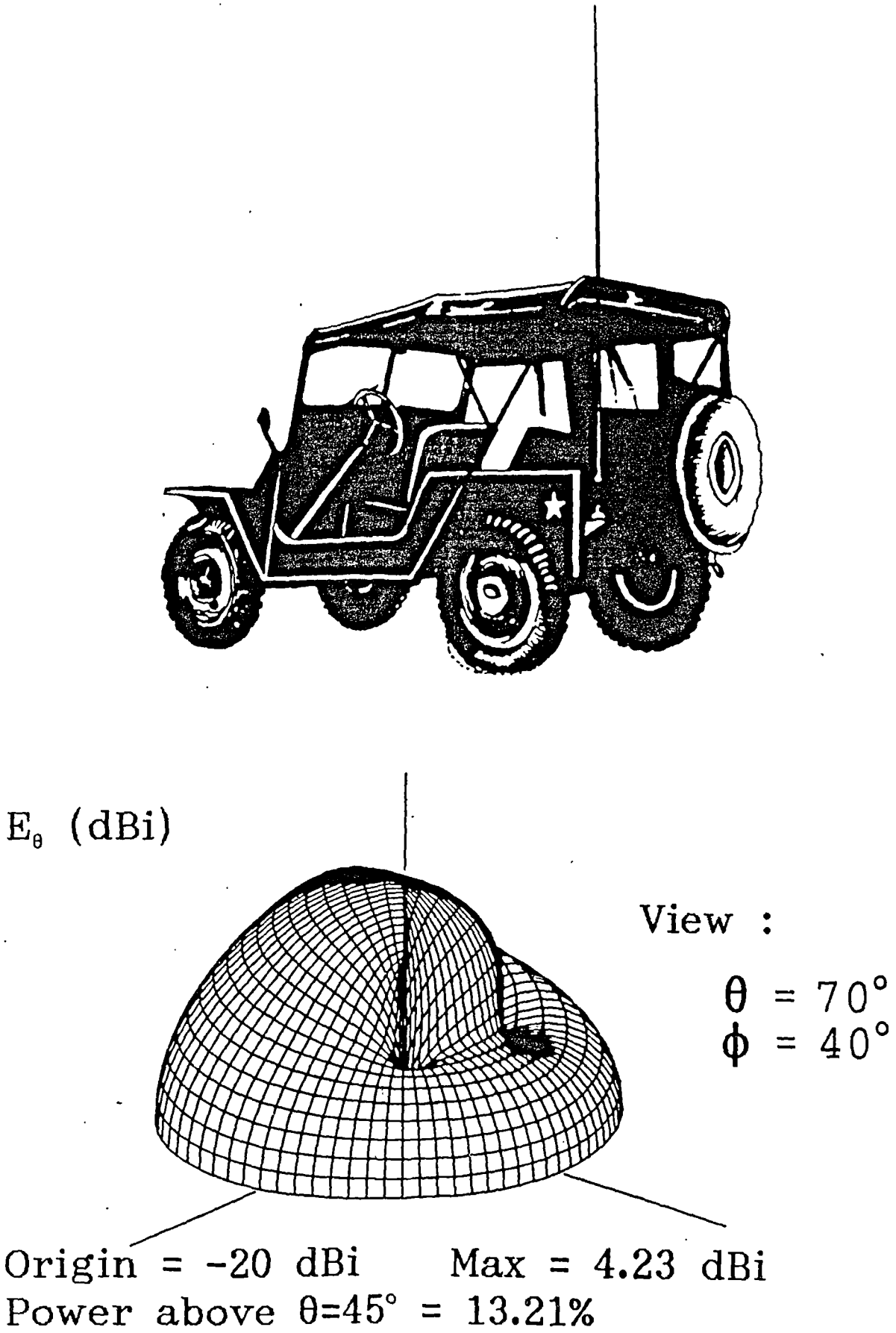

Figure 1 Computed far-field pattern of a whip antenna on a vehicle at 10 MHz.

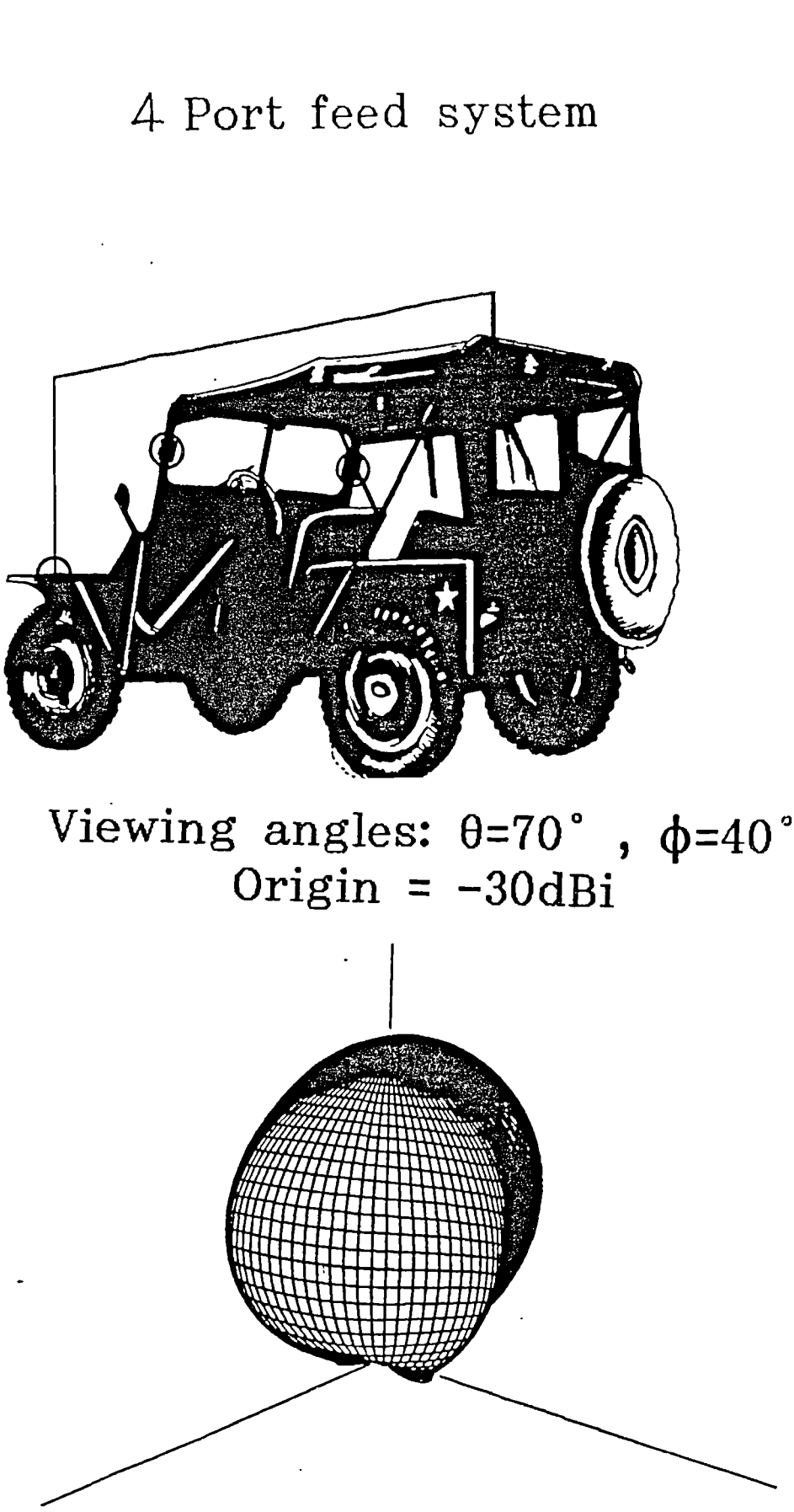

Figure 2 Computed pattern using the Characterisitc Modes of the vehicle plus loop at 10 MHz.

SYNTHESIS OF RADIATION PATTERNS FOR HF MOBILE COMMUNICATIONS USING THE METHOD OF CHARACTERISTIC MODES

K P Murray, B A Austin

University of Liverpool, UK.

INTRODUCTION

Mobile antenna systems have always presented engineers with a challenge. One particular problematic situation is when the antenna and structure on which it is mounted are comparable in size. Here induced current on the structure may dramatically alter the antennas characteristics. Much effort has therefore been applied, using the Method of Moments, in the development of modelling techniques for accurate analysis of the problem. In this paper an alternative approach is presented using the method of Characteristic Modes (CM). The technique allows a set of orthogonal functions to be defined from the Moment Method impedance matrix data to represent the current flow. This permits the antenna and associated structure to be considered as one. Pattern synthesis may hence be achieved by optimizing the modes of the total structure.

CHARACTERISTIC MODES

Calculation

Garbacz [1] initially showed that all structures have associated with them an infinite set of basis functions or mode currents that are independent of any particular excitation. Harrington [2] further formalised the theory, presenting a straightforward method of calculation using the Method of Moments. The generalised impedance matrix $[Z]=[R+jX]$ for any given configuration is used in a so called weighted eigenvalue equation

$$[X]I_n = \lambda_n[R]I_n \qquad (1)$$

where λ_n and I_n are the set of N eigenvalues and eigenvectors or Characteristic Mode currents. N is defined by the order of the $[Z]$ matrix and hence the segmentation scheme used in the Moment Method solution. The modal currents I_n are orthogonal over the structures surface and the associated fields E_n too, are orthogonal over the sphere at infinity.

An important aspect of the solution of equation 1 is that if the $[Z]$ matrix is symmetrical, the resultant eigenvalues and mode currents are real. This is highly advantageous as useful physical insight into the radiation characteristics of a structure may be obtained merely by visual inspection. Also each eigenvalue defines the ratio of stored to radiated power associated with each mode. Thus, the smaller the modulus of the eigenvalue, the more significant a mode will be in the overall radiation.

In order to generate a symmetrical impedance matrix it is necessary to use a Galerkin-based Moment method code which employs the same expansion and testing functions in its representation of the current. This stipulation effectively rules out the use of NEC - The Numerical Electromagnetics Code but not its derivative MININEC. However MININEC, being written in BASIC, is severely limited by compiler constraints and relative execution time. In the work reported here MININEC has been translated into FORTRAN including an improved, faster matrix factorization routine. It has been shown [3] to produce accurate results, compared to NEC, for a wire grid model of a vehicle with dimensions $1.2\lambda \times 0.5\lambda \times 0.2\lambda$.

Pattern Synthesis

In utilizing the Characteristic Modes of a complex structure to achieve a desirable radiation pattern two different approaches were considered. Firstly Harrington [2] showed that if the attributes of an individual mode are favourable compared to the rest then a loading scheme may be defined to resonate it, enforcing $\lambda_n=0$. In many cases this one resonant mode will be dominant and the radiation attributes of the structure will almost be entirely due to it.

The second approach followed that of Pozar [4]. Given a desired far field pattern E_D, a least mean squared error approximation E_A may be defined as a linear summation of the characteristic modal fields such that

$$E_A = \sum_{n=1}^{N} a_n E_n \qquad (2)$$

where a_n is an unknown complex scaling factor. Calculation of a_n is facilitated by the definition of a suitable inner product involving E_D and each E_n over the sphere at infinity. Iterative routines may also be used to further reduce the mean squared error if the phase or polarisation of the final result is unimportant. The current flow I_A necessary to produce the approximating field is then simply

$$I_A = \sum_{n=1}^{N} a_n I_n \qquad (3)$$

A system of voltage sources, numbering the same as modes used in the synthesis, may then be implemented to physically realise the approximating pattern.

HF MOBILE ANTENNAS

Near Vertical Incidence Skywave (NVIS)

For certain applications there is a need to communicate within the HF skip-zone which falls between the first skywave return and the boundary of the groundwave. This region is usually always beyond line-of-sight (BLOS) and is frequently obscured by terrain features. Hence, in the absence of man-made relay facilities such as repeaters or satellites, radio communication is only possible by using the near vertical incidence skywave (NVIS)

mode. This clearly requires radiation angles close to the zenith as shown in figure 1. Conventional vertical whip antennas are therefore inherently unsuitable for this purpose. Figure 2 shows the computed far-field pattern of a typical vertical whip mounted on a Land Rover. Notice that the percentage of power radiated into the cone defined by $\theta<45°$ amounts to just 13.21% of the total. Two approaches to overcome the problem have involved either the use of tilted whip [5] or a vertically mounted loop [6].

Another constraint on NVIS antenna systems is the frequency of operation. Because of the need for vertical incidence upon the ionosphere (usually the F2 layer) the operating frequency must be close to the prevailing critical frequency f_c. It may therefore be necessary sometimes to use frequencies as low as 1.5MHz.

Vehicle Characteristic Modes

The two approaches described above to overcome the NVIS problem have neglected the effect of the mounting structure in the antenna design. The method of Characteristic Modes however, enables current flowing on the rest of the structure to be utilised to beneficial effect. Figure 3 shows a wire grid model of a Land Rover with the NVIS loop antenna described in [6]. The modes of this structure were calculated for a number of frequencies in the range 3-12MHz. Figure 3 also shows four so-called mode current maxima. These points are four of a range of points, of which, one or more consistently exhibited a maximal current magnitude for each member of the modal set. These points are therefore amongst the most effective positions at which to situate voltage sources for greatest mode current excitation.

For Characteristic Mode pattern synthesis these four points were defined as feed ports. A so called generalised port impedance matrix $[Z_p]$ [2] specifying the interaction between these four ports was then defined. This effectively allowed the complete structure to be represented as a four-port network. The Characteristic Modes of this formulation were then calculated. Hence a manageable four mode configuration was defined.

Figure 4 shows the desired target far-field pattern that was specified for use with the synthesis routine. The pattern is of the form of a 4th order polynomial function. Notice the favourable nature of the pattern with nearly 90% of the total radiated power within the cone $\theta<45°$. Also there are no abrupt changes which were found previously to overly constrain the approximating pattern. Table I shows how the relative mean squared error of the approximating pattern varied as the number of modes used is increased at a frequency of 10MHz. Also shown is the mean squared error of the pattern of the loop fed alone conventionally as described in [5]. Clearly when using only the two most significant modes a substantial improvement compared to the loop fed conventionally is obtained. The third most significant mode seems inherently unsuitable for this application as only a insignificant improvement is noticeable compared to using modes 1 and 2 only. Using all four modes though yields the best result with a relative mean squared of around 20%.

Feed System Implementation

Clearly the relative mean squared error of a synthesized pattern reduces as the number of modes used is increased. The clear disadvantage of utilising a relatively large number of modes though is that the required feed system will increase in complexity. Two specific examples using the above synthesis data are described below.

In the first instance the individual characteristics of each mode were examined separately. Clearly the attributes of mode 2 seem substantially more suitable for NVIS than the other three. This is shown in table I by the dramatic decrease in relative mean squared error as mode 2 is introduced into the synthesis procedure. To investigate a four port loading scheme was calculated to resonate mode 2 and hence make it dominant mode of the system. Assuming then that the effect of all other modes is negligible a single voltage source was used to excite the structure with the aim of producing a far-field pattern that is predominantly that of mode 2. Secondly the four voltage sources necessary to realise the four mode approximation were calculated.

To assess the resultant computed patterns figure 5 firstly shows the 3D plot of the loop fed conventionally with a single voltage source at the front base. Secondly figure 6 shows the pattern of the structure with the ports loaded to produce mode 2 resonance. Lastly figure 7 shows the 4 port feed system pattern. Clearly there is a progressive improvement regarding suitability for NVIS. Table II shows the resultant input impedances. The complexity of the 4 port system is clearly apparent. Notice though that the intermediate case of the loaded ports present an input impedance that is comparable with that of the conventionally fed loop. Table II also lists the percentage power radiated into $\theta<45°$.

CONCLUSION

A new technique for the analysis and synthesis of vehicle-mounted antenna systems has been presented. An application of the method for NVIS communication is presently under investigation.

ACKNOWLEDGEMENT

The support of the SERC for this work is gratefully acknowledged.

REFERENCES

1. Garbacz, R.J., 1968, "A generalised expansion for radiated and scattered fields", Ph.D. dissertation, The Ohio State University.

2. Harrington, R.F., 1975, "Characteristic Modes for antennas and scatterers", Topics in Applied Physics - Numerical and Asymptotic Techniques in Electromagnetics, vol.3, pp.52-57, Springer Verlag.

3. Murray, K.P. and Austin, B.A., 1992, "The use of Characteristic Modes for antenna analysis and far-field pattern synthesis", ACES-UK Chapter Newsletter, no.1, pp.2-10.

4. Pozar, D.M., 1984, "Antenna synthesis and optimization using weighted Inagaki modes", IEEE Trans. on Antennas and Propagation, vol.AP-32, pp.159-165.

5. Wallace, M.A., 1992, "HF radio in Southwest Asia, (Operation Desert Storm), IEEE Comms. Magazine, vol.30, no.1, pp.58-61.

6. Burberry, R.A., 1982, "HF loop antennas for air, land and sea mobiles", Proc. 2nd IEE International Conf. on HF. Comms and Tech., no.206, pp.18-22.

Table I Variation of the relative mean squared error as the number of modes is increased.

Number of Modes	Relative mean squared error
1	0.7156
2	0.3663
3	0.3656
4	0.2018
Loop fed conventionally	0.5484

Table II Synthesized patterns feed system data.

Configuration		Feed voltage magnitude	Feed voltage phase	R_{in}	X_{in}	Percentage power in $\theta<45°$
Loop fed conventionally (1 voltage source)		1.0000	0.00	7.55	307.91	24.82
Loaded feed system (1 voltage source, 4 loads)		1.0000	0.00	4.53	0.47	40.12
4 mode feed system (4 voltage sources)	Port 1	0.6845	178.60	-1.54	39.95	53.52
	Port 2	0.8174	-178.27	1.13	29.94	
	Port 3	1.0000	0.00	1.87	124.94	
	Port 4	0.6860	0.95	-1.45	65.19	

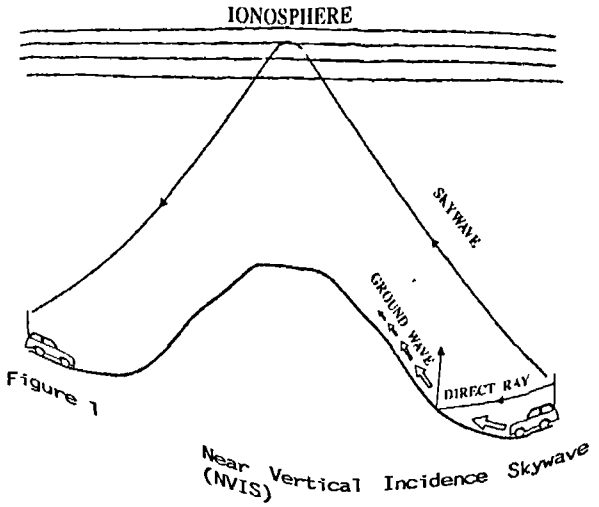

Figure 1

Near Vertical Incidence Skywave (NVIS)

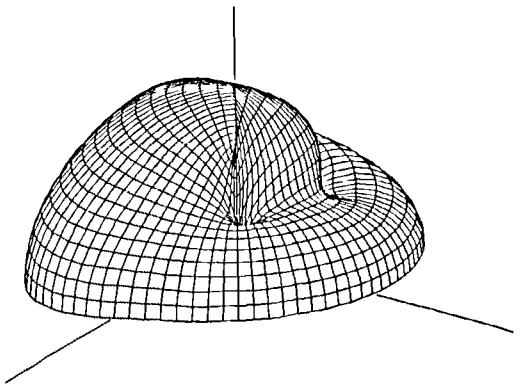

Figure 2 Far-field pattern of a vertical whip antenna mounted on a Land Rover

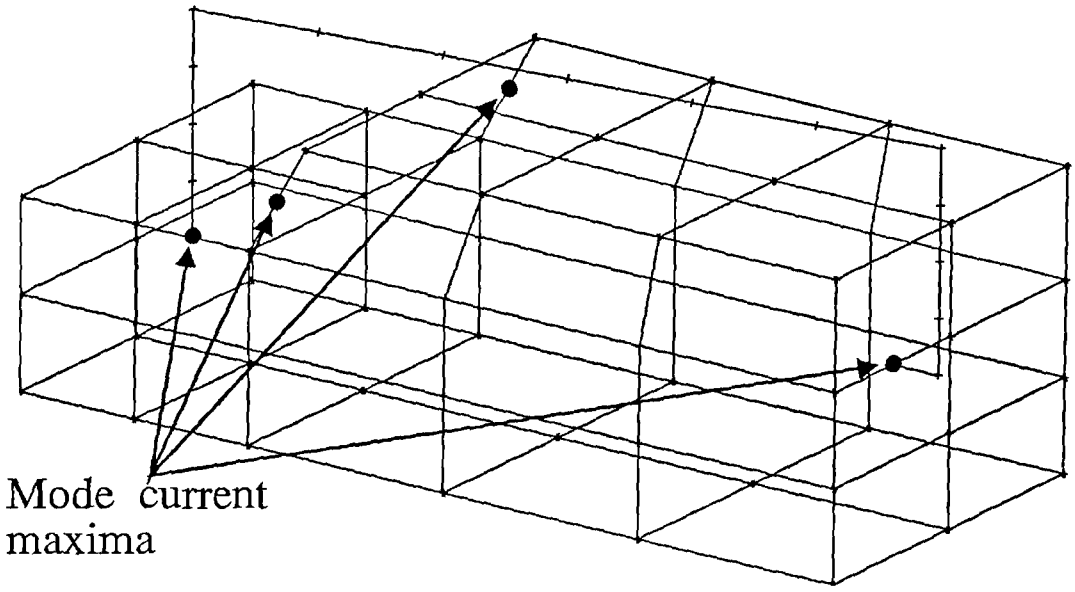

Figure 3 Land Rover wire grid model with mode current maxima

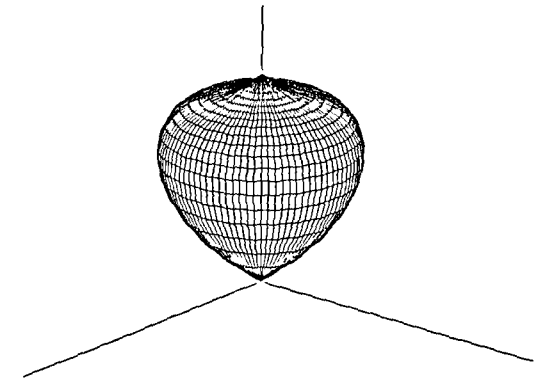

Figure 4 Target far field pattern

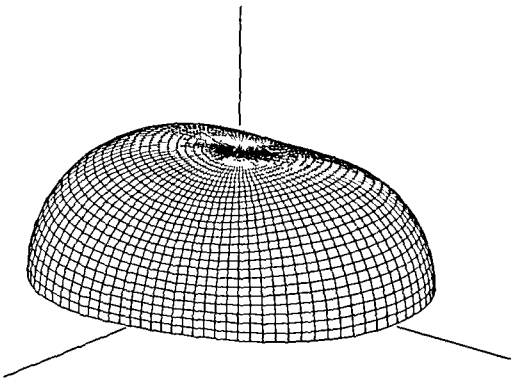

Figure 5 Conventionally fed loop antenna far-field

Pattern viewing angles θ=70°, ϕ=40°

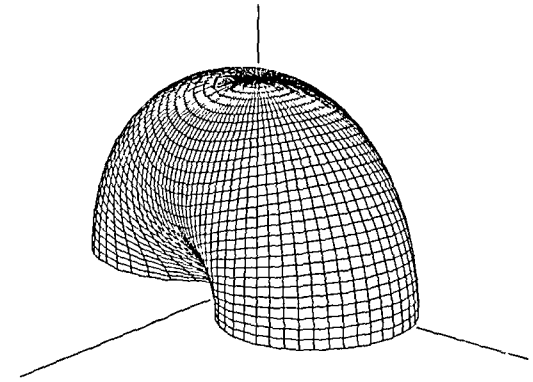

Figure 6 Loaded feed system far-field (1 voltage source, 4 loads)

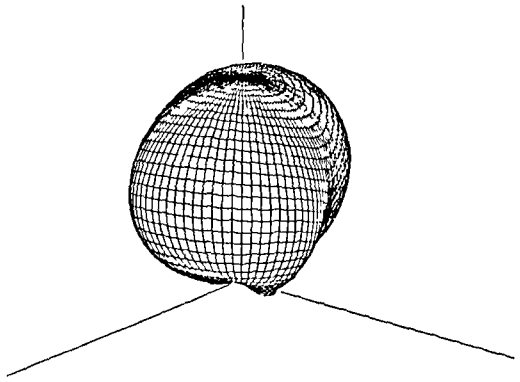

Figure 7 Four mode synthesized far-field (4 voltage sources)

REFERENCES

1. Antelme, F. and Straub, P., (1990). "A compact short range HF skywave antenna", Proceeding of the SAIEE/IEEE Joint AP/MTT-90 Conference, pp.129-136.

2. Austin, B.A. and Murray, K.P. (1991). "The generation of antenna Characteristic Modes from the impedance matrix using the Moment Method", Proceedings of the Seventh International Conference on Antennas and Propagation (ICAP-91), IEE Conference Publication No.333, vol.2, pp.713-716.

3. Austin, B.A. and Najm R.K., (1991). "Wire grid modelling of vehicles with flush-mounted window antennas", Proceedings of the Seventh International Conference on Antennas and Propagation (ICAP-91), IEE Conference Publication No. 333, vol.2, pp.950-953.

4. Austin, B.A., (1993). " An assessment of MININEC and its use in the teaching of antenna theory", Applied Computational Electromagnetics Society Journal, Special issue on Computer Applications in Electromagnetics Education, vol.8, no.1, pp.7-28.

5. Baker, D.C., (1991). "On the functioning of a helicopter-borne HF loop antenna", Applied Computational Electromagnetics Society Journal, vol.6, no.2, pp.53-73.

6. Balanis, C.A., (1982). "Antenna Theory", Harper and Row, New York.

7. Baldwin, P.J., Boswell, A.G.P., Brewster, D.C. and Allwright, J.S., (1991). "Iterative calculation of ship-borne HF antenna performance", IEE Proceedings H, vol.138, pp.151-158.

8. Beezley, B., (1992). "The MN4 Manual", Brian Beezley, 507 Taylor St., Vista, Calif, CA 92084, USA.

9. Bhattacharya, S., Long, S.A. and Wilton, D.R., (1987). " The input impedance of a monopole antenna on a cubical conducting box", IEEE Trans. on Antennas and Propagation, vol.AP-35, pp.756-762.

10. Burberry, R.A., (1982). "HF loop antennas for air, land and sea mobiles", Proceedings of the 2nd Conference on HF Communications and Techniques, IEE Conference Publication No. 206, pp.18-22.

11. Burke, G.J. and Poggio, A.J., (1981). "Numerical Electromagnetics Code Method of Moments", Lawrence Livermore National Laboratory, Technical Document UCID-18834, Calif., U.S.A.

12. Chu, W.C., Long, S.A. and Wilton, D.R., (1990). "The radiation pattern of a monopole antenna attached to a conducting box", IEEE Trans. on Antennas and Propagation, vol.38, pp.1907-1912.

13. Collin, R.E. and Zucker, F.J., (1969). "Antenna Theory - Part 1", McGraw Hill, New York.

14. Collin, R.E., (1985). "Antennas and Radiowave Propagation", McGraw Hill, New York.

15. Cox, J.W.R. and Vongas, G., (1991). "Calculated and measured radiation characteristics of an HF loop antenna mounted upon a helicopter", Proceedings of the 5th International Conference on Radio Systems and Techniques, IEE Conference Publication No. 339, pp.73-78.

16. Cox, J.W.R., (1991). "Comparison of predicted aircraft wire antenna terminal impedance (using NEC) with measurement in the HF band", Proceedings of the Seventh International Conference on Antennas and Propagation (ICAP-91), IEE Conference Publication No. 333, vol.2, pp.717-720.

17. Djordjevic, A.R., Bazdar, M.B., Vitosevic, G.M., Sarkar, T.K. and Harrington, R.F., (1990). "Analysis of Wire Antennas and Scatterers: Software and user's manual", Artech House, Boston.

18. Eley, A.S., Barr, E.E. and Choi, J.H., (1991). "Near vertical incidence skywave antenna examination", Proceeding of the 5th International Conference on HF Systems and Techniques, IEE Conference Publication No.339, pp.79-83.

19. Elliot, P.G. and McBride, T., (1990). "Wire grid Moment Method (NEC) models of a patch antenna", Applied Computational Electromagnetics Society Journal, vol.5, no.2, pp.146-160.

20. Ferguson, T.R. and Balestri, R.J., (1988). "Efficient solution of large moments problems: Wire grid modelling criteria and conversion to surface currents", Applied Computational Electromagnetics Society Journal, vol.3, No. 1, pp.55-81.

21. Garbacz, R.J., (1968). "A Generalized Expansion for Radiated and Scattered Fields" , Ph.D dissertation, The Ohio State University.

22. Garbacz, R.J. and Turpin, R.H., (1971). "A generalized expansion for radiated and scattered fields", IEEE Trans. on Antennas and Propagation, vol.AP-19, pp.348-358.

23. Garbacz, R.J. and Newman, E.H., (1980). "Characteristic Modes of a symmetric wire cross", IEEE Trans on Antennas and Propagation, vol.AP-28, pp.712-715.

24. Goodman, J.M., (1992). "HF Communications Science and Technology", Van Nostrand Reinhold, New York.

25. Gourlay, A.R., and Watson, G.A., (1973). " Computational Methods for Matrix Eigenproblems", John Wiley and Sons.

26. Griffiths, D.A. and Baker, A.R., (1990). "A low profile loop antenna for communications using NVIS", IEE Colloquium on "Flat plate and low profile mobile antennas", no.6, pp.7/1- 7/7.

27. Hagn, H.H. and Van der Laan, J.E., (1970). "Measured relative responses toward the zenith of short whip antennas on vehicles at high frequency", IEEE Trans. on Vehicular Technology, vol.VT-19, pp.230-236.

28. Hagn, G.H., (1973). "On the relative response and absolute gain toward the zenith of HF field-expedient antennas Measured with an ionospheric sounder", IEEE Trans on Antennas and Propagation, vol.AP-21, pp.571-574.

29. Hagn., H.H. and Vincent, W.R., (1974). "Comments on the performance of selected low-power HF radio sets in the Tropics", IEEE Trans. on Vehicular Technology, vol.VT-23, pp.55-58.

30. Harrington, R.F., (1968). "Field Computation by Moment Methods", The Macmillan Company, New York.

31. Harrington, R.F. and Mautz, J.R., (1971a). " Theory of Characteristic Modes for conducting bodies", IEEE Trans. on Antennas and Propagation, vol. AP-19, pp.622-628.

32. Harrington, R.F. and Mautz, J.R., (1971b). "Computation of Characteristic Modes for conducting bodies", IEEE Trans. on Antennas and Propagation, vol.AP-19, pp.629-639.

33. Harrington, R.F. and Mautz, J.R., Chang, Y., (1972). "Characteristic Modes for dielectric and magnetic bodies", IEEE Trans. on Antennas and Propagation, vol.AP-20, pp. 194-198.

34. Harrington, R.F. and Mautz, J.R., (1972). "Control of radar scattering by reactive loading", IEEE Trans. on Antennas and Propagation, vol.AP-20, pp.446-454.

35. Harrington, R.F. and Mautz, J.R., (1974a). "Pattern synthesis for loaded *N*-port scatterers", IEEE Trans on Antennas and Propagation, vol.AP-22, pp.184-190.

36. Harrington, R.F. and Mautz, J.R., (1974b). "Optimization of radar cross section of *N*-port loaded scatterers", IEEE Trans. on Antennas and Propagation, vol.AP-22, pp.697-701.

37. Harrington, R.F., (1975). "Characteristic Modes for antennas and scatterers", Topics in Applied Physics - Numerical and Asymptotic Techniques in Electromagnetics, vol.3, pp.52-87, Springer-Verlag.

38. Herbsteit, J.W. and Crichlow, W.Q., (1964). "Measurement of the attenuation of radio signals by jungles", Radio Science, vol.68D, no.8, pp.903-906.

39. Hilbert, M. and Balmain, K.G., (1985). "Characteristic Mode analysis of symmetric and asymmetric log-periodic dipole antennas", IEEE AP-S International Symposium: Antennas and Propagation - Symposium Digest, pp.199-202.

40. Hilbert, M., Tilston, M.A. and Balmain, K.G., (1989). "Resonance phenomena of log-periodic antennas: characteristic-mode analysis", IEEE Trans. on Antennas and Propagation, vol.AP-37, pp.1224-1233.

41. Hill, D.A. and Wait, J.R., (1977). "Analysis of alternating current excitation of a wire rope by a toroidal coil", Journal of Applied Physics, vol.48, no.12, pp.4893-4897.

42. IGUANA (1987). "User Guide for the Interactive Graphics Utility for Automated NEC Analysis", Version 4.1, Navel Ocean Systems Centre, San Diego.

43. Inagaki, N.I., (1978). "Eigenfunctions of Hermitian iterated operator and its application to numerical analysis", Digest International Symposium Antennas and Propagation Japan, pp.295-298.

44. Inagaki, N.I. and Garbacz, R.J., (1982). "Eigenfunctions of composite Hermitian operators with application to discrete and continuous radiating systems", IEEE Trans on Antennas and Propagation, vol. AP-30, pp.571-575.

45. Jesch, R.L., (1985). "Measured vehicular antenna performance", IEEE Trans. on Vehicular Technology, vol.VT-34, pp.97-107.

46. Jones, J.E., (1976). "Analysis of the symmetric centre-fed V-dipole antenna", IEEE Trans on Antennas and Propagation, vol.AP-24, pp.316-322.

47. Julian, A.J., Logan, J.C. and Rockway, J.W., (1982). "MININEC: A Mini-Numerical Electromagnetics Code", Naval Ocean Systems Centre Technical Document 516.

48. King, R.W.P. and Harrison, C.W., (1969). "Antennas and Waves: A Modern Approach", M.I.T. Press.

49. King, R.W.P., (1971). "Tables of Antenna Characteristics", IFI/Plenam Data Corporation, New York.

50. Kraus, J.D., (1988). "Antennas", McGraw Hill, New York.

51. Kubina, S.J., (1989)."Measurement and computer simulation of antennas on ships and aircraft for results of operational reliability", AGARD Lecture Series No.165, pp.5/1-5/28.

52. Kubina, S.J., (1991). "Computer modelling of performance of installed antennas", Proceedings of the Seventh International Conference on Antennas and Propagation (ICAP-91), IEE Conference Publication 333, pp.840-844.

53. Kummer, W.H., (1992). "Basic array theory", Proc. of the IEEE, vol.80, No.1, pp.127-140.

54. Kuo, D.C., Chao, H.H., Mautz, J.R., Strait, B.J. and Harrington, R.F., (1972). "Analysis of radiation and scattering by arbitrary configurations of thin wires", IEEE Trans on Antennas and Propagation, vol.AP-20, pp.814-815.

55. Laird, R.T, (1985). "GRAPS: Graphical Plotting System", Naval Ocean Systems Centre Technical Document 820.

56. Leather, P.S.H., (1991). Personal communication.

57. Lee, K.S.H., Marin, L. and Castillo, J.P., (1976). "Limitations of wire grid modelling of a closed surface", IEEE Trans on Electromagnetic Compatibility, vol.EMC-18, pp.123-129.

58. Lewallen, R., (1991). "MININEC: The Other Edge of the Sword", QST, pp.18-22, February issue.

59. Li, S.T., Logan, J.C., Rockway, J.W. and Tam, D.W.S., (1983). "Microcomputer Tools for Communication Engineering", Artech House, Boston.

60. Lin, Y.T. and Richmond, J.H. (1975). "EM modelling of aircraft at low frequencies", IEEE Trans. on Antennas and Propagation, vol.AP-23, pp.53-56.

61. Lindenmeier, H.K., (1989). "Antenna on land vehicles for improved communications", AGARD Lecture Series No.165, pp.7/1-7/19.

62. Liu, D., Garbacz, R.J. and Pozar, D.M. (1990). "Antenna synthesis and optimization using Generalized Characteristic Modes", IEEE Trans. on Antennas and Propagation, vol.38, pp.862-868.

63. Logan, J.C., and Rockway, J.W. (1986). "The new MININEC (version 3): A Mini-Numerical Electromagnetics Code.", Naval Ocean Systems Centre Technical Document 938.

64. Logan, J.C. (1988). "The MININEC System: Microcomputer Analysis of Wire Antennas", Artech House, Boston.

65. Ludwig, A.C. (1987). "Wire grid modelling of surfaces", IEEE Trans. on Antennas and Propagation, vol.AP-35, pp.1045-1048.

66. Maslin, N.M., (1987). "HF Communications - A Systems Approach", Pitman, London, pp.81-86.

67. Mautz, J.R. and Harrington, R.F. (1973). "Modal analysis of loaded *N*-port scatterers", IEEE Trans. on Antennas and Propagation, vol.AP-21, pp.188-199.

68. Mayhan, J.T. (1990). "Characteristic Modes and wire grid modelling", IEEE Trans. on Antennas and Propagation, vol.38, pp.457-469.

69. Miller, E.K. (1983). "Numerical modelling techniques for antennas", AGARD Lecture Series No.131, pp.7/1-7/29.

70. Miller, E.K. (1989). "A selective survey of computational electromagnetics for antenna applications", AGARD Lecture Series No.165, pp.2/1-2/29.

71. Miller, E.K. (1989). "MININEC in FORTRAN", IEEE Antennas and Propagation Society Newsletter, vol.31, no.6, pp.28-29.

72. Moore, J. and Pizer, R. (1986). "Moment Methods in Electromagnetics", Research Studies Press, New York.

73. Monteath, G.D. and Knight, P., (1960). "The performance of a balanced aerial when connected to a coaxial cable", Proceedings of the IEE, vol.107, pp.712-715.

74. NAG FORTRAN library manual (1981). Mark 8, volume 4.

75. Najm, R.K., (1991). "Simplified 3-D Mesh Generator", Applied Computational Electromagnetics Society Journal, vol.6, no.2, pp.86-98.

76. Najm, R.K., (1992). "Wire-Grid Modelling of Glass Mounted Vehicular Antennas at VHF", Ph.D Thesis, University of Liverpool, UK.

77. NEEDS, (1988). "NEEDS: The Numerical Electromagnetic Engineering Design System", Version 1.0, The Applied Electromagnetics Society.

78. Nalbantoglu, A.H. (1982). "New computation method for Characteristic Modes", Electronics Letters, vol.18, No.23, pp.994-996.

79. Newman, E.H., (1979). "Small antenna location synthesis using Characteristic Modes", IEEE Trans. on Antennas and Propagation, vol.AP-27, pp.530-531.

80. Nishikawa, L.A. (1984). "Effect of automobile body and earth on radiation patterns of antennas for FM radio", Trans. of the IECE of Japan, vol.E-67, No.10.

81. Oyekanmi, L.A. and Watkins, J. (1989). "Selecting wire radius for grid/mesh models", Applied Computational Electromagnetics Society Journal - Special edition on "Electromagnetics computer code validation, pp.43-57.

82. Paknys, R.J. (1991). "The near field of a wire grid model", IEEE Trans on Antennas and Propagation, vol.39, pp.994-999.

83. Pavey, N.A.D., (1980). "Guide to aircraft high frequency communications antenna systems", RAE Technical Report 80156.

84. Plonus, M.A. (1986). "Applied Electromagnetism", McGraw Hill, New York.

85. Poggio, A.J. and Miller, E.K. (1973). "Integral equation solution of three dimensional scattering problems", Computational Techniques for Electromagnetics, Mitrra, R. editor, Permagon, chapter 4.

86. Pozar, D.M. (1984). "Antenna synthesis and optimization using Weighted Inagaki Modes", IEEE Trans. on Antennas and Propagation, vol.AP-32, pp.159-165.

87. Richmond, J.H. (1966). "A wire grid model for scattering by conducting bodies", IEEE Trans. on Antennas and Propagation, vol.AP-14, pp.782-786.

88. Richmond, J.H. (1974a). "Radiation and Scattering by Thin Wire Structures in the Complex Frequency Domain", NASA Contractors Report 2396.

89. Richmond, J.H. (1974b). "Computer Program for Thin-Wire Structures in a Homogeneous Conducting Medium", NASA Contractors Report 2399.

90. Shaw, P.J. (1991). "Design of Antennas for the PCN Radio System", M.Sc Thesis, University of Liverpool, UK.

91. Stutzman, W.L. and Thiele, G.A. (1981). "Antenna Theory and Design", John Wiley and Sons, New York.

92. Trueman, C.W. and Kubina, S.J., (1990). "Verifying wire grid model integrity with program CHECK", Applied Computational Electromagnetics Society Journal, vol. 5, no. 2, pp 17-42.

93. Turpin, R.H. (1969). "Basis Transformation, Least Square, and Characteristic Mode Techniques for Thin Wire Scattering Analysis", Ph.D dissertation, The Ohio State University.

94. Wait, J.R. and Hill, D.A., (1973). "Excitation of a homogeneous conductive cylinder of finite length by a prescribed axial current distribution", Radio Science, vol.8, no.12, pp.1169-1176.

95. Wallace, M.A., (1992). "HF radio in Southwest Asia", IEEE Comms. Magazine, vol.30, no.1, pp.58-61.

96. Yee, A.O. and Garbacz, R.J., (1973). "Self- and mutual-admittances of wire antennas in terms of Characteristic Modes", IEEE Trans. on Antennas and Propagation, vol.AP-21, pp.868-871.